Fabrication and Characterization of graphene-based ink for flexible electronic

D.S. Saidina

UNIVERSITÉ DE LORRAINE

Ecole doctorale C2MP

Thèse

Présentée et soutenue publiquement pour l'obtention du titre de

DOCTEUR de L'UNIVERSITÉ DE LORRAINE

Spécialité : Chimie

Présentée par :

MOHD SAIDINA DANDAN SATIA

Fabrication et caractérisation d'encres à base de graphène pour l'électronique souple

Thèse soutenue publiquement le 22 août 2019 à Penang (Malaisie) devant le jury composé de :

Fauziah Ahmad	Professeur, Universiti Sains Malaysia	Président du Jury
Jesús Santos Pena	Maître de Conférences, Université de Tours	Rapporteur
Ishak Bin Ahmad	Professeur, Universiti Kebangsaan	Rapporteur
Claire Hérold	Directeur de Recherche, Université de Lorraine	Directeur de thèse
Mariatti Binti Jaafar	Professeur, Universiti Sains Malaysia	Directeur de thèse
Sébastien Fontana	Maître de Conférences, Université de Lorraine	Co-directeur de thèse
Tuti Katrina Abdullah	Maître de Conférences, Universiti Sains Malaysia	Invitée
Syazana Ahmad Zubir	Maître de Conférences, Universiti Sains Malaysia	Invitée

IJL, Campus Artem, 2 allée André Guinier, BP 50840, 54011 Nancy Cedex

Université de Lorraine – Pôle M4 : matière, matériaux, métallurgie, mécanique

FABRICATION AND CHARACTERIZATION OF GRAPHENE-BASED INK

MOHD SAIDINA BIN DANDAN SATIA

UNIVERSITI SAINS MALAYSIA

2019

FABRICATION AND CHARACTERIZATION OF GRAPHENE-BASED INK

by

MOHD SAIDINA BIN DANDAN SATIA

Thesis submitted in fulfilment of the requirements

for the degree of

Doctor of Philosophy

October 2019

ACKNOWLEDGEMENT

In the name of Allah, the Most Beneficent and the Most Merciful. All praises and thanks be to Allah for the strength, knowledge, ability and opportunity to undertake this research study and complete it satisfactorily. His blessings have made this achievement possible. Alhamdulillah.

First, deepest appreciation to my main supervisors in Universiti Sains Malaysia (USM), Malaysia and Université de Lorraine, France; Prof. Ir. Dr. Mariatti Jaafar and Prof. Claire Hérold for their guidance and supervision throughout this research. Their constant support, encouragement and credible ideas have been great inspirations in the completion of the thesis. Also to my co-supervisors; Dr. Syazana Ahmad Zubir and Dr. Sébastien Fontana, for their helpfulness and continuous support in the completion of the research.

Acknowledgements are also extended to the School of Materials and Mineral Resources Engineering, Universiti Sains Malaysia and Institut Jean Lamour, Université de Lorraine for the great facilities and working space. Also, warmest appreciation to the SMMRE's and IJL's staffs for the administrative and technical supports provided.

Special thanks to the Ministry of Higher Education Malaysia (MyBrain15), Fundamental Research Grant Scheme (FRGS; Grant No. 6071385) and Campus France for granting the research fund used for this project.

To my dear friends Shahrul Affendi, Alif Nur Faizal, Andre Ningkan, Nurliyana, Naqib, Badrul, Dr. Nawal, Dr. Brigitte, Yoni Levy, Lilian, Anna, Hugo, Xavier, Tristan, Olivier, Illies and Syafiq, who always be there for me and kept me going on my path to success in whatever manner possible. Thanks for the friendship and memories.

Lastly, to the biggest source of my strength; my father and my late mother Hj. Dandan Satia Bin Bukah & Allahyarhamah Saimah Binti Pidu, my beloved sisters Samee'ah and Syawal, my brother, Saidani and his wife, Hafizatunisa and their children Hiliy and Hilfiy. Thank you for your tremendous love and constant encouragement that helped me through the difficult moments of reaching my dreams. Not forgetting my lovely cousins Ain, Kamisah, Khadijah, Syikin and Syafiqah, my adopted family Jasmi and Saliza, and their daughters Izni, Izzati, Ika, Munirah and Ida, my aunts and uncles, for their love and care. To those contributed in this research one way or another, your kindness means a lot to me. Thank you!

I would like to dedicate this work to my father and my late mother. This one is for both of you!

TABLE OF CONTENTS

LIST OF TABLES

Page

LIST OF FIGURES

Page

LIST OF SYMBOLS

m	Metre
%	Percentage
J	Joule
g	Gram
°C	Degree Celsius
L	Litre
V	Volt
W	Watt
Pa	Pascal
N	Newton
S	Siemens
Ω	Ohm
sq	Square
min	Minutes
h	Hour
S	Siemens
s	Second
η	Viscosity
γ	Surface energy
θ_c	Contact angle
P	Poise
π	Pi
ζ	Zeta potential
Hz	Hertz
vol.%	Volume percent
psi	Pounds per square inch

θ	Theta
λ	Wavelength
Å	Angstrom
°	Degree
eV	Electronvolt
ρ	Resistivity
σ	Conductivity
t	Thickness
R	Sheet resistance
f	Correction factor
L	Length
a.u.	Arbitrary unit
d	Interlayer distance
L_c	Crystallite size
k	Constant
wt.%	Weight percent

LIST OF ABBREVIATIONS

2D	Two-dimensional
GNPs	Graphite nanoplatelets
GO	Graphene oxide
CVD	Chemical vapor deposition
LPE	Liquid phase exfoliation
RGO	Reduced graphene oxide
GF	Graphene foam
AuNPs	Gold nanoparticles
AgNPs	Silver nanoparticles
CuNPs	Copper nanoparticles
3D	Three-dimensional
NMP	N-Methyl-2-pyrrolidone
DMSO	Dimethylsulfoxide
DMF	N,N-Dimethylformamide
IPA	2-propanol
EG	Ethylene glycol
PG	Propylene glycol
SG	Synthetic graphite
PV	Polyester varnish
PET	Polyethylene terephthalate
SEM	Scanning electron microscopy

EDS	Energy dispersive spectroscopy
HRTEM	High resolution transmission electron microscopy
XRD	X-ray diffraction
XPS	X-ray photoelectron spectroscopy
FTIR	Fourier-transform infrared spectroscopy
BET	Brunauer-emmett-teller
TGA	Thermogravimetric analysis
THF	Tetrahydrofuran
PI	Polyimide
FGO	Few-layered graphene oxide
PEN	Poly(ethylenenaphthalate)
CNTs	Carbon nanotubes
PANI	Polyaniline
PPy	Polypyrrole
PEDOT:PSS	Poly(3,4-ethylenedioxythiophene)-poly(styrenesulfonate)
MWCNT	Multi-walled carbon nanotube
SWCNT	Single-walled carbon nanotube
PDMS	Polydimethylsiloxane
PVDF	Polyvinylidene fluoride
TPU	Thermoplastic polyurethane
SAED	Selected area electron diffraction
FWHM	Full-width at half maximum

FABRIKASI DAN PENCIRIAN DAKWAT BERASASKAN GRAFEN

ABSTRAK

Tujuan utama kajian ini dijalankan adalah untuk membangunkan dakwat berasaskan grafen dengan kestabilan, sifat-sifat elektronik dan fizikal yang baik untuk percetakan elektronik dengan menggunakan teknologi salutan semburan dan percetakan inkjet. Pertama, perbandingan untuk bahan seperti-grafen yang berbeza menunjukkan bahawa busa grafen (GF) mempamerkan permukaan yang tertinggi dengan nilai 2136 m^2g^{-1}. Sementara itu, grafit nanoplatlet (GNPs) dan grafit sintetik (SG) mempamerkan struktur hablur yang tinggi dengan kewujudan puncak (002) yang tajam dan sempit, dan zarah yang berkualiti tinggi dengan nisbah I_D/I_G yang rendah. Kedua, keputusan menunjukkan bahawa kelikatan dan sudut sentuhan dakwat yang konduktif meningkat dengan ketara dengan penambahan pengisian GF, GNPs dan SG dalam penguat varnis poliester (PV). Penambahan 10% isipadu GNPs meningkatkan konduktiviti elektrik PV sebanyak 186 %, dan hanya 40 % untuk SG dan 10 % untuk GF pada jumlah pengisi yang sama. Seterusnya, didapati bahawa GNPs disebar di dalam glikol etilena (EG) mempamerkan kestabilan yang baik dengan penurunan sebanyak 85% daripada kepekatan awal selepas sebulan, kelikatan dan kebolehbasahan berbanding glikol propilena (PG) dan 2-propanol (IPA). Selain itu, GF disebar di dalam pelarut campuran IPA:EG pada nisbah 1:1 menunjukkan penurunan sebanyak 50 % sahaja daripada kepekatan awal selepas sebulan berbanding dengan dakwat GNPs pada nisbah campuran yang sama. Untuk bahagian akhir, dakwat GF, dakwat hibrid GF/poli(3,4-etilenadioksitiofena) poli(stirenasulfonat) (PEDOT:PSS) menunjukkan kestabilan yang baik berbanding dakwat GF dan dakwat hibrid GF/nanopartikel perak (AgNPs) di mana dakwat menunjukkan penurunan kepekatan sebanyak 30 % selepas sebulan, peningkatan kekonduksian permukaan sebanyak 100 % pada 50 lapisan cetakan dan

faktor tolok sebanyak 4.3. Kesimpulannya, hibrid GF/PEDOT:PSS yang bercetak mempunyai potensi untuk digunakan sebagai aplikasi sensor regangan.

FABRICATION AND CHARACTERIZATION OF GRAPHENE-BASED INK

ABSTRACT

The main aim of the present study is to develop graphene-based ink with excellent stability, electrical and physical properties for printing electronics by utilizing spray coating and inkjet printing techniques. Firstly, comparison on the different types of graphene-like materials showed that graphene foam (GF) exhibited the highest surface area with the value of 2136 m^2g^{-1}. Meanwhile, graphite nanoplatelets (GNPs) and synthetic graphite (SG) displayed highly crystalline structures with the presence of sharp and narrow (002) peak, and high-quality particles with lower I_D/I_G ratio. Secondly, results showed that viscosity and contact angle of the conductive inks increased significantly with increasing GF, GNPs and SG filler loadings in a polyester varnish (PV) binder. The incorporation of 10 vol.% GNPs improved the electrical conductivity of PV by 186 %, and only 40 % for SG and 10 % for GF at the same filler loading. Next, it is found that GNPs dispersed in ethylene glycol (EG) exhibited better stability with 85 % decrement of the initial concentration after a month, viscosity and wettability than those of propylene glycol (PG) and 2-propanol (IPA). On the other hand, GF dispersed in IPA:EG mixed solvent at ratio of 1:1 showed only 50 % decrement from the initial concentration after a month compared to those of GNPs inks at the same mixed ratio. In the last part, GF/poly(3,4-ethylenedioxythiophene) poly(styrenesulfonate) (PEDOT:PSS) hybrid ink exhibited better stability than GF ink and GF/silver nanoparticles (AgNPs) hybrid ink where the ink showed 30 % decrement from the concentration after a month, 100 % improvement in surface conductivity at 50 printed layers and gauge factor of 4.3. As a conclusion, printed GF/PEDOT:PSS hybrid ink has the potential to be used for strain sensor applications.

FABRICATION ET CARACTERISATION DE L'ENCRE A BASE DE GRAPHENE

RÉSUMÉ

L'objectif principal de la présente étude est de développer des encres à base de graphène présentant d'excellentes propriétés de stabilité, électriques et physiques pour l'électronique d'impression en utilisant des techniques de revêtement par pulvérisation et d'impression par jet d'encre. Premièrement, la comparaison des différents types de matériaux similaires au graphène a montré que la mousse de graphène (GF) présentait la plus grande surface spécifique avec une valeur de 2136 m^2g^{-1}. Par ailleurs, les nanoplaquettes de graphite (GNPs) et le graphite synthétique (SG) présentaient des structures hautement cristallines avec la présence d'un pic aigu et étroit (002) et de particules de haute qualité avec un rapport I_D/I_G inférieur. Deuxièmement, les résultats ont montré que la viscosité et l'angle de contact des encres conductrices augmentaient significativement avec l'augmentation des charges de GF, GNPs et SG dans un liant de vernis polyester (PV). L'incorporation de 10 % en volume de PNB a amélioré la conductivité électrique du PV de 186 %, et seulement 40 % pour la SG et 10 % pour le GF avec la même charge de remplissage. Ensuite, il a été constaté que les PNB dispersés dans l'éthylène glycol (EG) présentaient une meilleure stabilité avec une diminution de 85% de la concentration initiale après un mois, une viscosité et une mouillabilité supérieures à celles du propylène glycol (PG) et du 2-propanol (IPA). D'autre part, le GF dispersé dans un solvant mélangé IPA:EG avec un rapport de 1:1 n'a montré qu'une diminution de 50 % par rapport à la concentration initiale après un mois comparant à ceux des encres GNP dans le même rapport de mélange. Dans la dernière partie, l'encre hybride GF/poly(3,4-éthylènedioxythiophène) poly(styrène-sulfonate) (PEDOT:PSS) a montré une meilleure stabilité que l'encre hybride GF et

l'encre hybride GF/nanoparticules d’argent (AgNPs) où l'encre a montré 30 % de réduction de concentration après un mois, 100 % d'amélioration en termes de conductivité superficielle à 50 couches imprimées et un facteur de gauge de 4.3. En conclusion, l'encre hybride imprimée GF/PEDOT:PSS a le potentiel d'être utilisée pour les applications de capteurs de contrainte.

CHAPTER 1

INTRODUCTION

1.1 Background

Recent years have witnessed a revolution in graphene due to its distinctive physicochemical properties, tremendous mechanical performance and its unique electrical and thermal conductivities (Novoselov *et al*., 2004). Presently, graphene has been widely used in various electronic applications including as the conductive inks for printable flexible electronics. Graphene expression consists of a prefix of "*graph*" from graphite and suffix "*ene*" from C-C double bonds (Bianco *et al*., 2013; Ghany *et al*., 2017). Graphene by definition is a single atomic layer of carbon atoms packed into two-dimensional (2D) honeycomb lattice structure. The atoms are arranged in hexagonal structure creating a sheet of sp^2 tightly bonded carbon. Graphene has been considered as "the thinnest, most flexible and strongest material known" that conducts heat and electricity very well (Jaworski *et al*., 2013; Brownson and Banks, 2014). The thickness (number of layers) in 2D carbons goes from 0.34 nm (monolayer graphene) up to several micrometers. In 1947, Wallace in his study has explained that almost all 'graphene-like materials' are different from the idealized 2D 'graphene structure'. Several types of graphene-like materials had been existing from monolayer to multilayer graphene, turbostratic carbon, graphite nanoplatelets (GNPs), graphene foam (GF) and graphene oxide (GO) (Choucair *et al*., 2009; Bianco *et al*., 2013).

To date, several methods for the mass production of graphene have been explored including chemical vapor deposition (CVD), liquid phase exfoliation (LPE), graphite oxide route leading to graphene oxide (GO) or reduced graphene oxide (RGO), electrochemical route and solvothermal method (Chen *et al*., 2004; Choucair

et al., 2009; Novoselov *et al*., 2012; Low *et al*., 2013, Speyer *et al*., 2015). Among these methods, LPE method is considered one of the simplest methods and yields larger quantities of graphene, however the number of graphene layers is inconsistent as the layers may reaggregate and this method introduces chemical and physical defects in the graphene layers, which may not be suitable to be used as conductive inks (Parvez *et al*., 2015). Choucair *et al*. (2009) reported that solvothermal method is an alternative bottom-up approach for the production of graphene-like materials, low cost of raw materials, has the ability to yield graphene in large scale, etc. According to Ma *et al*. (2014) and Speyer *et al*. (2015), solvothermal reaction method has been widely studied previously for the production of graphene foam (GF).

Conductive ink made of graphene has become a topic of interest due to its superior electrical properties in comparison of various conductive nanomaterials, conductive polymers and other carbon-based materials while at the same time reducing production costs (Arapov *et al*., 2014). An ideal conductive ink should be inexpensive, simple preparation, good printability, low viscosity, good stability, good adhesion to the substrate and high electrical conductivity values even after printing (Choi *et al*., 2015; Liu *et al*., 2015; Stoppa and Chiolerio, 2014). According to the statistic of scientific journals related to conductive inks which were taken from Scopus as in Figure 1.1, it shows that the number of scientific publications exhibited 416% improvement specifically from 2009 to 2018.

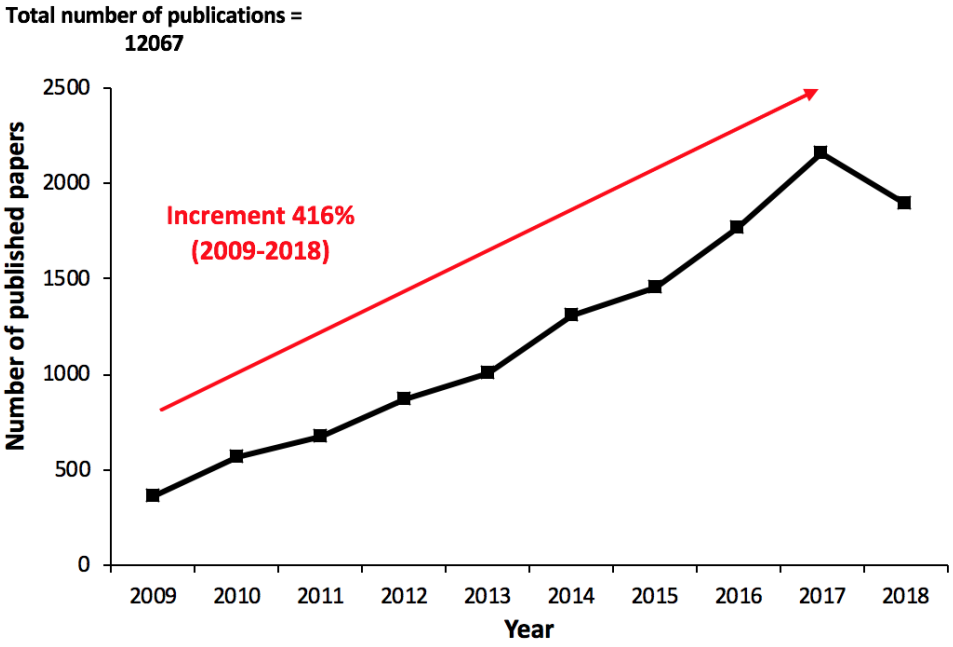

Figure 1.1 The number of published papers for conductive inks 2009-2018 from Scopus by searching for the topic "conductive ink" (data acquired on October 2019)

Furthermore, conductive ink is one of the main elements in the printing industry such as inkjet printing, spray coating, screen printing, etc for flexible electronic applications. Figure 1.2 illustrates the market value share for conductive inks in printed electronic applications including organic light-emitting diode (OLED), organic and inorganic photovoltaics, flexible displays, radio-frequency identification (RFID), healthcare devices, thin film transistor, solar cells, sensors, smart textiles, batteries, memories, and antenna (Capasso *et al*., 2015; Suganuma, 2014; Denneulin *et al*., 2011; Kamyshny and Magdassi, 2014; Li *et al*., 2010). The market value share for conductive inks is expected to increase gradually up to 2026.

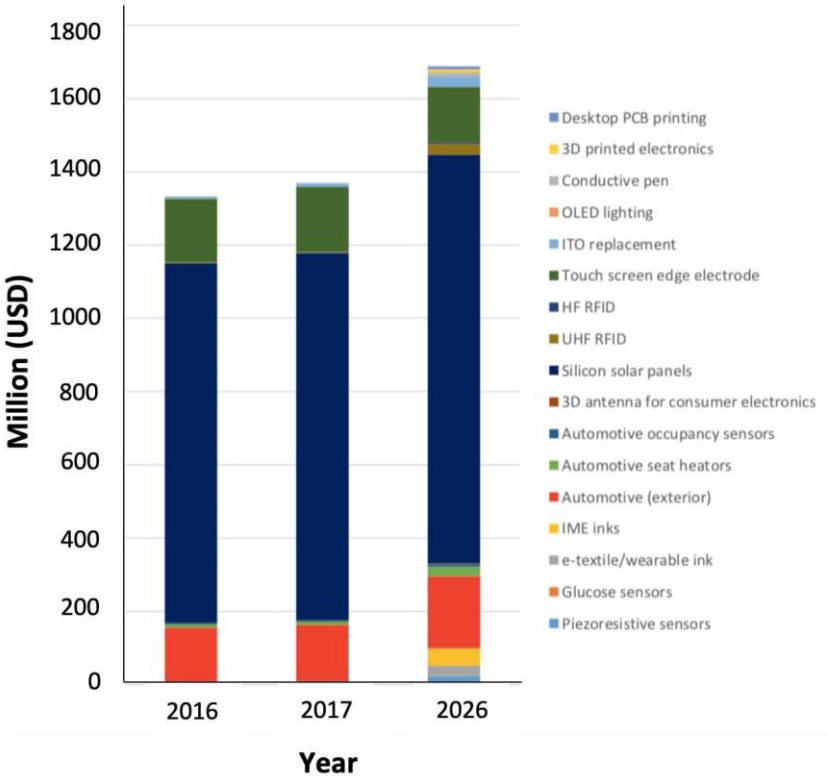

Figure 1.2 Market value share (million USD) for conductive inks in emerging sectors 2016-2026 (Zervos, 2016)

1.2 Problem statements

Numerous researches of the conductive nanomaterials and conductive polymer inks have been done for the production of printed electronic applications. Among them, metal-based inks such as gold nanoparticles (AuNPs), silver nanoparticles (AgNPs) and copper nanoparticles (CuNPs) have received a great attention due to their excellent electrical conductivity. AuNPs and AgNPs suffer from high cost and require high sintering temperature which limiting their functions to be used with flexible substrates (Cui *et al*., 2010; Nie *et al*., 2012; Kastner *et al*., 2017), making CuNPs a good alternative due to the low cost and high electrical conductivity. However, CuNPs have issues with oxidation under heat and humidity conditions which limits its applications (Kang *et al*., 2010). Meanwhile for conductive polymers, the electrical

conductivity is still considered to be very low as compared to those of metal-based inks (Perinka *et al*., 2013). Due to that, considering the advantages of graphene over other conductive nanoparticles and conductive polymers, graphene-based inks have been widely explored since the past 10 years (Cheng *et al*., 2017; Tran *et al*., 2018), however more effort still need to be considered before they can be used in practical applications. Extensive works to produce good quality graphene-based inks are required. Ink formulation and properties mainly influence the printing quality and it must be optimized in order to achieve patterns without a coffee ring effect and homogeneity of the printed patterns.

Most of the graphene-based inks reported in the literature were prepared by utilizing GNPs and GO as the fillers. Due to the nature of graphene which is hydrophobic, it is very difficult to achieve stable dispersions in various types of common solvents. Addition of surfactant in the conductive ink is required to improve the solubility of the conductive ink, however it reduces the conductivity value. Meanwhile, GO suffer from low electrical conductivity due to the high oxygen-based functional groups content (around 8%). Therefore, reduction process is important to remove the functional groups, however this process involves highly toxic materials which is not environmentally friendly and introduced defects which compromise the conductivity value (Pei and Cheng, 2012). Due to that, alternative graphene-like material which has good electrical properties and quality is preferred to be used in the preparation of conductive ink. Based on the literature studies, reports on utilizing graphene foam (GF) produced by using solvothermal reaction method for conductive ink are very limited. According to Salunkhe *et al*. (2016), Tang *et al*. (2016) and Ma *et al*. (2017), the unique structure of GF which is constructed of three-dimensional (3D) interconnected network with very high surface area to avoid aggregation yet

maintaining the electrical conductivity can be considered to be explored for the fabrication of graphene-based conductive ink.

Coleman (2013) and Nicolosi *et al*. (2013) reported that most of graphene-based inks were produced by using effective solvents such as N-Methyl-2-pyrrolidone (NMP), Dimethylsulfoxide (DMSO) and N,N-Dimethylformamide (DMF) due to the surface tension that is closed to 40 mJm^{-2}. However, these solvents suffer from highly toxic especially for women which may damage fertility or the unborn child (hazard code = H360) (Byrne et al. 2016). In addition, these solvents have high boiling points (>150 °C) which are not suitable to be used with plastic substrates, that require low processing temperature. Alternative solvents with low boiling points, less toxic and high surface tension are preferred in the preparation of good dispersion conductive ink. Acetone, 2-propanol (IPA) and ethanol are some of the common alternative solvents that have low boiling points, however these solvents exhibit low surface tension approximately 23 mJm^{-2}, that lead to poor graphene dispersion (Tran *et al*., 2018). From the literature review, reports on preparing graphene-based ink by using ethylene glycol (EG) and propylene glycol (PG) are limited. These solvents have surface tension close to 40 mJm^{-2} and are less toxic than NMP and DMF solvents, as reported by Byrne et al. (2016), but these solvents suffer from high boiling points. Therefore, it is expected that by mixing these solvents with other common solvents that have low boiling point, could produce graphene-based ink with excellent dispersion stability and physical properties.

Various printing techniques including screen printing, spray coating, 3D printing, inkjet printing, etc have been utilized in the fabrication of conductive ink patterns for various electronic applications (Khan *et al*., 2015). Among these printing

techniques, spray coating and inkjet printing received more attentions due to the simple printing process, high repeatability, economical and save time compared to other printing techniques. However, these printing techniques often suffer from nozzle clogging due to the aggregation of the particles in the conductive inks. Thus, the ink properties such as viscosity, surface tension, contact angle and surface energy should be optimized to meet the specific printing requirements. Hoath (2016) reported that an ideal ink should possess low viscosity and high surface tension in order to flow through the nozzle easily without coagulate or stuck in the nozzle.

1.3 Objectives

The main objective of this research work is to produce graphene-based inks using alternative common solvents for printed electronics. In order to achieve it, the following steps are required:

1. To compare the characteristics of the synthesized graphene foam with commercial graphite nanoplatelets and synthetic graphite.
2. To investigate the ink properties of graphene-based materials mixed with polyester varnish binder and determine the electrical properties of the conductive ink patterns fabricated using spray coating technique.
3. To determine the dispersion stability and physical properties of graphite nanoplatelets and graphene foam dispersed into various types of common solvents and mixed solvents.
4. To identify the stability of graphene-based ink and graphene hybrid-based inks and investigate the electrical properties of the conductive ink patterns fabricated using inkjet printing technique.

1.4 Scope of study

This research has been devoted to produce graphene-based ink by using GF as novel material with surface area of 2000-2300 m^2g^{-1} which has been prepared via solvothermal reaction method. GNPs and synthetic graphite (SG) were also used in the preparation of graphene-based inks for comparison.

Two commonly printing techniques such as spray coating and inkjet printing were utilized in the fabrication of the printed patterns. The graphene-based materials were first mixed with polyester varnish (PV) binder and deposited onto a flexible substrate using a customized motor-controlled air spray coating. Secondly, GF and GNPs fillers were dispersed into various types of alternative less toxic solvents including EG, IPA and PG and also, the mixture of EG and IPA mixed solvents before being printed onto polyethylene terephthalate (PET) substrate via inkjet printing.

The characteristics of the synthesized GF and commercial GNPs and SG were examined by scanning electron microscopy (SEM), high resolution transmission electron microscopy (HRTEM), X-ray diffraction (XRD), Raman spectroscopy, X-ray photoelectron spectroscopy (XPS), Fourier-transform infrared spectroscopy (FTIR), Brunauer-emmett-teller (BET), thermogravimetric analysis (TGA) and electrical conductivity. Meanwhile the dispersion stability and physical properties of the graphene-based inks via visual observation, zeta potential analysis, UV-Vis spectrophotometer, HRTEM, viscosity and wettability were investigated.

1.5 Thesis overview

This thesis consists of five chapters. Chapter 1 (Introduction) discusses the introduction of the overall research by introducing graphene, conductive ink and printing methods for graphene-based inks and printing pattern productions. The

motivations for conducting present study are expressed after identifying current hurdles related to the highly toxic (hazardous) and high boiling point solvent in the production of graphene ink. Based on that, a set of objectives are then outlined. This chapter ends with the description about the scope of study and thesis overview by chapters.

Chapter 2 (Literature Review) gives an overview of the recent progress in conductive inks which include graphene ink, other conductive materials ink and graphene-conductive material hybrid ink, respectively. Besides that, the properties of the conductive inks are also discussed. The printing techniques for the fabrication of flexible electronics and the overview of research work are summarized.

Chapter 3 (Materials and Method) describes the materials and methods used throughout this study. Detailed information on the materials, chemicals, equipment and methodologies to conduct the experimental works are described within this chapter. The characterization techniques are also discussed in this chapter.

Chapter 4 (Results and Discussion) is the heart of this thesis where results and discussion are presented. It is divided into four sections. First section discusses the characterization of the synthesized GF and compare with commercial GNPs and SG. Second section covers the properties of graphene-based inks mixed with PV and conductive ink patterns fabricated using spray coating. Third section explores the stability of graphene-based materials dispersed into various types of alternative common solvents and mixed solvents. Finally, fourth section describes the production of conductive ink patterns using inkjet printing method.

Chapter 5 (Conclusion and Future Recommendations) presents the conclusions from this research and some recommendations for future studies in this related field.

CHAPTER 2

LITERATURE REVIEW

2.1 Conductive ink materials

Conductive ink becomes an important element in printing industry such as screen printing, spray coating, inkjet printing, gravure printing, *etc*. A conductive ink is a thermoplastic viscous paste that conducts electricity by inculcating conductive materials (Banfield, 2013). To be specific, the conductive inks are suspensions of conductive nanomaterials either in water or a solvent medium with or without an addition of a surfactant or polymer that acts as a stabiliser. These solvents must evaporate rapidly after deposition but not dry out quickly at the printhead nozzles while idle for short periods of time. To obtain high electrical conductivity of conductive inks, conductive nanomaterials are normally introduced; the sizes of these materials should be at least 50 times less than the printing nozzle to avoid clogging of the nozzles (Huang and Wu, 2019).

An ideal conductive ink should be inexpensive, simple to prepare, and offer good printability, low viscosity, good stability, good adhesion to the substrate, high electrical conductivity after printing and post-printing processing, and dry in preferentially densify manner at substrate surface without a coffee ring effect (Choi *et al*., 2015; Liu *et al*., 2015; Stoppa and Chiolerio, 2014). Coffee ring was formed on the printing substrate when a drop dries at room temperature, as obvious outflow induces edge growth process and forms ring-like pattern, as illustrated in Figure 2.1 (a). However, as the substrate temperature increases, the transition from a coffee ring to a uniform dried deposit was occurred, as presented in Figure 2.1 (b) (Li *et al*., 2016; He and Derby, 2017).

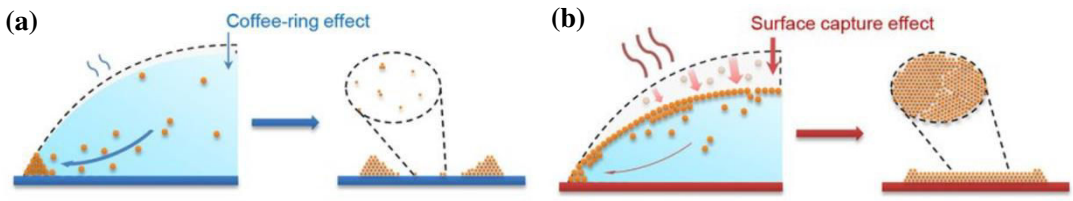

Figure 2.1 Schematic of (a) coffee-ring effect at low drying temperature and (b) surface capture effect at high drying temperature (Li *et al*., 2016)

Various solvents have been widely studied to disperse graphene for conductive ink applications and interfacial tension can be considered as one of the main criteria on graphene dispersion. Higher interfacial tension between solid and liquid often leads to poor stability of the dispersion (Israelachvili, 2011). Coleman (2012) reported that solvents with the surface tension of approximately 40 mNm^{-1} can minimize their interfacial tension with graphene. Hernandez *et al*. (2008) and Khan *et al*. (2011) reported that NMP is considered to be the most widely used solvent for dispersing graphene and the sonication of graphite with N-Methyl-2-pyrrolidone (NMP) can produce stable graphene dispersion at concentration between 0.01 to 2 $mgmL^{-1}$. Majee *et al*. (2016) produced stable graphene ink at high concentration of 3.2 $mgmL^{-1}$ using shear exfoliation of graphite in NMP. Other solvents including Dimethyl sulfoxide (DMSO) and N,N-Dimethylformamide (DMF) have also been established as effective solvents to prepare graphene ink with good dispersion stability (Li *et al*., 2013; Tran *et al*., 2018). However, these solvents suffer from high boiling point (>150°C) which restricted them to be used with plastic substrates, as it requires low treatment temperature. Besides that, these solvents are expensive and highly toxic making them not practical to be widely utilized in the industry.

Due to that, low boiling point and less toxic solvents are preferable. Several

examples of common low boiling point solvents including acetone and ethanol were alternatively used, however, these solvents have low surface tension (<30 mJm^{-2}) that lead to poor graphene dispersion. Table 2.1 describes the chemical properties such as surface tension, boiling point and chemical formula of common solvents used for graphene ink dispersion.

Table 2.1 Chemical properties of common solvents used for graphene ink dispersion (Materials Safety Data Sheet; DataPhysics Instruments GmbH)

Solvent	**Chemical formula**	**Surface tension (mNm^{-1})**	**Boiling point (°C)**
NMP	C_5H_9NO	40.8	202
DMF	C_3H_7NO	37.1	153
DMSO	C_2H_6OS	43.5	189
2-propanol (IPA)	C_3H_8O	23	83
Tetrahydrofuran (THF)	C_4H_8O	26.4	66
1,2-Dichlorobenzene	$C_6H_4Cl_2$	36.6	181
Cyclohexanol	$C_6H_{12}O$	34.4	162
Chlorobenzene	C_6H_5Cl	33.6	131
Toluene	C_7H_8	28.4	111
Acetone	C_3H_6O	27.6	56
Ethanol	C_2H_6O	22.1	78
Water	H_2O	72.8	100

2.1.1 Graphene-based ink

Since its isolation by Novoselov and Geim in 2004, graphene has attracted various investigations into its unique physicochemical, mechanical and electrical properties. Graphene has been considered as "the thinnest, most flexible and strongest material known" that conducts heat and electricity very well (Jaworski *et al*., 2013; Brownson and Banks, 2014). Graphene has unique physicochemical properties with large specific surface area (2630 m^2g^{-1}), high optical transparency (97.7%), extraordinary electron mobility (200 000 $cm^2V^{-1}s^{-1}$) and thermal conductivity (5000 $Wm^{-1}K^{-1}$), extremely high mechanical strength (elastic modulus 0.25 TPa and tensile strength 42 Nm^{-1}) and possibility of mass-production at low cost (Shen *et al*., 2012; Guo and Mei, 2014; Ghany *et al*., 2017). These properties arise from the two-dimensional crystallographic nature of graphene. Table 2.2 describes the definitions of 'graphene-like materials' as proposed by Bianco *et al*. (2013).

Table 2.2 Comparison of graphene-like materials terms (Bianco *et al*., 2013)

Graphene terms	Details
Graphene layer	• A single-atom-thick sheet of hexagonally arranged • sp^2-bonded carbon atoms and known as monolayer graphene
Turbostratic carbon	• 3D sp^2-bonded carbon atoms and known as rotationally faulted • No defined registry of the layers • Prepared at low temperature and resist the development of 3D crystalline order upon very high temperature heat treatment

Table 2.2 *Continued*

Bilayer graphene, trilayer graphene	• 2D (sheet-like) materials • Consists 2 or 3 well-defined, countable and stacked graphene layers of extended lateral dimension
Multi-layer graphene	• 2D (sheet-like) material • Consists of a small number (between 2 to 10) of well defined, countable and stacked graphene layers of extended lateral dimension
Few-layer graphene	• 2D (sheet-like) material • A subset of multi-layer graphene with layer numbers from 2 to 5
Graphite nanoplates, graphite nanosheets, graphite nanoflakes	• 2D graphite materials • Thickness and/or lateral dimension less than 100 nm
Graphene microsheet	• A single-atom-thick sheet of hexagonal arranged • sp^2-bonded carbon atoms that is not an integral part of a carbon material but is freely suspended • Lateral dimension between 100 nm to 100 μm
Graphene oxide (GO)	• Chemically modified graphene prepared by oxidation and exfoliation, followed by extensive oxidative modification of the basal plane • Monolayer material with a high oxygen content
Reduced graphene oxide (rGO)	• GO that has been reductively processed by chemical, thermal, *etc* methods to reduce its oxygen content

To date, several methods for the production of graphene have been explored, and these methods are divided into two categories: (1) bottom-up approach (from carbon precursors) i.e. elaboration on silicon carbide, chemical vapour deposition, solvothermal reaction, *etc*, and (2) top-down approach (from graphite) i.e. micromechanical cleavage, liquid phase exfoliation, chemical reduction of GO and exfoliation of graphite intercalation compounds, *etc*. The various graphene elaboration methods allow a wide choice in terms of size, quality and price depending on the applications. Figure 2.2 depicts the comparison of quality against price (for mass production) for graphene elaboration methods. Most graphene that were used in electronic applications are fully dependent on the quality of the prepared graphene, types of defects, substrate, *etc* which strongly affected by the production method (Novoselov *et al*., 2012). The bottom-up approaches can produce graphene with fewer defects; however, these methods suffer from high complexity, low yield and the high cost of metal substrates. Meanwhile, top-down approaches produce graphene in high yield, use solution-based processability and are easy to implement due to the use of the existing form of a bulk material (Chen *et al*., 2004; Choucair *et al*., 2009; Novoselov *et al*., 2012; Low *et al*., 2013, Speyer *et al*., 2015).

Graphene foam (GF) also known as 3D graphene, is one of the graphene-like materials and can be synthesized using various bottom-up approaches including solvothermal method. As reported by Jiang and Fan (2014) and Liu *et al*. (2014), GF has a unique porous structure, unlike sheet-like structure as seen in 2D graphene-like materials. GF also has a very large specific surface area compared to other common graphene-like materials due to the 3D topography which prevents the restacking generally observed in 2D graphene-like materials. The voids with micron-scale were separated by thin carbon walls, as illustrated in Figure 2.3.

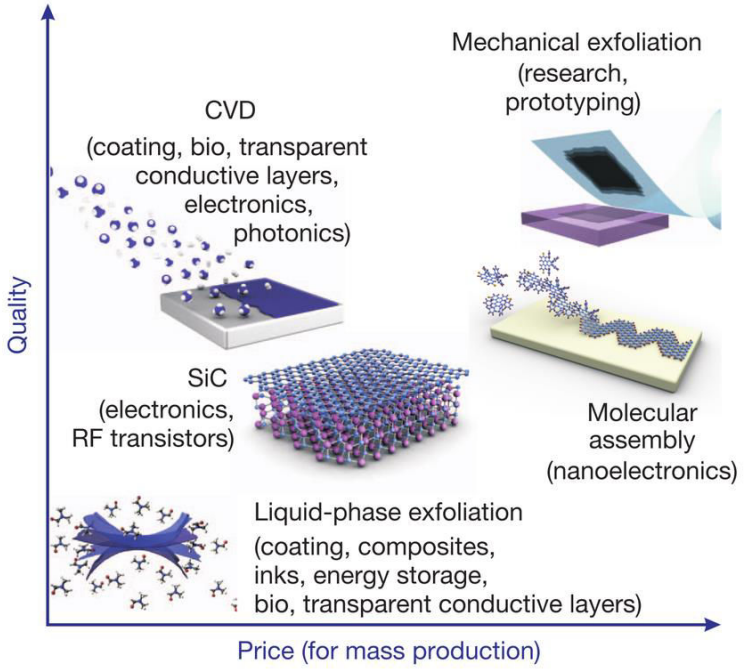

Figure 2.2 Comparison of quality against price (for mass production) for graphene elaboration methods (Novoselov *et al*., 2012)

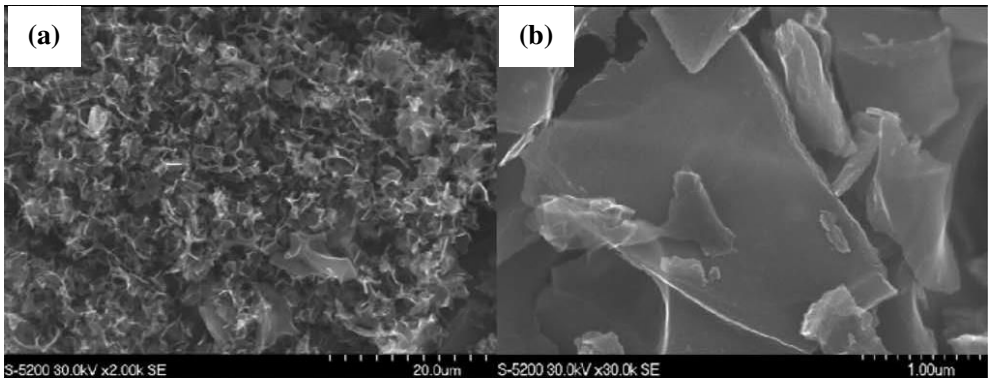

Figure 2.3 SEM images of graphene foam (GF) (Liu *et al*., 2014)

Graphene conductive inks have the potential to revolutionize the printed conductor field by replacing metallic inks, conductive polymer inks and other carbon material inks, while at the same time reducing biological hazards and production costs (Arapov *et al*., 2014). Huang *et al*. (2011) reported that a series of inkjet printing processes using water-soluble single-layered GO (SGO) and few-layered GO (FGO)

have been printed on diverse flexible substrates. Based on these findings, the electrical conductivity of GO and FGO after 25 printed layers on a polyimide (PI) substrate are 5.0×10^2 Sm^{-1} and 9.0×10^2 Sm^{-1}, respectively. According to Huang *et al*. (2011), the low conductivity of GO printed on PI substrate compared to FGO could be attributed to the high number of oxygen-containing groups in the GO sample (Figure 2.4).

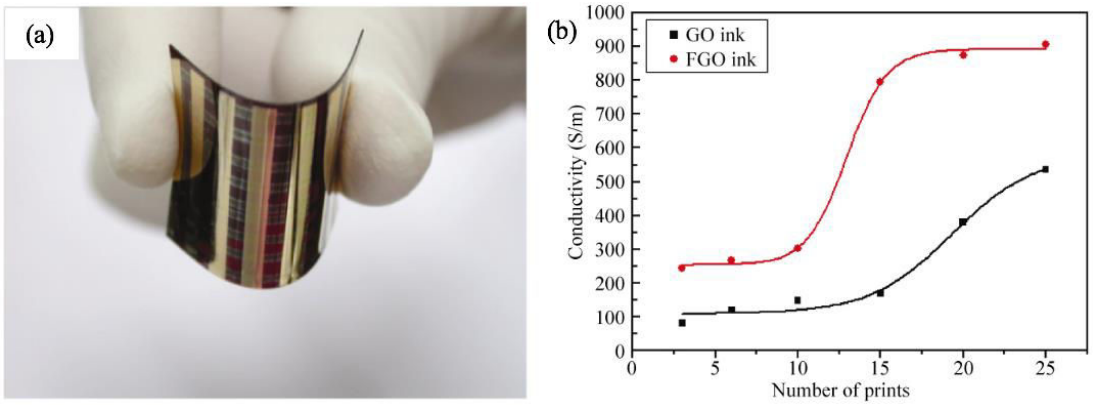

Figure 2.4 (a) Photograph of a printed pattern on PI substrate and (b) the electrical conductivity of the printed patterns on PI (Huang *et al*., 2011)

Arapov *et al*. (2014) presented a comparison of two graphene inks: one prepared by the solubilisation of expanded graphite in the presence of a surface-active polymer and the other by covalent graphene functionalisation followed by redispersion in a solvent but without surfactant. Based on their findings, the conductivity levels for expanded graphite-based inks and functionalised graphene are approximately 1–2 $k\Omega sq^{-1}$ and 2 $M\Omega sq^{-1}$, respectively, for 15 printed layers. This technique is simple and efficient, and therefore has a potential to be used for large-area printing of conductive films. Meanwhile, Gao *et al*. (2014) fabricated highly conductive pristine graphene electrodes by inkjet printing using ethyl cellulose-stabilised ink prepared from pristine graphene. No graphene sheets were observed to settle at the bottom of the bottle even

after 9 months. This stability is reported to be due to the strong hydrophobic interactions between ethyl cellulose (as the stabilising polymer) and the graphene sheets countering the van der Waals forces between the graphene flakes, thereby inhibiting the aggregation of the graphene. The printed films have high conductivity with the value of 9.24×10^3 Sm^{-1} after 30 printed layers annealed at 300 °C for 30 min.

In 2016, Miao *et al*. reported a simple method of inkjet printing of graphene nanoplatelets (GNPs) using an electrochemical process in an inorganic-salt-based electrolyte without using stabiliser. The electrical conductivity of printed pristine GNPs film improved from 44 Sm^{-1} to approximately 2.5×10^3 Sm^{-1} after 20 printed layers after a simple thermal treatment of annealing at 300 °C for 1 h (Figure 2.5). Meanwhile, Majee *et al*. (2017) reported an efficient inkjet printing of water-based pristine GNPs ink by a shear-exfoliation process with the aid of bromine intercalation in aqueous media using a water-soluble cellulose stabiliser, i.e. (hydroxypropyl)methyl cellulose. The electrical conductivity was 1.4×10^3 Sm^{-1} when the printed GNPs film was dried at 100 °C and increased to about 3×10^4 Sm^{-1} after an additional treatment of dipping the film in an aqueous iodine solution prior to drying. In contrast, a conductivity of about 2.4×10^4 Sm^{-1} was obtained after annealing the film at elevated temperature in air. The electrical conductivity of the doped GNPs films improved further to 10^5 Sm^{-1} after annealing in air at 300 °C. This shows a positive effect of the combination of iodine doping and thermal annealing on conductivity enhancement for printed GNPs films. In 2017, Secor *et al*. demonstrated graphene inks with nitrocellulose as a synergistic polymer stabiliser. The printed graphene films on glass had electrical conductivity values of 1.0×10^4 Sm^{-1} and 4.1×10^4 Sm^{-1} when annealed at 200 °C and 350 °C, respectively.

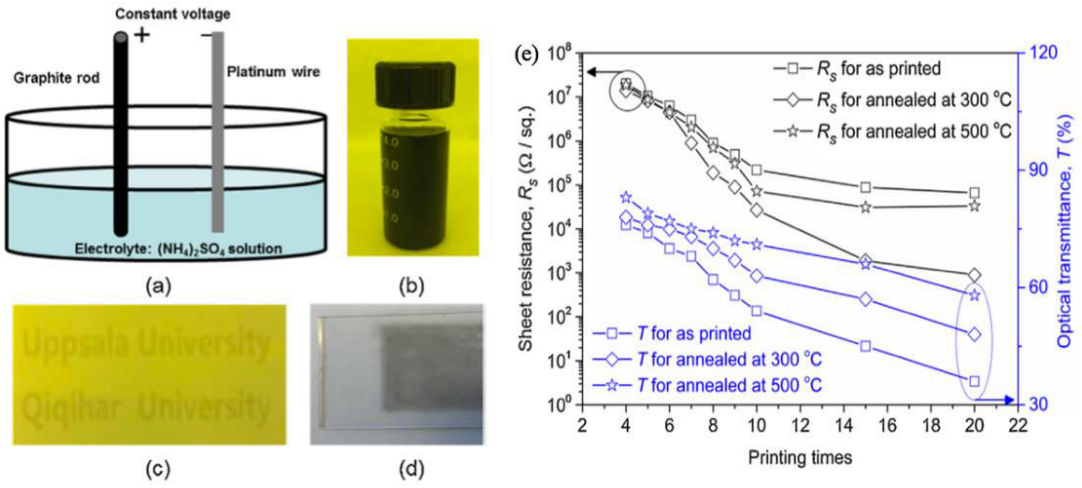

Figure 2.5 (a) Schematic experimental setup for the electrochemical exfoliation process, photo pictures of (b) electrochemical-GNPs ink ready for inkjet printing, (c) printed patterns on a plastic substrate and (d) printed test sample on a glass substrate, and (e) variations of sheet resistance and optical transmittance with number of prints at different annealing temperatures (Miao *et al.*, 2016)

Table 2.3 presents the comparison of graphene-based inks and electrical properties based on the literature. It is observed that graphene inks based on various types of graphene-like materials have been successfully synthesized using sonication as mixing method and inkjet printing as a fabrication method. Based on Table 2.3, most of the graphene-based inks were prepared using GNPs, GO and rGO as the fillers. From the findings, it can be observed that types of solvent, number of printed layers, annealing temperature and type of substrate influenced the electrical properties of the printed films. However, higher annealing temperature (100 – 350 °C) and longer annealing duration (> 30 min) of printed graphene films restricted the used of polymer substrate for the fabrication of flexible printed electronics.

Table 2.3 Comparison of the various types of graphene inks and electrical conductivity from literature (Huang *et al*., 2011; Secor *et al*., 2013; Gao *et al*., 2014, Secor *et al*., 2015; Miao *et al*., 2016, Majee *et al*., 2017; Secor *et al*., 2017)

Graphene material	**Solvent and surfactant**	**Substrate**	**Printing layers**	**Electrical conductivity (Sm^{-1})**
SGO and FGO	Deionized water	Polyimide (PI) and PET	25	5.5 X 10^2 (SGO) and 9.0 X 10^2 (FGO)
Graphene and ethyl cellulose	Cyclohexanone and terpineol	Si/SiO_2 wafers	10	2.5 X 10^4
Pristine graphene flakes	Ethyl cellulose and cyclohexanone	Hexamethyldisilazane-treated glass slides	30	9.24 X 10^3
Graphene and ethyl cellulose	Cyclohexanone and terpineol	Poly(ethylene naphthalate) (PEN)	(not mentioned)	2.5 X 10^4
Electrochemical GNPs	DMF, EG and glycerol	Plastic and glass	20	2.5 x 10^3
GNPs	Water soluble cellulose	Glass and PET	20	10^5
Graphene and nitrocellulose	Ethyl lactate, octyl acetate, ethylene glycol diacetate	Glass	(not mentioned)	1.0 X 10^4 (200 °C) and 4.1 X 10^4 (350 °C)

2.1.2 Other conductive materials-based ink

2.1.2(a) Ink based on conductive nanomaterials

Other than graphene, several types of commonly used conductive materials are also reported in the literature. Silver nanoparticles (AgNPs) are another promising nanomaterial for flexible electronics. Until now, AgNPs-based inks have represented the most important commercial nanotechnology-derived product and the one most widely studied worldwide, other than graphene (Rajan *et al*., 2016). Kastner *et al*. (2017) investigated and optimised the printing of a reactive silver ink made of silver acetate dissolved in aqueous ammonium hydroxide. Based on the findings, the conductivity value of the printed film on glass was 4.42×10^6 Sm^{-1} after annealing at 120 °C for several minutes, with the pattern thickness ranging from 150 to 133 nm. For printed silver films on acrylate-based coatings, the conductivity value was 2.9×10^5 Sm^{-1} with a pattern thickness of 150 nm.

Besides that, gold nanoparticles (AuNPs) are known as the most stable metal nanoparticles and have been used in printing highly conductive elements. The unique properties of AuNPs make them useful in various applications, such as colourants, metal coatings, electronics, optics and chemical catalysis (Iwakoshi *et al*., 2005). Despite the excellent electrical conductivity and excellent printability of AgNPs and AuNPs, various work still needs to be done considering the high cost and high sintering temperature (>200 °C) and long sintering required, which make them inadvisable for use on a large scale, especially in industrial applications and not compatible for flexible polymer substrates such as PEN and PET due to their low glass-transition temperatures (Kamyshny *et al*., 2005; Kim *et. al*., 2014).

Copper nanoparticles (CuNPs) are a good alternative for gold and silver nanoparticles due to their high electrical conductivity and low price (Tsai *et al*., 2015). However, the main problem of CuNPs is that they are easily oxidised under heat and humidity conditions, which limits their applications. It is also difficult to produce homogeneous nanoparticles and ensure good dispersion within the ink, as the material is not stable in most common solvents (i.e. water, isopropyl alcohol, acetone, *etc*) which causes sedimentation (Lee *et al*., 2008).

Carbon nanotubes (CNTs) have drawn considerable attention over other nanomaterials by being electrically heterogeneous (either metallic or semiconducting) in nature. This make them attractive for numerous applications in electronics (Denneulin *et al*., 2011). However, the stability of CNTs suspensions in water is still a topic of interest because the nanoparticles tend to aggregate easily due to their high van der Waals forces of attraction; moreover, there are toxicological issues. Besides that, CNTs require selective growth, functionalisation and sorting processes for separation in order to exploit in full their electronic properties (Sabba and Thomas, 2004; Kernan and Blau, 2008).

2.1.2(b) Ink based on conductive polymers

Several conductive polymers have been intensively investigated, considering their low cost and that no sintering process is required; in particular, polyaniline (PANI), polypyrrole (PPy), poly(3,4-ethylenedioxythiophene)-poly(styrenesulfonate) (PEDOT:PSS), *etc*. PANI has been considered as one of the most promising conducting polymers due to its unique properties, including high electrical conductivity for a polymer material, excellent environmental stability and partial solubility in various solvents. It is the most versatile polymer due to its simplicity, low cost of preparation,

thermal and chemical stability and processability (Kulkarni *et al*., 2013; Song *et al*., 2015; Stempien *et al*., 2015).

PPy is also a conducting polymer of moderate environmental stability and suitable for multifunctional applications. The electrical and physical properties of the polymeric films are fully dependant on the preparation conditions, such as the electrochemical method of polymerisation, concentration of monomer and doping agent and other synthesis conditions. The polymer is not conducting in its neutral state and only becomes conducting when it is oxidised. The conductivity value is in the range of 10^{-3} to 10^{2} Ωcm^{-1} (Schlenoff and Xu, 1992; Abdulla and Abbo, 2012; Popli and Patel, 2015).

PEDOT:PSS is a polymer mixture of poly(3,4-ethylenedioxythiophene (PEDOT) and polystyrene sulfonate (PSS). PEDOT:PSS is also regarded as one of the most technologically promising electrically conductive polymers, due to its water dispersibility, good electrical conductivity and excellent processability (Hong and Kanicki, 2004; Ha *et al*., 2015; Sharbati, 2016). The electrical conductivity of pristine PEDOT:PSS dispersion is less than 10 Scm^{-1} and can be improved by post-treatment with some compounds such as ethylene glycol (Groenendaal *et al*., 2000; Kim *et al*., 2011; Abroshan *et al*., 2011).

Table 2.4 represents the brief comparison between existing inks made of several types of conductive polymers with conductive nanomaterials.

Table 2.4 Comparison of several types of conductive materials-based inks (Kordás *et al*., 2006; Lee *et al*., 2008; Kang *et al*., 2010; Cui *et al*., 2010; Nie *et al*., 2012; Perinka *et al*., 2013; Zhang *et al*., 2015; Kastner *et al*., 2017)

Ink material	**Sintering temperature (°C)**	**Resistivity (Ωcm)/ Surface resistance (Ωsq^{-1})/ Conductivity (Scm^{-1})**
AuNPs	(not mentioned)	0.8 X 10^5 Scm^{-1}
AgNPs	150	17 μΩcm
	230	3.1 μΩcm
AgNPs	30	31.6-26.5 μΩcm
AgNPs	120	4.42 X 10^6 Sm^{-1}
CuNPs	200	3.6 μΩcm
CuNPs	200	36.7 nΩm
PEDOT:PSS	(not mentioned)	1.1 $mScm^{-1}$
MWCNT	(not mentioned)	40 $k\Omega sq^{-1}$
MWCNT-COOH	(not mentioned)	1.1 X 10^6 Ωsq^{-1}
MWCNT-COOH-PSS	(not mentioned)	3.5 X 10^3 Ωsq^{-1}

2.1.3 Graphene hybrid-based ink

Recently, researches on graphene hybrid inks by adding metallic nanoparticles or conductive polymers to improve the original properties of graphene have been widely developed. Based on the comparison of literature review on graphene hybrid-based inks

reported since 2014, the values of electrical conductivity of some graphene hybrid-based inks is still considered very low for some flexible electronic applications. The values of electrical conductivity reported are in the range of 0.29 to 2.0 X 10^3 Scm^{-1}. The annealing temperatures used by the researchers are in the range of 100 – 245 °C. Several hybrid inks that been used by previous researchers are GNP/PANI, Ag/rGO, Ag@Au NTPs-GO, rGO/carbon black and PEDOT:rGO/AuNPs (Xu *et al*., 2014; Zhang *et al*., 2016; Li *et al*., 2017).

Xu e*t al*. (2014) formulated graphene nanoplatelets/polyaniline (GNP/PANI) inks for the fabrication of GNP/PANI thin-film electrodes. GNP/PANI thin film is then printed on the quartz substrate and the values of conductivity for GNP and GNP/PANI thin film are 3.67 Scm^{-1} (5 prints, thickness ~ 41 μm) and 0.29 Scm^{-1} (5 prints, thickness ~28 μm), while the pure PANI conductivity is only 10^{-9} S/cm (Li *et al*., 2009). Zhang *et al*. (2016) reported that well dispersed of Ag/rGO composite was obtained by anchoring AgNPs on the surface of rGO sheet, which served as one of promising conductive ink fillers for printable flexible electronics. An optimum conductivity of 2.0 X 10^3 Sm^{-1} with a baking process at 100 °C was observed. This simple and cost-effective method is applicable for the future application in printed flexible electronics (Figure 2.6). Li *et al*. (2017) synthesized the Ag@Au nanotriangle platelets and graphene oxide hybrid (Ag@Au NTPs-GO) nanomaterial ink. The patterns show no undesirable coffee ring effects and the inkjet-printed rGO-based lines with ~ 7 μm width and a film with high transparency ~98% are achieved. The value of sheet resistance is 146.8 Ωsq^{-1} after preparation and slightly increased to 149.5 Ωsq^{-1} after 100 days. This method is applicable for highly stable integrated circuit boards and highly transparent devices.

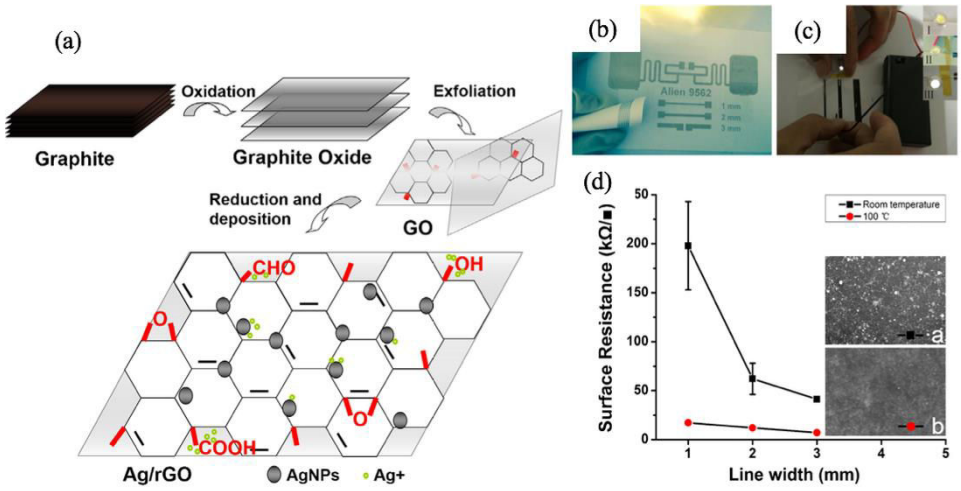

Figure 2.6 (a) The route to synthesize Ag/rGO composite by reducing both the Ag and GO, (b) different patterns obtained by inkjet printing on office paper, (c) conductive tracks in different width on PET for circuit test and (d) surface resistance and the surface morphology of the printed conductive tracks (Zhang *et al.*, 2016)

2.2 Conductive ink properties

There are many printing techniques to deposit the conductive ink onto substrates for example flexography printing, inkjet printing, gravure printing, and screen printing. Basically, characteristics of good conductive ink are good stability, good printability, good adhesion with the substrates, high resolution, minimum printer maintenance and long shelf life. However, ink stability and properties of conductive inks such as density, viscosity, surface tension, elasticity, velocity, droplet size, and impact of droplet on dry surface are affected to the droplet jetting during printing and consequently final properties of printed conductive patterns. Among these characteristics, ink stability, viscosity and surface tension dominate the behavior of conductive ink during printing and quality of printed conductive patterns especially for inkjet printing (Gao *et al.*, 2014). A printable conductive ink requires a stable dispersion, low viscosity and high

surface tension in order to flow through the nozzle easily without leak, dry out, break away or coagulate within the nozzle.

2.2.1 Viscosity

Viscosity, η is a fundamental characteristic of all fluids and one of the critical properties of printing inks. It is affected by numerous parameters, e.g. temperature and pressure. The viscosity value decreases when the temperature increases (Viswanath *et al*., 2007; Hoath, 2016). Inkjet printing requires low viscosity of conductive ink compared to other printing methods because conductive ink with high viscosity will clog the nozzle (Stoppa and Chiolerio, 2014). The results indicate that rheological behaviour and dispersion state of conductive inks used in inkjet printing significantly affects conductive inks printability and the quality of a produced pattern, and so it should be carefully controlled (Dybowska-Sarapuk *et al*., 2018).

According to Cummins and Desmulliez (2012) and Ihalainen *et al*. (2015), the viscosity of an ideal conductive ink for inkjet printing should be in the range 1 to 25 mPas to avoid problems during printing process including nozzle clogging, satellite or double droplet. If the conductive ink is highly viscous, the jetting frequency will be reduced as the rate of reservoir filling is decreased. Meanwhile for conductive ink that is too less viscous, high frequency jetting might cause unstable droplet ejection.

Figure 2.7 illustrates the rheological behavior of graphene ink at various temperatures (Dybowska-Sarapuk *et al*., 2018). The viscosity of the conductive ink is considered to be stable at high shear rate and then started to decrease with an increasing of shear rate, exhibiting common behavior of fluid which is called shear-thinning or pseudoplastic. Besides that, it can also be observed from Figure 2.7 that the viscosity values decreased with an increasing of temperature. The viscosity of graphene ink at

room temperature is approximately between 7.5 to 10 mPas which can be considered as acceptable for inkjet printing process. According to Shaw (1996) and Woo *et al*. (2013), the viscosity is higher at low shear rate due to the attraction between the particles that creates flocculation in the inks, therefore causes an immobility of the solvent suspending the particles. In contrast, the viscosity at higher shear rate is lower as the flocculation breaks down and aids the mobility of solvent entrapped between particles.

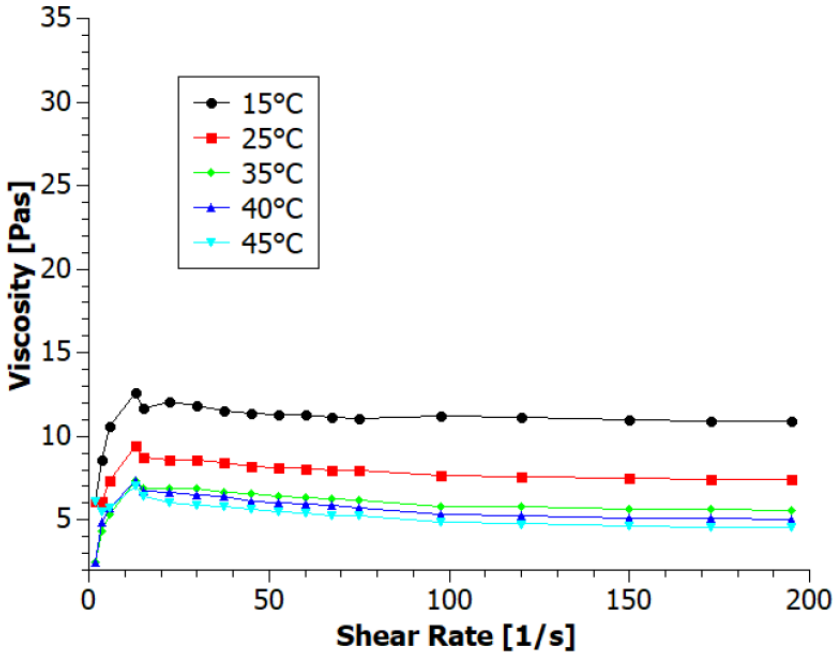

Figure 2.7 Viscosity curves of graphene ink with dispersing agent at various temperatures (Dybowska-Sarapuk *et al*., 2018)

2.2.2 Surface tension

According to the cohesive intermolecular forces in the liquid, there is an asymmetric attractive force on the molecules at interface between liquid and air, which gives rise to the tension at the surface as displayed in Figure 2.8 (a). Surface tension is highly dependent on temperature, most decrease slightly with increasing temperature.

Adhesive force and attractive force between unlike molecules enable the liquid to adhere onto surface of materials. In deposition of ink droplets onto surface of substrates, the shape of droplets after deposition depends on the relative strengths of these forces of molecules. Surface tension of liquid causes the force to act in plane of free surface perpendicularly on the surface, which can be measured in term of surface energy.

Surface tension and surface energy are comparable properties. Both are a quantification of how unfavorable the interface is, in which surface tension is referring to liquid-gas interface (γ_{LG}) and surface energy is referring to solid-gas interface (γ_{SG}). The surface tension of the liquid does not change, but rather the surface energy of the solid is stronger than liquid's surface tension and overpowers it, causing the liquid to spread over the solid surface. The main difference between surface tension and surface energy is that surface tension measures the force per unit length of the surface (Nm^{-1}) while surface energy measures the amount of work that needs to be done per unit area in order to stretch it (Jm^{-2}).

An ideal situation of droplet spreading onto substrate surface is obtained only for one equilibrium contact angle is obtained as shown in Figure 2.8 (b). The surface energy relation between liquid, solid and gas interfaces can be expressed by Young's equation $\gamma_S = \gamma_{SL} + \gamma_L \cos\theta$, in which γ_L is the surface energy of the liquid, γ_{SL} is the surface energy between solid to liquid interface, and γ_S is the surface energy of the solid (Michel *et al.*, 2016). At high γ_{SL}, the adhesive force dominate and ink droplet will be pulled towards the surface, known as wet characteristics or hydrophilicity. In contrast, at low γ_{SL}, adhesive force is negligible and ink droplet will tend to bead up on the surface, known as hydrophobicity. This means the ink droplet has cohesion force into

droplet more than the adhesive force between droplet and surface of substrate. The behavior of an ink droplet on surfaces is illustrated in Figure 2.8 (c, d). In practice, there are two relatively reproducible angles in the largest and smallest contact angles where the difference between these two angles is often called contact angle hysteresis. Figure 2.9 indicates the different wetting behaviors of droplet spreading on substrate surface (Hoath, 2016).

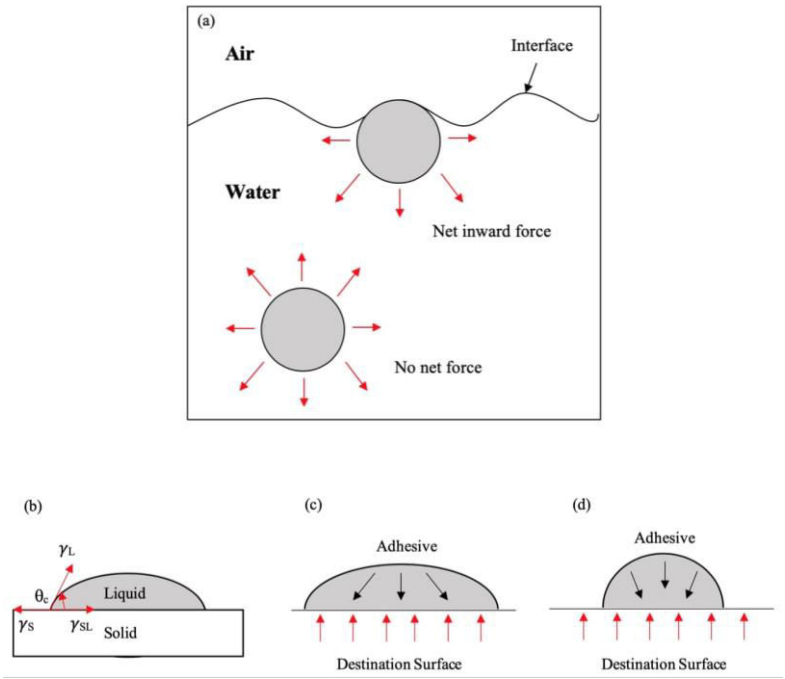

Figure 2.8 Schematic of (a) surface tension from intermolecular forces, (b) droplet onto substrate surface with an ideal contact angle (θ_c), and comparison of droplet shapes with (c) high surface energy and (d) low surface energy on the substrates

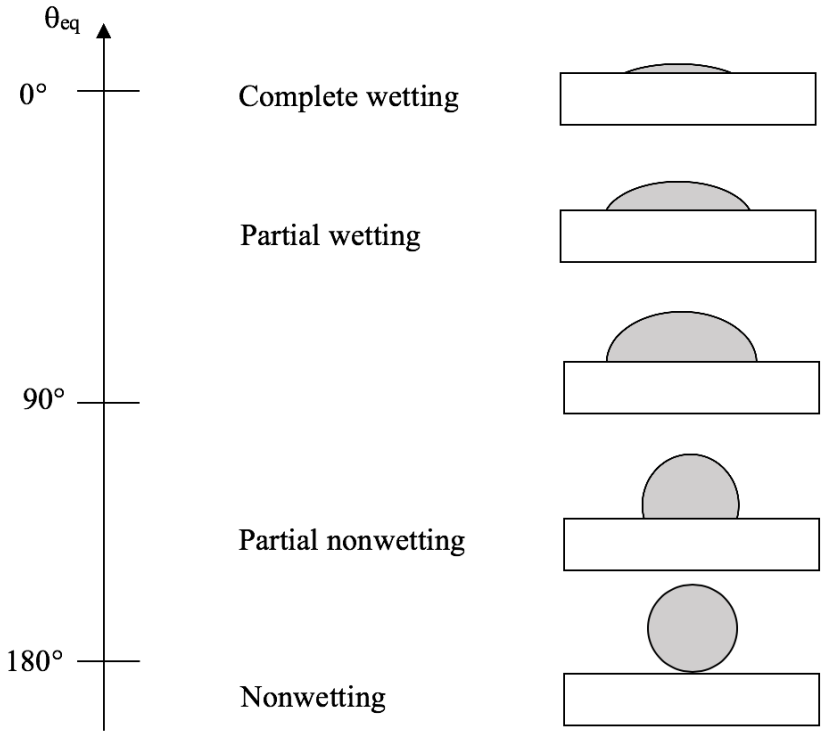

Figure 2.9 Schematic of wetting behaviors of a droplet onto substrate surface at different contact angles (θ_{eq})

The recommended values of surface tension for conductive ink used in inkjet printing should be within the range of 25-50 mNm^{-1} in order to generate stream of droplets (Cummins and Desmulliez, 2012). Li *et al*. (2018) reported that the surface tension of GO dispersion increased slowly when the concentration of GO increased, as in Figure 2.10. The concentration of GO should be as high as possible in a certain range to ensure the printed circles has enough thickness to lead to a good electrical conductivity. However, the surface tension of GO dispersion was too high to print (>70 mNm^{-1}). Thus, surfactants (e.g. SDS and TX-100) were introduced in the GO dispersion as these compounds could lower the surface tension between two liquids or between a liquid and a solid efficiently. The surface tension of GO/SDS hybrid dispersion

decreased with an increasing of dispersion concentration. Noted that the amount of surfactants should be as little as possible.

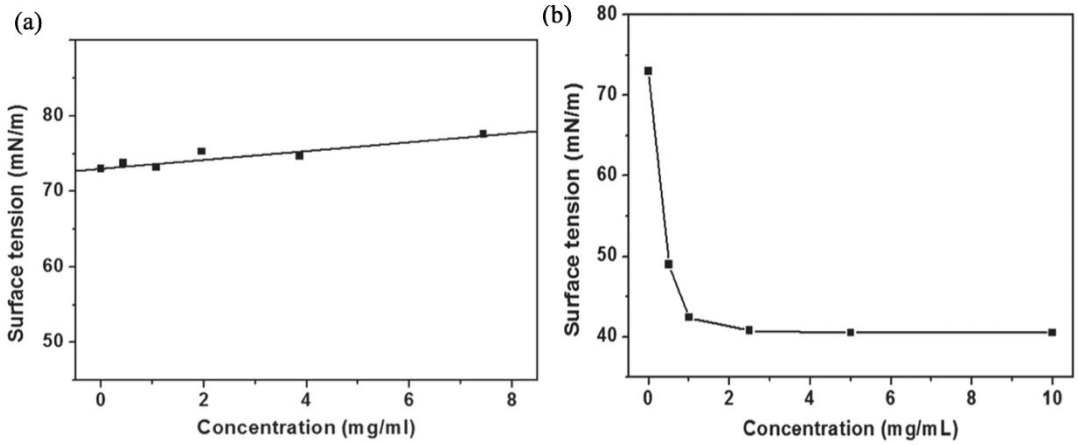

Figure 2.10 Plot of surface tension (20 °C) of (a) GO dispersion and (b) GO/SDS hybrid dispersion varied with dispersion concentration (Li *et al*., 2018)

Table 2.5 presents the comparison of viscosity and surface tension of various types of conductive inks from literature.

Table 2.5 Comparison of viscosity and surface tension of various types of conductive inks from literature (Wu *et al*., 2009; Jeong *et al*., 2011; Denneulin *et al*., 2011; Vaseem *et al*., 2012; Öhlund *et al*., 2012; Capasso *et al*., 2015; Deng *et al*., 2017)

Ink Material	**Solvents**	**Viscosity (cP)**	**Surface tension (mNm^{-1})**
AgNPs	Deionized water	1.66-5.09	-
AgNPs	Water	5.47	40.799
AgNPs	Water	4.5	41
AgNPs	Triethylene glycol monoethyl ester	12.9	37.3

Table 2.5 *Continued*

CuNPs	Deionized water	4.8-5.3	37.3 - 41.2
Graphene and AgNPs	Cyclohexanone/ terpineol	16-18	30
Carboxylic acid-functionalized SWCNT	PEDOT:PSS	6	28
Exfoliated graphene	N-Methyl-2-pyrrolidone (NMP)	3.14	(Not mentioned)
Exfoliated graphene	Ethanol/water	2.47	30.9

2.2.3 Solubility parameters

Other than viscosity and surface tension which dominate the behavior of conductive ink during printing, it is also important to understand the miscibility of liquid-liquid mixtures or the solubility of solids in liquids (Hughes *et al*., 2013). Hilderbrand and Hansen solubility parameters are commonly used to investigate suitable solvents for the dispersion of graphene and other solutes.

Successful solvents are governed by two criteria; (1) for nonpolar solutes, the Hilderbrand solubility parameters (δ_T) of solvent and solute must be very close to each other and (2) for polar solutes, good solvents are those where solvent and solute have similar values of all three Hansen solubility parameters (δ_D, δ_P and δ_H are the dispersion forces, polar forces and hydrogen-bonding forces) (Barton, 1983; Hansen, 2007). Hernandez *et al*. (2010) reported the dispersibility of graphene in 40 solvents and shown that good solvents for graphene were characterized by a Hilderbrand solubility parameter of δ_T ~ 23 $MPa^{1/2}$ and Hansen solubility parameters of δ_D ~ 18 $MPa^{1/2}$, δ_P ~ 9.3 $MPa^{1/2}$ and δ_H ~ 7.7 $MPa^{1/2}$.

2.3 Conductive ink stability

The stability of the conductive ink can be characterized using various techniques including ultraviolet-visible spectrophotometer and zeta potential analysis to further understand the behavior of the conductive ink. The details of these techniques are described in the following subsection.

2.3.1 Ultraviolet-visible spectrophotometer

Ultraviolet-visible (UV-Vis) spectrophotometer is one of the most popular analytical techniques because it is very versatile and able to examine the behavior of the sample. The spectrophotometers send the UV-Vis light through a sample and then the intensity of the beam is measured to identify the absorbance. Besides that, the concentration of the sample (in liquid or solid form) can be measured too (Johnson *et al*., 2015).

As reported by Johra *et al*. (2014), the absorption peak at 235 nm for GO sample in Figure 2.11 corresponds to π–π* transitions of the remaining sp^2 C=C bonds. The spectrum is further shifted to longer wavelength around 265 nm after reduction of GO to graphene. The reduction of GO to graphene increased the π–conjugation which reduces the required energy for the transition that corresponds to the observed shift of the absorption to the longer wavelength region. Meanwhile, the absorption peak at 265 nm for graphene corresponds to sp^2 C=C bonds (Zhou *et al*., 2009). GO has higher intensity peak than graphene due to higher degree of oxidation. The higher degree in oxidation of GO is attributed to the effect of concentration of the oxidizing agent, *i.e.* potassium permanganate which increased the oxidation level (Peng *et al*., 2013; Emiru and Ayele, 2017).

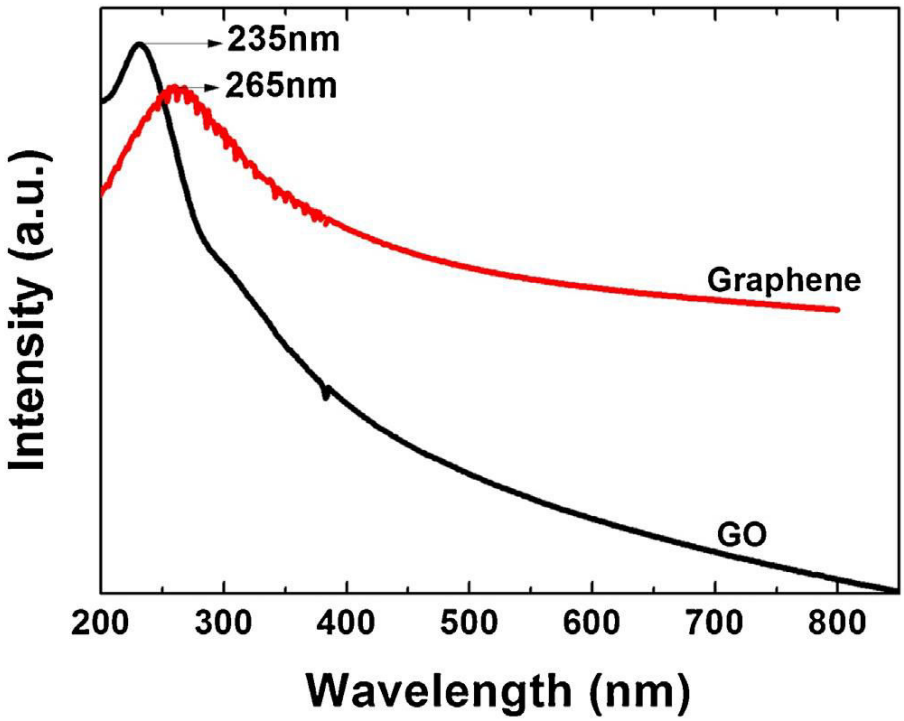

Figure 2.11 UV spectra of graphene and GO (Johra *et al*., 2014)

According to Hernandez *et al*. (2008), the concentration of graphene dispersion can be measured at 660 nm using the Beer-Lambert law (Equation 2.1) even though the UV-vis spectrum of graphene appears flat and featureless in the visible-IR region but the optical density is dependent on concentration. The conductive ink is considered to be stable when there is no change in concentration over certain period of time or no sedimentation is observed.

$$A = \alpha C l \qquad 2.1$$

where; absorbance- A, concentration- C, cell length- l and absorption coefficient, α = 2460 $mLmg^{-1}m^{-1}$ (Lotya *et al*., 2009; Lotya *et al*., 2010; Khan *et al*., 2010; Torrisi and Carey, 2018).

2.3.2 Zeta potential analysis

According to Johnson *et al*. (2015), a charge may be developed at the interface creating a potential when the material is immersed in a solvent. The model can be presented as an electric double layer with three distinct regions known as Stern layer (a closely bound layer of oppositely charged ions), a diffuse layer and the bulk solvent. The zeta, ζ potential is defined as the potential at the shear plane within the diffuse layer, in which all components move as a single kinetic unit with the particle, as illustrated in Figure 2.12.

Graphene can be positively or negatively charged when it was dispersed in an organic solvent and the used solvents covered a wide range of electron-donor properties (Liu *et al*., 2012). Graphene in water is typically negatively charged (Liu *et al*., 2012; Konkena and Vasudevan, 2012). Negatively charged graphene is attributed to the Lewis acid-base interaction, which was originally defined by Lewis (Lewis, 1923). As reported by Gutmann (1978), the Lewis concept can be quantified through the donor and acceptor number. The charging was negatively charged in solvents with higher donor numbers and positively charged in lower donor numbers. Liu *et al*. (2012) reported zeta potentials of graphene dispersed in water and various organic solvents with respect to donor and acceptor numbers, as shown in Figure 2.13. The surface charge of graphene in water and various solvents were negative due to higher donor numbers than acceptor numbers.

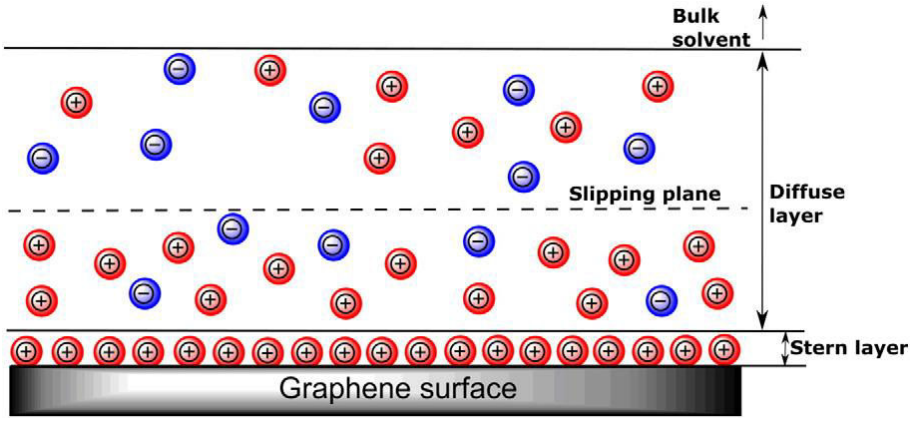

Figure 2.12 Schematic of the ζ potential double layer model for a negatively charged graphene sheet (Johnson *et al*., 2015)

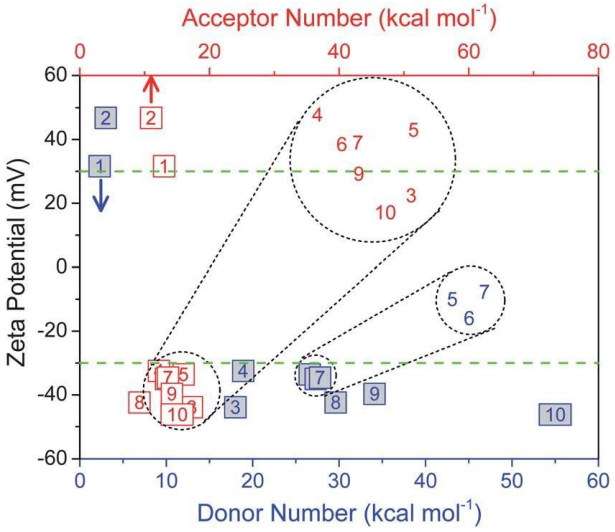

Figure 2.13 Zeta potentials of graphene dispersions against donor number (blue, shaded square) and acceptor numbers (red, open square)

ζ-potential is often correlated to the dispersion stability which is affected by several factors including temperature, solvent, ionic strength and pH (Hunter, 1981). The dispersion is considered to be stable at higher magnitude of ζ-potential |>30 mV|. According to Schramm (2005), the dispersion shows good stability when the ζ-potential is more than 30 mV or less than -30 mV. The |ζ>30 mV| is an optimum for good

stabilization of nano dispersion (Freitas and Müller, 1998). Highly charged particles prevent the particles from aggregation due to electric repulsion. The dispersion is considered unstable when ζ-potential |<30 mV| as the attraction overcome repulsion and will cause the mixtures to foam coagulate and aggregate (Müller *et al*., 1994). Liu *et al*. (2012) reported that the ζ-potential of exfoliated graphite in several organic solvents including NMP, DMF, *etc* exhibited $|\zeta| \geq 30$ mV showing good stability.

2.4 Flexible electronics

Flexible electronics often called as flex circuits have created a vibrant market over the past few years. Several factors have contributed towards the increment of flexible electronics, including more ruggedness, bendable, lightweight, portable and less cost, with respect to production as compared to rigid substrate electronics. In order to make the structure flexible, all the components must bend up to some degree without losing their function.

Figure 2.14 shows several images of recent developments in the field of flexible electronics including (a) stretchable strain sensor for patients to monitor their health at home and (b) flexible circuit film displayed by research group in Penn State's University Park Campus (Penn State, 2013; Diabetes Queensland, 2017). Two basic approaches have been widely used to fabricate flexible electronics (Cheng and Wagner, 2009); (1) transfer and bonding of completed circuits to a flexible substrate and (2) fabrication of the circuits directly on the flexible substrate.

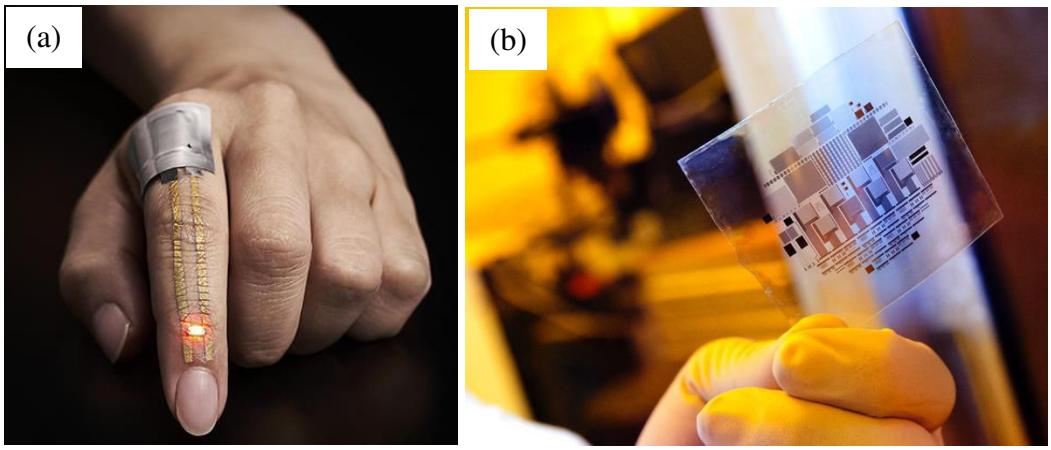

Figure 2.14 Recent developments in the field of flexible electronics; (a) stretchable strain sensor, (b) flexible circuit film (Penn State, 2013; Diabetes Queensland, 2017)

2.4.1 Methods to fabricate flexible electronics

Two main approaches involve in fabrication of flexible electronics; (1) contact printing and (2) non-contact printing. In contact printing, the patterned structures with inked surfaces acquired physical contact with the substrate. Several examples of contact printing technologies are flexography, gravure, soft-lithography and roll-to-roll (R2R) printing. Meanwhile for non-contact printing, the solution is dispensed through openings or nozzles and structures are defined by moving the stage (substrate holder) in a pre-programmed pattern. It involves screen printing, aerosol-jet, 3D printing, spray coating, inkjet printing (Khan *et al*., 2015).

Among these two techniques, non-contact printing technologies receive more attentions due to its simplicity, affordability, speed, adaptability to the fabrication process, reduced material wastage, high resolution of patterns and easy control by adjusting few parameters. In this section, screen printing, spray coating and inkjet printing technologies will be explained in detail.

2.4.1(a) Screen printing

Screen printing is widely used in electronics production due to its ability to produce thin and thick layer from various paste-like materials including conductive ink. Screen printing is a non-contact printing technique where the ink is placed upon a screen mesh and it is pushed by moving a rubber squeegee across the mesh screen. The screen is a negative of the required image and the results of this process, which is the pattern on the substrate can be obtained below the screen mesh. The inks used for screen printing method are comprised of a powdered metallic or non-metallic conductor, a binding agent and a solvent (Gonzalez-Macia *et al*., 2010). Figure 2.15 shows the principle operation of the screen printing process. Two different types of screen printing; (1) flat bed, in which the ink poured on the mesh screen is squeegeed to swipe over the screen resulting in the transfer through the stencil openings to the substrate beneath it and (2) rotary screen printing, same principle as in flat bed but in this case the web of the screen is folded while the squeegee and ink are placed inside the tube (Khan *et al*., 2015).

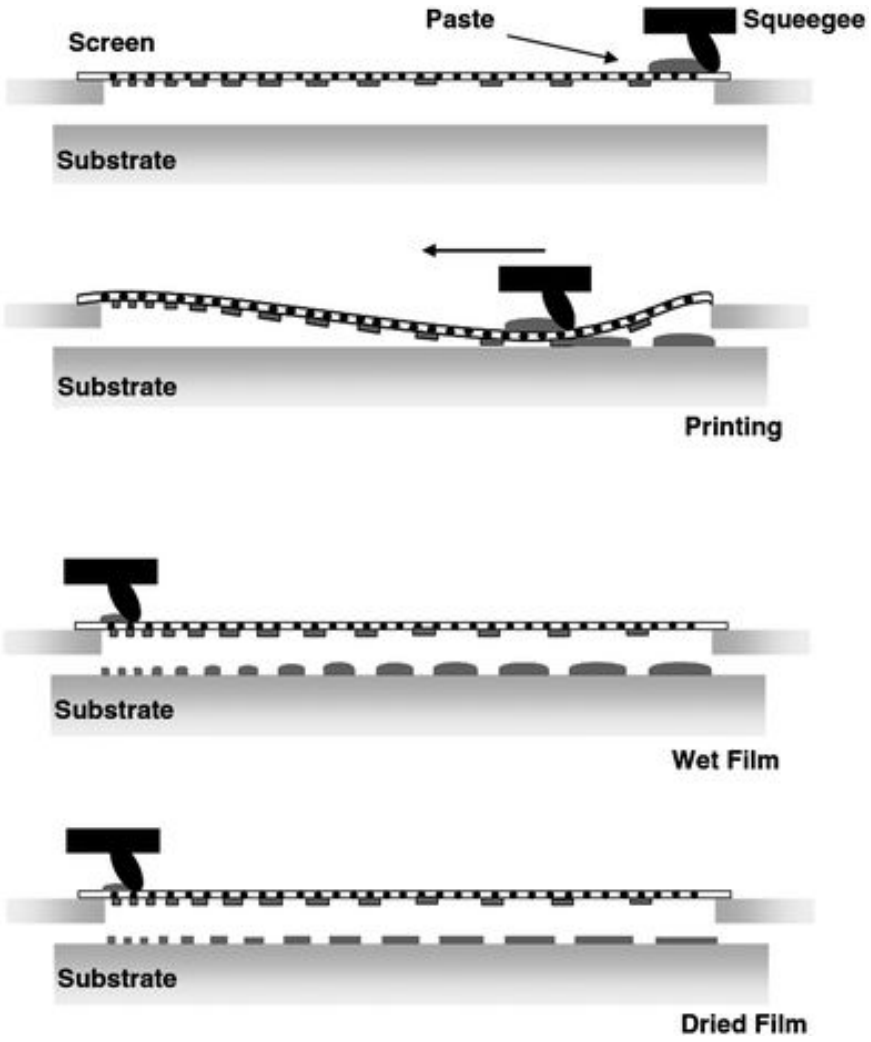

Figure 2.15 Schematic of the screen printing process (Gonzalez-Macia *et al*., 2010)

2.4.1(b) Spray coating

Spray coating is a non-contact printing technique that has been widely used for electronic printing due to its numerous advantages including low cost, time-saving which does not require long printing speed, high repeatability and simple set-up (Abdellah *et al*., 2012). Spray coating can be defined as a process to adhere coating material on the substrate surface by an air atomizing spray gun. The coating material in liquid state is pressurized and fed into an air spray gun in which the material is mixed with pressurized air, atomized and finally flew to deposit on the target surface.

There are several types of spray coating techniques including electrostatic spray technique, air pressure spray technique, hybrid spray technique, *etc* (Elmolla, 2017). Air pressure spray technique has been widely used for laboratory work and in the industry for many years due to the simple set-up and continuous process in which the nozzle has two parts; a large external nozzle with size of 250 μm and a small internal nozzle with size of 100 μm. Figure 2.16 illustrates the schematic diagram of air pressure spray coating technique. This dual-nozzle has large diameter of the internal nozzle which can be useful to overcome the nozzle clogging problem and used a high air pressure to avoid air turbulence and to obtain smaller droplets for forming a thin film with good surface roughness (Kim *et al*., 2014; Elmolla, 2017).

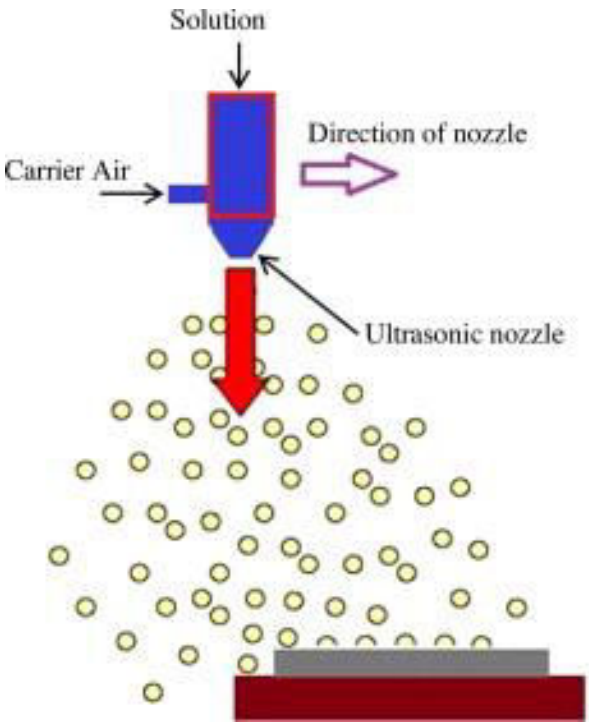

Figure 2.16 Schematic of an air pressure spray coating process (Zabihi *et al*., 2015)

Carey *et al*. (2018) deposited graphene/PEDOT:PSS hybrid inks onto plastic substrate using spray coating with an air-assist spray nozzle and exhibited film conductivity of 10^4 Sm^{-1}, as presented in Figure 2.17. The films were sprayed homogenously with low aerial roughness of 48 nm by controlling the surface tension and boiling point with the values of 30 mNm^{-1} and 79 °C, respectively.

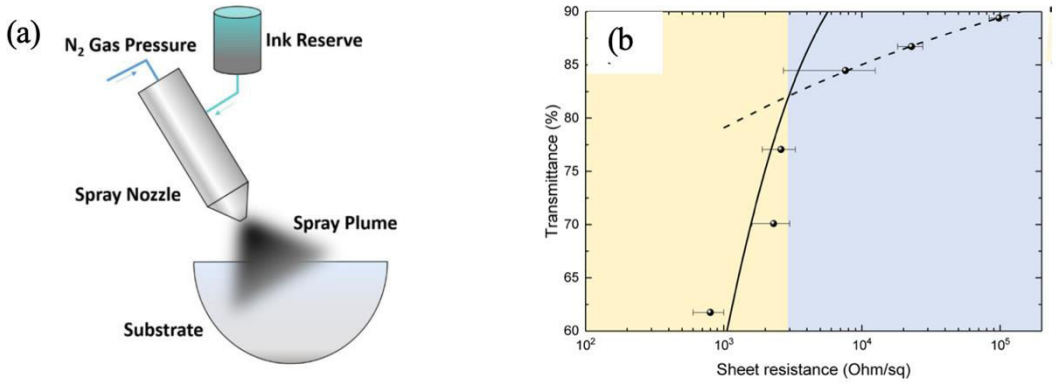

Figure 2.17 (a) Schematic of the spray coating process and (b) optical transmittance as a function of the sheet resistance (Carey *et al*., 2018)

2.4.1(c) Inkjet printing

Inkjet printing, known as digital printing, is a non-contact printing technique where micro-sized ink droplets are ejected directly onto a substrate from a jet device driven by an electronic signal. Inkjet printing is considered as a popular method in the conventional printing industry due to fine pattern generation, non-contact injection, solution saving effects, high repeatability and scalability. Inkjet printing technologies can be classified as continuous or drop-on-demand, as illustrated in Figure 2.18 (Singh *et al*., 2010; Aleeva and Pignataro, 2014; Mariani *et al*., 2015).

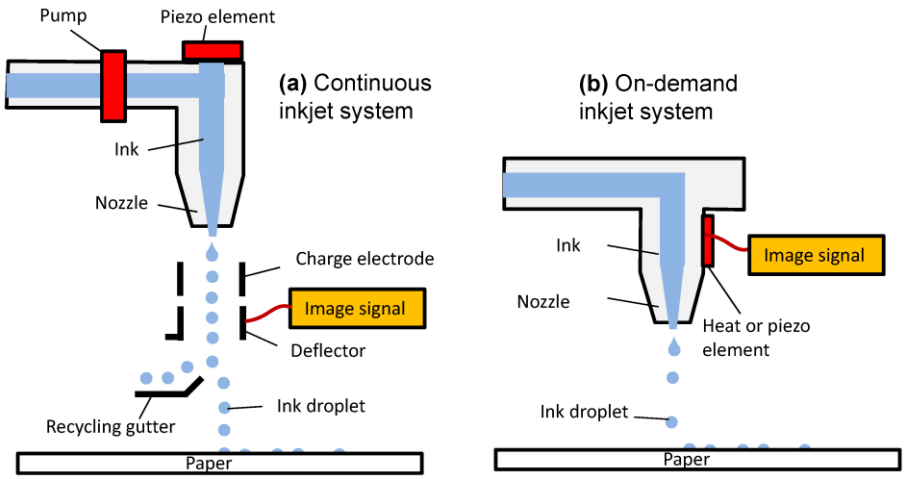

Figure 2.18 Schematic of inkjet printing (a) continuous inkjet system and (b) on-demand inkjet system (Lau and Shrestha, 2017)

In continuous inkjet printing, the ink is pumped through a nozzle, which is charged according to the image and controlled electronically to aim the droplets onto the substrate. The excess droplets are recirculated from the gutter. This method has a fast rate of 0.5 µL droplet generation at 80 – 100 kHz (Le, 1998; Wallace *et al*., 2007). Today most inkjet printers are based on the drop-formation process, known as demand-mode printing. This method has a slower ejection rate of 2–500 pL droplet generation at 30 kHz. The demand-mode method provides smaller drops and higher placement accuracy than continuous inkjet printing, and does not need a recirculation system. Therefore, this method is of simple design and results in less wasted ink (Le, 1998; Wallace *et al*., 2007; Lau and Shrestha, 2017).

Majee *et al*. (2017) formulated a water-based graphene ink by a shear-exfoliation process. The graphene ink at a concentration of approximately 8.5 $mgmL^{-1}$ has a viscosity of 9 – 12 mPas at 30 °C, and was printed using a Dimatix DMP-2831 printer equipped with a 10 pL drop cartridge. Drop spacing was maintained at 20 µm

for all printed patterns. These conditions are suitable for the inkjet printing process. More recently, Karim *et al*. (2017) formulated an rGO ink by rigorous stirring, with a viscosity of 1.35 mPas and surface tension of 65 mNm^{-1}. The film was printed using Dimatix DMP-2800 printer equipped with a 10 pL drop cartridge. The nozzle plate consisted of a single row of 16 nozzles of 21.5 μm diameter spaced at 254 μm with a typical drop diameter of 27 μm.

Inkjet printing technique has been known due to its versatility to fabricate printed electronics especially in the research and development phase by jetting conductive inks onto flexible substrates. Therefore, inkjet printing technique was used as the printing method in this study, alongside with spray coating technique which was also used for comparison.

2.4.2 Flexible electronics for the strain sensor

In recent years, flexible strain sensors have attracted considerable attention with increasing demand in areas such as wearable electronics, soft robotics and health-monitoring devices. According to the statistic of scientific journals related to flexible strain sensors which were taken from Scopus as in Figure 2.19, it shows that the number of scientific publications exhibited 416% improvement specifically from 2009 to 2018. Strain sensor is a component of soft electronics that is integrated in flexible substrate and being used to monitor the shape, stress, strain, force and pressure. Filippidou *et al*. (2015) reported that strain sensors respond to the applied strain with different mechanisms which depend on the type of material, micro/nano-structure and fabrication process.

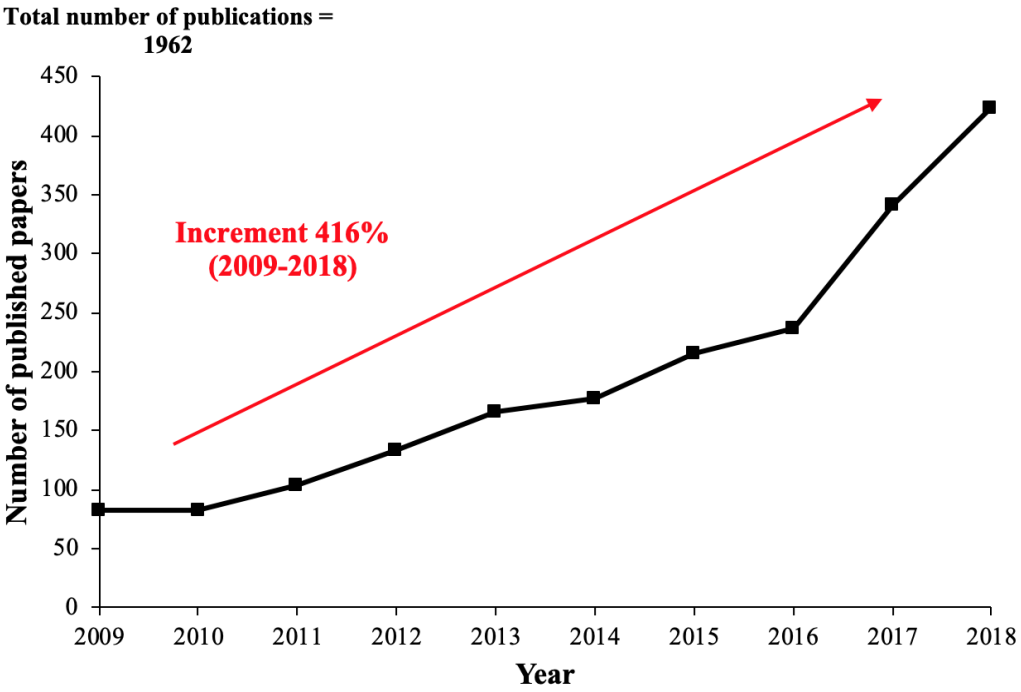

Figure 2.19 The number of published papers for flexible strain sensors 2009-2018 from Scopus by searching for the topic "flexible strain sensors" (data acquired on October 2019)

Strain sensors are being used to record the ageing infrastructure integrity such as aircraft through structural health monitoring (Laflamme *et al*., 2012). Meanwhile for monitoring human body motions can be classified into two categories (Lipomi *et al*., 2011): (1) detection of large-scale motions such as bending movements of the hands, arms and legs, and (2) detection of small-scale motions such as fine movements in the chest and neck during breathing, speaking and swallowing. Strain sensors are also employed for monitoring the civil infrastructural integrity, which is important for the high standard safety requirements in the mechanical and electrical engineering industries (Zhou *et al*., 2006). However, strain sensors that have been fabricated using conventional methods are not flexible, rigid and are separated from the substance or medium that is being monitored leading to incorrect or unreliable results (Cochrane *et*

al., 2007). Therefore, flexible strain sensors fabricated using direct printing techniques have received increasing attention and been considered as a promising solution to overcome the limitations of conventional strain sensors. Gaikwad *et al*. (2013) reported that printed and flexible strain sensors offer mechanical flexibility and are relatively cost efficient.

The performance of strain sensors can be characterized by various parameters including sensitivity or gauge factor, stretchability, linearity, hysteresis, durability, response and recovery time, long time stability, electrical conductivity, fabrication cost, *etc* (Filippidou *et al*., 2015). The gauge factor is one of the main performance parameters and often used to measure the data for strain sensors under variable strains, which is the standard for quantifying the piezoresistive sensitivity (Li *et al*., 2012). According to Meng *et al*. (2019), the gauge factor can be defined as the ratio of relative change in electrical resistance to the applied mechanical strain. A strain gauge sensor is basically a sensor used for the measurement of various physical parameters like stress, strain, *etc*. The desired pattern of the strain gauge sensor is shown in Figure 2.20 (Correia *et al*., 2013). The working principle of the strain gauge is based on the piezoresistive effect. When a metal conductor is stretched or compressed, the dimension of conductor changes. Change in dimension means a change in radius and length of the conductor (Pan *et al*., 2014). Since the resistance of a conductor is directly proportional to its length and inversely proportional to its area of cross-section, therefore a change in dimension of the conductor will cause a change in the resistance. It has also been observed that the resistivity of the conductor changes due to strain in the conductor. This change in resistivity due to strain is called the piezoresistive effect.

Figure 2.20 Schematic of the strain sensor gauge (Correia *et al*., 2013)

Commonly, polymers including polydimethylsiloxane (PDMS), polyurethane and natural rubber were used as stretchable substrate. As reported by Jeon and Ha (2016) in their studies, PDMS has become the most popular stretchable polymer substrate for fabricating strain gauge sensor due to its flexibility, biocompatibility, low cost, low toxicity, *etc*. These stretchable polymer substrates were coupled with conductive nanomaterials including carbon blacks, carbon nanotubes, graphene and metal nanoparticles/ nanowires. To date, graphene has been utilized as a promising next generation material for strain sensors replacing the traditionally used carbon black due to its remarkable electronic and mechanical properties (Bae *et al*., 2013; Tian *et al*., 2014; Wang *et al*., 2014; Park *et al*., 2015).

Wang *et al*. (2013) prepared graphene/PDMS composite strain sensor by direct film casting. The results indicated a gauge factor reaching 233 under a strain of 2%. It was observed that high gauge factor was obtained, however poor strain range make this composite not suitable to be used in modern devices. In 2019, Zhang *et al*. reported that graphene foam/natural rubber composite was prepared by casting natural rubber latex into graphene foam. The results showed that the gauge factor of the flexible sensor reached 210 in the strain range of 10-40%. Detailed specifications of graphene-based

strain sensors are summarized in Table 2.6. High gauge factors were obtained when the strain range percentage was large and it is necessary to obtain high sensitivity and high strain range simultaneously for the development of flexible strain sensor with outstanding performance.

Table 2.6 Performances of flexible graphene-based strain sensors (Eswaraiah *et al*., 2011; Wang *et al*., 2013; Filippidou *et al*., 2015; Liu *et al*., 2016; Lin *et al*., 2016; Chun *et al*., 2017; Zhang *et al*., 2019)

Materials	**Methods**	**Strain range (%)**	**Gauge factor**
Graphene/PVDF	Casting	0.27	-
Graphene/PDMS	Casting	2	233
Graphene/TPU	Compression molding	30	17.7
Graphene/CNT/TPU	Compression molding	30	35.78
Graphene/rubber	Hot compression	100	82.5
Graphene/PDMS	Compression	20	42.2
Graphene foam/rubber	Casting	40	210
GNP/PDMS	Spin coating	0.2	3
PEDOT:PSS/PI	Inkjet printing	3	<1

2.5 Summary

Numerous researches on graphene-based inks have been done since the past 10 years, however more effort need to be considered before they can be used in practical applications. Extensive works to produce large scale, good quality, low-cost of graphene-based ink and eco-friendly fabrication method are required. Based on intended applications and desired printing process, there are some factors needed to be considered for conductive inks formulation. These factors are printing methods, conductive materials, factors affecting ink performances and factors affecting electrical conductivity. Apart of these factors, conductive inks should be stable against aggregation and precipitation in order to provide reproducible performances. There are few challenges in producing excellent electrical properties and stable conductive which can be divided into few parts such as graphene materials, ink dispersant solvent and ink stability.

Based on the literature studies, graphene-based materials such as GNP, GO and rGO were used as the fillers to fabricate graphene-based inks, knowing that GNP has poor solubility in various types of common solvents, GO sheets suffer from low electrical conductivity and rGO required highly toxic solvents. Other than that, it is observed that printed graphene films exhibited high electrical conductivity values ($>10^3$ S/m) after being annealed at high temperature (100 – 350 °C). However, the need for low annealing temperature and short annealing duration are required in order to meet the requirements for printing process on the plastic substrate and therefore for the fabrication of flexible electronic applications.

Most of the solvents used in the fabrication of graphene-based inks are highly toxic and have high boiling points (>150 °C). The usage of these common solvents such

as NMP, DMF, *etc* limit the development of graphene-based ink technology. Other than that, addition of stabilizer or surfactant often gives negative effect to the electrical properties of the printed pattern. Thus, non-toxic and low boiling point solvents without an addition of stabilizer or surfactant should be considered for the development of graphene-based inks.

Moreover, based on the literature studies, the ink properties including viscosity, surface tension, contact angle and surface energy play a vital role in determining the printing quality and should be optimized to meet the printing requirements. The prepared conductive inks should have good stability for a certain period of time without sedimentation. Other than that, limited studies have been conducted to investigate the effect of inkjet printing GNP and GF as conductive inks on plastic substrate and bio-friendly polymer substrate for flexible strain sensors.

CHAPTER 3

MATERIALS AND METHOD

Chapter 3 provides information of materials, methodologies and characterization used for the experimental work in this study. This chapter is divided into three sections; namely materials, experimental methods and characterization techniques, respectively. Section 3.1 explains the details of the raw materials, solvents and chemicals used throughout the experimental work. Section 3.2 covers the information about the method and parameters used in this study. Section 3.3 presents the characterization techniques that are used to characterize the raw materials, conductive inks and conductive ink patterns.

3.1 Materials

Starting materials that being used to produce graphene-based inks and graphene hybrid-based inks are listed in the following paragraphs, Section 3.1.1 and 3.1.2. Note that all the materials are commercial products except graphene foam (GF), which was prepared using solvothermal method based on previous work by Speyer *et al*. (2015). The preparation of GF was carried out at Carbon Materials Group (E205)'s laboratory, Institut Jean Lamour, Université de Lorraine, France.

3.1.1 Raw materials

3.1.1(a) Graphene-based materials

Several types of graphene-like materials were used as a filler in the preparation of conductive inks. These include GF, graphite nanoplatelets (GNPs) and synthetic graphite (SG). GF in black powder form was prepared using solvothermal method based on previous work (Speyer *et al*., 2015). Starting materials of anhydrous ethanol (>99.8%) and gases of argon and nitrogen for GF production were supplied by Sigma Aldrich and Air Liquide, respectively. Ethanol, sodium and nitrogen gas were used in the solvothermal process, meanwhile argon was used to collect the solvothermal product. Both GNPs and SG with reference number of TIMREX BNB90 graphite-AA-130 and TIMREX SFG 44-75 were supplied by Timcal Group, Switzerland. General properties of the graphene-based materials are shown in Table 3.1.

Table 3.1 General properties of various types of graphene-like materials (Materials Safety Data Sheet)

Materials	Physical state	Color	Density (gcm^{-3})
GNPs	Powder	Black	2.2
SG	Powder	Gray to black	3.0

3.1.1(b) Silver nanoparticles

Silver nanoparticles, AgNPs were supplied by Sigma Aldrich were used as hybrid filler in the production of graphene hybrid-based ink. Table 3.2 shows the properties of AgNPs powders.

Table 3.2 General properties of silver nanoparticles (Materials Safety Data Sheet)

Properties	Description/value
Physical state	Powder
Color	Silver
Density (gcm^{-3})	10.49

3.1.1(c) Poly(3,4-ethylenedioxythiophene)-poly(styrenesulfonate)

Poly(3,4-ethylenedioxythiophene)-poly(styrenesulfonate), PEDOT:PSS conductive polymer supplied by Sigma Aldrich was also used as hybrid material in the production of graphene hybrid-based ink. Table 3.3 presents the general properties of PEDOT:PSS.

Table 3.3 General properties of PEDOT:PSS (Materials Safety Data Sheet)

Properties	Description/value
Physical state	Liquid
Color	Blue
Density (gcm^{-3})	0.985

3.1.2 Solvents and chemicals

All of the solvents used to disperse graphene-based materials and chemicals involved in this research were purchased from local and oversea suppliers. Polyester varnish (PV) was used as a binder in the preparation of graphene-based material inks for spray coating and supplied by AEV Ltd., United Kingdom. Xylene thinner was used as a solvent for PV and also supplied by AEV Ltd., United Kingdom. Table 3.4 presents the general properties of PV. Meanwhile, solvents including ethylene glycol (EG), 2-Propanol (IPA), propylene glycol (PG), N,N-Dimethylformamide (DMF) and N-Methyl-2-pyrrolidone (NMP) were used to disperse graphene-based materials in the preparation of conductive ink for inkjet printing. EG, IPA and DMF solvents were supplied by Merck. PG and NMP solvents were supplied by Sigma Aldrich. Table 3.5 presents the details and chemical formula of the solvents and chemicals.

Table 3.4 General properties of PV (Materials Safety Data Sheet)

Properties	**Description/value**
Physical state	Liquid
Color	Straw (pale yellow)
Density (gcm^{-3})	0.92
Viscosity (P)	3
Solvent	Xylene thinner

Table 3.5 General properties and chemical formula of various types of solvents and chemicals (Materials Safety Data Sheet)

Solvents and chemicals	**Density (gcm^{-3})**	**Boiling point (°C)**	**Chemical formula**
PV	0.92	150-203	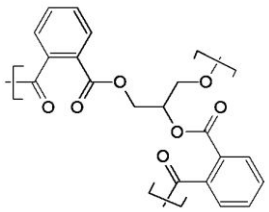
Xylene thinner	0.87	138-142	
EG, ≥99.5%	1.11	197.6	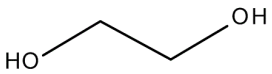
IPA, ≥99.8%	0.786	82.4	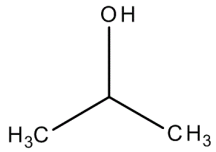
PG, ≥99.5%	1.036	187	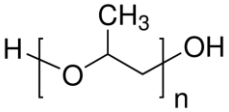
DMF, ≥99.0%	0.94	153	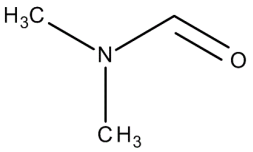
NMP, 99.5%	1.028	202	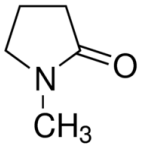

3.2 Experimental methods

Figure 3.1 shows the flowchart of the research overview of this research work. The experimental methods are divided into three stages, namely synthesis of graphene foam, production of graphene-based ink via spray coating and production of graphene-based ink via inkjet printing for strain sensor. Further explanation regarding the methodologies are described in the following sections.

3.2.1 Synthesis of graphene foam

Graphene foam (GF) was prepared using a solvothermal-based process according to the method reported by Speyer *et al*. (2015). The experiment was carried out at Carbon Materials Group (E205)'s laboratory, Institut Jean Lamour, Université de Lorraine, France. In this method, 15 mL of ethanol and 6 g of sodium were mixed (1:1 stoichiometric mixture) under inert atmosphere in a Parr autoclave, as shown in Figure 3.2 (a). Nitrogen gas at a pressure of 100 bar was then injected into the reactor. Next, the autoclave was heated at 220 °C until the internal pressure reached 200 bar for 72 h and finally cooled down to room temperature. The solvothermal product which was sodium ethoxide was then collected under argon atmosphere.

About 5 g of sodium ethoxide was weighed and placed inside a vertical tubular oven (Figure 3.2 (b)). The oven was heated at 850 °C with a heating rate of 20 °Cmin^{-1} for 4 h, followed by cooled down to room temperature. The pyrolysis products contained carbon, sodium carbonate, sodium hydroxide and hydrocarbons gaseous. The pyrolysis products were sonicated and washed with ethanol, hydrochloric acid and distilled water to remove sodium carbonate and sodium hydroxide, and finally filtered using vacuum filtration as presented in Figure 3.2 (c). The washed sample was then dried at 100 °C for 24 h.

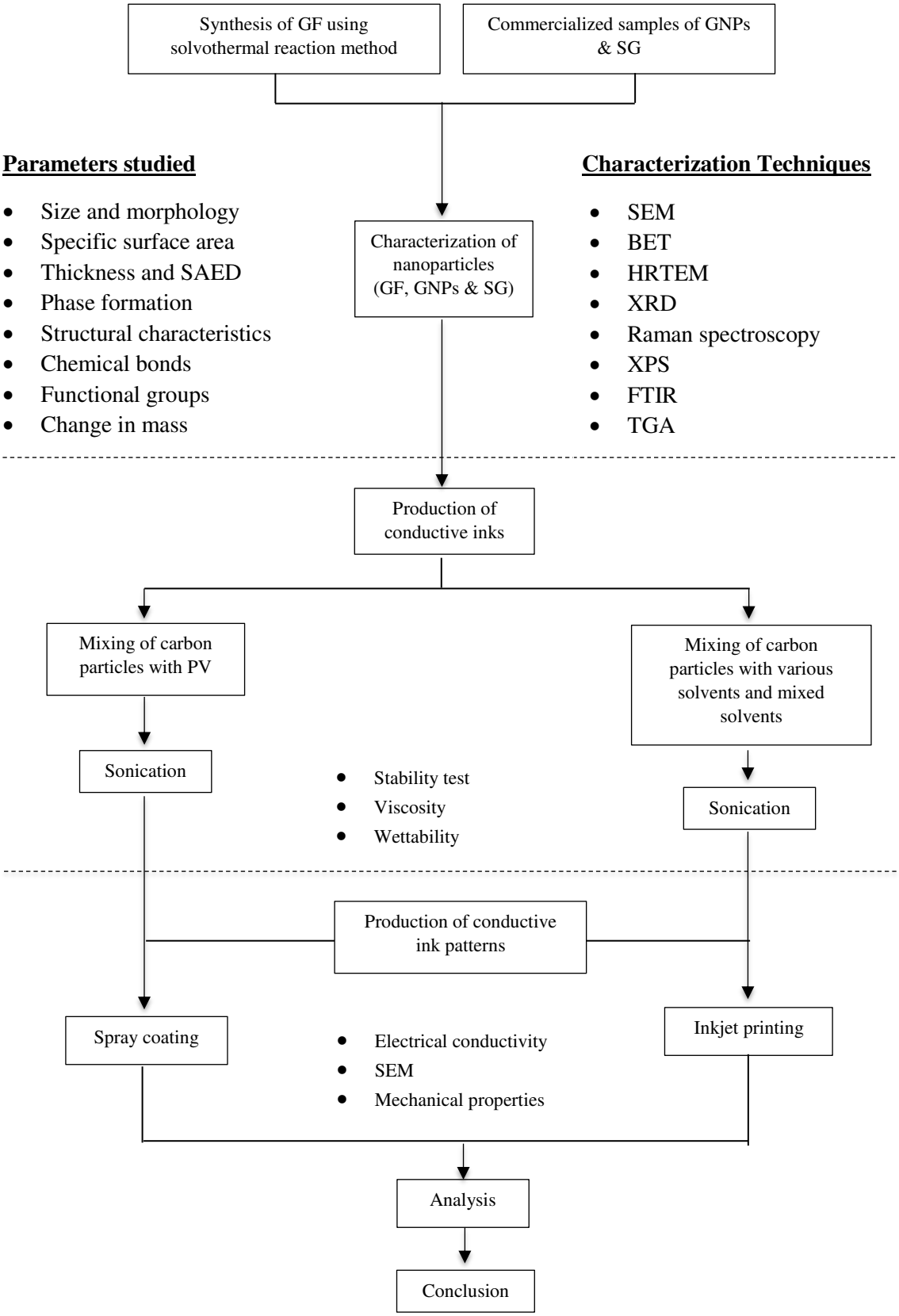

Figure 3.1 Overall research flowchart

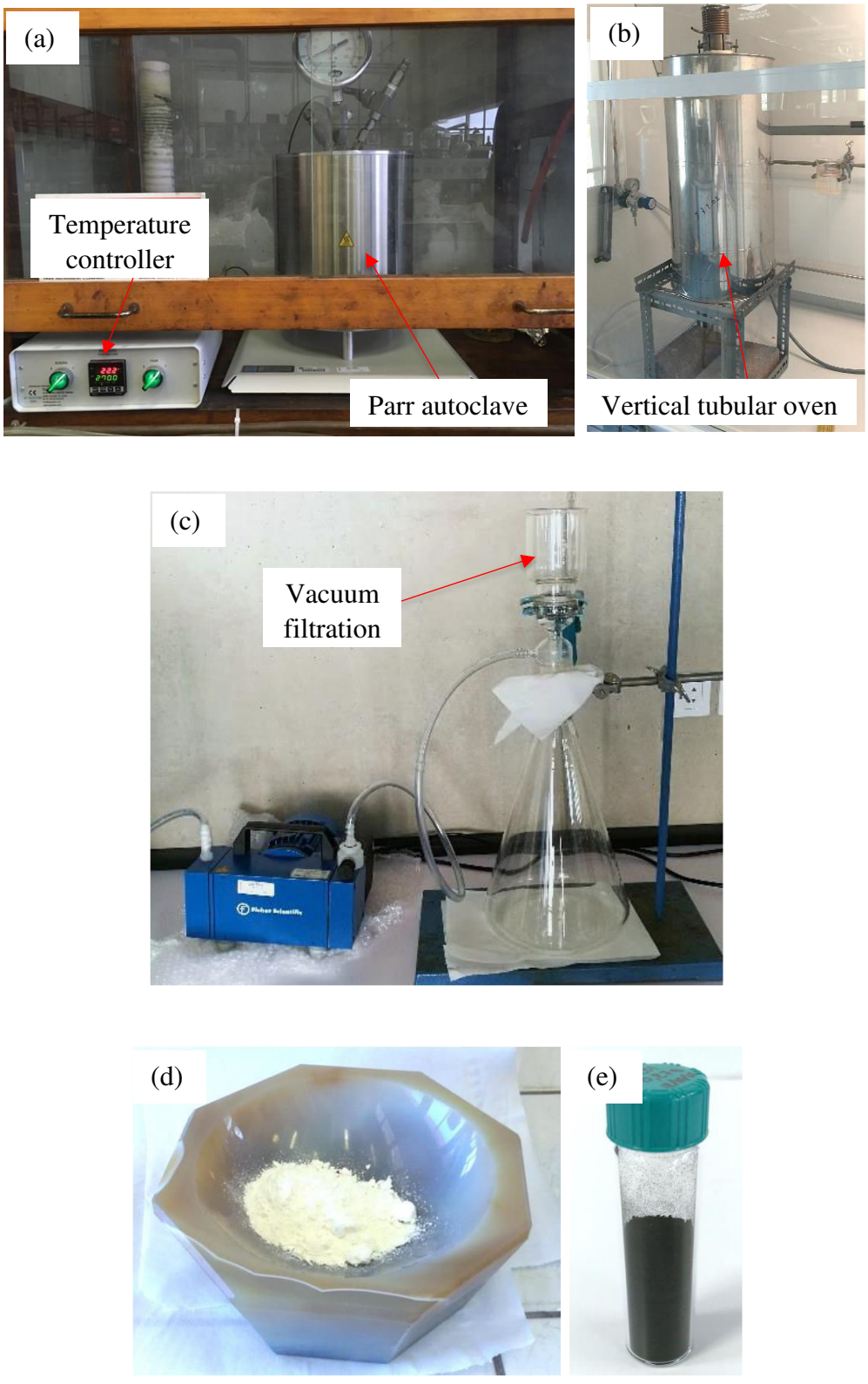

Figure 3.2 (a) Solvothermal reaction to produce sodium ethoxide, (b) pyrolysis reaction for producing graphene foam, (c) washing and filtration of pyrolysis products, (d) sodium ethoxide and (e) product of pyrolysis

3.2.2 Production of graphene-based ink for spray coating

3.2.2(a) Preparation of ink

The loading of graphene-based materials in the PV binder were varied from 2 vol.% to 20 vol.%. The formulations were sonicated at room temperature for 15 min with 175 W power density in order to achieve uniform and homogenous dispersion of the filler in the PV binder. The temperature of the mixture was increased during sonication process, therefore, to avoid the mixture from overheat, the beaker was immersed in a water bath to reduce the temperature.

3.2.2(b) Fabrication of conductive ink pattern

In order to achieve a highly uniform deposition, a customized motor-controlled air spray coating was fabricated to deposit the mixture of conductive ink and PV onto a flexible substrate, as shown in Figure 3.3. The experiment was carried out at Carbon Materials Group (E205)'s laboratory, Institut Jean Lamour, Université de Lorraine, France. The flexible substrate used in this study was organic transparency film. The flexible substrate was placed on the preheated metal substrate. The metal substrate temperature, the spray length and the air pressure were fixed at 100 °C, 0.16 m and 4 psi, respectively. The conductive ink pattern produced by spray coating was cured at 130 °C for 4 h in an oven. The schematic of flow work for the fabrication process of conductive ink pattern is shown in Figure 3.4.

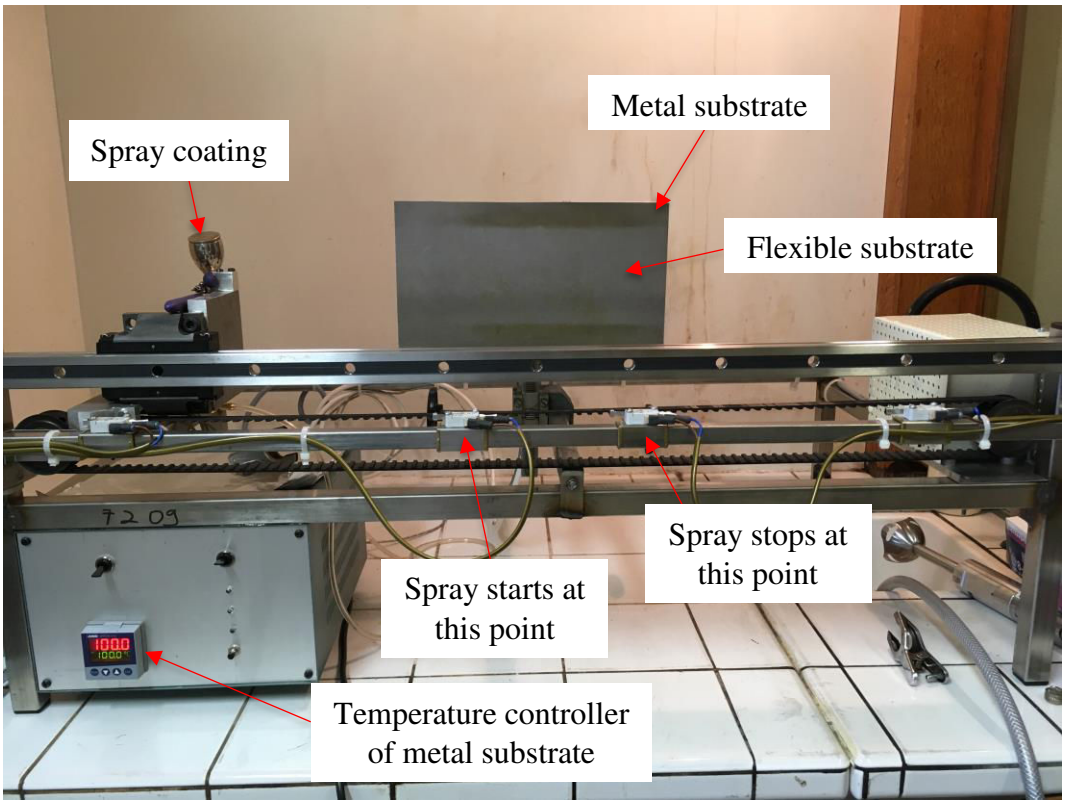

Figure 3.3 Photograph of the customized motor-controlled air spray coating

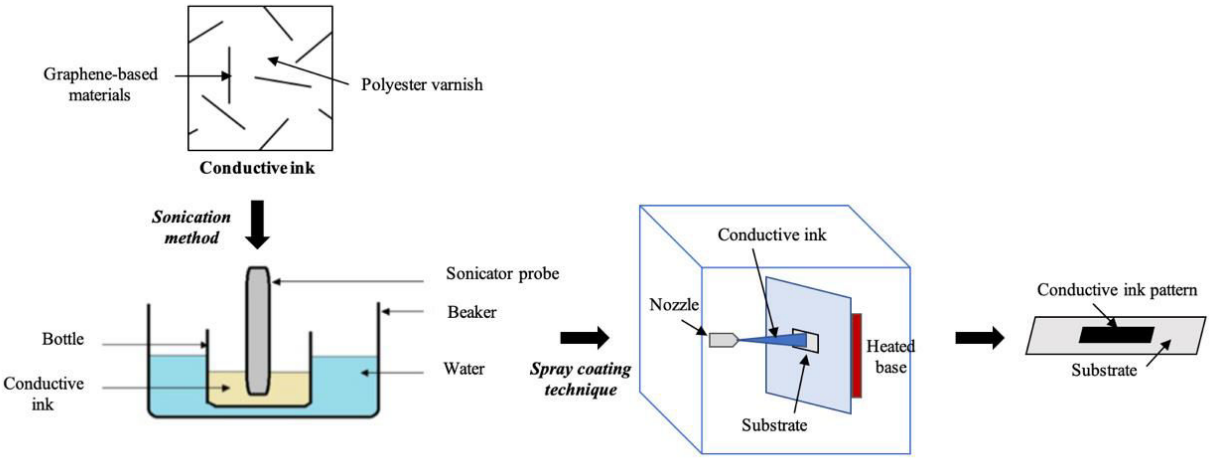

Figure 3.4 Schematic of the fabrication process of conductive ink pattern using spray coating technique

3.2.3 Production of graphene-based ink for inkjet printing

3.2.3(a) Different types of solvents

GNPs were further used as a filler in the preparation of conductive ink. About 0.05 $mgmL^{-1}$ concentration of GNPs dispersed in EG solvent were prepared. The formulations were sonicated at room temperature for an hour with approximately 200 W power density. Once the sonication was completed, the ink supernatant was then collected. The same procedure was used to prepare GNPs dispersed in PG, IPA, NMP and DMF solvents.

3.2.3(b) Mixed solvents

About 0.05 $mgmL^{-1}$ concentration of GNPs dispersed in the mixture of IPA and EG solvents. Ratio of mixed solvents of IPA:EG was varied from 1:4, 2:3, 1:1, 3:2 and 4:1, respectively. The formulations were sonicated at room temperature for an hour with approximately 200 W power density. Once the sonication was completed, the supernatant of GNPs ink was then collected. The same procedures as discussed in this section to produce GNPs inks were utilized to prepare GF inks for the comparison purpose. The numbers in front of samples are referring to the ratio of IPA:EG mixed solvents. The details of the ratios used in IPA:EG mixed solvents are listed in Table 3.6.

Table 3.6 Description of the sample codes for GNPs and GF dispersed into various ratios of IPA:EG mixed solvents

Sample description	Sample code
IPA:EG mixed solvents at ratio of 1:4	IPA:4EG
IPA:EG mixed solvents at ratio of 2:3	2IPA:3EG
IPA:EG mixed solvents at ratio of 1:1	IPA:EG
IPA:EG mixed solvents at ratio of 3:2	3IPA:2EG
IPA:EG mixed solvents at ratio of 4:1	4EG:EG

3.2.3(c) Fabrication of conductive ink pattern

The concentration of GF ink, GF/AgNPs hybrid ink and GF/PEDOT:PSS hybrid ink dispersed in IPA:EG solvents at the ratio of 1:1 were fixed at 4 $mgmL^{-1}$. The same procedure was used to prepare GF ink as mentioned in Section 3.2.3(a). In this study, the printing layers were varied from 10 to 50 layers, respectively. Printing process was carried out using Squink Multilayer PCB Printer (BotFactory Inc., United States) with approximately 6 μm of advance ink cartridge nozzle and 80 °C of metal substrate, as shown in Figure 3.5. The flexible substrate used was polyethylene terephthalate (PET), manufactured by DuPont Mylar A with the thickness of 125 μm and opaque white appearance (GTS Flexible Materials Ltd., United Kingdom). The schematic of flow work for the fabrication process of conductive ink pattern is shown in Figure 3.6.

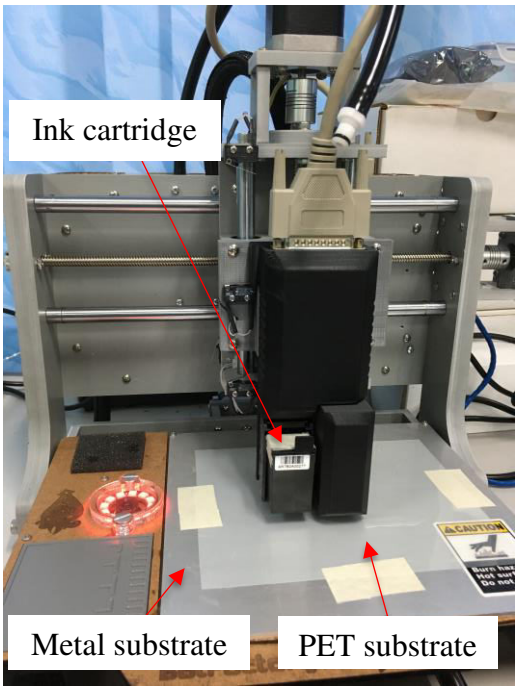

Figure 3.5 Photograph of the inkjet printing

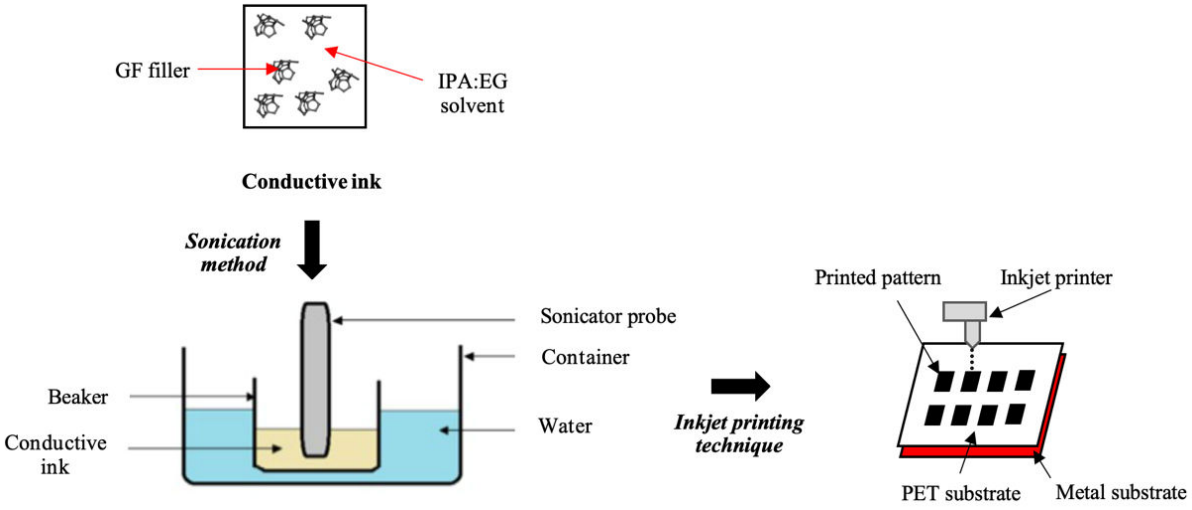

Figure 3.6 Schematic of the fabrication process of conductive ink pattern using inkjet printing technique

3.3 Characterization techniques

Several techniques were used for the raw materials and conductive ink characterizations and will be further discussed in this section.

3.3.1 Scanning electron microscopy

Scanning electron microscopy (SEM) is a type of non-destructive characterization method that can be used to observe the morphology of the sample at high magnification and resolution image. In this study, the flake size and morphology of the graphene-like materials, as well as the morphology of the conductive ink patterns were characterized by using SEM model QUANTA FEG450 at School of Chemical Engineering's laboratory, Universiti Sains Malaysia and model JEOL JSM-6010LA at Carbon Materials Group (E205)'s laboratory, Institut Jean Lamour, Université de Lorraine, France. The graphene-based materials were sprinkled onto the surface of sticky carbon tape for SEM analysis.

Meanwhile, energy dispersive spectroscopy (EDS) was used to confirm the presence of carbon element in the graphene-like materials and to identify other possible elements present in the material obtained using the solvothermal-based process.

3.3.2 High resolution transmission electron microscopy

High resolution transmission electron microscopy (HRTEM) is a type of non-destructive characterization method and very common tool for graphene-like materials characterization to observe the morphology and the structure. In HRTEM image at the edge of graphene-like particle, each fringe line represents a layer of graphene and if it is a monolayer graphene, only one line will be visible; it is possible to observe lattice arrangement of the graphitic material through selected area electron diffraction (SAED)

too at the HRTEM image. For this study, FEI TECNAI G20 at Science and Engineering Research Centre (SERC)'s laboratory, Universiti Sains Malaysia was used. The graphene-like materials were dispersed in ethanol and a drop of the dispersion was deposited on a copper grid covered with a holey carbon film followed by solvent evaporation in open air at room temperature.

3.3.3 X-ray diffraction

X-ray diffraction (XRD) analysis is an effective non-destructive analysis of crystalline materials and provide details information about the phase and crystal structure of the graphene-based materials. The data from XRD patterns were analyzed by using the EVA software (Bruker) based on the International Centre for Diffraction Data (ICDD). The X-ray analysis data was collected in the form of intensity peak against diffraction angle, 2θ. The relation between wavelength and diffraction angle was determined by using Bragg's Law in Equation 3.1.

$$n\lambda = 2dsin\theta \quad (3.1)$$

where n is an integer, λ is the wavelength of incident x-rays beam, d is the distance between atomic layers and θ is the diffraction angles. In this study, XRD analysis was carried out using Bruker D8 Advance Diffractometer with molybdenum radiation (λ MoKα_1 = 0.70930 Å) in the range of 2θ ($10° \leq 2\theta \leq 45°$). The sample powder was placed in Lindemann glass capillary tubes with 1.5 mm diameter. The characterization was carried out at Carbon Materials Group (E205)'s laboratory, Institut Jean Lamour, Université de Lorraine, France.

3.3.4 Raman spectroscopy

Raman spectroscopy is widely used to determine the quality and number of layers of graphene-like materials. It is a point-based characterization which gives better overview of the plane as it covers a larger area of sampling. In this study, the structural characteristics of the graphene-like materials were analyzed using Renishaw inVia Raman spectrometer at SERC's laboratory, Universiti Sains Malaysia operating at λ = 633 nm HeNe laser (20 mW), on a spectral range 100-3200 cm^{-1}. The sample powder was placed in a special specimen holder.

3.3.5 X-ray photoelectron spectroscopy

X-ray photoelectron spectroscopy (XPS) is a powerful tool to characterize the material's surface chemistry with high selectivity. It is mostly used to identify the binding energy which can be further used to determine the specific chemical bonds and the functionalities in the graphene-like materials. For graphene materials, the main peak is the C 1s band at ~285 eV which represent sp^2 C=C bond. A good quality of graphene with low amount of oxygen content would produce a sharp and narrow C 1s peak. In this study, the XPS spectra were obtained using AXIS Ultra DLD, Kratos at SERC's laboratory, Universiti Sains Malaysia equipped with Al Kα X-ray source (1486.6 eV). The graphene-like materials were sprinkled onto the surface of sticky carbon tape for XPS analysis.

3.3.6 Fourier-transform infrared spectroscopy

Fourier-transform infrared spectroscopy (FTIR) analysis was performed to identify functional groups of the graphene-like materials. In the present study, FTIR analysis was carried out using Perkin-Elmer Spectrum One spectrometer, Waltham, MA. About 2 mg of sample powder was mixed with about 98 mg of potassium bromide

(KBr) prior to compacting into thin plates with a hydraulic press at a pressure of 500 psi for 1 minute. The samples were scanned from 4000 to 1000 cm^{-1} in open air environment with a resolution of 2 cm^{-1} for 4 scans. All FTIR spectra were obtained in transmittance mode.

3.3.7 Physisorption of Nitrogen at 77 K

Physisorption of nitrogen at 77 K is performed with a Micromeritics ASAP 2020 Surface Area and Porosity Analyzer at School of Chemical Engineering's laboratory, Universiti Sains Malaysia. The samples were degassed during 4 h at 350 °C with before analysis. The specific surface area of the graphene-like materials was calculated with the BET model and the micropore volume was determined using the t-plot model.

3.3.8 Thermogravimetric analysis

Thermogravimetric analysis (TGA) is a technique in which the mass of the sample is monitored against time or temperature of the sample. TGA was done using Setsys Evolution Setaram thermobalance at Carbon Materials Group (E205)'s laboratory, Institut Jean Lamour, Université de Lorraine, France to determine the change in mass or weight loss of the graphene-like materials with respect to temperature. About 3 mg of samples were placed in a crucible and heated under dry air at temperature range between 20 to 1000 °C with a heating rate of 3 °Cmin^{-1}. The decomposition temperature and weight of residue were reported in this study.

3.3.9 Visual observation

The stability of GNPs and GF inks were investigated at their current pH via visual observation to evaluate the effectiveness of GNPs and GF dispersions and the stability of the resulting inks. All inks with a fixed concentration of 0.05 mgmL^{-1} were

observed and compared within certain period of time.

3.3.10 Zeta potential analysis

The zeta (ζ) potential is a well-known technique to evaluate the stability of a system by understanding the degree of electrostatic repulsion. The ζ-potential values were calculated based on the Helmholtz-Smoluchowski equation, as shown in Equation 3.2 (Ries Jun, 1970).

$$\xi = \frac{4\pi\mu\eta}{D} \tag{3.2}$$

where μ, η and D are the electrophoretic mobility, velocity and dielectric constant of the liquid at the boundary layer, respectively. In this study, ζ-potential of GNPs and GF inks were characterized by using Zetasizer Nano Instrument model Nano ZS ZEN3600, Malvern, UK. Three measurements consisting of 100 runs were performed for GNPs and GF dispersions at current pH and the average results were reported.

3.3.11 Ultraviolet-visible spectrophotometer

Spectral analysis through ultraviolet-visible (UV-Vis) spectrophotometer is used to study the electronic structure of atomic and molecular species of a compound in the region from 200 nm to 1000 nm. In this study, UV-Vis was performed by using UV-Vis spectrophotometer model Varian Cary 50 Conc, Agilent Technologies with absorption spectra between 200 and 800 nm to measure the absorbance of GNPs and GF inks. Initial concentration of the conductive inks was fixed at 0.05 $mgmL^{-1}$ and the supernatant of the conductive inks were used to obtain a detectable transmission during the measurements. Besides that, the stability of the conductive inks was evaluated by calculating the concentration of the conductive inks at 660 nm within a certain period of time, using Lambert-Beer law in Equation 3.3 (Khan *et al*., 2010; Lotya *et al*., 2010).

$$A = \alpha CL \tag{3.3}$$

where A, α, C and L are the absorbance, absorption coefficient with the value of 2460 $mLmg^{-1}m^{-1}$, concentration of the conductive ink and cell length, respectively.

3.3.12 Viscosity

A rheometer is used to measure the rheological properties of the materials. Unlike a viscometer which can only be used to measure the viscosity, η of a fluid under a limited range of conditions, a rheometer is capable of measuring η and elasticity of non-Newtonian materials under a wide range of conditions. η is a fundamental characteristic of all fluids which measures the resistance of liquid to flow or shear deformation. This resistance is caused by cohesive intermolecular force with giving rise to friction between adjacent layers of fluids in relative motion. In this study, the ink viscosity, η was measured by cone and plate rheometer model Physica MCR 301, Anton Paar Malaysia Sdn. Bhd. at the shear rate within a range of 1-500 s^{-1}.

3.3.13 Measurement of contact angle

The contact angle, θ_c is an indication of the wetting performance of liquids applied to solids and the angle is usually measured between the base and the tangent at the point of contact between conductive ink and the substrate. In this study, the contact angle was measured by the sessile drop method with a droplet volume of 5 μL using a goniometer model Rame hart Instrument. Co, USA on the substrate. The samples were placed in a Contact Angle Goniometer that is attached to the Image analyzer. Each sample was subjected to 10 measurements in each 4-angle position: vertical left, vertical right, horizontal left and horizontal right. DROPimage Advanced software was used to obtain the contact angle.

The surface energy of the conductive inks that indicate intermolecular interactions at the interfaces of a solid surface with its environment was identified. The surface energy relation between liquid, solid and gas interfaces can be calculated by using Young's equation in Equation 3.4 (Michel *et al*., 2016).

$$\gamma_S = \gamma_{SL} + \gamma_L \cos\theta \tag{3.4}$$

where γ_L is the surface energy of the liquid, γ_{SL} is the surface energy between solid to liquid interface, and γ_S is the surface energy of the solid.

3.3.14 Electrical conductivity

The electrical conductivity of the films and the sprayed patterns was measured at room temperature using four-point probe measurement. The sheet resistivity was calculated using Van Der Pauw's method according to the Equation 3.5. The electrical conductivity was calculated using Equation 3.6. The samples were placed at the centre of a copper plate and connected to the power source and voltmeter. This method was based on two voltage measurements, by shifting the two measuring devices. The power source was Keithley 220 current source and the voltmeter was a Keithley 2010 multimeter. To obey Ohm's law, three current values for the measurements were applied at 50, 100 and 150 μA, respectively.

$$\rho = \left(\frac{\pi d}{ln2}\right)\left(\frac{R_A + R_B}{2}\right) f \tag{3.5}$$

$$\sigma = \frac{1}{\rho} \tag{3.6}$$

where ρ, σ, t, $R_A + R_B$ and f are resistivity, conductivity, sample thickness, sheet resistance and correction factor, respectively. The principle of the measurement is shown in Figure 3.7.

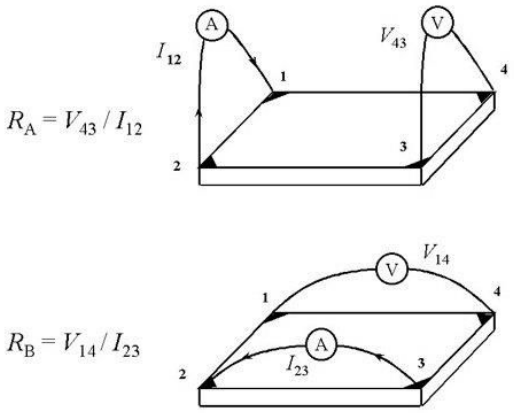

Figure 3.7 The principle of Van der Pauw's measurement

For polyester varnish, the surface resistivity was measured using Prostat PRS-812 Resistance Meter and then calculated using Equation 3.6 to determine the electrical conductivity.

3.3.15 Mechanical properties

The tensile test was performed to investigate the mechanical behavior of printed ink on the substrate, and therefore confirm their suitability for flexible interconnects. In this study, the strain sensing characteristics were tested by using a mechanical Instron 3366 tensile testing machine with a crosshead speed of 1 mmmin^{-1} and uniform strain/release cycle of 5%, 10% and 20%, respectively. The change in resistance of the conductive ink patterns were investigated when the strain from 0 to 20% was applied.

The gauge factor is defined as the ratio of per unit change in resistance to the per unit change in length and can be calculated using Equation 3.7.

$$GF = \frac{\frac{\Delta R}{R_O}}{\frac{\Delta L}{L_O}} \tag{3.6}$$

where $\frac{\Delta R}{R_O}$, $\frac{\Delta L}{L_O}$ and GF are per unit change in resistance, per unit change in length and gauge factor, respectively.

CHAPTER 4

RESULTS AND DISCUSSION

The results of the experiment conducted as well as the related discussion are presented in this chapter. The division of the section is based on the objectives as stated in Chapter One. The first section discusses on the characterization of the synthesized graphene foam (GF) and compare with commercial graphite nanoplatelets (GNPs) and synthetic graphite (SG). Section two covers on the ink properties of graphene-based materials mixed with polyester varnish (PV) binder and the electrical conductivity of the sprayed patterns. Followed by the section which explains the stability of graphene-based materials dispersed into various types of common solvents and mixed solvents. The electrical properties of printed patterns and performance of strain sensor fabricated using inkjet printing are discussed in the last part of the thesis. The discussion is based on the results obtained and supported by the results reported by previous researchers.

4.1 Properties of graphene foam and commercial graphene-based materials

The first objective of the present research is to compare the characteristics of the synthesized GF via solvothermal reaction method with commercial GNPs and SG. In this work, the morphology, phase formation, functionalities, structural characteristics and electrical properties of graphene-based materials were investigated.

4.1.1 Morphology

Figure 4.1 shows the scanning electron microscopy (SEM) images of the graphene-based materials; (a) GF, (c) GNPs and (e) SG. Based on the micrographs, it was observed that the structure for GF is a porous 3D network. The porous GF was formed due to the reaction between ethanol and sodium during solvothermal process. Ethanol is encapsulated into sodium in a clathrate-like structure. Meanwhile, 2D network of GNPs and SG represent the typical sheet like morphology with folding and crumbles over the sheets. The graphene layers are stacked together by weak van der Waals forces. Energy dispersive spectroscopy (EDS) spectrum of GF (Figure 4.1 (b)) shows signals for the presence of carbon, oxygen and sodium with weight percentages of 77.62, 20.03 and 2.35%, respectively. The presence of oxygen and sodium is attributed to the sodium carbonate (Na_2CO_3), formed upon the pyrolysis reaction. Meanwhile for EDS spectra of GNPs (Figure 4.1 (d)) and SG (Figure 4.1 (f)), only carbon signal was observed with weight percentage of 100%.

The size distribution of the graphene-based materials was summarized in Figure 4.2 (a-c) based on the SEM image analysis of over 150 particles. The measurement was taken at more than 6 different locations using ImageJ software. The lateral size of GF, GNPs and SG particles are distributed over a broad range with mean values of 32 μm, 38 μm and 44 μm, respectively. In addition, average lateral size, BET surface area and pore volume of the particles are reported in Table 4.1. GF exhibited the lowest average lateral size, but the highest BET surface area than those of GNPs and SG, is attributed to the high porosity which lead to extremely high in surface area. As reported by Chen *et al*. (2011), GF structure has high surface area because of its many nanoscopic pores.

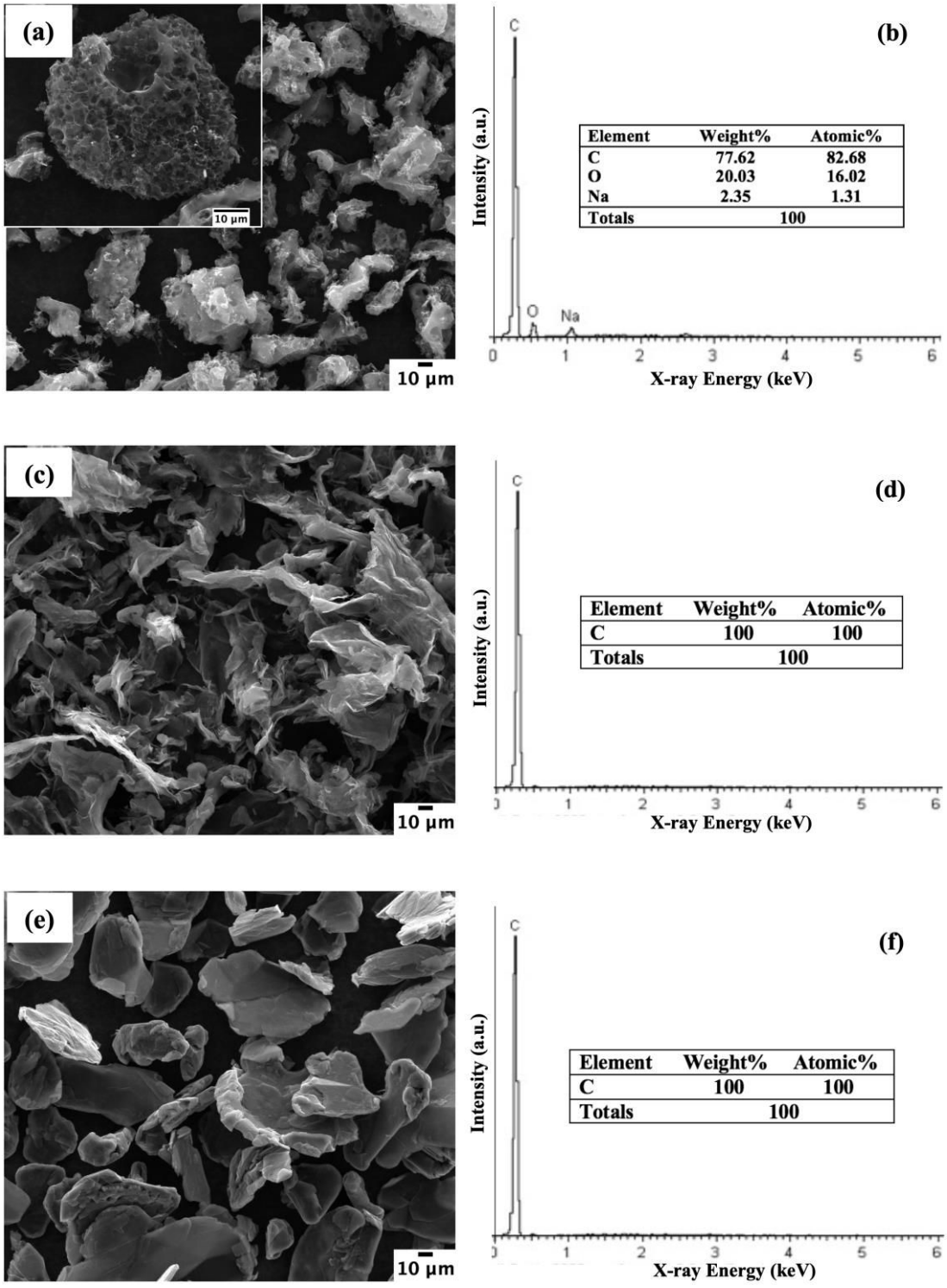

Figure 4.1 SEM micrographs of (a) GF, (c) GNPs and (e) SG particles [1000X mag.], the inset is an image of porous GF at 2000X mag., EDS analysis of (b) GF, (d) GNPs and (f) SG particles

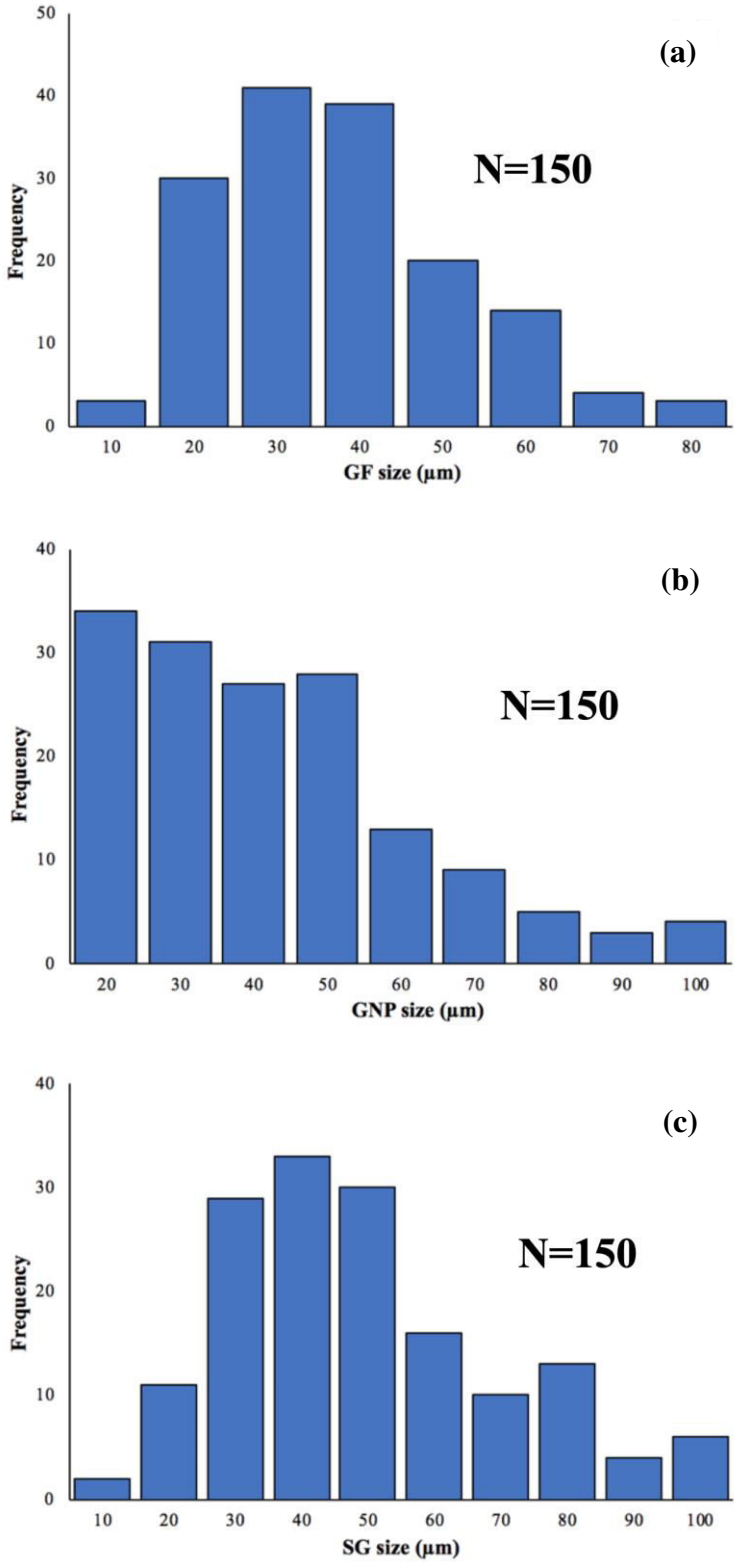

Figure 4.2 Lateral size distribution histogram measured by ImageJ of (a) GF, (b) GNPs and (c) SG particles

Table 4.1 Average lateral size, BET surface area and pore volume of the graphene-based materials

Sample	Average lateral size (μm)	BET surface area (m^2g^{-1})	Pore volume (cm^3g^{-1})
GF	32 ± 14.10	2136	0.138
GNPs	38 ± 21.51	25	0.003
SG	44 ± 20.75	3	0.001

Figure 4.3 illustrates the high resolution transmission electron microscopy (HRTEM) images of (a, b) GF, (c, d) GNPs and (e, f) SG particles. Based on Figure 4.3 (a), it is observed that GF consists of folded edges almost throughout the GF structure and amorphous carbon regions can be seen. Amorphous carbon can be seen by observing of highly buckled GF particle. The presence of amorphous carbon region is due to the crystallization of GF which is considered by Speyer *et al*. (2015) as incompleted. Eleven parallel lines could be observed from the image captured by HRTEM, an early indication that it was a multi-layer graphene. Meanwhile GNP and SG samples indicated transparent sheet-like structures and suggested that the carbon particles presented better crystallinity with ordered planar regions. The number of graphene layers for GNP and SG are 10 layers and 46 layers, respectively. Besides that, GNP and SG also exhibited crumpled and less folded edges as compared to GF. The folded edges appeared more in GF structure than in GNP and SG structures. This is due to the tendency of GF particles to overlap, as a result of the high surface area of the extended thin layers. The interlayer distance for GF, GNP and SG were 0.33nm, 0.34 nm and 0.33 nm, respectively.

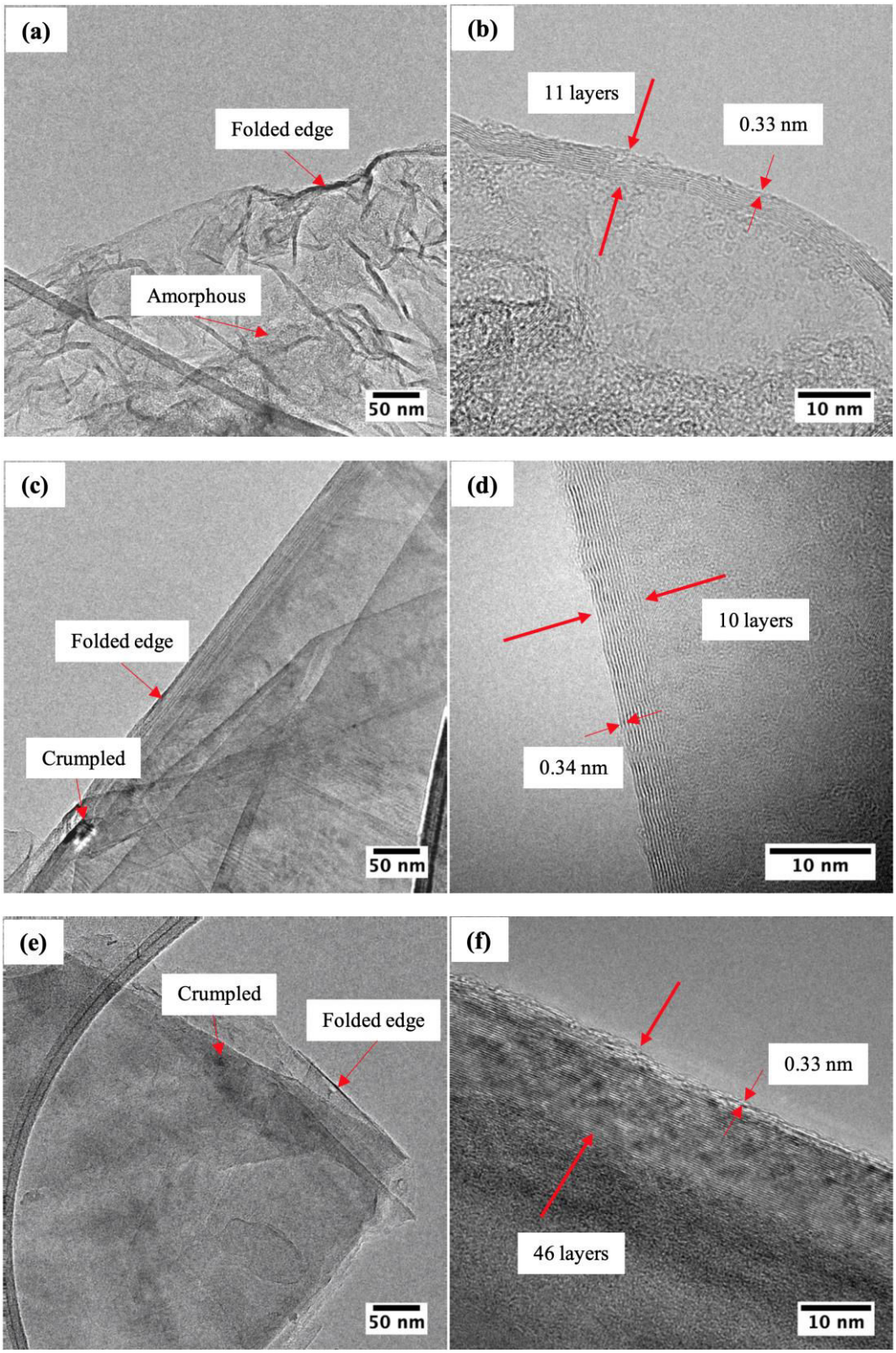

Figure 4.3 HRTEM micrographs of (a, b) GF, (c, d) GNPs and (e, f) SG particles at magnifications of (a, c, e) 97kX and (b, d, f) 690 kX

The crystallographic structure of the graphene-based materials was characterized by selected area electron diffraction (SAED), as shown in Figure 4.4 (a-c). According to Egerton (2005), SAED pattern was used to identify the crystallinity of the material, whether the sample is amorphous (diffuse ring), crystalline (bright spots) or polycrystalline (small spots making up a rings). The SAED for GF particle exhibited diffraction ring pattern which indicate polycrystalline features in an amorphous material. On the other hand, the symmetrical and isolated points arranged in a hexagonal pattern shows the high crystallinity of GNPs particle. Meanwhile the SAED for SG with 46 layers exhibited the disorderly lattice arrangement showing how thick the particle was. Similar patterns were observed by Htwe *et al*. (2019) in their study on the formation of graphene using an electrochemical exfoliation process.

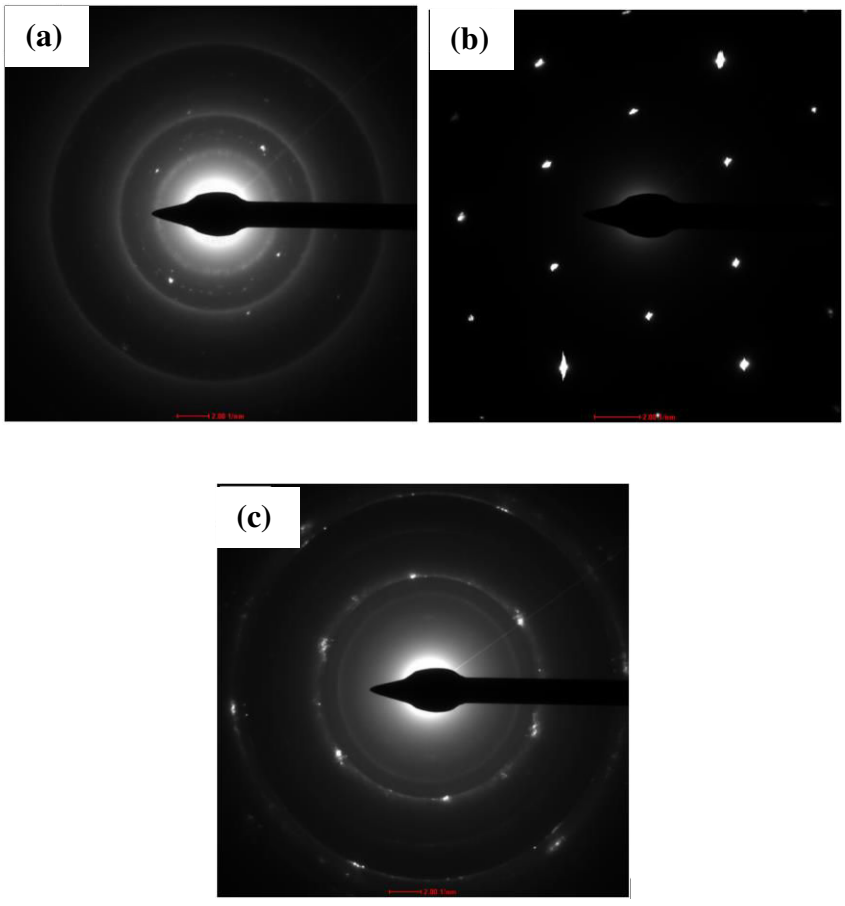

Figure 4.4 SAED of (a) GF, (b) GNPs and (c) SG particles

4.1.2 X-ray diffraction analysis

Figure 4.5 illustrates the X-ray diffraction (XRD) patterns of graphene-based materials. The indexation of the XRD patterns revealed that GF sample contained hexagonal graphite (space group *P*6$_3$/*mmc,* a = 246 pm, c = 671 pm) and a set of graphitic structures with stacking faults, noted turbostratic carbons (space groups *P*6$_3$/*mmc* or *R*-3*m*, a = 252 pm, c varying from 412 pm to 4324 pm) and orthorhombic carbon (space group *Cmma*, a = 458 pm, b = 530 pm, c = 563 pm). A space group is the symmetry group of a configuration in space, usually in three dimensions. A space group P6$_3$/*mmc* referring to the hexagonal structure and *Cmma* referring to the orthorhombic structure. This is consistent with the TEM observations, as shown in Figure 4.3 (a, b). The GF presented supplementary crystalline phases: sodium carbonate (Na_2CO_3) (space group C12/*m*1, a = 891 pm, b = 524 pm, c = 605 pm, β = 101.32°) resulting from the reaction of pyrolysis. Na_2CO_3 with monoclinic structure was found using EVA software, in which the diffraction peak corresponding to Na_2CO_3. Besides that, the presence of Na_2CO_3 is consistent with the nature of reactants. Similar observation was reported by Speyer *et al*. (2015). In spite of a washing step with concentrated hydrochloric acid, there was Na_2CO_3 remained in the sample because it is trapped into cavities of the graphene structures. Orthorhombic graphite and turbostratic carbons were both described as intermediate phases occurring in the graphite-to-diamond phase transition (Ownby *et al*., 1992; Fayos, 1999).

Meanwhile for sample GNPs and SG samples, the presence of sharp narrow (002) peak at 2θ value of 12° which corresponds to an interlayer distance, *d* of 0.33 nm and therefore confirms the crystalline structure of GNPs and SG samples. This is also related to the distance between the different layers of the GNPs and SG structures (Carotenuto *et al*., 2013).

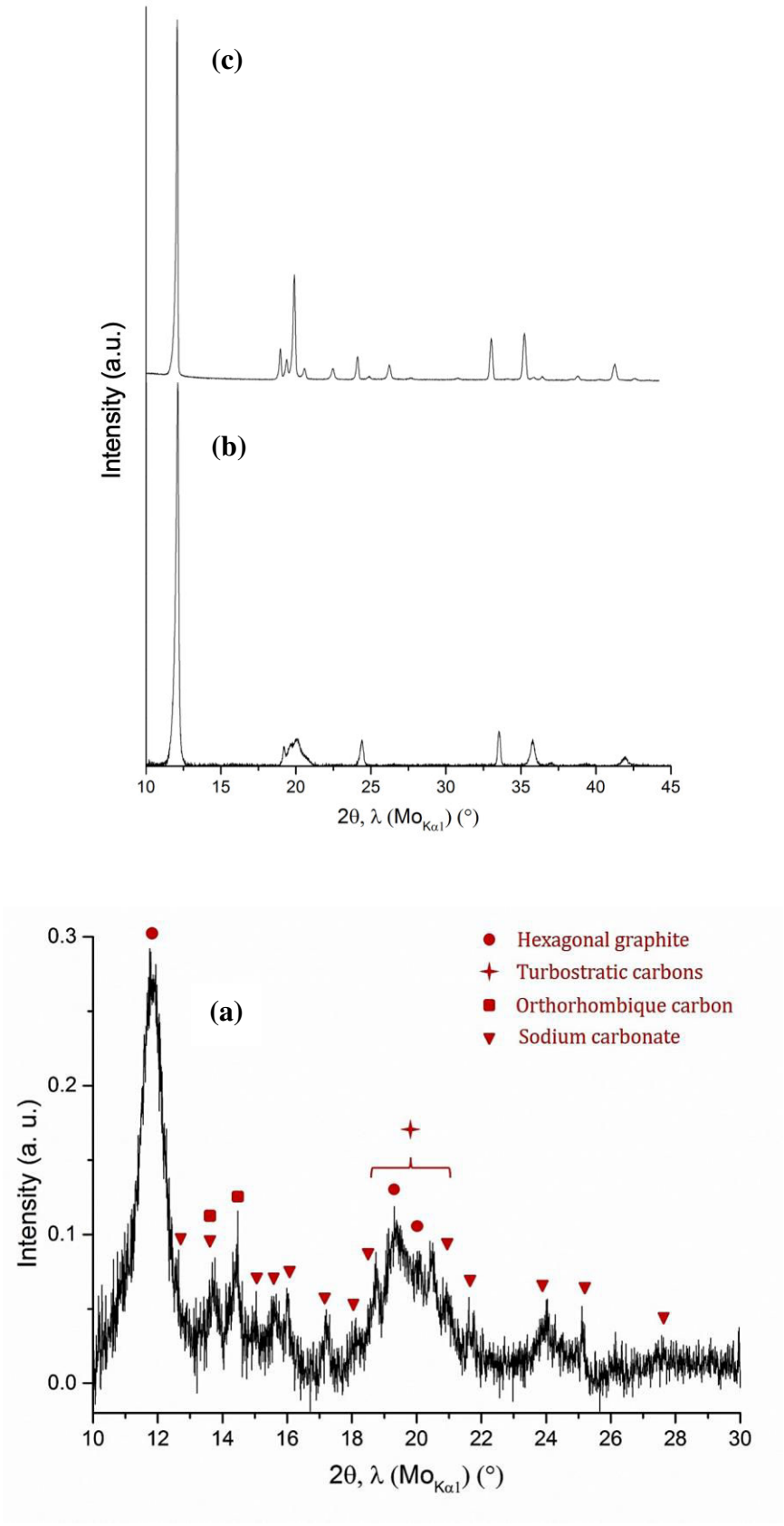

Figure 4.5 XRD patterns of (a) GF, (b) GNPs and (c) SG particles

GNPs and SG have high crystallinity than GF due to the sharp and narrow of (002) peak as shown in Figure 4.5, corresponding to the stacking of GNPs and SG particles were well-ordered. Meanwhile, the (002) peak of GF was broader and weak, showing the stacking of GF particle was not well-ordered due to the presence of semi-crystalline phase in GF, as confirmed by HRTEM images (Figure 4.3 (a,b)).

The full widths at half-maximum of the (002) peak (FWHM) were studied to determine the crystallite size (Amaro-Gahete *et al*., 2019). This is attributed to the strong peak at 12° (2θ), corresponding to the graphite reflection and preferred orientation of graphite (Simón et al., 2018). The crystallite size, L_c of the graphene-based materials was determined using the Scherrer's equation, $L_c = k\lambda_{Mo}/\beta cos\theta$ at (002) peak, where k is a constant (k =0.91), λ_{Mo} is the wavelength of X-ray (Å), β is the full-width at half maximum (FWHM) of the (002) peak (radian) and θ is the Bragg angle (°). Meanwhile the average number of graphene layers (n) was calculated using the following equation, $n = L_c/d$ where d is the interlayer distance. Results are reported in Table 4.2. Based on the obtained results, the graphene-based materials consist of multi-layer graphene. It is worth noting that XRD allows the detection of a thicker regions of samples. However, Scherrer's equation provides higher median values as compared to the thin regions observed by HRTEM. Moreover, hexagonal graphite is just one part of the sample and other crystalline structures must be taken account.

Table 4.2 The crystallite size (L_c), interlayer distance (d) and number of layers (n) of the graphene-based materials

Sample	Crystallite size, L_c (nm)	Interlayer distance, d (nm)	Number of layers, n
GF	3.8	0.33	11
GNPs	3.7123	0.34	11
SG	4.8253	0.33	15

4.1.3 Fourier-transform infrared spectroscopy analysis

Figure 4.6 shows the fourier-transform infrared (FTIR) spectra of GF, GNPs and SG particles. FTIR analysis provides evidence for the presence of oxygen-containing functional groups attached to the graphene-based materials. The FTIR spectrum of GF is slightly similar to GNPs and SG spectra. However, the peak appeared at around 3417 cm^{-1} for sample GF is broad and intense than those of GNPs and SG which attributed to the presence of stretching vibrations of hydroxyl group (O-H) in relation to the hydrogen bonding between network of GF particle. The large particles of samples GNPs and SG act as a barrier for the oxidation which only allow small number of oxygens containing groups are retaining throughout the graphite layers. Thus, the characteristic O-H stretching is weak and less intense in the spectra of GNPs and SG. A similar trend was observed by Manoratne *et al*. (2017).

The weak peak near 2924 cm^{-1} and 2854 cm^{-1} corresponding to the asymmetric and symmetric stretching vibration of C-H groups. Meanwhile, the strong peak at 1625 cm^{-1} and weak peak at 1578 cm^{-1} and 1440 cm^{-1} are attributed to the C=C stretching vibration indicated the skeletal vibration of the graphitic zone, aromatic sp^2 carbon ring

and C=O stretching vibration. The moderate peak at 1320 cm^{-1}, 1374 and 1047 cm^{-1} corresponding to C-O-H bending, O-H bending and C-O stretching, respectively.

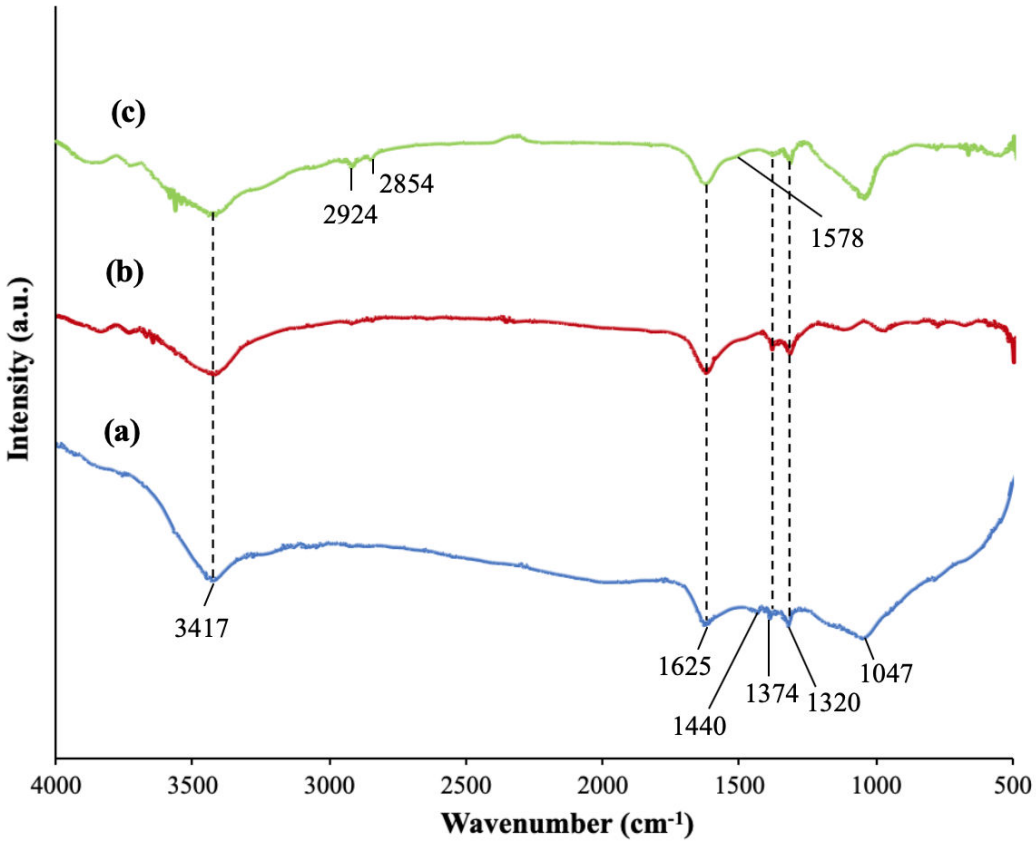

Figure 4.6 FTIR spectra of (a) GF, (b) GNPs and (c) SG particles

4.1.4 Raman spectroscopy analysis

Figure 4.7 shows the Raman spectra of the graphene-based materials. Raman spectroscopy is a versatile tool to get useful information about carbonaceous materials. There are three disorder-related bands that are prominent for Raman spectra of graphite, including the D peak at around 1350 cm^{-1}, G peak at around 1580 cm^{-1} and 2D peak at around 2700 cm^{-1}. By using the Raman spectra, it is possible to identify the amounts of defects and their types (D band), in-plane sp^2 hybridized carbon atoms (G band),

stacking order and the number of layers (2D band) in graphene samples (Ferrari *et al*., 2006; Cançado *et al*., 2008).

In general, similar peaks were observed in the three types of graphene-based materials. In Figure 4.7 for GF sample, Raman spectrum showed peaks at 1329 cm^{-1} (D-band), 1589 cm^{-1} (G-band) and 2663 cm^{-1} (2D-band). For GNPs sample, Raman spectrum exhibited peaks at 1339 cm^{-1} (D-band), 1581 cm^{-1} (G-band) and 2689 cm^{-1} (2D-band). Meanwhile for SG sample, Raman spectrum presented peaks at 1346 cm^{-1} (D-band), 1580 cm^{-1} (G-band) and 2685 cm^{-1} (2D-band). The broadened of D-band and G-band of GF spectrum is attributed to the presence of amorphous carbon. Besides that, two additional peaks were observed for GF spectrum at around 1150 cm^{-1} (A-band) corresponds to nanocrystalline diamond and sp^3 defects, also at around 1450 cm^{-1} (B-band) corresponds to nanocrystalline graphite and sp^2 clusters in a sp^3 matrix (Ferrari and Robertson, 2000; Ferrari and Robertson, 2001; Speyer *et al*., 2018).

The defect of the particles can be determined by measuring the intensity ratio of the D and G peaks (I_D/I_G) (Tang *et al*., 2012). Based on Table 4.3, the intensity ratios of the D-band to the G-band (I_D/I_G) of GF, GNPs and SG were calculated as 1.07, 0.34 and 0.56, respectively. Higher value of I_D/I_G can be related to the higher degree of disorder or higher defect concentration. From the result, GF sample exhibited the highest value of I_D/I_G compared to those of GNPs and SG samples meaning that large area of graphene foam has low structural quality. Besides that, for AB-stacked graphene, the number of layers could be derived from the ratio of peak intensities for 2D and G (I_{2D}/I_G). The ratios of I_{2D}/I_G for GF, GNPs and SG were 0.42, 0.70 and 0.74, respectively which indicates the graphene-based materials consist of multi-layer graphene.

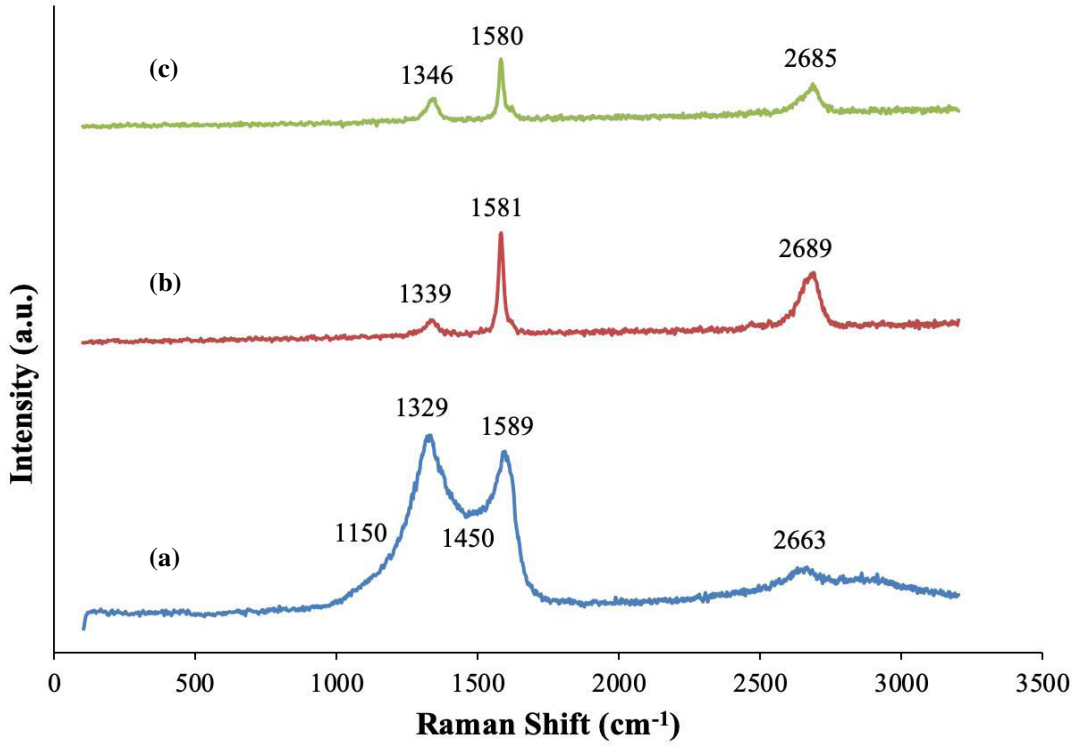

Figure 4.7 Raman spectra of (a) GF, (b) GNPs and (c) SG particles

Table 4.3 Raman intensity of the graphene-based materials

Sample	I_D	I_G	I_{2D}	I_D/I_G	I_{2D}/I_G
GF	1511	1400	594	1.07	0.42
GNPs	312	918	642	0.34	0.70
SG	351	622	458	0.56	0.74

4.1.5 X-ray photoelectron spectroscopy analysis

The surface characterization, chemical composition, types of carbon and oxygen bonds and the percentage of oxygen present in the graphene-based materials were investigated by using X-ray photoelectron (XPS), as illustrated in Figure 4.8 (a-c). The XPS spectra are dominated by a featured around 284 eV and 532 eV corresponding to C 1s and O 1s. The peak corresponding to C 1s suggests sp^2 hybridized carbon atoms

in the graphene-based materials, meanwhile the peak relate to O 1s indicated the presence of various oxygen functionalization in the carbon particles structure (Yang *et al*., 2009; Sahoo and Mallik, 2015; Htwe *et al*., 2019). For GF particle, chloride and sodium were detected as contaminants, as a results of sodium carbonate was trapped in carbon structures even after washing with concentrated hydrochloric acid. The carbon, oxygen and O/C ratio were obtained through elemental analysis measurement by XPS analysis, as presented in Table 4.4. The graphene-based materials showed approximately 0.050, 0.008 and 0.017 weight ratio carbon to oxygen corresponding to GF, GNPs and SG particles, respectively. Higher oxygen content in GF particle is attributed to the sodium carbonate formed during the pyrolysis reaction, parallel with the SEM-EDS and XRD results in Section 4.1.1 and 4.1.2.

The peak at around ~284 eV was deconvoluted in order to understand the oxygen functionality in the graphene-based materials. Further deconvolution of C 1s peak as presented in Figure 4.9 shows that the majority of the binding energy comes from sp^2 C=C, C-O, C=O and O-C=O bonds. The main peak at binding energy of 284.5 eV is assigned to the C=C bond which represent sp^2 hybridized carbon atoms in the graphene-based materials sheet. Three peaks at 286.0, 287.5 and 288.5 eV corresponding to C-O (epoxide), C=O (carbonyl) and O-C=O (carboxyl COOH) (Johra *et al*., 2014). These results correlated with the FTIR analysis indicates the presence of oxygen functional groups. Besides that, the multi-layer GNPs have quite good quality, followed by SG and GF, in agreement with Raman results in Section 4.1.4.

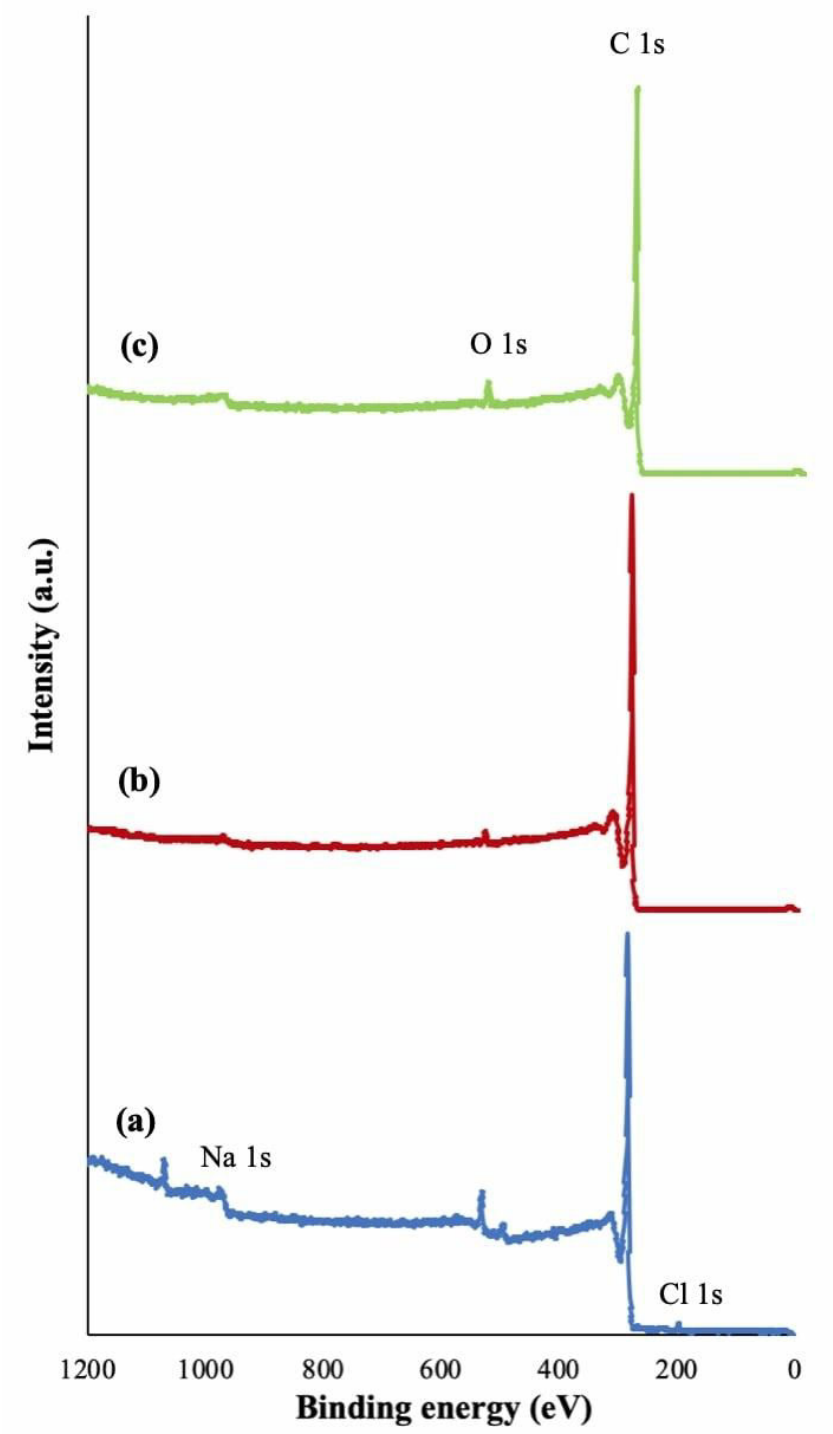

Figure 4.8 XPS spectra of (a) GF, (b) GNPs and (c) SG particles

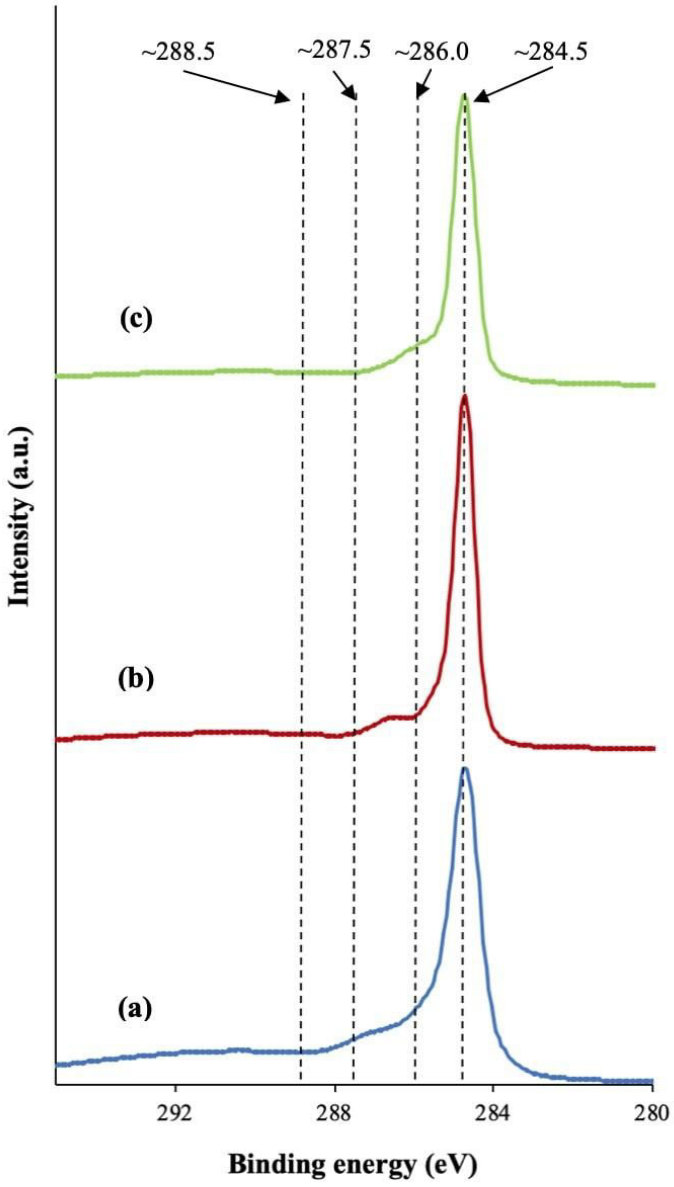

Figure 4.9 C 1s spectra band highlighted of (a) GF, (b) GNPs and (c) SG particles

Table 4.4 The elemental compositions of carbon (C 1s), oxygen (O 1s) and O/C atomic ratio of the graphene-based materials

Sample	C (wt%)	O (wt%)	O/C
GF	93.98	4.64	0.050
GNPs	99.17	0.83	0.008
SG	98.31	1.69	0.017

4.1.6 Thermal properties

Thermal stability of the particles is an important factor in processing and during application at high temperature since it affects the performance of the materials. Figure 4.10 and Table 4.5 show the TGA curves and thermal analysis data of the graphene-based materials. Only one degradation step was observed for all samples. GF thermogram exhibited a major loss between 300 ºC and 450 ºC due to the decomposition of amorphous carbon which started at around 300 ºC to 500 ºC (Dillon *et al*., 1999). GF has low thermal stability than GNPs and SG due to low crystallinity and the presence of impurities; *e.g.* Na_2CO_3. The final mass loss of sample GF at 1000 ºC has approximately 10% by weight remaining due to the presence of residual Na_2CO_3. This is in accordance with XRD results in Section 4.1.2 which indicated Na_2CO_3 may be trapped in carbon structures formed due to the reaction of pyrolysis. Meanwhile, GNPs thermogram shown a major loss between 500 ºC and 780 ºC and SG thermogram exhibited a major loss between 600 ºC to 850 ºC. According to Turkdogan and Vinters (1969), graphite starts burning above 700 ºC to 800 ºC. The residue at 1000 ºC for both GNPs and SG samples were almost equal to zero.

The initial degradation temperature, $T_{5\%}$ (ºC), onset degradation temperature, T_{onset} (ºC) and weight of residue at 1000 ºC are reported in Table 4.5. The TGA results showed that GNPs and SG exhibited higher $T_{5\%}$ and T_{onset} compared to GF. The results revealed that GNPs and SG have better thermal stability compared to GF.

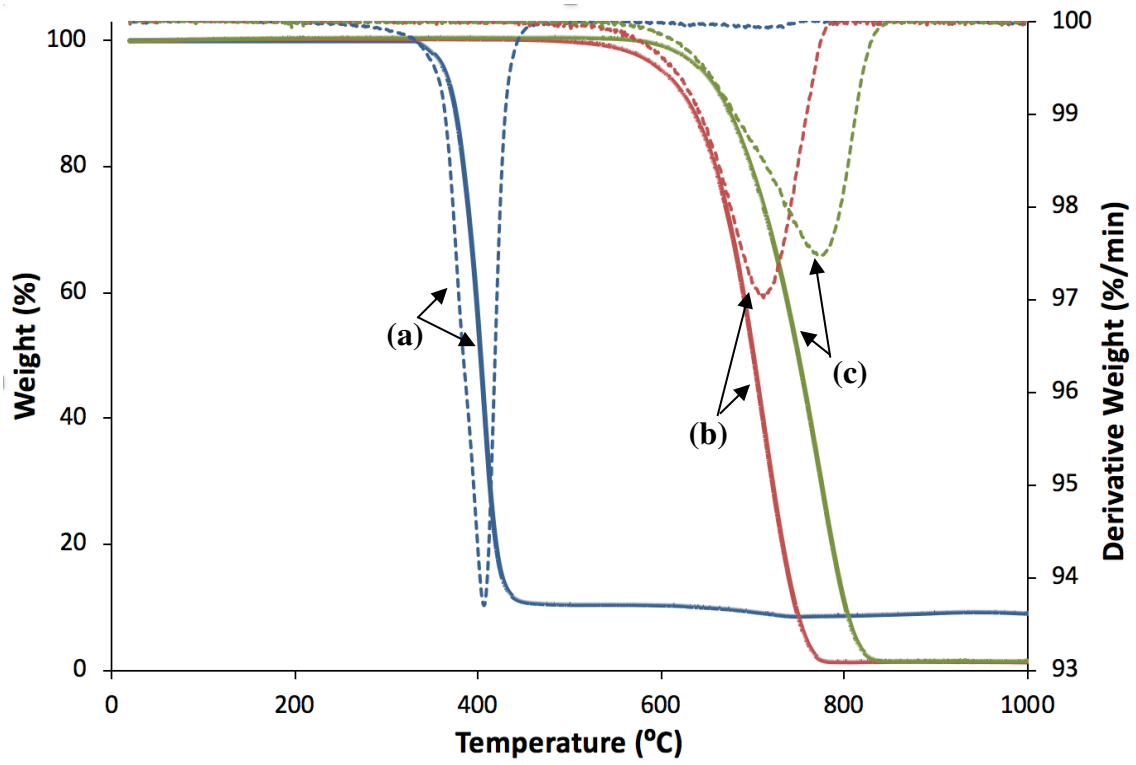

Figure 4.10 Weight loss (solid line) and derivative weight loss (dotted line) of (a) GF, (b) GNPs and (c) SG particles with respect to temperature

Table 4.5 Decomposition temperature and weight of residue of the graphene-based materials

Sample	Initial degradation temperature, $T_{5\%}$ (°C)	Onset degradation temperature, T_{onset} (°C)	Weight of residue at 1000 °C (%)
GF	364	370	10
GNPs	603	650	0
SG	646	685	0

4.2 Properties of graphene-based materials mixed with polyester varnish binder

The second objective of the present research is to investigate the ink properties of graphene-based materials mixed with polyester varnish (PV) binder and determine the electrical conductivity of the sprayed patterns. The properties of conductive inks made from various graphene-like materials including the viscosity, contact angle and surface energy were investigated.

4.2.1 Visual observation

The graphene-based materials mixed with PV binder were observed over time, before and after 15 minutes of sonication time, as presented in Figure 4.11. As can be observed, the graphene-based materials dispersed well with PV after sonication which turned from yellowish solution into black solution.

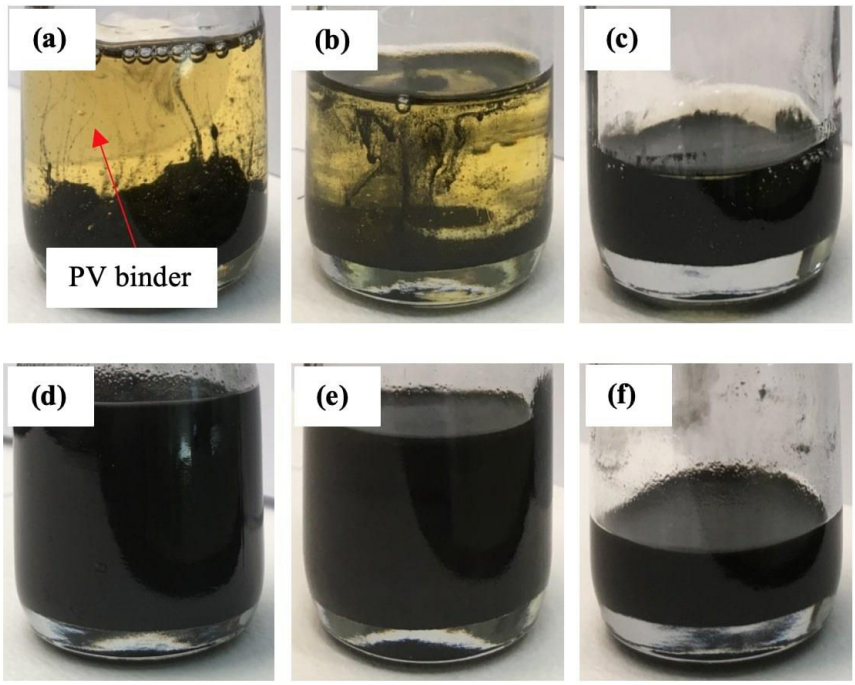

Figure 4.11 Photographs of (a, d) GNPs ink, (b, e) SG ink and (c, f) GF ink were observed at (a-c) before sonication and (d-f) after sonication

4.2.2 Viscosity analysis

Figure 4.12 (a) illustrates the viscosity, η curves of graphene-based materials inks at 5 vol.% as a function of shear rate. It was observed that the η for all inks decreased with increasing shear rate within a range of 1.5-500 s^{-1}, exhibiting shear-thinning flow behaviors. The η is considered to be stable at high shear rates value. The attraction between the graphene-based materials induces flocculation in the inks which causes an immobility of the solvent suspending the particles and therefore increased the η at low shear rate (Woo *et al*., 2013). In comparison, at higher shear rate, the flocculation breaks down and promotes the mobility of solvent entrapped between particles causes the η to be decreased.

Meanwhile Figure 4.12 (b) shows the η variation as a function of filler loadings. It is clearly indicated that the addition of graphene-based materials at 5 vol.%, at 500 s^{-1} shear rate showed increment in η of the inks by 114% (GNPs ink), 55% (SG ink) and 16% (GF ink) as compared to the unfilled PV binder (η = 0.18 Pas). The η values of the inks were different even at the same filler loading due to the different size and shape of the fillers. Even though GF exhibited the highest BET surface area as compared to GNPs and SG which supposed to increase the η value of the ink, different trend was observed. The small increment in the η value of GF ink is attributed to aggregation between the GF particles, as confirmed by HRTEM analysis in Section 4.1.1. Similar observation was observed by Vallés *et al*. (2014) as the viscosity of GO suspension increased slightly due to aggregation between the GO flakes.

Figure 4.12 (c-e) shows that the η curves as a function of shear rates predicted by the Carreau model, as well as the experimental data. The Carreau model was used to describe the shear thinning behaviour of the polymers and conductive inks. The liquid

acts as a Newtonian fluid at a low shear range and as a power-law fluid at a high shear range (Ankireddy *et al*., 2013; Dybowska-Sarapuk *et al*., 2018). The prediction η was calculated using Carreau model, as shown in Equation 4.1.

$$\eta(\gamma) = \eta_\infty + (\eta_0 - \eta_\infty)(1 + (\chi\gamma)^2)^{\frac{n-1}{2}} \quad (4.1)$$

where: η_∞- viscosity at infinite shear rate, η_0 – viscosity at zero shear rate, χ – relaxation time, n – power index. The $\eta_\infty = 0$, $\eta_0 > 0$, $\chi < 1$ and $n < 1$, respectively. From Figure 4.12 (c-e), the Carreau model agreed relatively well with the experimental data over a wide range of the shear rate for GNPs ink, SG ink and GF ink.

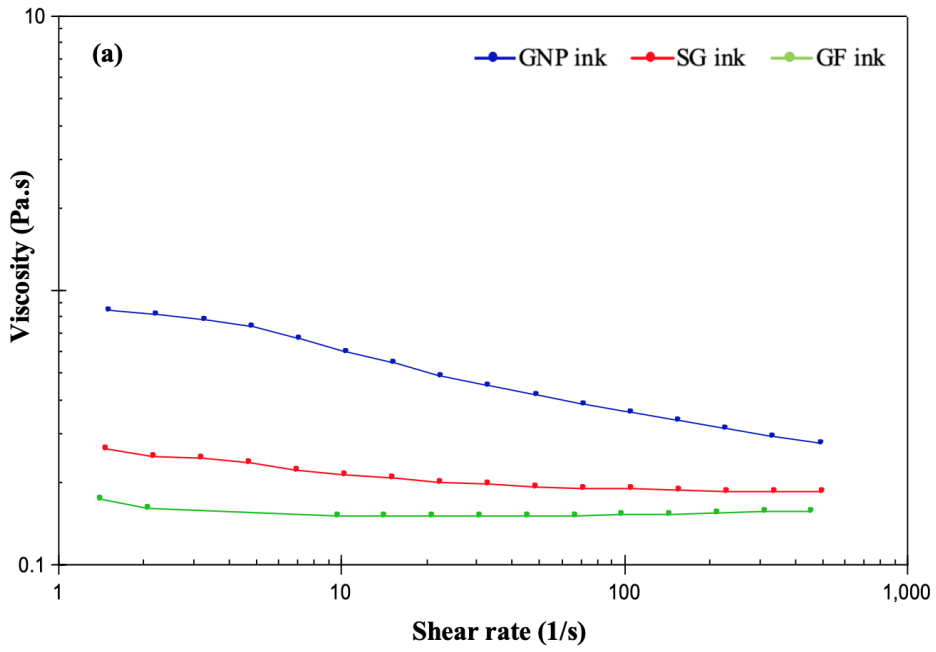

Figure 4.12 (a) Viscosity curves of conductive inks at 5 vol.% as a function of shear rate, (b) viscosity variation as a function of filler loadings at 500 s-1 shear rate, and viscosity curves of (c) GNPs ink, (d) SG ink and (e) GF ink with fitted Carreau Model curve

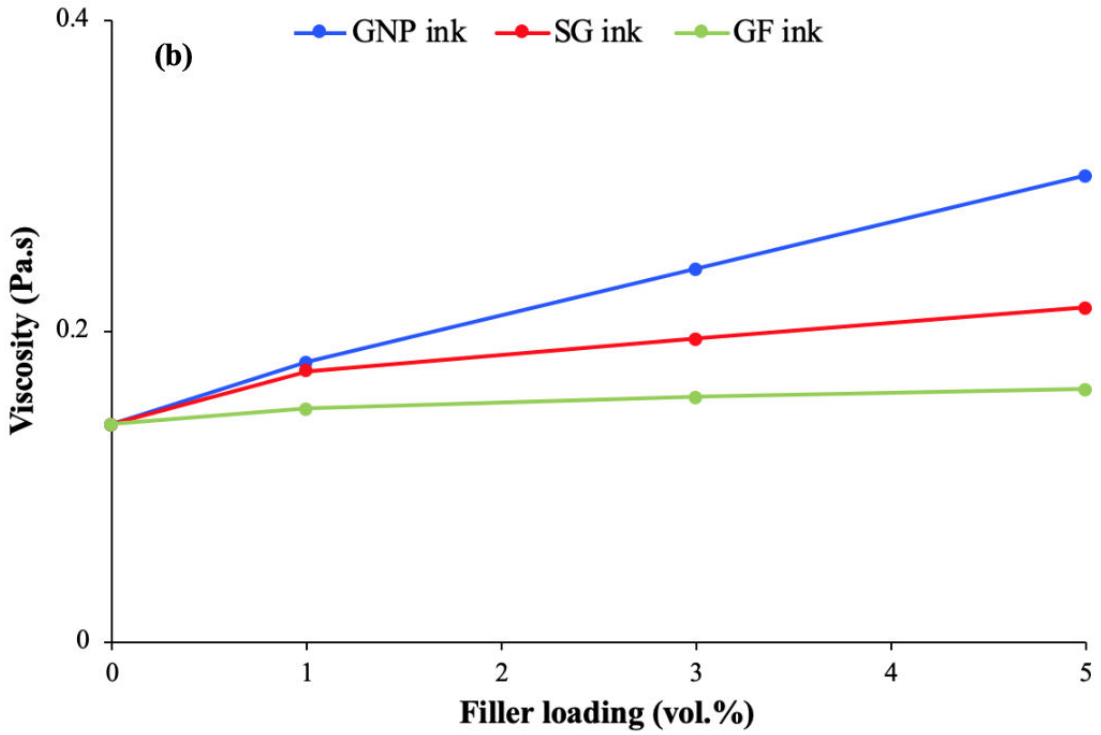

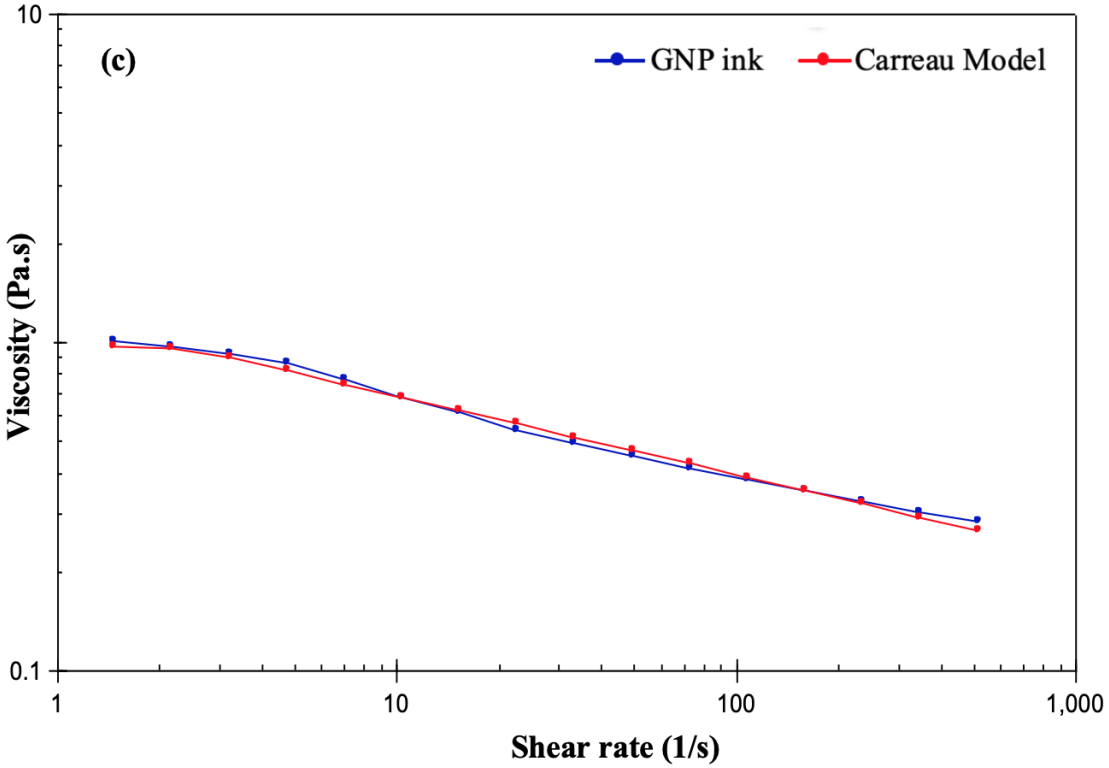

Figure 4.12 *Continued*

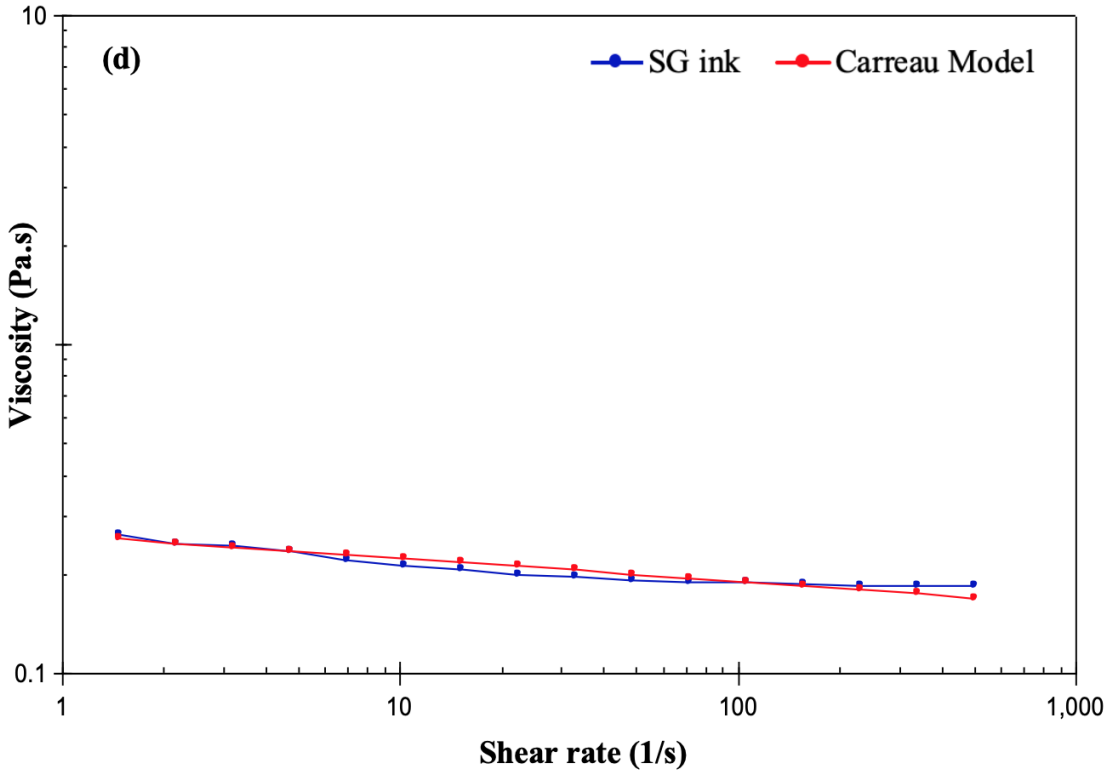

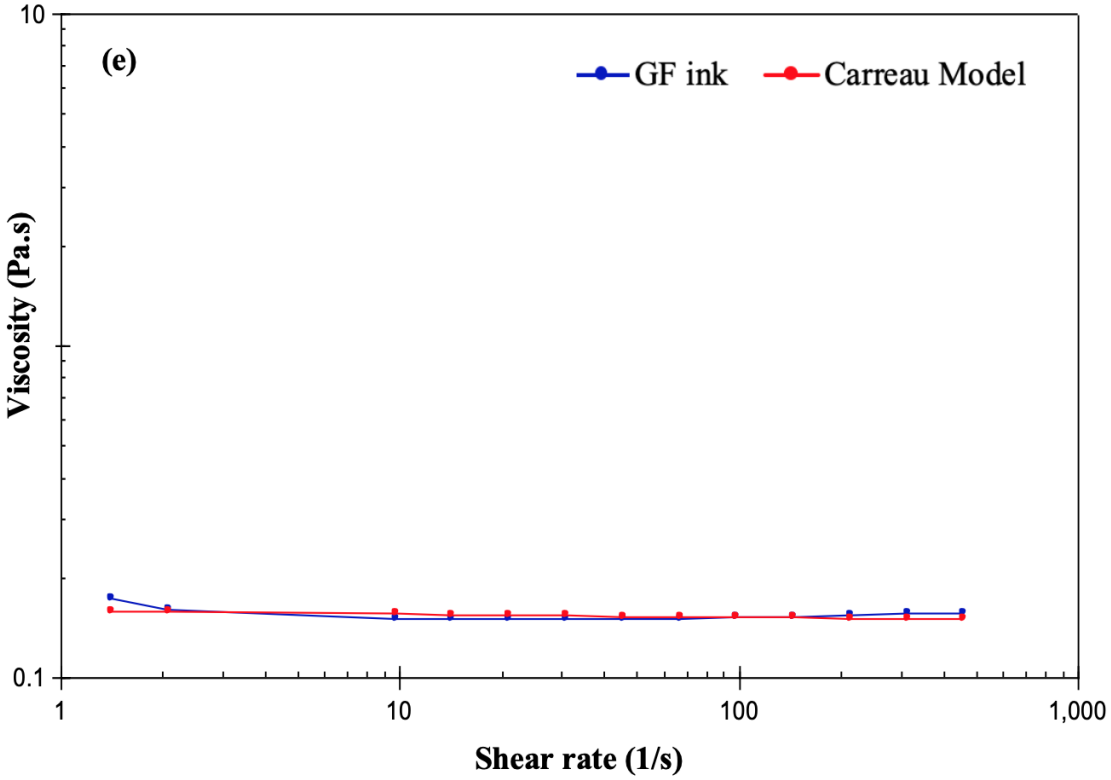

Figure 4.12 *Continued*

4.2.3 Surface wettability analysis

Besides the physical properties of the prepared inks, surface wettability of the ink with the substrate is also the factor which influence the spray pattern quality. Contact angle, θ_c is an indication of the wetting performance of liquids applied to solids. The contact angle is measured as the angle between the base and the tangent at the point of contact between conductive ink and surface of transparency film. Figure 4.13 (a, b) illustrates the droplet shape just before it lands on the transparency substrate and when the drop settled on the substrate. Figure 4.13 (c) indicates that the θ_c for all conductive inks increased with an increasing of filler loadings in PV binder due to lowering the surface energy (γ_{SL}). Lowering the γ_{SL} means the cohesive force dominate, caused the ink droplet to bead up on the film surface and therefore, increased the θ_c. The increment of graphene-based materials in PV binder also affects the droplet θ_c on the substrate due to the change in η but the conductive inks still showing hydrophilic characteristics, $\theta_c < 90°$ which lead to a better ink-substrate combination.

GF ink has the lowest θ_c than those of GNPs and SG inks. GF surface was grafted with hydroxyl group (OH) and more oxygen content, as explained in Section 4.1.3, which changed the polar properties from hydrophobic to hydrophilic. GNPs and SG consist almost entirely of carbon and hydrogen atoms, and have hydrophobic characteristics. Meanwhile PV binder has a hydrophilic characteristic due to ester groups in polyester chain are polar. Due to that, GF has better affinity for PV binder as they attract to each other and reduced the θ_c.

The surface energy relation between liquid, solid and gas interfaces can be expressed by Young's equation $\gamma_S = \gamma_{SL} + \gamma_L \cos\theta$, where γ_L is the surface energy of the liquid, γ_{SL} is the surface energy between solid to liquid interface, and γ_S is the

surface energy of the solid (Michel *et al*., 2016). The γ_{SL} from the measured θ_c for all conductive inks were calculated and shown in Figure 4.14. The γ_{SL} slightly decreased with an increasing of the graphene-based materials loadings. This is attributed to the high amounts of graphene-based materials presented at the surface of the droplets at high filler loadings and therefore, reduced the γ_{SL} of the conductive inks. However, the slight decrement in γ_{SL} was not influenced the sprayed pattern quality between conductive ink and the substrate, where the θ_c is still <90°. The result is parallel with the previous work by Ankireddy *et al*. (2013) where the γ_{SL} of the silver nanoparticle-based inks decreased with increasing concentration of the particles in the inks.

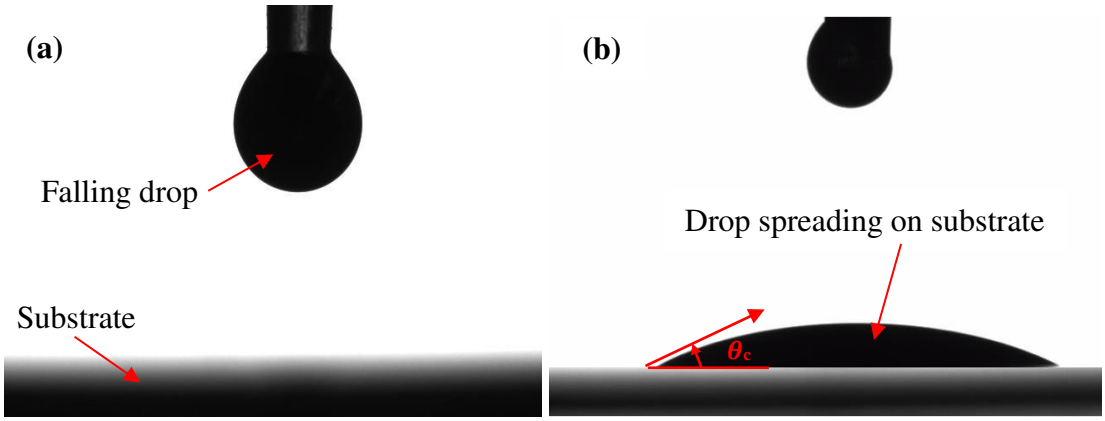

Figure 4.13 Illustration of contact angle measurement (example: 1 vol.% GF ink) when: (a) drop falling and (b) as the drop settled on the surface of the substrate, (c) contact angle variation as a function of filler loadings, inset showing (i) small and (ii) high contact angle

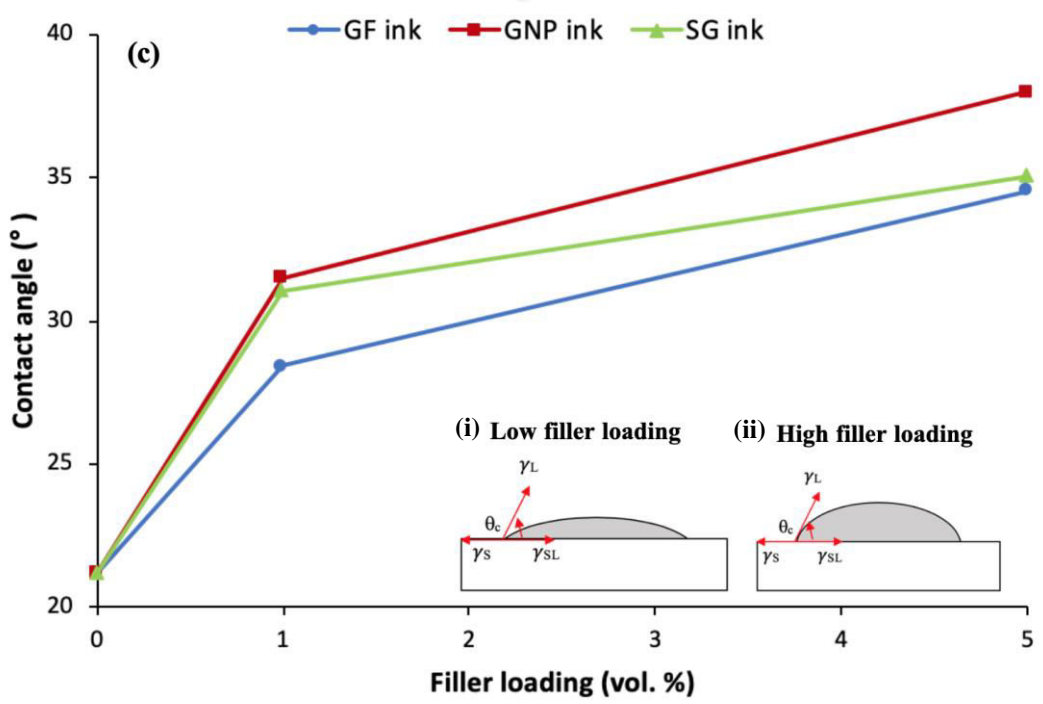

Figure 4.13 *Continued*

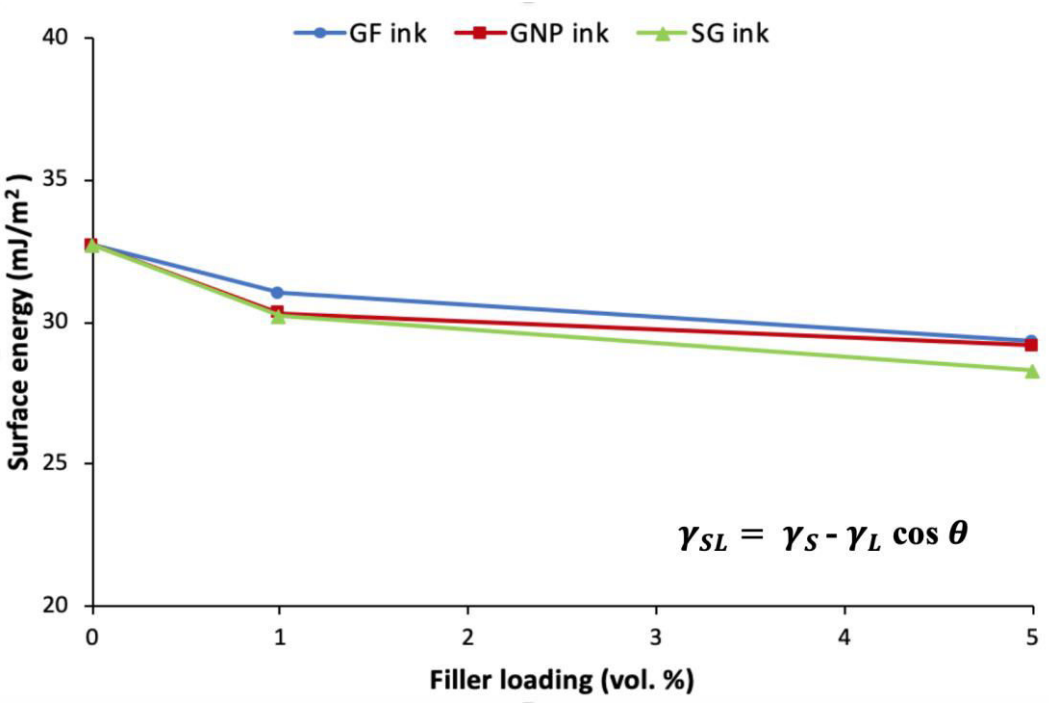

Figure 4.14 Surface energy as a function of filler loadings including Young's equation

4.2.4 Electrical conductivity properties

The conductive ink patterns made of various graphene-based materials at different loading in PV binder were fabricated in order to determine the percolation threshold. Figure 4.15 presents the electrical conductivity of various conductive inks as a function of filler loadings. Obvious different filler loadings were used in the formulation of conductive inks due to the η. Based on the formulations, higher amount of GF filler was used to mix with polyester varnish as compared to GNPs and SG at the same filler loading due to the low density of GF. However, the conductive inks become very difficult to dispense at higher filler loading due to high η.

It can be observed that the electrical conductivity of all samples increased evidently with increasing filler loadings (Figure 4.15). Conductive ink made of GNPs shows the highest electrical conductivity, followed by SG ink and GF ink at all filler loadings. Even though GF exhibited the highest BET surface area than those of GNPs and SG which supposed to increase the electrical conductivity of the conductive ink pattern, however different trend was observed. This is due to other factors that influenced the electrical conductivity of GF ink including the low crystallinity of GF particle attributed to the presence of semi-crystalline structure and the (002) peak was broader and weak, which reduced the electrical conductivity of GF ink in accordance to low order as there was no regularity in conduction mechanism. Another factor is high oxygen content as the oxide disrupted the C=C bonding network in GF, and low quality of GF particle due to the presence of defect as the defect hinder the charge transport by decreasing the electron movement, as shown in HRTEM, XRD, XPS and Raman analysis, respectively. Due to the above factors, the electrons in GF could not move rapidly through the interconnected network of low-quality GF. Meanwhile the higher

electrical conductivity at all filler loadings of GNPs ink and SG ink were attributed to the large lateral size, high crystalline structure and high quality of GNPs and SG flakes.

For GNPs ink, the percolation threshold is obtained between 4 vol.% and 4.5 vol.% GNP. On further increasing GNPs loading, the electrical conductivity is observed to be increased with values of 1.26 Scm^{-1} at 5 vol.% to 1.86 Scm^{-1} at 10 vol.%. Meanwhile for SG ink and GF ink, the percolation threshold could be observed when SG loading is in between 8 vol.% and 9 vol.% and when GF loading is in between 9 vol.% and 10 vol.%.

A simple electronic circuit was composed of a 9.0 V battery, the sprayed conductive pattern, a capacitor and the LED to demonstrate the behaviour of conductive ink patterns towards the LED brightness. Inset showing digital images of an electronic circuit set up and LED brightness for various types of conductive ink patterns at 10 vol. %. The LED connected to GNPs ink pattern showed the brightest followed by SG ink pattern and GF ink pattern. GNPs ink exhibited remarkable improvement of electrical conductivity, followed by SG ink and GF ink at 10 vol.% than unfilled polyester varnish binder by 186%, 40% and 10%, respectively.

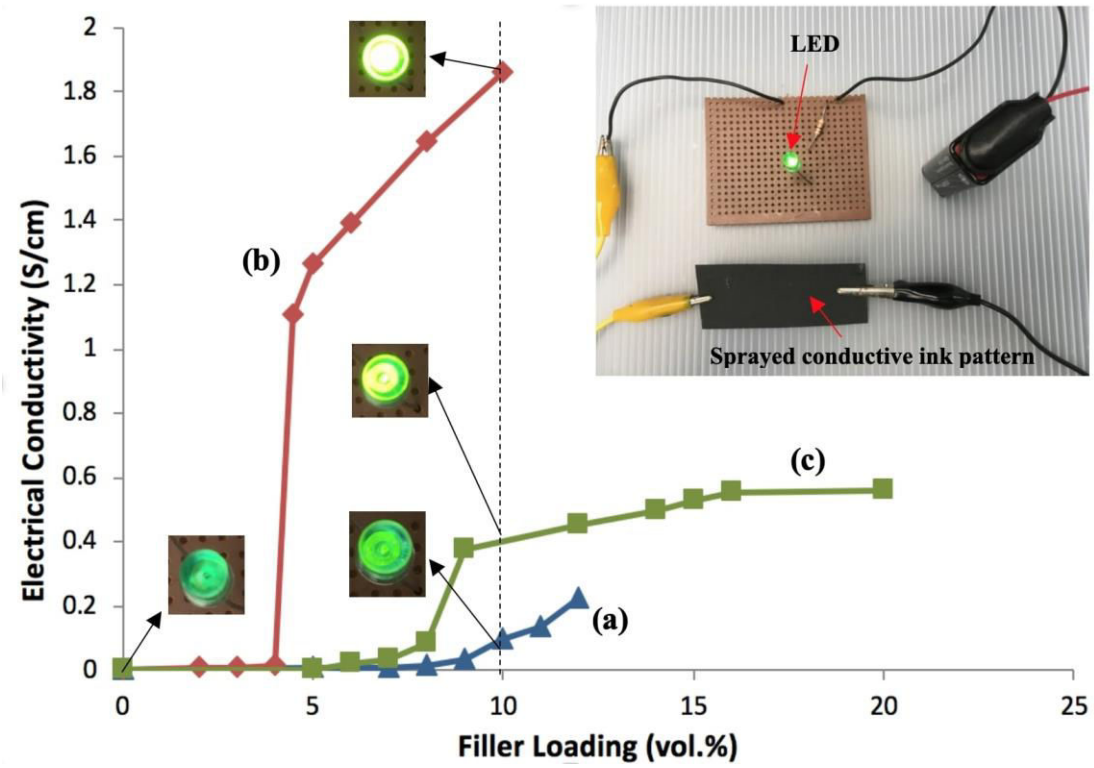

Figure 4.15 Electrical conductivity of (a) GF ink, (b) GNPs ink and (c) SG ink as a function of filler loading, inset showing digital images of an electronic circuit set up and LED brightness for various types of conductive ink patterns at 10 vol. %

The electrical conductivity of the conductive ink patterns is strongly dependent on their morphology which was investigated by SEM analysis. Figure 4.16 (a-e) shows the morphology of the cross section conductive ink patterns with respect to the filler loadings which provides insight into the process of conductive network formation. The conductive ink patterns at low filler loadings (shown in Figure 4.16 (a) and (c)) indicates that some conductive paths were not connected which indicating that low filler loadings were not sufficient to support a completed network and more voids could be seen. However, when the amount of graphene-based materials was increased, as shown in Figure 4.16 (b), (d) and (e), the network became obviously denser and the conductive paths were well established, as indicated by red arrow.

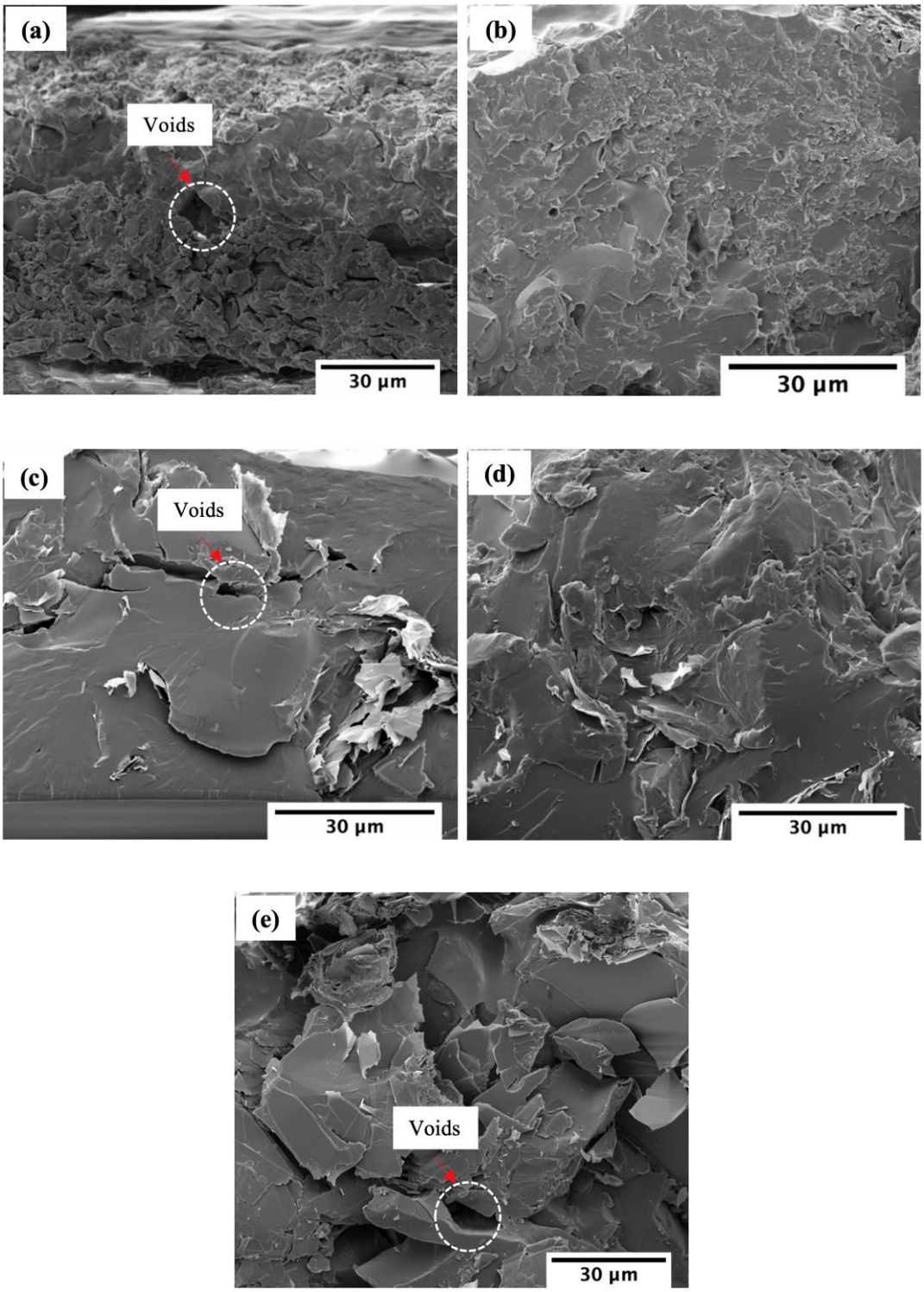

Figure 4.16 SEM micrographs of cross-section conductive ink patterns made of (a) 7 vol.% GF (b) 12 vol.% GF, (c) 2 vol.% GNPs (d) 4.5 vol.% GNPs (e) 9 vol.% SG [2,500-3,500X mag.]

Table 4.6 compares the values of maximum electrical conductivity and corresponding percolation threshold measured in the current study with those reported in the literature for graphene filled or mixed with polymer. The GNP ink produced in the present study (column highlighted in grey) exhibited a maximum conductivity of 1.86 Scm^{-1}, which is higher than the typical 10^{-6} to 1.58 Scm^{-1} values observed in the literature. Meanwhile, SG ink and GF ink (column highlighted in grey) showed moderate values of maximum conductivity that remain interesting in spite of the quite high amount of filler loading.

Table 4.6 Comparison of the maximum electrical conductivity and percolation threshold between present study and graphene-filled polymer from literature (Hu *et al*., 2012; Wang *et al*., 2015; Chiu *et al*., 2016; Alam *et al*., 2016; Ma *et al*., 2017; Wang *et al*., 2018; Jun *et al*., 2018)

Filler	**Binder/ matrix**	**Percolation starts (vol. %)**	**Percolation end (vol. %)**	**Electrical conductivity at end point of percolation (Scm^{-1})**
rGO	Ultrahigh molecular weight polyethylene	0.028	0.4	0.1
Thermally rGO	Polyamide-6	0.11	1.8	10^{-2}
Graphene	Polyacrylic acid hydrogel	0.4	1.25	10^{-6}

Table 4.6 *Continued*

Graphene nanosheets	Syndiotactic polystyrene	0.46	2.5	0.82
Graphene nanosheets	Syndiotactic polystyrene	0.24	0.73	0.8
Chemically expanded graphite	Poly(methyl methacrylate)	0.29	5.67	1.58
GNP	Polypropylene	2.99	9.3	1.7×10^{-2}
GNP	PV	4.5	10	1.86
SG	PV	9	20	0.4
GF	PV	10	12	0.22

4.3 Properties of graphene-based inks

Based on the physical properties and electrical properties shown in Section 4.2, graphite nanoplatelets (GNPs) and graphene foam (GF) were selected for further investigation. The third objective is to determine the stability of GNPs and GF dispersed into various types of common solvents and mixed solvents. This section is further divided into two subsections; effect of GNP dispersed in various types of common solvents and effect of GNP and GF dispersed in mixed solvents. The dispersion stability of graphene-based inks was investigated using visual observation, zeta potential analysis, UV-Vis spectrophotometer, viscosity and wettability.

4.3.1 Effect of GNPs dispersed in various types of common solvents

4.3.1(a) Visual observation

Figure 4.17 shows the sedimentation of GNPs dispersed in various solvents at different periods of time, between day 1 (after sonication) and day 7. From Figure 4.17, GNPs dispersed in NMP is partially stable up to one week. It is observed that dark appearance can be seen even after a week. Meanwhile GNPs in EG, PG and DMF are stable up to day 3 and as for GNPs in IPA is only stable for one day, resulting in a distinct separation of transparent liquid above the black precipitation. GNPs are known for its poor dispersibility in various types of solvents due to the nature of graphene which is hydrophobic (Bai, 2017). The GNPs particles reaggregate easily due to the strong van der Waals attraction and this has been proven by aggregation and sedimentation of GNPs near the bottom of the bottle. The schematic of GNPs dispersed in less toxic solvent after a period of time is shown in Figure 4.18. This schematic shows three phases; (i) clear solvent without GNPs, (ii) GNPs started to aggregate after certain period of time and (iii) GNPs finally sedimented and settled at the bottom.

Table 4.7 presents the general properties of these solvents including surface tension, Hildebrand solubility parameter (δ_T) and Hansen solubility parameters. As stated in Table 4.7, solvents including EG, PG, DMF and NMP have high surface tension that are closed to the surface tension of graphene with the value of 40 mNm^{-1} which can minimize the interfacial tension with graphene. Higher interfacial tension between graphene and solvent often leads to poor stability of the dispersion (Coleman, 2013; Nicolosi *et al*., 2013).

Other than surface tension, solubility theories such as Hansen solubility parameters and Hildebrand solubility parameter can also be used to further understand

the solvent-graphene interaction, $\delta_T^2 = \delta_D^2 + \delta_P^2 + \delta_H^2$, where δ_T, δ_D, δ_P and δ_H are the Hildebrand solubility parameter and, dispersion forces, polar forces and hydrogen-bonding forces of Hansen solubility parameters, respectively (Hernandez *et al*., 2010). The Hildebrand solubility parameter of solvent must be closed to Hildebrand solubility parameter of graphene, δ_T ~ 23 $MPa^{1/2}$ to produce stable graphene dispersion (Hernandez *et al*., 2010). From Table 4.7, IPA, DMF and NMP solvents have δ_T very close to 23 $MPa^{1/2}$ indicated that GNPs in IPA, DMF and NMP have stable dispersions. Unfortunately, GNPs dispersed in some solvents displayed poor dispersibility. Meanwhile, for Hansen solubility parameters, good solvents for graphene should have δ_D in the range of 15 $MPa^{1/2}$ to 21 $MPa^{1/2}$, δ_P ~ 12 $MPa^{1/2}$ and δ_H ~ 9 $MPa^{1/2}$. From these parameters, only NMP solvent has very close to these values showing good dispersibility. This is in agreement with the visual observations in Figure 4.17.

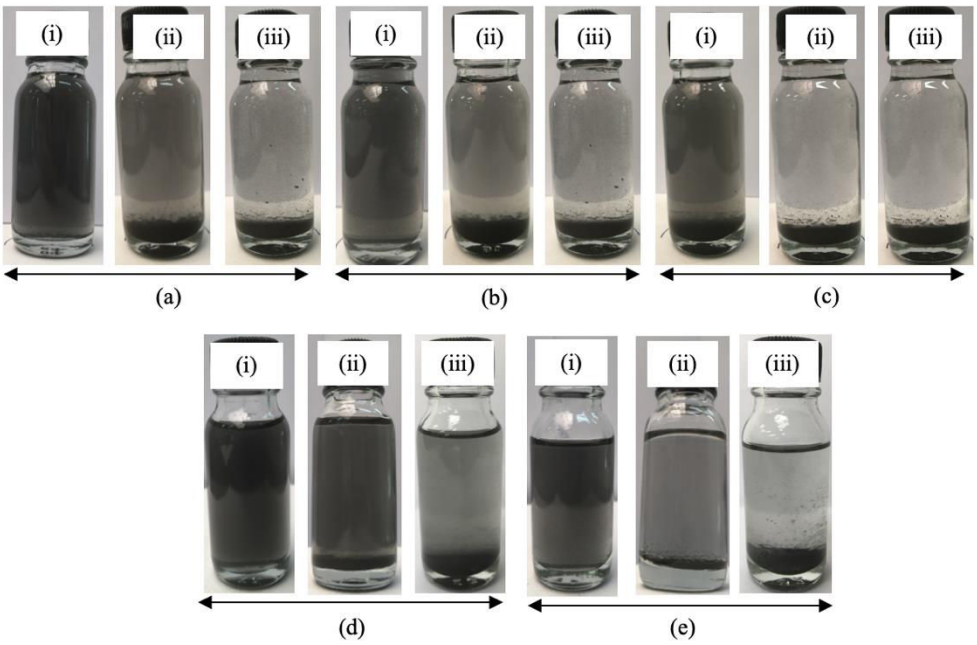

Figure 4.17 Photographs of GNPs dispersed in (a) EG, (b) PG, (c) IPA, (d) NMP and (e) DMF. Figure (i), (ii) and (iii) refer to the image after sonication (day 1), day 3 and day 7, respectively

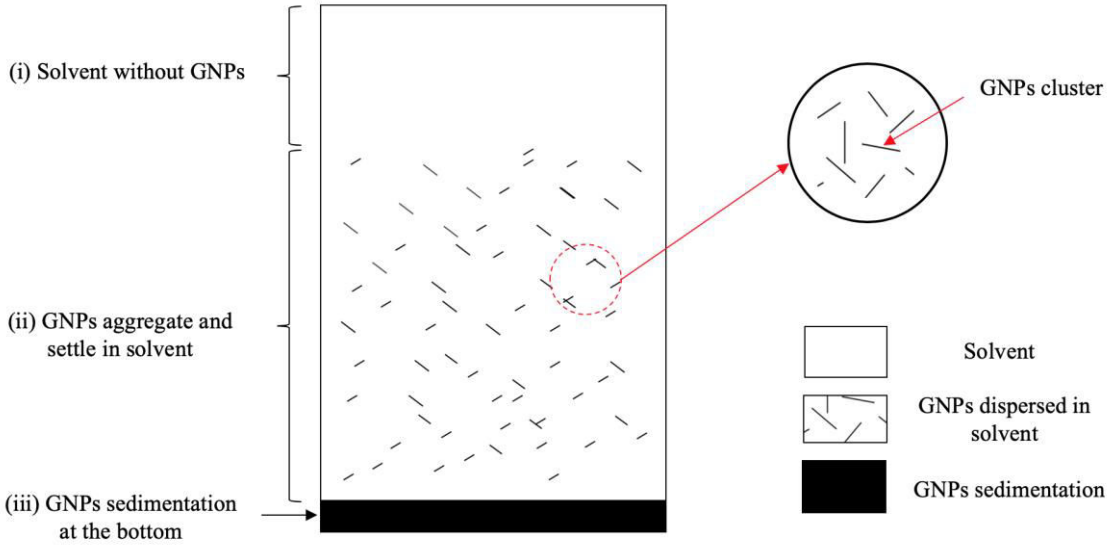

Figure 4.18 Schematic of GNPs dispersed in solvent after a period of time

Table 4.7 General properties of various types of solvents (Hernandez *et al*., 2010; Johnson *et al*., 2015)

Solvents	**Surface tension (mNm^{-1})**	**Hildebrand solubility parameter, δ_T ($MPa^{1/2}$)**	**Hansen solubility parameters ($MPa^{1/2}$)**		
			δ_D	δ_P	δ_H
EG	48.4	33	17	11	26
IPA	23.3	23.6	15.8	6.1	16.4
PG	45.6	30.7	16.8	9.4	23.3
DMF	34.4	24.9	17.4	13.7	11.3
NMP	44.6	23	18	12.3	7.2

4.3.1(b) Zeta potential analysis

The zeta, ζ potential was measured to understand the GNPs dispersions surface charge and predicting the long-term stability of GNPs dispersed in various solvents, as shown in Figure 4.19. The measured pH values of GNPs dispersed in EG, PG, IPA, NMP and DMF solvents after sonication were 5, 5, 5, 6 and 7, respectively. From Fig. 4.19, the GNPs surfaces were negatively charged in three dispersions but positively charged in two dispersions. For all solvents studied, other than EG and PG solvents, ζ-potentials were negative due to Lewis charge transfer of interfacial solvent molecules and the GNPs (Johnson *et al*., 2015). Lewis' theory is based on the transfer of electrons. The charging GNPs were negatively charged in IPA, NMP and DMF solvents due to higher donor numbers and positively charged in EG and PG solvents due lower donor numbers. The same observation was reported by Liu et al. (2012) as the surface charge of graphene in various common solvents were negative due to higher donor numbers than acceptor numbers.

According to Yu et al. (2017), ζ-potential can be described as the indicator of stability of a colloidal system and the theoretical limit is 30 mV. For electrostatic reasons, colloidal particles are expected to be stable at higher magnitude of ζ-potential |>30 mV|. Highly charged particles prevent the particles from agglomeration due to electric repulsion. It can be observed that GNPs dispersed in EG solvent exhibited ζ-potential values of 31.3 mV, which was considered to be stable compared to GNPs dispersed in PG and IPA solvents with ζ-potential |<30 mV|, indicating that GNPs have a high tendency to agglomerate. For comparison purposes, GNPs dispersed in NMP and DMF showed ζ-potential values of -32.8 mV and -16.6 mV, respectively, which indicated that GNPs dispersed in NMP were also stable.

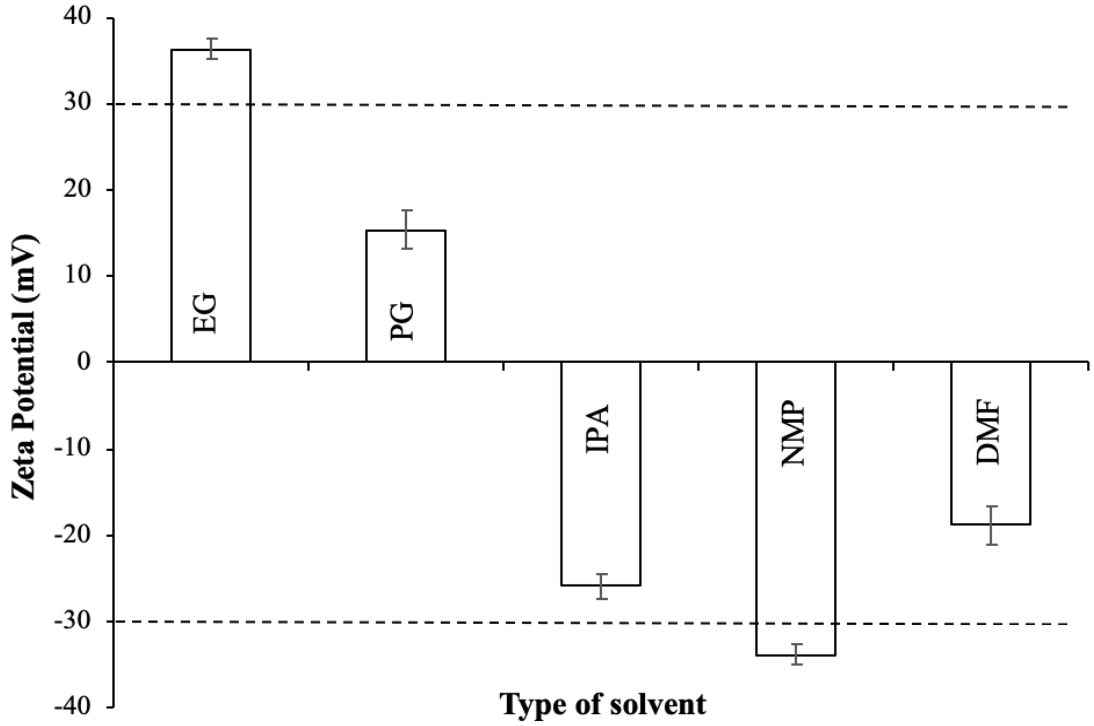

Figure 4.19 Zeta potentials of GNPs dispersed in various types of solvents

4.3.1(c) UV-Vis spectrophotometer analysis

Figure 4.20 shows the UV-Vis spectra of GNPs dispersed in various types of solvents, measured at different periods of time, between day 1 (refers to D1) and day 5 (refers to D5). It is observed that the GNPs dispersed in various types of solvents exhibited the maximum absorption peak at 265 nm. The spectra of GNPs dispersed in various types of solvents are very similar to those reported by Zhou *et al*. (2009) and Johra *et al.* (2014). They reported a maximum (λ_{max}) around 265 nm. The absorption peak at 265 nm in Figure 4.20 corresponding to the π-π* transition of the C-C aromatic ring in the GNPs inks.

Moreover, GNPs dispersed in NMP exhibited the highest absorption intensity from day 1 to day 5 which indicated better dispersion stability, followed by GNPs dispersed in EG, DMF, IPA and PG solvents, respectively. In contrast, the absorption

intensity for all samples decreased after day 5, especially for GNPs dispersed in IPA showing that the dispersion stability was reduced.

The stability of the conductive inks were further evaluated by calculating the concentration of GNPs inks at 660 nm using Lambert-Beer's equation $A = \alpha CL$, where A, α, C and L are the absorbance, absorption coefficient with the value of 2460 $mLmg^{-1}m^{-1}$, concentration of the conductive ink and cell length, respectively (Khan *et al*., 2010; Lotya *et al*., 2010). Figure 4.21 illustrates the concentration of GNPs dispersed in various types of solvents measured for one month. Different concentration of GNPs inks at Day 1 corresponding to the different concentration of ink supernatant was collected for UV-Vis measurement, as a result of Van der Waals forces of attraction between particles and the particles settled at the bottom due to gravitational effect. From Figure 4.21, it is observed that the concentration of GNPs dispersed in IPA dropped to 95% of its original concentration after one month of ink preparation, followed by GNPs dispersed in EG and PG by decrement of ~85%. Meanwhile, about 81 to 89% decrement of its initial concentration were measured for GNPs dispersed in NMP and DMF.

Over time, the concentrations were expected to decrease due to the gravity, aggregation and agglomeration caused by strong van der Waals forces between GNPs particles. The quantitative assessment matches well with the visual observation and zeta potential as discussed in Figure 4.17 and Figure 4.19, respectively.

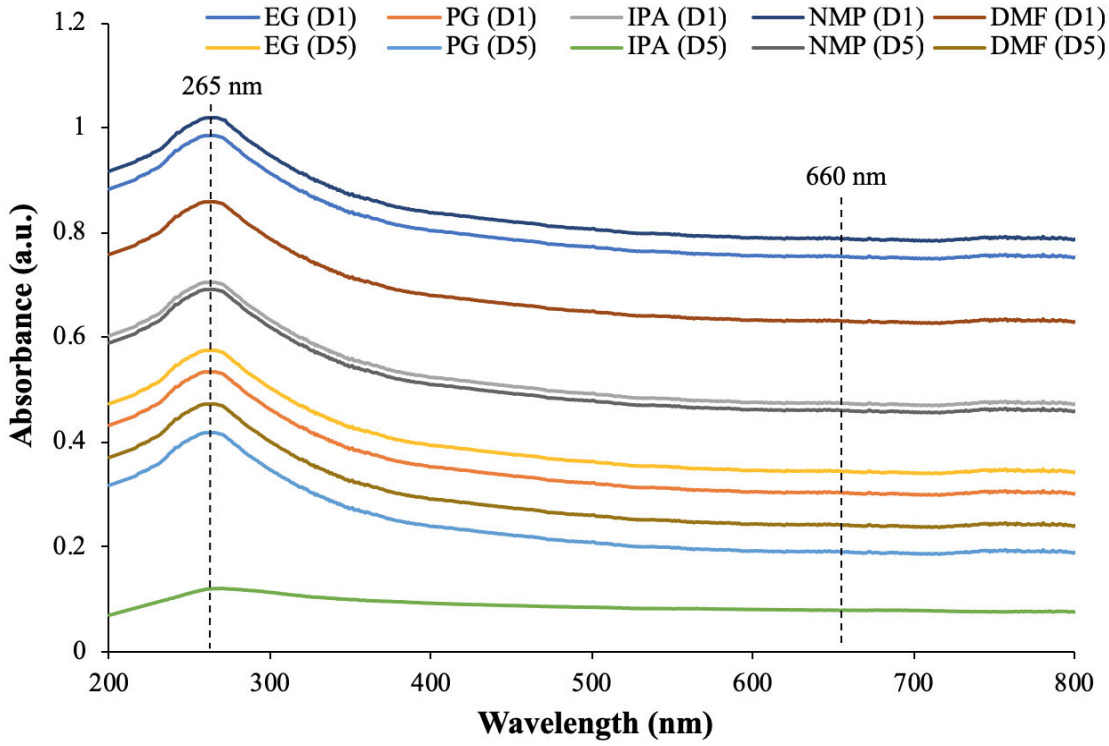

Figure 4.20 UV-Vis absorption spectra of GNPs dispersed in various types of solvents at different periods of time

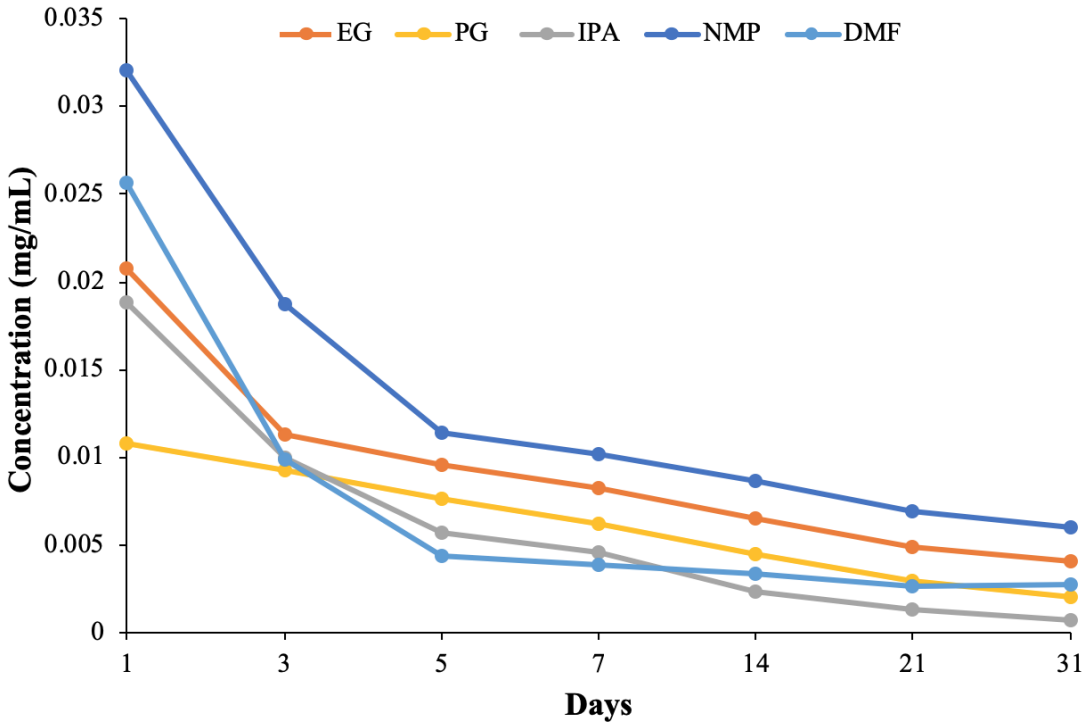

Figure 4.21 Concentration of GNPs dispersed in various types of solvents as a function of time

4.3.1(d) Viscosity analysis

An ideal viscosity, η of conductive ink for inkjet printing should be in the range between 1 to 20 mPas to avoid problems during printing process including nozzle clogging, satellite or double droplet (Ihalainen *et al*., 2015). Table 4.8 presents the η values of the solvents and GNPs dispersed in various types of solvents. It is observed that the η of all GNPs inks slightly increased with an addition of GNPs into various types of solvents. GNPs (PG) has the highest η due to the higher η of the solvent. PG is an alcohol with two OH groups on adjacent carbon atoms, similarly to EG. The two OH groups lead to extensive intermolecular hydrogen bonding, which results in high η (Adrjanowicz *et al*., 2016). The measured η of all GNPs inks were approximately between 0.6 to 38.2 mPas. All GNPs inks can be considered as acceptable for inkjet printing except GNPs dispersed in PG and DMF. Highly viscous conductive ink will reduce the jetting frequency as the rate of reservoir filling is decreased. As for conductive ink that is less viscous enough, high frequency jetting might cause unstable droplet ejection (Ihalainen *et al*., 2015).

Table 4.8 Viscosity of solvents and GNPs dispersed in various types of solvents

Sample	Viscosity of the solvent (mPas)	Viscosity of GNPs ink (mPas)
GNPs (EG)	14.5	15.1
GNPs (PG)	37	38.2
GNPs (IPA)	1.3	2.2
GNPs (NMP)	2.1	2.6
GNPs (DMF)	0.4	0.6

Figure 4.22 illustrates the viscosity, η curves of GNPs dispersed in (a) PG, (b) EG, (c) NMP, (d) IPA and (e) DMF solvents as a function of shear rate. As can be seen, the η for GNPs inks decreased with increasing shear rate within a range of 1.5-500 s^{-1}, showing shear-thinning flow behaviors. A first region in which the dispersions were found to exhibit shear thinning effect in which the η decreased very rapidly while the stress remained approximately constant with increasing shear rate, as observed in GNPs (PG) due to lower initial concentration of GNPs (PG), as presented in Figure 4.21. According to Vallés *et al*. (2014), this observation of pseudo-yield stress suggested that in this first region the network reformed as it was sheared, as the Brownian motion of the particles was dominating over the hydrodynamic forces. A second region was seen at higher shear rates where the shear stress was described by a power law. The transition between these two regions depended on the concentration of GNPs dispersions and indicated the moment from which the hydrodynamic forces on the particles started to dominate over their Brownian motion. As the initial concentrations increased as observed in GNPs (NMP) and GNPs (DMF), the first region extended until very high shear rates in which the η decreased slowly and finally constant at the second region.

According to Woo *et al*. (2013), the η is considered to be stable at high shear rates value as the attraction between the graphene-like particles induces flocculation in the inks which causes an immobility of the solvent suspending the particles and therefore increased the η at low shear rate. Meanwhile at higher shear rate, the flocculation breaks down and promotes the mobility of solvent entrapped between particles causes the η to be decreased.

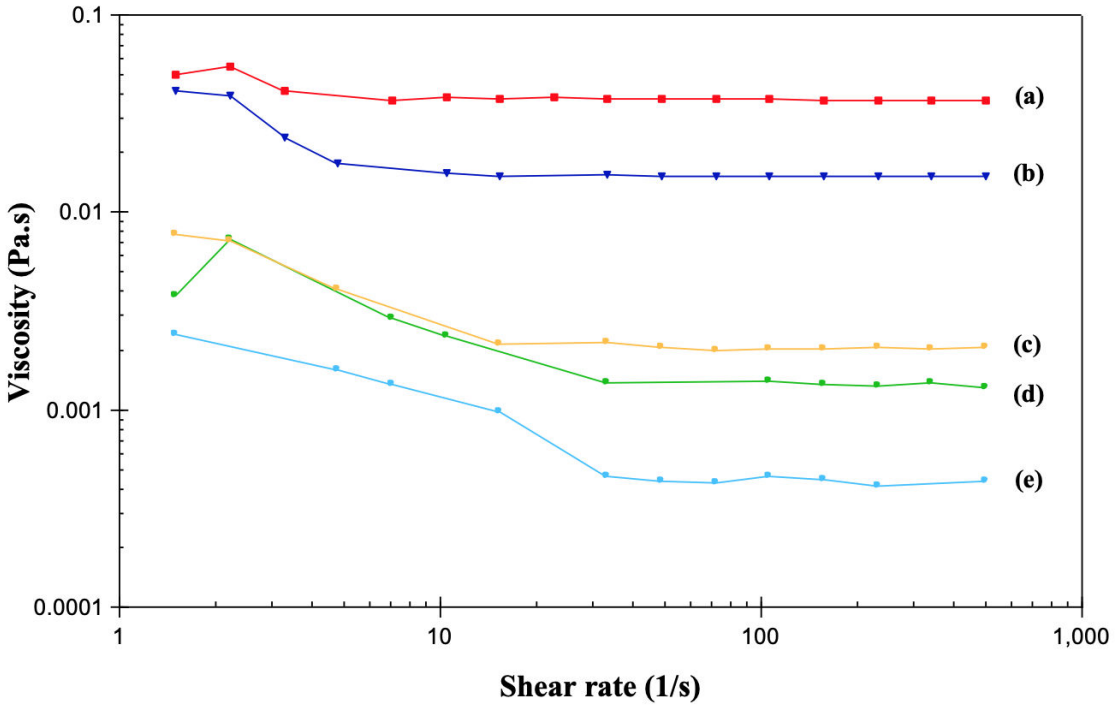

Figure 4.22 Viscosity curves of GNPs dispersed in (a) PG, (b) EG, (c) NMP, (d) IPA and (e) DMF solvents as a function of shear rate

4.3.1(e) Surface wettability analysis

Figure 4.23 shows the contact angle of GNPs dispersed in various types of solvents. As can be observed that the GNPs dispersed in all solvents exhibited small contact angle, θ_c which were less than 90° correspond to good wettability. For wettability study, the higher the surface tension of the solvent behaves as partial wetting (hydrophobic), thus increased the θ_c. As can be observed, the dispersed GNPs in EG exhibited the highest θ_c followed by GNPs dispersed in PG, NMP, DMF and IPA. This is in agreement in which the θ_c increased with an increasing of the surface tension of the solvent (Table 4.7).

The same observation was reported by Bharatidasan et al. (2015), as the θ_c of few layered graphene oxide (FGO) in water was higher than FGO in EG and coconut

oil with the θ_c values of 111°, 71° and 33.9° due to the high surface tension of water than other liquids with the values of 72.9 mNm^{-1}, 47.7 mNm^{-1} and 33.4 mNm^{-1}, respectively. Besides that, Pietrikova *et al*. (2016) reported if the contact angle, θ_c is larger than 90° can cause strong hydrophobic effect on the substrate surface and therefore, resulted in the agglomeration of ink drops on the substrate.

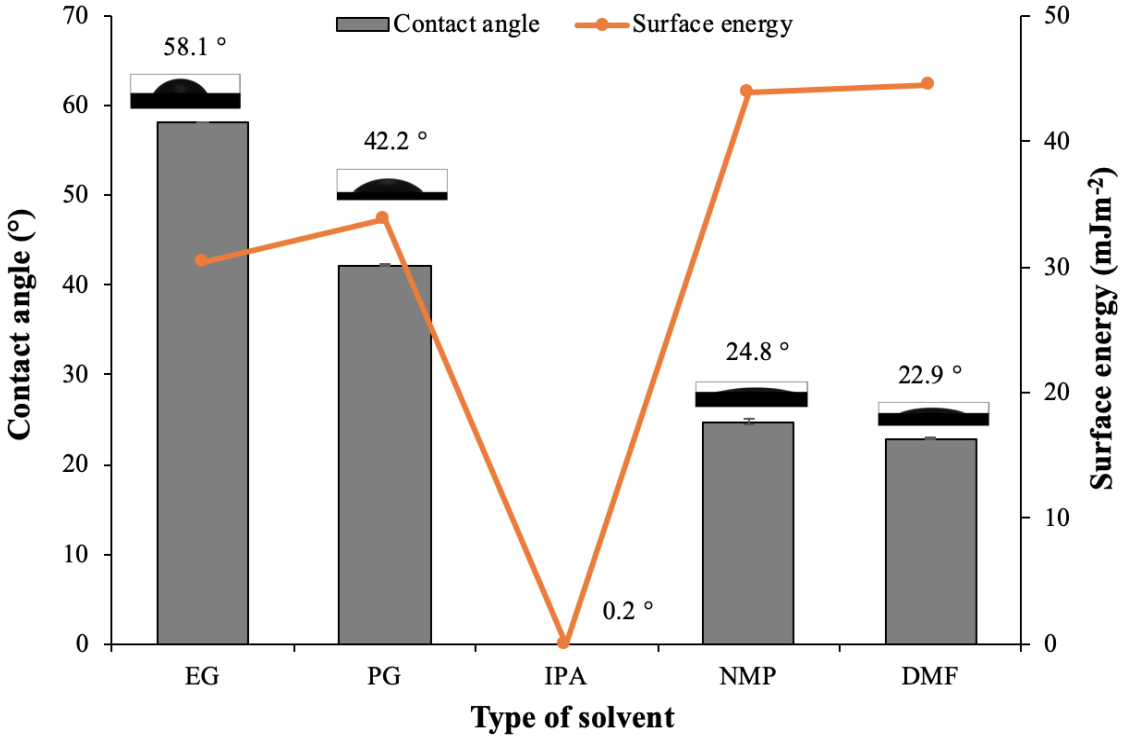

Figure 4.23 Contact angle of GNPs dispersed in various types of solvents, inset showing the drop settled on the surface of the substrate

The γ_{SL} from the measured θ_c of various GNPs inks were calculated and shown in Figure 4.24. The γ_{SL} is found to be maximum for GNPs dispersed in NMP and DMF solvents (>40 mJm^{-2}). In order to reduce the surface energy of the system, GNPs should properly interact with the solvent. Lower γ_{SL} of GNPs dispersed in EG as compared to other solvents is an indication of the tendency of GNPs ink to become less reactive with

the surrounding. The polymer chains preferentially interact with GNPs surface when the γ_{SL} become lower and therefore decreasing the interaction with the surroundings (Haghi *et al*., 2018).

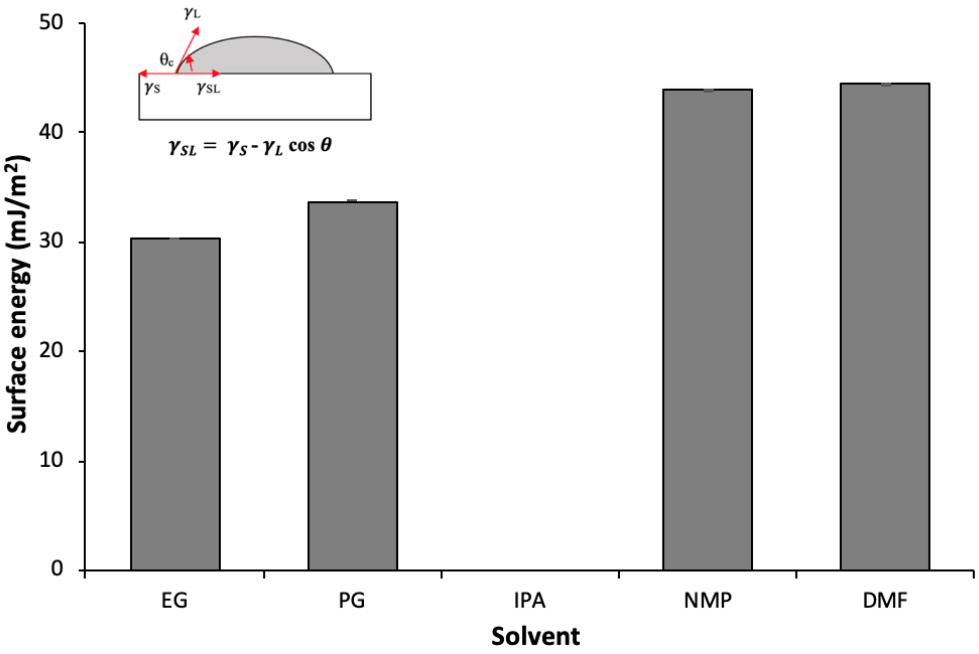

Figure 4.24 Surface energy of GNPs dispersed in various types of solvents, inset showing a contact angle including Young's equation

The comparison properties of GNPs dispersed in various types of solvents are shown in Table 4.9. Here, it could be summarized that GNPs dispersed in NMP solvent presented the best stability amongst all studied solvents, however this solvent including DMF suffer from toxicity and have high boiling points which were not suitable to be used with plastic substrates, that require low processing temperature and also because of safety and environmental issues.

In contrast, GNPs dispersed in EG which was less toxic, presented better dispersion stability, viscosity and wettability compared to those of GNP dispersed in

PG and IPA solvents. Nevertheless, from ζ-potential analysis, GNPs dispersed in IPA indicated good stability compared to that of GNPs dispersed in PG, however this dispersion was stable in less than a week. According to Dang *et al*. (2013), the prepared ink should be stable at least during the printing process. Therefore, in the next section, GNPs were dispersed in EG and IPA mixed solvents due to the positive results shown in this section and also because of the high surface tension and less toxic solvent of EG and low boiling point solvent of IPA. The GNPs dispersions were further compared with GF dispersions at various ratios of IPA:EG mixed solvents.

Table 4.9 Comparison properties of GNPs dispersed in various types of solvents

Sample	Zeta potential (mV)	Concentration decrement (%)	Viscosity (mPas)	Contact angle (°)	Surface energy (mJm^{-2})
GNP (EG)	36.3	85	15.1	58.1	31.9
GNP (PG)	15.3	85	38.2	42.2	37.9
GNP (IPA)	-25.9	95	2.2	0.2	-
GNP (NMP)	-33.8	81	2.6	24.8	43.6
GNP (DMF)	-18.8	89	0.6	22.9	45.9

Note: '-' indicates perfect wettability; N/A indicates not available

4.3.2 Effect of GNPs and GF dispersed in mixed solvents

4.3.2(a) Visual observation

The GNPs and GF dispersed in various ratios of IPA:EG mixed solvents were observed visually over time, between day 1 (after sonication) and day 7, as shown in Figure 4.25. As can be observed, GF inks presented better dispersion stability as the

dispersion remained a uniform dark color compared to GNPs inks. Higher oxygen content in GF about 4.64 wt% (as confirmed by XPS analysis in Table 4.4) showed that GF is more hydrophilic than GNPs with 0.83 wt% and therefore, makes it more easily to be dispersed in the solvent. Figure 4.25 (d-f) shows minimum sedimentation could be observed in GF inks with a dark appearance after day 7 storage time. GF dispersed in IPA:EG solvent at ratio of 1:1 shows the best dispersion stability compared to those of GF inks at mixed ratios of 1:4 and 4:1, respectively. Meanwhile for GNPs inks, it is observed that GNPs agglomerated and sedimented along the bottom of the bottle as the solvents appeared even clearer after day 7. Nethravathi and Rajamathi (2008) and Zhou *et al*. (2011) reported that the agglomeration is due to the increase in the hydrophobicity and the π-π stacking interaction between GNPs sheets, as confirmed in Figure 4.1 (a, c).

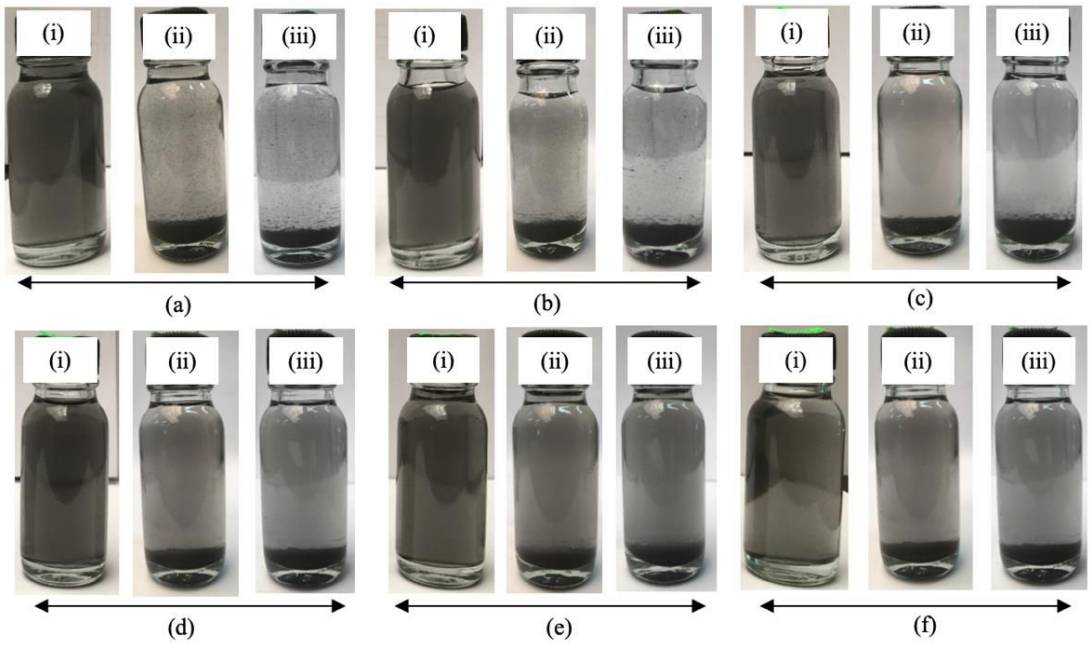

Figure 4.25 Photographs of (a-c) GNPs and (d-f) GF in various ratios of IPA:EG mixed solvents. Figure (a, d) IPA:4EG, (b, e) IPA:EG and (c, f) 4IPA:EG refer to the image after sonication (day 1), day 3 and day 7, respectively

4.3.2(b) Zeta potential analysis

Figure 4.26 shows the ζ-potential of GNPs and GF dispersed in various ratios of IPA:EG mixed solvents. The measured pH value of GNPs and GF inks after sonication was 5. The GNPs and GF surfaces were negatively charged in all dispersions mainly attributed to Lewis charge transfer of interfacial solvent molecules and the GNPs and GF particles (Johnson *et al*., 2015). The values of ζ-potential indicate that, all contents of GF in mixed solvents are in good stability, meanwhile for GNPs dispersions only stable at mixed ratios of 3:2 and 4:1, respectively. According to Rajan *et al*. (2016), ζ-potentials with absolute values larger than $\pm$30 mV indicated stable dispersion because of the inter particles electrostatic repulsion. It is apparent that GF inks are more stable compared to GNPs inks at all mixed ratios.

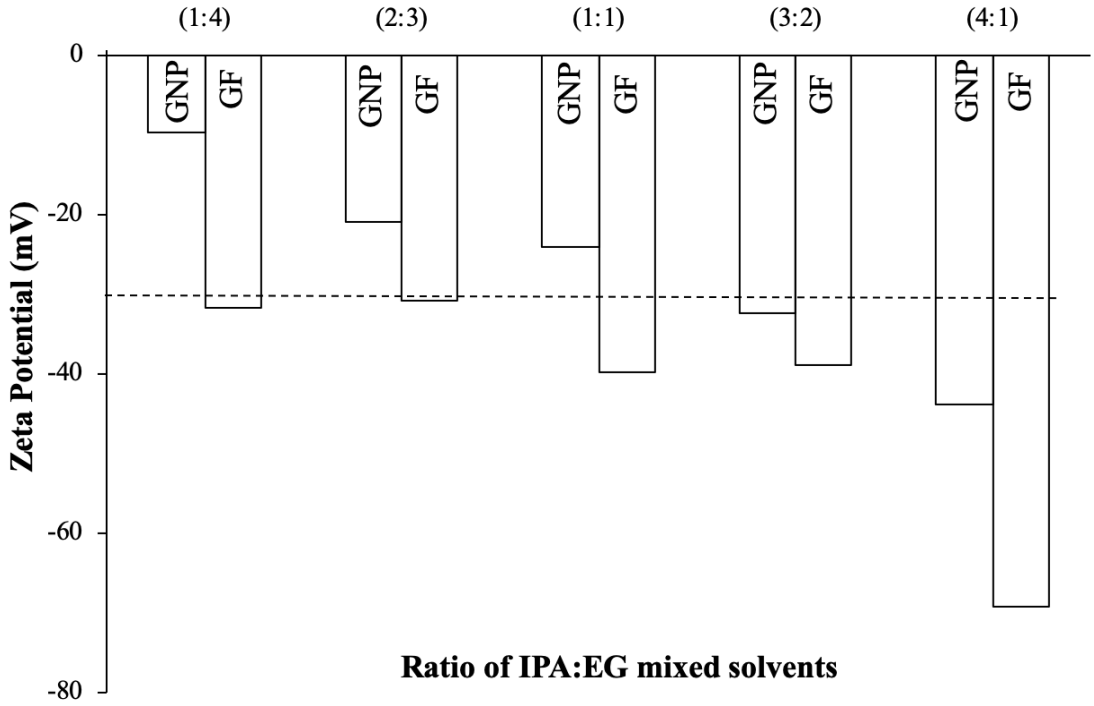

Figure 4.26 Zeta potentials of GNPs and GF dispersed in various ratios of IPA:EG mixed solvents

4.3.2(c) UV-Vis spectrophotometer analysis

The stability of GNPs and GF dispersed in IPA:EG solvent at certain period of time was studied by using UV-Vis spectroscopy. Figure 4.27 shows the UV-Vis absorption spectra of GNPs ink and GF ink in IPA:EG solvent at different periods of time, between day 1 (refers to D1), day 3 (refers to D3) and day 5 (refers to D5). It was found that both GNPs and GF inks exhibited the highest absorption peak at 265 nm which attributed to the sp^2 C=C bonds. The absorption intensity of GF ink demonstrated a slight decrement compared to GNPs ink over time as shown in Figure 4.27, confirming that GF ink has better dispersion stability. The intensity of all inks gradually decreased over time possibly due to the re-agglomeration of the particles.

Besides that, the dispersion stability of GNPs and GF in mixed solvents were further evaluated by investigating their concentrations over certain periods of time, as illustrated in Figure 4.28. Different concentration of GNPs and GF inks at Day 1 corresponding to the different concentration of inks supernatant were collected for UV-Vis measurement, as a result of Van der Waals forces of attraction between particles and the particles settled at the bottom due to gravitational effect. Based on the calculated concentrations in Figure 4.28, GNPs dispersed in IPA:EG at mixed ratios of 1:4 and 4:1 show a significant decrement after one month (>90%) as compared to GNPs dispersed in IPA:EG at 1:1 ratio (>80%). Meanwhile for GF dispersions, a slight decrement after a month could be seen in GF dispersed in mixed solvents at ratio of 1:1 (~50%) as compared to those of 1:4 and 4:1 mixed ratios with the percentage decrement about 60%. These observations strongly suggest that GF dispersed in IPA:EG mixed solvents at all ratios were stable than GNPs dispersions. This is in accordance with the visual observation and ζ-potential analysis which have been discussed in Figure 4.25 and Figure 4.26.

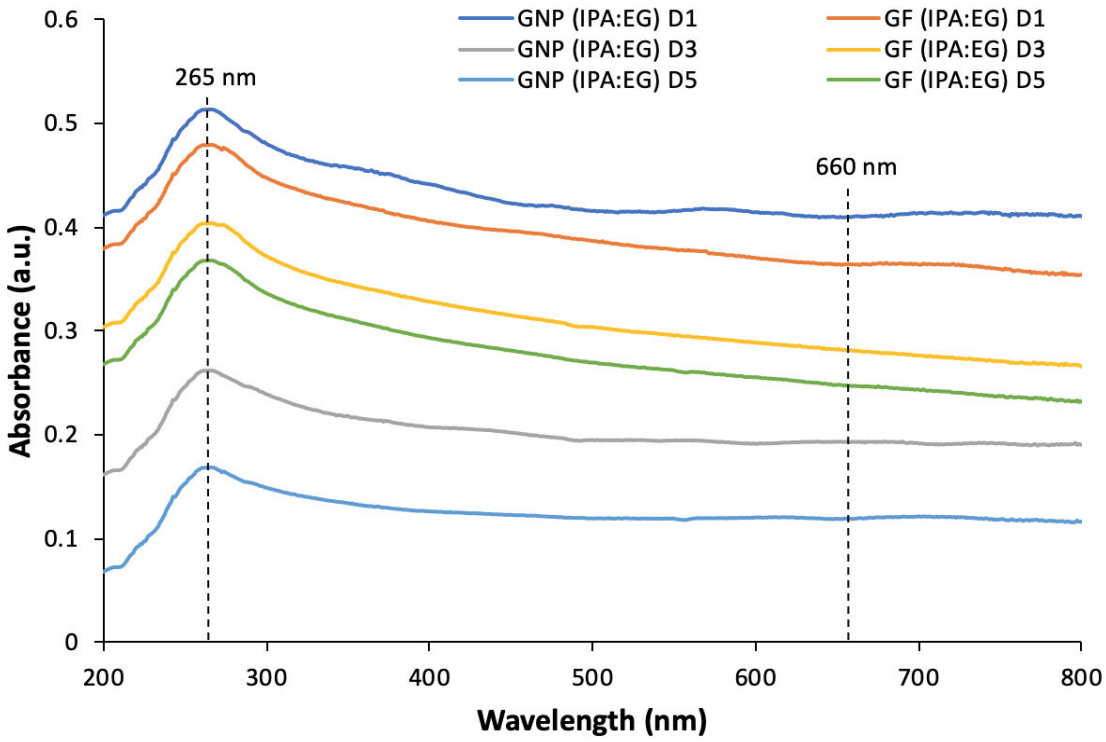

Figure 4.27 UV-Vis absorption spectra of GNPs inks and GF inks in IPA:EG solvent at different periods of time

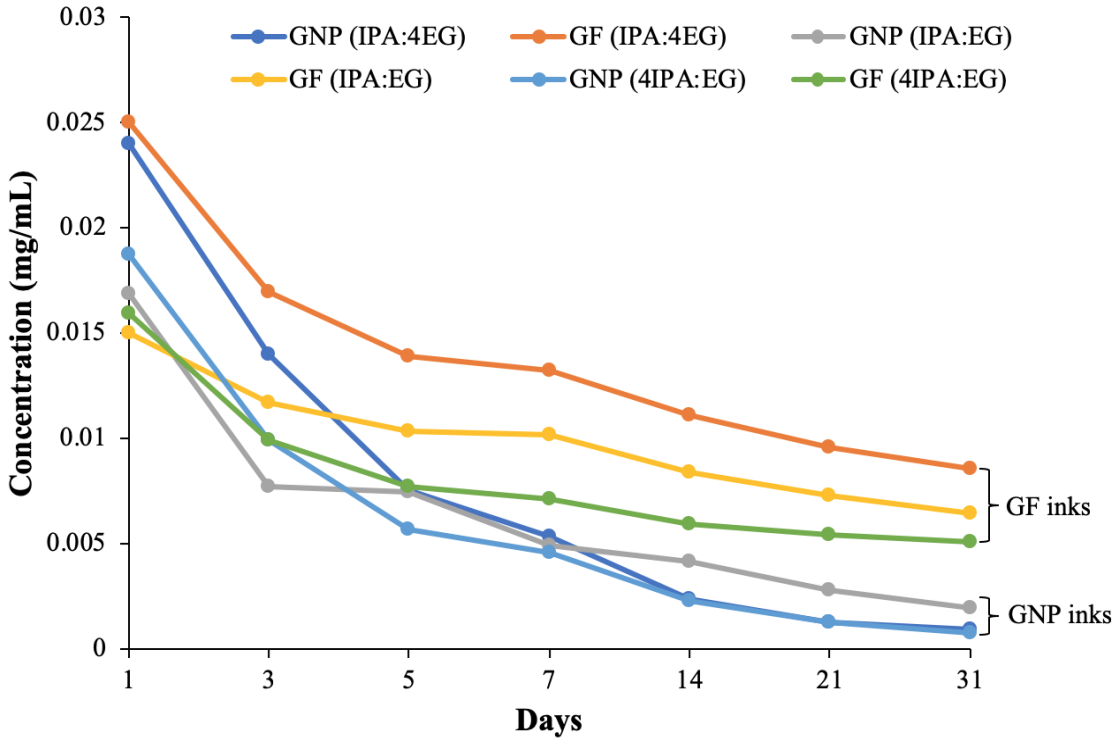

Figure 4.28 Concentration of GNPs inks and GF inks in various ratios of IPA:EG mixed solvents as a function of time

4.3.2(d) Viscosity analysis

Table 4.10 presents the viscosity, η values of mixed solvents and η values of GNPs and GF dispersed in various ratios of IPA:EG mixed solvents. It is observed that the η values of all inks increased with an addition of GNPs and GF into mixed solvents at all ratios. Also, the η values of GNPs inks and GF inks decreased with an increasing of IPA content in IPA:EG mixed solvents. This is in agreement with the low η of IPA as discussed in Table 4.8. It is observed that the η values of GNPs inks and GF inks exhibited in the range between 3.5 to 14 and 5 to 14.3 mPas, respectively. These findings suggested that GNPs inks and GF inks can be considered as acceptable for inkjet printing. Besides that, it was found that the η of GF ink was slightly higher than GNPs ink even at the same mixed ratio. Based on the formulations, higher amount of GF filler at the same vol.% is due to the low density of GF with the value of 1.06 gcm^{-3} compared to GNPs of 2.2 gcm^{-3}.

Table 4.10 Viscosity of mixed solvent and viscosity of GNPs and GF in various ratios of IPA:EG mixed solvents

Sample	IPA:EG mixed ratio	Viscosity of mixed solvent (mPas)	Viscosity of GNP(GF) ink (mPas)
GNPs (GF)	1:4	11.3	14 (14.3)
	2:3	8.2	9.5 (11)
	1:1	6.9	8 (10)
	3:2	5.2	6 (8)
	4:1	2.5	3.5 (5)

*values in the bracket refer to the GF dispersions

4.3.2(e) Surface wettability analysis

Figure 4.29 shows the contact angle and surface energy of GNPs and GF in various ratios of IPA:EG mixed solvents. Based on the θ_c values, it is found that the θ_c of GNPs and GF dispersions tended to decrease with an increasing of IPA content in the mixed solvents. This is in agreement with the complete wetting shown by GNPs dispersed in IPA, as discussed in Figure 4.23. The images of a drop of conductive ink dispensed from the ganiometer on PET substrate and photographed by software for θ_c measurement are shown in Figure 4.30. As expected, better wettability could be observed for GF inks as compared to GNPs inks due to an improvement in the dispersion stability of GF inks, and therefore leads to the lower θ_c values presented in GF inks. According to Park *et al*. (2013) and Wan *et al*. (2013), a small θ_c causes fast ink evaporation and excessive absorption than the big θ_c.

The γ_{SL} from the measured θ_c of GNPs and GF in various ratios of IPA:EG mixed solvents increased with an increasing of IPA content in the mixed solvents. As can be observed that the difference in γ_{SL} of GF inks at all mixed ratios were very small, by 6% compared to those of GNPs inks by 17%. The particles should properly interact with the solvent in order to reduce the γ_{SL} of the system.

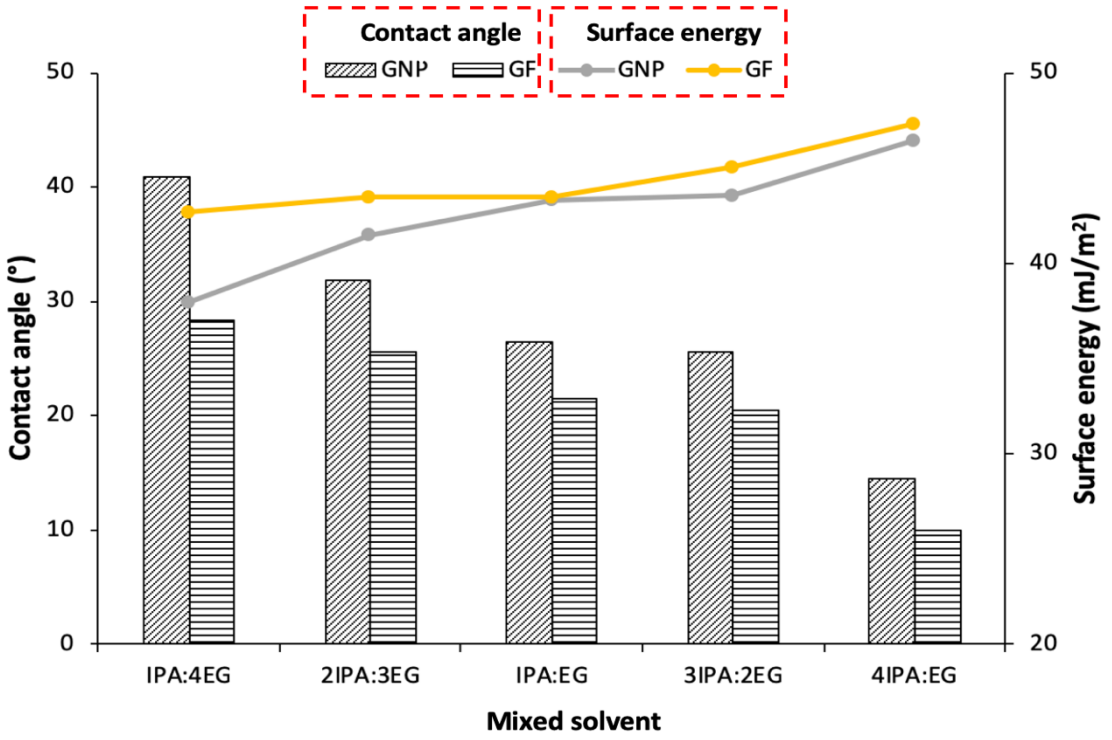

Figure 4.29 Contact angle and surface energy of GNPs and GF in various ratios of IPA:EG mixed solvents

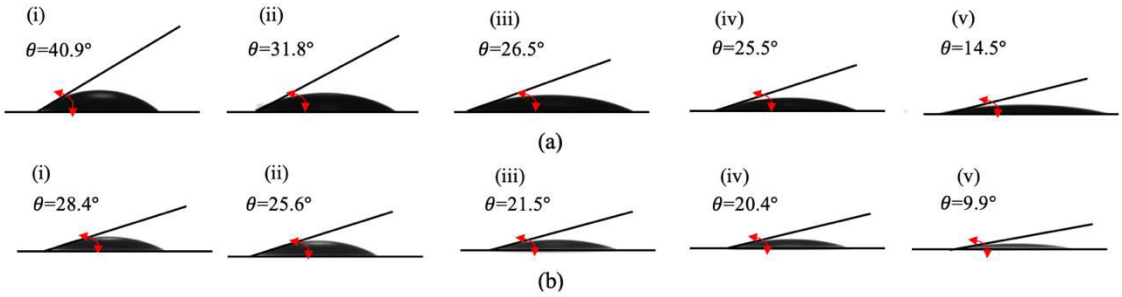

Figure 4.30 The droplet of (a) GNPs inks and (b) GF inks at various ratios of IPA:EG mixed solvents (i) 1:4, (ii) 2:3, (iii) 1:1, (iv) 3:2 and (v) 4:1 on PET substrate

4.3.2(f) Morphology

Morphology of GF dispersed in IPA:EG at 1:1 ratio was observed to identify the stability effect at day 1 and day 5. The HRTEM images of GF in IPA:EG at 1:1 ratio are shown in Figure 4.31. Noted that, agglomerates appear as dark regions in the

HRTEM images. Based on Figure 4.31, darker region could be observed for GF dispersion after day 5 (Figure 4.31 (iii)), indicated that the particles were agglomerated as compared to the GF particles at day 1 (Figure 4.31 (i)). These results are consistent with the visual observation and UV-Vis analysis as discussed in Figure 4.25 and Figure 4.27, respectively.

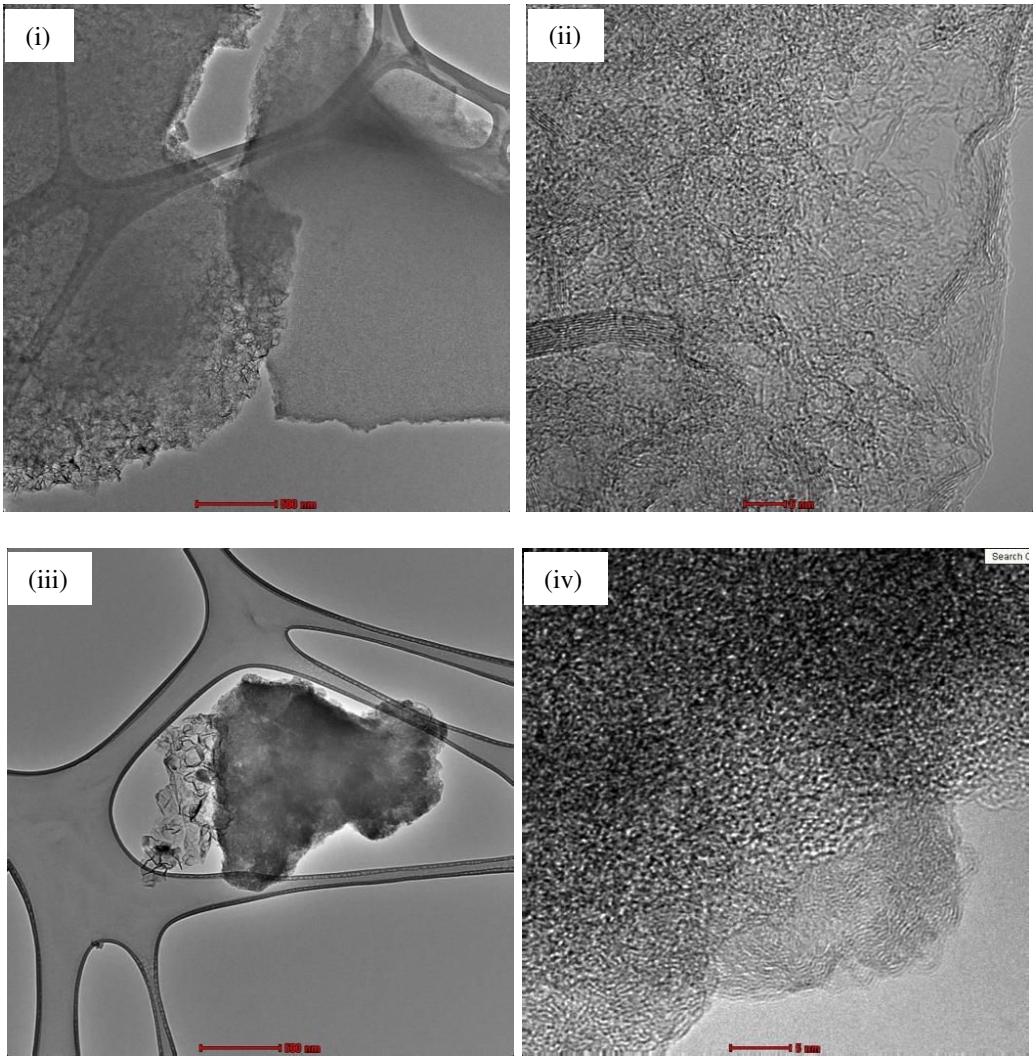

Figure 4.31 HRTEM micrographs of GF particles in IPA:EG mixed solvents at 1:1 ratio at magnifications of (i, iii) 15kX and (ii, iv) 690kX. Figure (i-ii) and (iii-iv) refer to the image after sonication (day 1) and day 5, respectively

The summary of the properties of GNPs and GF in various ratios of IPA:EG mixed solvents are compared in Table 4.11. From the table, GNPs dispersed in IPA:EG at mixed ratios of 3:2 and 4:1 exhibited lower ζ-potential ≤-30 mV than other dispersions at other mixed ratios. However, these dispersions have higher % of concentration decrement after one-month storage, around 90% due to the sedimentation of GNP particles. Meanwhile for GF dispersions, the ζ-potential were lower ≤-30 mV at all mixed ratios and presented good viscosity and wettability. Besides that, the % of concentration decrement after one-month storage for GF dispersed in IPA:EG at mixed ratio of 1:1 was only 50% as compared to dispersions at 1:4 and 4:1 mixed ratios with the values of 60% for both. Therefore, from the findings, GF dispersed in IPA:EG mixed solvents at ratio of 1:1 presented the best stability, good viscosity and wettability than those of GNPs inks and can be considered to be used as conductive ink for printing applications.

Table 4.11 Comparison properties of GNPs and GF in various ratios of IPA:EG mixed solvents

Sample	IPA:EG mixed ratio	Zeta potential (mV)	Concentration decrement (%)	Viscosity (mPas)	Contact angle (°)	Surface energy (mJm^{-2})
GNPs (GF)	1:4	-9.7 (-31.7)	90 (60)	14 (14.3)	40.9 (28.4)	37.9 (42.7)
	2:3	-21.1 (-30.9)	N/A	9.5 (11)	31.8 (25.6)	41.5 (43.5)
	1:1	-24.2 (-39.8)	80 (50)	8 (10)	26.5 (21.5)	43.6 (43.5)
	3:2	-32.6 (-38.9)	N/A	6 (8)	25.5 (20.4)	43.3 (45.1)
	4:1	-43.8 (-69.4)	90 (60)	3.5 (5)	14.5 (9.9)	46.5 (47.3)

*values in the bracket refer to the GF dispersions; N/A indicates not available

4.4 Properties of graphene-based ink and graphene hybrid-based inks

In this work, graphene-based ink and graphene hybrid-based inks at fixed concentrations of 4 mg/mL were prepared using IPA:EG mixed solvents at ratio of 1:1. Two materials were used for graphene hybrid-based inks including AgNPs and PEDOT:PSS. The effect of graphene on the stability, viscosity, surface wettability, electrical conductivity and morphology of graphene and graphene hybrid as conductive inks were investigated.

4.4.1 Stability of GF ink, GF/AgNPs and GF/PEDOT:PSS hybrid inks

Visual observation of GF ink, GF/AgNPs and GF/PEDOT:PSS hybrid inks at concentration of 4 $mgmL^{-1}$ observed from day 1 (after sonication) until day 7 was shown in Figure 4.32. For GF ink (Figure 4.32 (a)), small amount of settling was observed at day 7 indicated that GF is partially stable up to a week. On the other hand, GF/AgNPs hybrid ink was only stable for one day as the hybrid ink appeared clearer at day 7. Sedimentation of high amounts of GF and AgNPs were observed at the bottom of the bottle at day 7, indicating the dispersion of GF and AgNPs in IPA:EG solvents were not stable. This is attributed to the high interfacial tension between GF (~40 mNm^{-1}), AgNPs (~7.2 Nm^{-1}) and IPA:EG mixed solvents (~36 mNm^{-1}) and also, the high density of AgNPs (10.49 gcm^{-3}) that leads to poor stability of the dispersion (Nanda *et al*., 2003). However for GF/PEDOT:PSS hybrid ink, it can be seen that the hybrid ink was visually homogeneous with dark appearance even until day 7, indicating that the dispersion of GF hybrid with PEDOT:PSS in IPA:EG mixed solvents was stable for a long period. Low interfacial tension between GF (~40 mNm^{-1}), PEDOT:PSS (~42.5 mNm^{-1}) and IPA:EG mixed solvents (~36 mNm^{-1}) leads to good stability of the hybrid ink dispersion (Dabczyński *et al*., 2018). Interfacial tension plays an important role

when a solid surface is immersed in a liquid medium. Higher interfacial tension between graphene and solvent (surface tension of the solvent was very high or low compared to the surface tension of graphene ~40 mNm^{-1}) leads to poor dispersibility as graphene particles tend to adhere to each other and the work of cohesion between them is high, therefore hindering their dispersion in the solvent (Lyklema, 1999; Israelachvili, 2011). Meanwhile, solvent or polymer that has surface tension closed to the surface tension of graphene with the value of 40 mNm^{-1} is considered to be the most suitable solvent or polymer for the dispersion of graphene, since they can minimize the interfacial tension between solvent or polymer and graphene, therefore leads to good dispersion stability (Israelachvili, 2011).

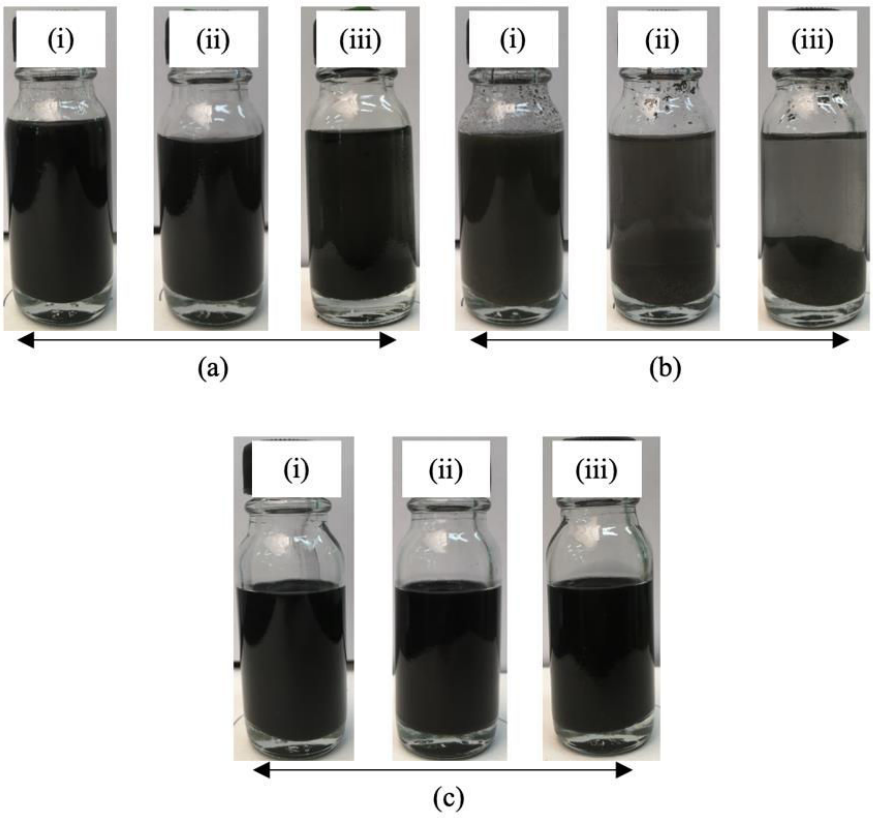

Figure 4.32 Photographs of (a) GF ink, (b) GF/AgNPs hybrid ink and (c) GF/PEDOT:PSS hybrid ink. Figure (i), (ii) and (iii) refer to the image after sonication (day 1), day 3 and day 7, respectively

UV-Vis spectroscopy was used to analyze the quality, nature and the stability of GF ink and GF hybrid inks. The UV-Vis absorption spectra of GF ink and GF hybrid inks are shown in Figure 4.33. As seen from Figure 4.33 (a), the highest absorption peak for GF ink was observed at 265 nm which attributed to the π- π* transition of the C-C aromatic ring in the GF ink (Johra *et al*., 2014).

The formation of AgNPs and PEDOT:PSS in GF hybrid inks were confirmed by the absorption peaks in the UV-Vis spectra, as shown in Figure 4.33 (b-c), respectively. As clearly seen, GF/AgNPs hybrid ink had absorbance peak at 418 nm, showing a peak associated with surface plasmon resonance of AgNPs. AgNPs absorb and scatter light with extraordinary efficiency due to the conduction electrons on the metal surface undergo a collective oscillation when they are excited by light at specific wavelength. This oscillation is called as a surface plasmon resonance (Bououdina, 2016). Saion *et al*. (2013) and Campillo *et al*. (2017) reported a maximum peak of AgNPs lies in between 404 to 418 nm. Meanwhile for GF/PEDOT:PSS ink, the maximum absorption was observed at 227 nm which refers to the aromatic rings of PSS (Mengistie *et al*., 2014; Saghaei *et al*., 2015).

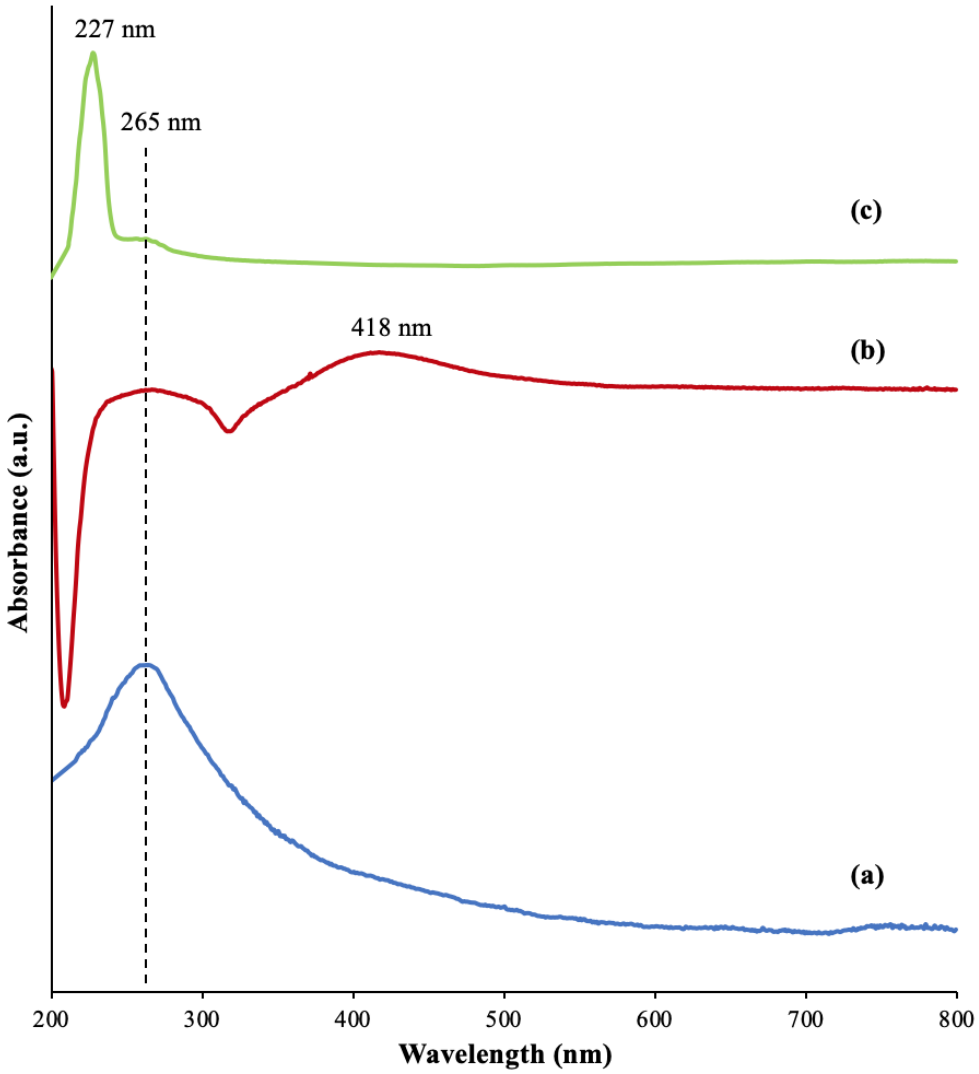

Figure 4.33 UV-Vis absorption spectra of (a) GF, (b) GF/AgNPs hybrid ink and (c) GF/PEDOT:PSS hybrid ink

The dispersion stability of GF and GF hybrid inks in IPA:EG mixed solvents were investigated by measuring their concentrations for a month, as illustrated in Figure 4.34. Based on the calculated concentrations using Lambert-Beer's equation, GF/PEDOT:PSS hybrid ink shows a slight decrement after one month (30%) as compared to those of GF ink and GF/AgNPs hybrid ink with the percentage decrement about 50% and 70%, respectively. From this observation, GF/PEDOT:PSS hybrid ink

was stable than those conductive inks. This result is parallel with the visual observation which has been discussed in Figure 4.32.

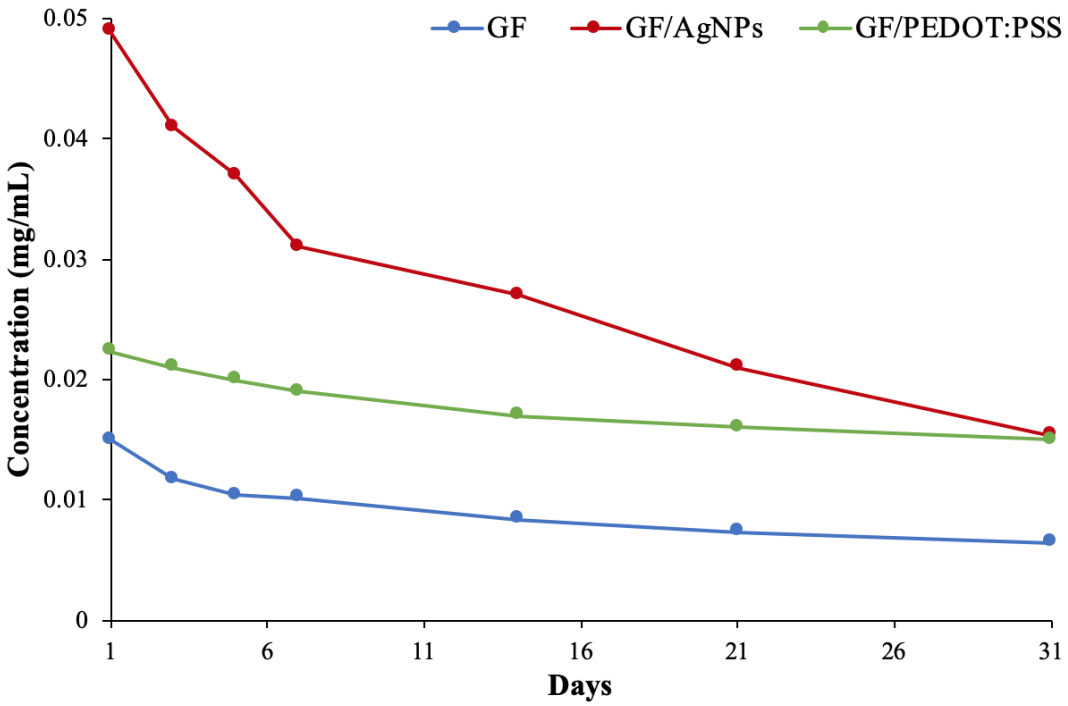

Figure 4.34 Concentration of GF ink, GF/AgNPs hybrid ink and GF/PEDOT:PSS hybrid ink as a function of time

Table 4.12 presents concentration decrement and zeta, ζ potential values of GF and GF hybrid inks. The values of ζ-potentials indicate that all inks are in good stability as the conductive inks have ζ-potential values less than -30 mV (Rajan *et al.*, 2016). GF/PEDOT:PSS hybrid ink exhibited the lowest ζ-potential with the value of -80.4 mV as compared to other conductive inks, indicating that this hybrid ink has the best stability than GF ink and GF/AgNPs hybrid ink, respectively. Zeta potential results in Table 4.12 generally support the results shown by visual observation and UV-Vis analysis.

Table 4.12 Concentration decrement and zeta potential of GF and GF hybrid inks

Ink	Concentration decrement (%)	Zeta potential (mV)
GF	50	-38.9
GF/AgNPs	70	-50
GF/PEDOT:PSS	30	-80.4

4.4.2 Physical properties of GF ink, GF/AgNPs and GF/PEDOT:PSS hybrid inks

Table 4.13 presents viscosity, η contact angle, θ_c and surface energy, γ_{SL} values of GF and GF hybrid inks. The data shows no significant difference in physical properties, in accordance with the dispersion stability, as explained in Section 4.4.1. The η for all inks range between 7.5 to 11.9 mPas, indicating that all inks are acceptable for inkjet printing. Figure 4.35 illustrates the η curves of GF ink and GF hybrid inks. The η for GF ink and GF hybrid inks decreased with increasing shear rate, indicating pseudoplastic (shear-thinning flow) behavior. Shear-thinning is a phenomenon in which the viscosity of the conductive ink decreases with increasing shear stress. This phenomenon is good in inkjet printing where the conductive ink has high viscosity under standard conditions but low viscosity when passing through the print head in order to avoid nozzle clogging (O'Mahony *et al*., 2019).

According to Khondoker *et al*. (2013), the surface wettability of the conductive ink with the substrate play an important role which significantly influence the printing quality. The measured values of the θ_c and γ_{SL} of GF ink and GF hybrid inks on the PET substrate are shown in Table 4.13. Based on Table 4.13, it was found that the θ_c for hybrid inks slightly increased with an addition of hybrid material; AgNPs and

PEDOT:PSS. However, the θ_c is still below 90°, which is considered as good adhesion between conductive ink and the PET substrate. The images of a drop of conductive ink dispensed from the ganiometer on the substrate are shown in Figure 4.36. The γ_{SL} from the measured θ_c of GF ink and GF hybrid inks range in between 39.4 to 41.1 mJm^{-2}, resulting the tendency of GF ink and GF hybrid inks to become less reactive with the surrounding.

Table 4.13 Comparison physical properties of GF and GF hybrid inks

Ink	Viscosity (mPas)	Contact angle (°)	Surface energy (mJm^{-2})
GF	7.5	32.9	41.1
GF/AgNPs	9.8	33	41.1
GF/PEDOT:PSS	11.8	37.3	39.4

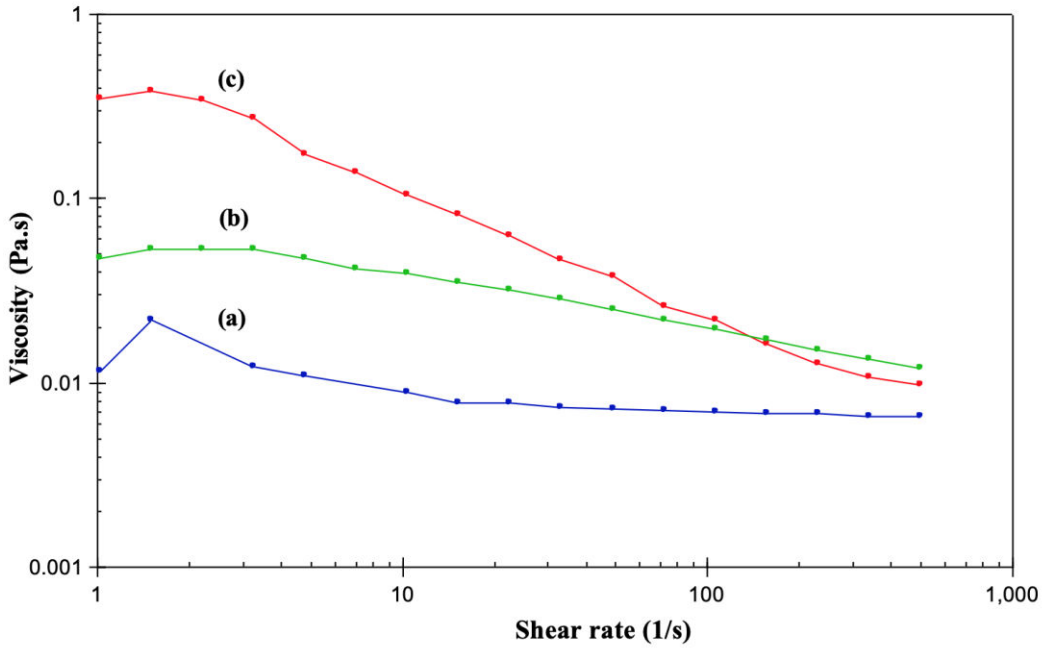

Figure 4.35 Viscosity curves of (a) GF ink, (b) GF/PEDOT:PSS hybrid ink and (c) GF/AgNPs hybrid ink as a function of shear rate

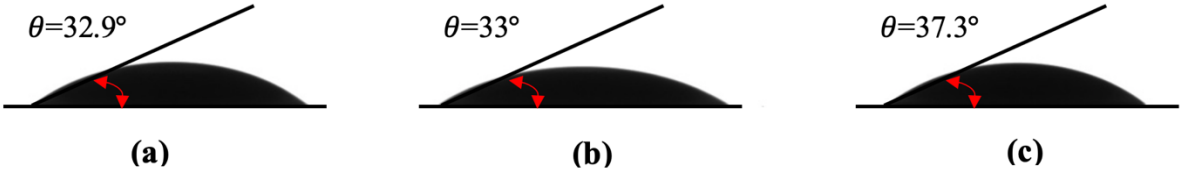

Figure 4.36 The droplet of (a) GF ink, (b) GF/AgNPs hybrid ink and (c) GF/PEDOT:PSS hybrid ink

4.4.3 Properties of printed GF ink and GF hybrid inks

Figure 4.37 shows the printed GF and GF hybrid inks on PET substrate at different number of printing layers. Based on Figure 4.37, as expected the inkjet printed color became darker with an increasing of printing layers, especially for GF/PEDOT:PSS hybrid ink. However for GF ink and GF/AgNPs hybrid ink, the printed color were less darker as compared to GF/PEDOT:PSS hybrid ink. It is believed that the printed sample with darker color has better connection and might influence the electrical properties. Denneulin *et al*. (2009) reported that as the number of printing layers increased, the conductive film became connected to each other and therefore reduced the sheet resistance.

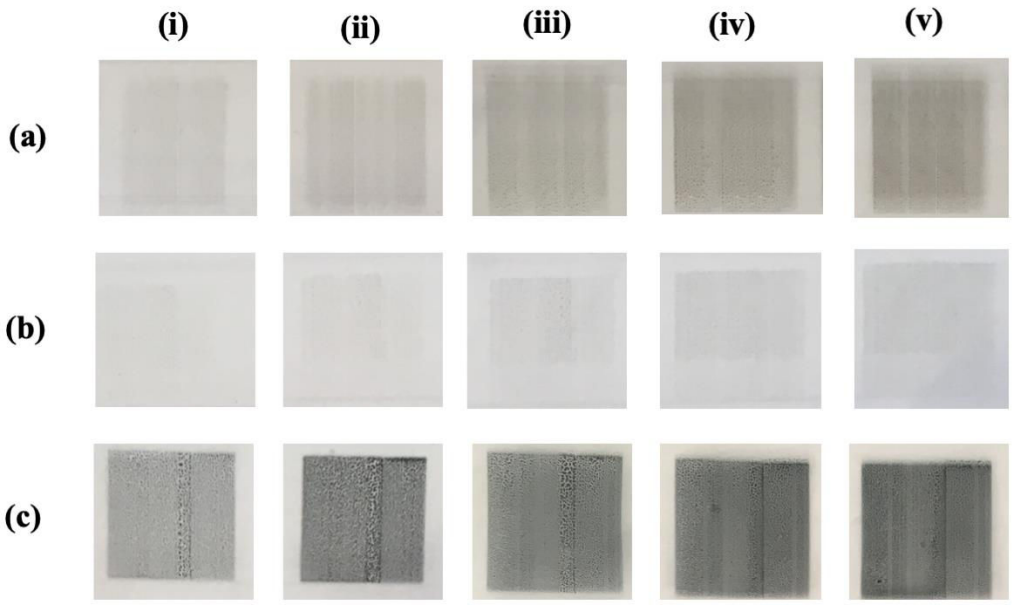

Figure 4.37 Photographs of printed (a) GF ink, (b) GF/AgNPs hybrid ink and (c) GF/PEDOT:PSS hybrid ink on PET substrate with different printing layers (i) 10 layers, (ii) 20 layers, (iii) 30 layers, (iv) 40 layers and (v) 50 layers

The conductive ink patterns made of GF ink and GF hybrid inks at different printing layers were fabricated using inkjet printing in order to determine the conductivity behavior. Figure 4.38 (a, b) presents the surface conductivity of GF ink and GF hybrid inks as a function of printing layer. As clearly seen, the surface conductivity of all inkjet printed samples increased evidently with increasing printing layer. Conductive ink made of GF/PEDOT:PSS hybrid shows the highest surface conductivity compared to those of GF ink and GF/AgNPs hybrid ink at all printing layers. GF/PEDOT:PSS hybrid ink exhibited remarkable improvement of surface conductivity from 10 printing layers to 50 printing layers, followed by GF/AgNPs hybrid ink and GF ink by 100%, 55% and 54%, respectively.

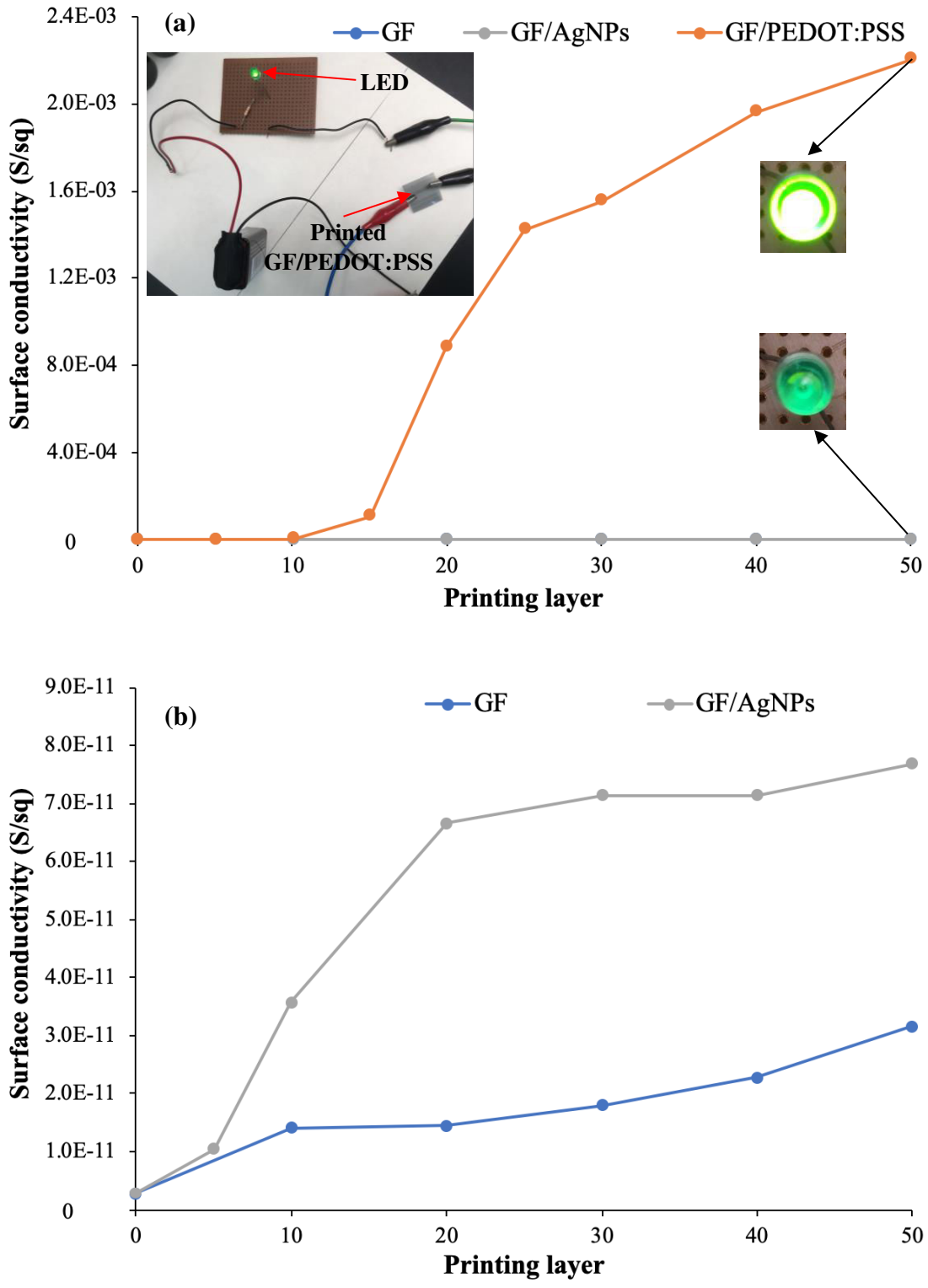

Figure 4.38 (a) Surface conductivity of GF ink and GF hybrid inks as a function of printing layer and (b) enlargement of surface conductivity of GF ink and GF/AgNPs hybrid ink, inset showing digital images of an electronic circuit set up and LED brightness for printed GF ink and GF hybrid inks

Even though the electrical conductivity of pure GF and AgNPs were higher than pure PEDOT:PSS, there is also other factors that influenced the surface conductivity of the printed patterns mainly including the ink stability. Dang *et al*. (2013) reported that the conductive ink should be stable at least during the printing process. As discussed in Section 4.4.1, GF/PEDOT:PSS shows the best stability amongst all conductive inks. Poor ink stability may lead to several problems during printing process which include nozzle clogged and conductive material trapped on the ink cartridge filter, as shown in Figure 4.39. Figure 4.39 (a, b) shows nozzle clogged and conductive material trapped on the ink cartridge filter due to poor ink stability. This results to poor printing quality and therefore affected the surface conductivity of the printed patters as discussed in Figure 4.38.

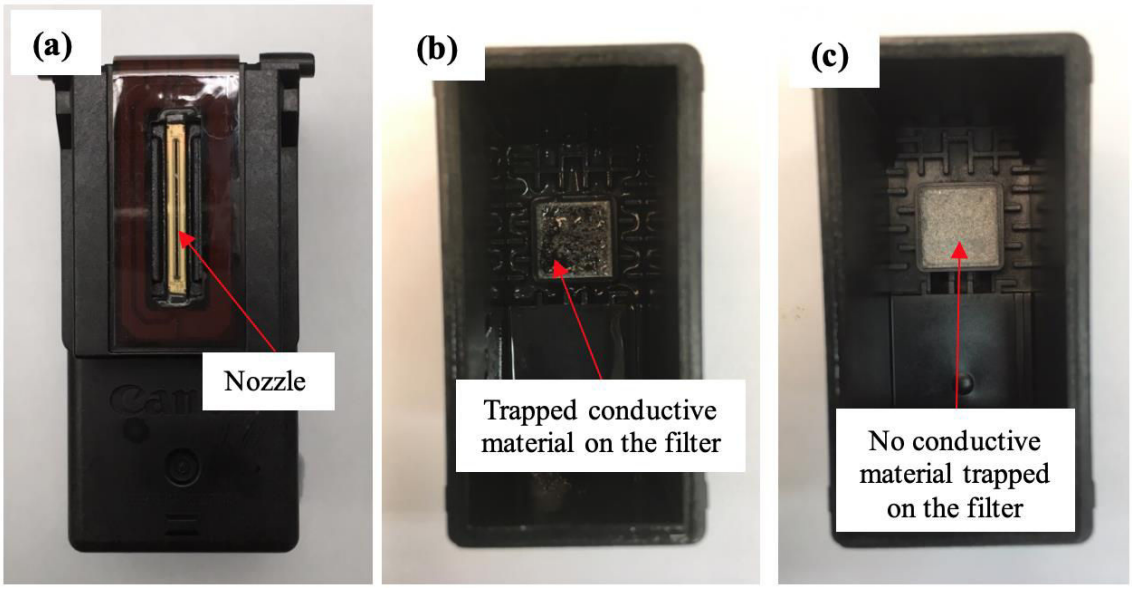

Figure 4.39 Photographs of ink cartridge problems due to poor stability including (a) nozzle clogged and (b) conductive ink trapped on the ink cartridge filter; in comparison with (c) no conductive material trapped on the cartridge filter

Besides that, the surface conductivity of the printed patterns is completely influenced by their morphology. Figure 4.40 shows the morphology of the top printed surface of GF ink and GF hybrid inks with respect to the printing layer that provides information of conductive network formation. Figure 4.40 (a-d) shows the conductive paths were not connected and spread randomly over the substrate showing that amount of GF and GF/AgNPs hybrid were not sufficient to support complete network. Meanwhile for GF/PEDOT:PSS hybrid (Figure 4.40 (e-f)), the network become denser and the conductive network was fully formed. The continuity of the printed patterns improved with an increasing of printing layer from 10 layers to 50 layers. The printed quality of the conductive inks improved as the number of printing layer increased. This observation is in accordance with the previous report by Gao *et al*. (2014) on the fabrication of graphene patterns on the glass substrate using inkjet printing method.

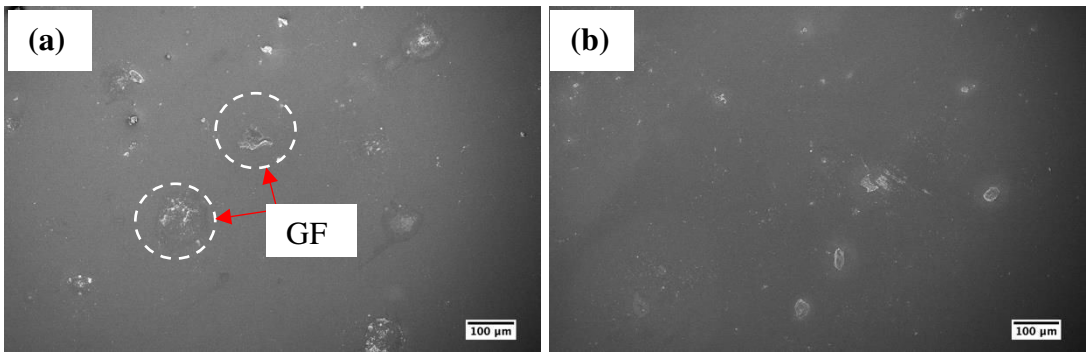

Figure 4.40 SEM micrographs of top printed surface made of (a, b) GF ink, (c,d) GF/AgNPs hybrid ink and (e, f) GF/PEDOT:PSS hybrid ink at (a), (c), (e) 10 printing layers and (b), (d), (f) 50 printing layers [100X mag.]

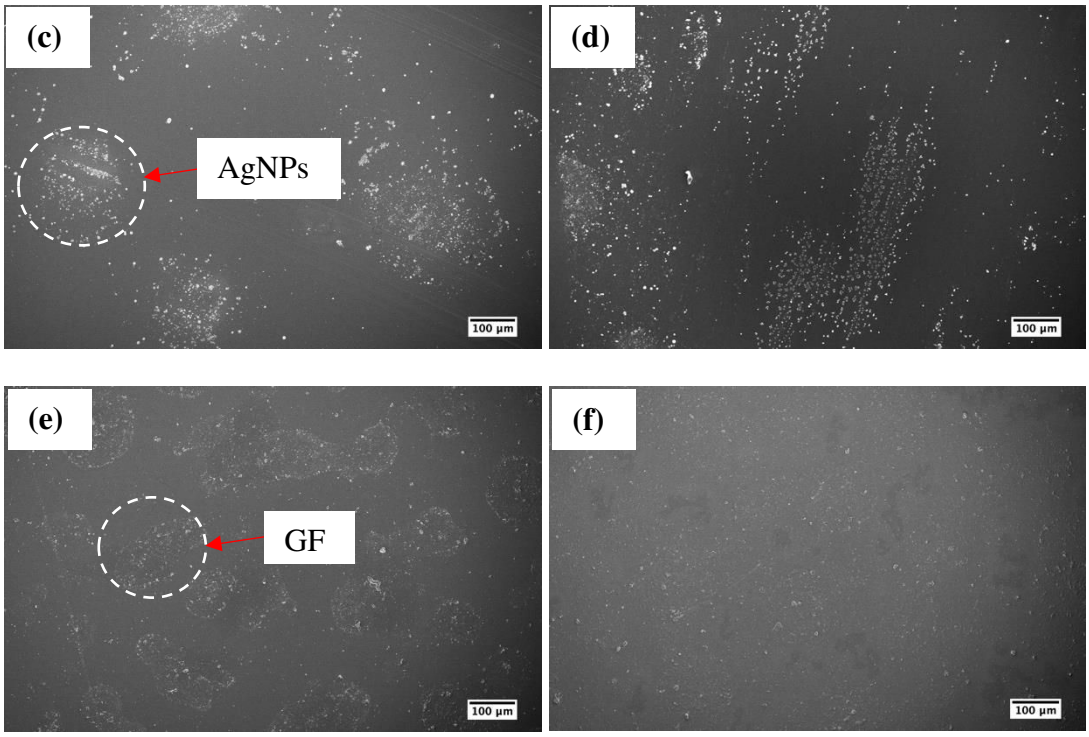

Figure 4.40 *Continued*

4.4.4 Properties of printed GF/PEDOT:PSS hybrid ink for strain sensor

Based on the results shown in Section 4.4.3, GF/PEDOT:PSS hybrid ink was selected for strain sensor characterization. Figure 4.41 presents the typical curves for the relative change of resistance of GF/PEDOT:PSS hybrid sensor. Different strain levels of ε = 1%, 2% and 3% were applied to GF/PEDOT:PSS hybrid printed sensor. The resistance was fully recovered for stretch/release cycles with maximum strain, ε = 3%. It is observed that the linearity of sensor at 1% is slightly better than those of sensor at 2% and 3% strain, respectively. Linearity has an important role for the strain sensor, as it enables the strain rate to be obtained more easily as soon as the resistance change in known. Good linearity means that the resistance change was gentle with sensor stretching (Shengbo *et al*., 2018). Non-linearity of sensor makes the calibration process complex and difficult (Hwang *et al*., 2015).

As shown in Figure 4.41, the relative change resistance of the strain for GF/PEDOT:PSS hybrid sensor was fully recovered to its original value after the stress being released from 1% up to 3%. The findings indicated the recovery performance and hysteresis behavior of the printed hybrid sensor. This results in the motion detection more accurate and reliable. Small hysteresis was observed during ε = 1%. Meanwhile, large hysteresis behavior could be seen when the printed sample was applied at ε = 3%. Large hysteresis behavior leads to the irreversible sensing performance sensor upon dynamic load (Liu and Choi, 2014). Based on the hysteresis curve, the performance of GF/PEDOT:PSS hybrid sensor at low strain 1% is better than those at high strain of 2% and 3%, respectively.

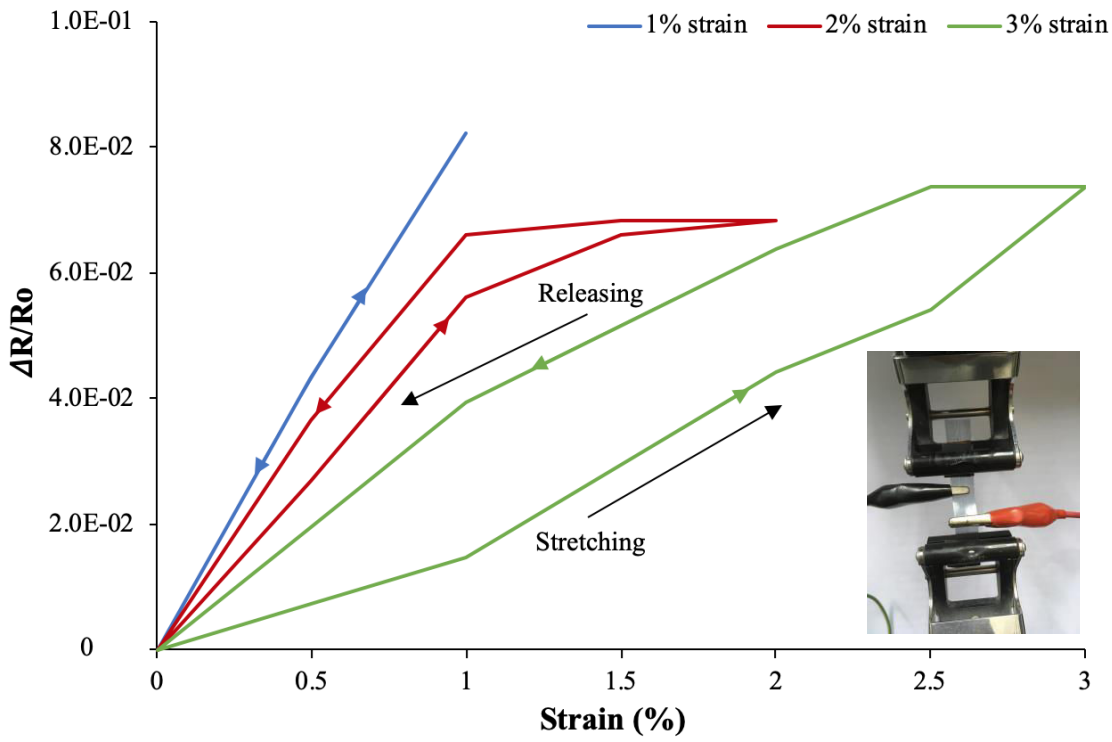

Figure 4.41 Relative change resistance and hysteresis behavior of GF/PEDOT:PSS hybrid sensor as a function of strain, inset showing digital image of an tensile test set up for printed GF/PEDOT:PSS hybrid sensor

Table 4.14 compares the values of gauge factor calculated in the present study with the previous works. The strain sensor produced in the present study (column highlighted in grey) exhibited gauge factor of 4.3 with strain range of 0-20%. Correia *et al*. (2013) have developed strain sensor made of PEDOT and Ag-ink printed on polyimide (PI) substrate with gauge factor up to 2.48 and 0.35, respectively. Meanwhile, Borghetti *et al*. (2016) reported that PEDOT:PSS-ink sensor and Ag-ink sensor with gauge factor values of <1 and 3.7 were produced by inkjet printing on PI substrate. Casiraghi *et al*. (2018) obtained gauge factor up to 125 with large sensitivity (>20%) for graphene printed on paper. Higher gauge factor value is required for the strain sensor due to sensitivity. Based on the comparison, it is observed that the sensitivity gauge factor of the strain sensor based GF/PEDOT:PSS obtained in the present study is higher compared to those of previous works reported by Correia *et al*. (2013) and Borghetti *et al*. (2016) but lower than Casiraghi *et al*. (2018). The prepared hybrid sensor has the capability to be used for low sensitive strain sensing application.

Table 4.14 Comparison of gauge factor between present study and from literature

Materials	**Methods**	**Gauge factor**	**Strain range (%)**
GF/PEDOT:PSS	Inkjet printing	4.3	0-20
PEDOT	Inkjet printing	2.48	Not mentioned
Ag	Inkjet printing	0.35	Not mentioned
PEDOT:PSS	Inkjet printing	<1	Not mentioned
Ag	Inkjet printing	3.7	Not mentioned
Graphene	Inkjet printing	125	20

CHAPTER 5

CONCLUSIONS AND FUTURE RECOMMENDATIONS

5.1 Conclusions

Based on the findings reported from the investigation done in the present research, the following conclusions are summarized based on the outline objectives:

1. Three different types of graphene-like materials; GF, GNPs and SG were utilized and compared. GF exhibited the highest BET surface area and pore volume, meanwhile GNPs and SG displayed large lateral size, high crystalline structure and high quality of particles. However, the small lateral size, low crystalline structure and high oxygen content of GF particle reduced its electrical properties.
2. Graphene-like materials were mixed with PV binder. An addition of filler loadings increased the viscosity and contact angle of the conductive inks. Conductive ink made of GNPs exhibited 186% improvement of electrical conductivity at 10 vol.% of filler loading compared to those of 40% and 10% shown by SG and GF, respectively. The micrographs of graphene-like materials in PV binder showed that the conductive inks were sprayed on the substrate evenly.
3. GNP dispersed in EG exhibited better dispersion stability and physical properties than those of GNP dispersed in PG and IPA. In contrast, GNPs dispersed in NMP and DMF solvents also presented good dispersion stability and wettability, however these solvents suffer from toxicity and high boiling points issues.
4. GNPs dispersions at various ratios of IPA:EG mixed solvents were compared

with GF dispersions. GF inks presented better stability and physical properties than those of GNP inks at all mixed ratios. GF dispersed in IPA:EG at mixed ratio of 1:1 shows the best dispersion stability amongst all the prepared inks with only 50% decrement from the initial concentration after a month.

5. GF/PEDOT:PSS hybrid ink has better stability than those of GF ink and GF/AgNPs hybrid ink with slight decrement from the concentration after a month with the values of 30%, 50% and 69%, respectively. The conductive pattern made of GF/PEDOT:PSS hybrid exhibits 100% improvement of surface conductivity with 50 printing layers compared to those of 55% and 54% shown by GF/AgNPs hybrid and GF, respectively. Strain sensor made of printed GF/PEDOT:PSS hybrid was prepared and exhibits gauge factor with the value of 4.3 with strain range of 0-20%.

5.2 Recommendations for future research

Many efforts have been made in this research to fulfill the objectives of the study on synthesis and characterization of graphene-based inks using common solvents for printed electronics. However, there are still much more room for improvement to further understand the behavior of graphene-based inks. The following lists are the recommendation works to be done for the improvement in further studies:

1. GNPs should be chemically treated in order to reduce the hydrophobicity of GNPs and improve the dispersion behavior with the solvents. The chemical treatment of GNPs should be carefully studied in order to maintain the electrical properties of GNPs.

2. Other fabrication method of conductive ink for flexible electronics should be studied such as 3D printing method. This method can be further used to fabricate conductive ink patterns on the flexible substrate for various electronic applications such as strain sensor.
3. Investigation on the addition of green polymer stabilizers could also be carried out in order to improve the stability of GNPs and GF ink dispersions. This could be helpful in improving the printing quality and electrical conductivity of the printing patterns.
4. Other types of graphene-like materials such as GO, rGO, FLG, *etc* should also be used for the preparation of graphene-based inks in order to investigate the ink dispersion behavior and electrical properties.
5. Graphene hybrid-based ink showing significant promise to improve the electrical properties of the conductive ink, however, the ink dispersion stability is still far from optimization. Thus, the main challenges still remained on formulation of low cost and printable graphene ink with appropriate characteristics in an eco-friendly solvents and fabrication methods.

REFERENCES

Abdellah, A., Virdi, K.S., Meier, R., Döblinger, M., Müller-Buschbaum, P., Scheu, C., Lugli, P., Scarpa, G. (2012). Successive spray deposition of P3HT/PCBM organic photoactive layers: material composition and device characteristics. Advanced Functional Materials 22(19), 4078-4086.

Abdulla, H.S., Abbo, A.I. (2012). Optical and Electrical Properties of Thin Films of Polyaniline and Polypyrrole. International Journal of Electrochemical Science. Int. J Electrochem. Sci. 7, 10666-10678.

Abroshan, H., Akbarzadeh, H., Taherkhani, F., Parsafar, G. (2011). Effect of water-methanol content on the structure of Nafion in the sandwich model and solvent dynamics in nano-channels; A molecular dynamics study. Mol. Phys. 109, 709-724.

Adrjanowicz, K., Kaminski, K., Tarnacka, M., Szutkowski, K., Popenda, L., Bartkowiak, G., Paluch, M. (2016). The effect of hydrogen bonding propensity and enantiomeric composition on the dynamics of supercooled ketoprofen-dielectric, rheological and NMR studies. Phys. Chem. Chem. Phys. 18, 10585-10593.

Alam, A., Meng, Q., Shi, G., Arabi, S., Ma, J., Zhao, N., Kuan, H.C. (2016). Electrically conductive, mechanically robust, pH-sensitive graphene/polymer composite hydrogels. Compos. Sci. Technol. 127, 119-126.

Aleeva, Y., Pignataro, B. (2014). Recent advances in up scalable wet methods and ink formulations for printed electronics. J. Mater. Chem. C 2, 6436-53.

Ankireddy, K., Vunnam, S., Kellar, J., Cross, W. (2013). Highly conductive short chain carboxylic acid encapsulated silver nanoparticle based inks for direct write technology applications. Journal of Materials Chemistry C 1, 572-579.

Arapov, K., Abbel, R., de With, G., Friedrich, H. (2014). Inkjet printing of graphene. Faraday Discuss. 173, 323-336.

Bae, S.H., Lee, Y., Sharma, B.K., Lee, H.J., Kim, J.H., Ahn, J.H. (2013). Graphene-based transparent strain sensor. Carbon 51, 236-242.

Bai, Y. (2017). Research on hydrophobicity of graphene composites. AIP Conference Proceedings 1794, 020008.

Banfield, R. (2013). Specialist Printing Worldwide: Issue One. https://www.appliedinksolutions.com/pdf/sp11340-43.pdf (accessed October 2018).

Barton, A.F.M. (1983). Handbook of solubility parameters and other cohesion parameters. CRC Press Inc.: Boca Raton, FL.

Bharatidasan, T., Narayanan, T.N., Sathyanaryanan, S., Sreejakumari, S.S. (2015). Above 170° water contact angle and oleophobicity of fluorinated graphene oxide based transparent polymeric films. Carbon 84, 207-213.

Bianco, A., Cheng, H.M., Enoki, T., Gogotsi, Y., Hurt, R.H., Koratkar, N., Kyotani, T., Monthioux, M., Park, C.R., Tascon, J.M.D., Zhang, J. (2013). All in the Graphene family - a recommended nomenclature for two-dimensional carbon materials. Carbon 65, 1-6.

Borghetti, M., Serpelloni, M., Sardini, E., Pandini, S. (2016). Mechanical behavior of strain sensors based on PEDOT:PSS and silver nanoparticles inks deposited on

polymer substrate by inkjet printing. Sensors and Actuators A:Physical 243, 71-80.

Bououdina, M. (2016). Emerging research on bioinspired materials engineering. Advances in Chemical and Materials Engineering (IGI Global, USA).

Brownson, D.A.C., Banks, C.E. (2014). The Handbook of Graphene Electrochemistry. Springer London Heidelberg NY Dordecht.

Byrne, F.P., Jin, S., Paggiola, G., Petchey, T.H.M., Clark, J.H. (2016). Tools and techniques for solvent selection: green solvent selection guides. Sustain Chem. Process 4, 7

Campillo, G.E., Vélez, E., Morales, G., Hincapié, C., Osorio, J., Arnache, O., Uribe, J.I., Jaramillo, F. (2017). Synthesis of silver nanoparticles (AgNPs) with antibacterial activity. IOP Conf. Series: Journal of Physics: Conf. Series 850, 012023.

Cançado, L.G., Takai, K., Enoki, T., Endo, M., Kim, Y.A., Misuzaki, H., Speziali, N.L., Jorio, A., Pimenta, M.A. (2008). Measuring the degree of stacking order in graphite by Raman spectroscopy. Carbon 46, 272-275.

Capasso, A., Del Rio Castillo, A.E., Sun, H., Ansaldo, A., Pellegrini, V., Bonaccorso, F. (2015). Ink-jet printing of graphene for flexible electronics: an environmentally approach. Solid State Commun. 224, 53-63.

Carey, T., Jones, C., Moal, F.L., Deganello, D., Torrisi, F. (2018). Spray-coating thin films on three-dimensional surfaces for a semi-transparent capacitive-touch device. ACS Appl. Mater. Interfaces 10, 19948-19956.

Carotenuto, G., Romeo, V., Nicola, S.D., Nicolais, L. (2013). Graphite nanoplatelet chemical cross-linking by elemental sulfur. Nanoscale Research Letters 8(1), 94.

Casiraghi, C., Macucci, M., Parvez, K., Worsley, R., Shin, Y., Bronte, F., Borri, C., Paggi, M., Fiori, G. (2018). Inkjet printed 2D-crystal based strain gauges on paper. Carbon 129, 462-467.

Chen, G., Weng, W., Wu, D., Wu, C., Lu, J., Wang, P., Chen, X. (2004). Preparation and Characterization of Graphite Nanosheets from Ultrasonic Powdering Technique. Carbon 42, 753-759.

Chen, Z., Ren, W., Gao, L., Liu, B., Pei, S., Cheng, H.M. (2011). Three-dimensional flexible and conductive interconnected graphene networks grown by chemical vapour deposition. Nature Materials 10, 424-428.

Cheng, C., Zhang, J., Li, S., Xia, Y., Nie, C., Shi, Z., Cuellar-Camacho, J.L., Ma, N., Haag, R. (2017). A water-processable and bioactive multivalent graphene nanoink for highly flexible bioelectronic films and nanofibers. Advanced Materials 30(5), 1705452.

Cheng, I.C., Wagner, S. (2009). Overview of Flexible Electronics Technology, Springer, Boston.

Chiu, Y.C., Huang, C.L., Wang, C. (2016). Rheological and conductivity percolations of syndiotactic polystyrene composites filled with graphene nanosheets and carbon nanotubes: A comparative study. Compos. Sci. Technol. 134, 153-160.

Choi, H.W., Zhou, T., Singh, M., Jabbour, G.E. (2015). Recent developments and directions in printed nanomaterials. Nanoscale 7, 3338-3355.

Choucair, M., Thodarson, P., Stride, J.A. (2009). Gram-scale Production of Graphene Based on Solvothermal Synthesis and Sonication. Nat. Nanotechnol., 30-33.

Chun, S., Choi, Y., Park, W. (2017). All-graphene strain sensor on soft substrate. Carbon 116, 753-759.

Cochrane, C., Koncar, V., Lewandowski, M., Dufour, C. (2007). Design and development of a flexible strain sensor for textile structures based on a conductive polymer composite. Sensors 7(4), 473-492.

Coleman, J.N. (2013). Liquid exfoliation of defect-free graphene. Acc. Chem. Res. 46(1), 14-22.

Correia, V., Caparros, C., Casellas, C., Francesch, L., Rocha, J.G., Lanceros-Mendez, S. (2013). Development of inkjet printed strain sensors. Smart Mater. Struct. 22, 105028.

Cui, W., Lu, W., Zhang, Y., Lin, G., Wei, T., Jiang, L. (2010). Gold nanoparticle ink suitable for electric-conductive pattern fabrication using in ink-jet printing technology. Colloids and Surfaces A: Physicochem. Eng. Aspects 358, 35-41.

Cummins, G., Desmulliez, M.P.Y. (2012). Inkjet printing of conductive materials: a review. Circuit Word 38, 193-213.

Dabczyński, P., Marzec, M.M., Pięta, Ł., Fijałkowski, K., Raczkowska, J., Bernasik, A., Budkowski, A., Rysz, J. (2018). Engineering a poly(3,4-ethylenedioxythiophene):(polystyrene sulfonate) surface using self-assembling molecules- a chemical library approach. ACS Omega 3, 3631-3639.

Dang, M.C., Dang, T.M.D., Fribourg-Blanc, E. (2013). Inkjet printing technology and conductive inks synthesis for microfabrication techniques. Adv. Nat. Sci: Nanosci. Nanotechnol. 4, 015009.

DataPhysics Instruments GmbH (2019). Surface tension values of some common test liquids for surface energy analysis. Retrieved from: https://www.dataphysics-instruments.com/Downloads/Surface-Tensions-Energies.pdf [Accessed August 2019].

Deng, D., Feng, S., Shi, M., Huang, C. (2017). In situ preparation of silver nanoparticles decorated graphene conductive ink for inkjet printing. J. Mater. Sci.: Mater. Electron. 28, 15411-15417.

Denneulin, A., Bras, J., Blayo, A., Khelifi, B., Roussel-Dherbey, F., Neuman, C. (2009). The influence of carbon nanotubes in inkjet printing of conductive polymer suspensions. Nanotechnology, 20(38), 385701.

Denneulin, A., Bras, J., Carcone, F., Neuman, C., Blayo, A. (2011). Impact of ink formulation on carbon nanotube network organization within inkjet printed conductive films. Carbon 49, 2603-2614.

Diabetes Queensland (2017). Breathable, flexible electronics allow long term on-skin health monitoring. Retrieved from: https://www.diabetesqld.org.au/media-centre/2017/july/breathable,-flexible-electronics-allow-long-term-on-skin-health-monitoring.aspx [Accessed May 2019].

Dillon, A.C., Gennett, T., Jones, K.M., Alleman, J.L., Parilla, P.A., Heben, M.J. (1999). A simple and complete purification of single-walled carbon nanotube materials. Adv. Mater. 11(16), 1354-1358.

Dybowska-Sarapuk, L., Kielbasinski, K., Arazna, A., Futera, K., Skalski, A., Janczak, D., Sloma, M., Jakubowska, M. (2018). Efficient Inkjet Printing of Graphene-Based Elements: Influence of Dispersing Agent on Ink Viscosity. Nanomaterials 8, 602.

Egerton, R.F. (2005). Physical principles of electron microscopy. An introduction to TEM, SEM and AEM. Springer, NY, USA, 108-110.

Elmolla, S.H.A. (2017). Inkjet printing & spray deposition techniques for flexible electronic applications. Technischen Universität München.

Emiru, T.F., Ayele, D.W. (2017). Controlled synthesis, characterization & reduction of graphene oxide: A convenient method for large scale production. Egypt. J. Basic Appl. Sci. 4, 74-79.

Fayos, J. (1999). Possible 3D carbon structures as progressive intermediates in graphite to diamond phase transition. J. Sol. State Chem. 148, 278-285.

Ferrari, A.C., Meyer, J.C., Scardaci, V., Casiraghi, C., Lazzeri, M., Mauri, F., Piscanec, S., Jiang, D., Novoselov, K.S., Roth, S., Geim, A.K. (2006). Raman spectrum of graphene and graphene layers. Phys. Rev. Lett. 9, 187401.

Ferrari, A.C., Robertson, J. (2000). Interpretation of Raman spectra of disordered and amorphous carbon. Phys. Rev. B 61, 14095.

Ferrari, A.C., Robertson, J. (2001). Origin of the 1150- cm^{-1} Raman mode in nanocrystalline diamond. Phys. Rev. B 63, 121405.

Filippidou, M.K., Tegou, E., Tsouti, V., Chatzandroulis, S. (2015). A flexible strain sensor made of graphene nanoplatelets/polydimethylsiloxane nanocomposite. Microelectronic Engineering 142, 7-11.

Freitas, C., Müller, R.H. (1998). Effect of light and T on zeta potential & physical stability in solid lipid nanoparticle (SLN). Int. J. Pharm. 168, 221-229.

Gaikwad, A.M., Steingart, D.A., Nga Ng, T., Schwartz, D.E., Whiting, G.L. (2013). A flexible high potential printed battery for powering printed electronics. Applied Physics Letters 102(23), 104.

Gao, Y., Shi, W., Wang, W., Leng, Y., Zhao, Y. (2014). Inkjet printing patterns of highly conductive pristine graphene on flexible substrates. Ind. Eng. Chem. Res. 53, 16777-16784.

Ghany, N.A.A., Elsherif, S.A., Handal, H.T. (2017). Revolution of graphene for different applications: state-of-the-art. Surfaces and Interfaces 9, 93-106.

Gonzalez-Macia, L., Morrin, A., Smyth, M.R., Killard, A.J. (2010). Advancend printing and deposition methodologies for the fabrication of biosensors and biodevices. The Analyst. 135(5), 845-867.

Groenendaal, L., Jonas, F., Freitag, D., Pielartzik, H., Reynolds, J.R. (2000). Poly(3,4-ethylenedioxythiophene) and Its Derivatives: Past, Present, and Future. Adv. Mater. 12, 481-494.

Guo, X., Mei, N. (2014). Assessment of the toxic potential of graphene family nanomaterials. J. Food Drug Anal. 22, 105-115.

Gutmann, V. (1978). The donor-acceptor approach to molecular interactions, Plenum Press, New York.

Ha, J., Park, J., Ha, J., Kim, D., Chung, S., Lee, C., Hong, Y. (2015). Selectively modulated inkjet printing of highly conductive and transparent foldable polymer electrodes for flexible polymer light-emitting diode applications. Org. Electron. 19, 147-156.

Haghi, A.K., Praveen, K.M., Thomas, S. (2018). Engineered Carbon Nanotubes and Nanofibrous Materials. Apple Academic Press Inc., USA.

Hansen, C.M. (2007). Hanses solubility parameters- A user's handbook. CRC Press: Boca Raton, FL.

He, P., Derby, B. (2017). Controlling coffee ring formation during drying of inkjet printed 2D inks. Adv. Mater. Interfaces 4, 1700944.

Hernandez, Y., Nicolosi, V., Lotya, M., Blighe, F.M., Sun, Z., De, S., *et al*., (2008). High-yield production of graphene by liquid-phase exfoliation of graphite. Nat. Nanotechnol. 3(9), 563-568.

Hernandez, Y., Lotya, M., Rickard, D., Bergin, S.D., Coleman, J.N. (2010). Measurement of multicomponent solubility parameters for graphene facilitates solvent discovery. Langmuir 26, 3208-3213.

Hoath, S.D. (2016). Fundamentals Of Inkjet Printing, Germany, Wiley-VCH.

Hong, Y., Kanicki, J. (2004). Opto-Electronic Properties of Poly (Fluorene) Co-Polymer Red Light-Emitting Devices on Flexible Plastic Substrate IEEE Trans. Electron. Dev. 51, 1562.

Htwe, Y.Z.N., Chow, W.S., Suda, Y., Thant, A.A., Mariatti, M., Appl. Surf. Sci. 469, 951-961.

Hu, H., Zhang, G., Xiao, L., Wang, H., Zhang, Q., Zhao, Z. (2012). Preparation and electrical conductivity of graphene/ultrahigh molecular weight polyethylene composites with a segregated structure. Carbon 50 (12), 4596-4599.

Huang, L., Huang, Y., Liang, J., Wan, X., Chen, Y. (2011). Graphene-based conducting inks for direct printing of flexible conductive patterns and their applications in electric circuits and chemical sensors. Nano Res. 4, 675-684.

Huang, T.S., Wu, W. (2019). Scalable manufacturing of inkjet-printed wearable energy storage devices. J. Mater. Chem. A.

Hughes, J.M., Aherne, D., Coleman, J.N. (2013). Generalizing solubility parameter theory to apply to one- and two- dimensional solutes and to incorporate dipolar interactions. J. Appl. Polym. Sci. 127, 4483-4491.

Hunter, R. (1981). Zeta potential in colloid science: principle and applications. Waltham: Academic Press.

Hwang, B.U., Lee, J.H., trung, T.Q., Roh, E., Kim, D.I., Kim, S.W., Lee, N.E. (2015). Transparent stretchable self-powered patchable sensor platform with ultrasensitive recognition of human activities. ACS Nano 9(9), 8801-8810.

Ihalainen, P., Määttänen, A., Sandler, N. (2015). Printing technologies for biomolecule and cell-based applications. Int. J. Pharm. 494, 585-592.

Israelachvili, J.N. (2011). Intermolecular and surface forces. Academic Press.

Iwakoshi, A., Nanke, T., Kobayashi, T. (2005). Coating Materials Containing Gold Nanoparticles. Gold Bull 38, 107-112.

Jaworski, S., Sawosz, E., Grodzik, M., Winnicka, A., Prasek, M., Wierzbicki, M., Chwalibog, A. (2013). In vitro evaluation of the effects of graphene platelets on glioblastoma multiforme cells. Int. J. Nanomedicine 8, 413-20.

Jeon, J.Y., Ha, T.J. (2016). Waterproof electronic-bandage with tunable sensitivity for wearable strain sensors. ACS Applied Materials & Interfaces 8(4), 2866-2871.

Jeong, S., Song, H.C., Lee, W.W., Lee, S.S., Choi, Y., Son, W., Kim, E.D., Paik, C.H., Oh, S.H., Ryu, B.H. (2011). Stable Aqueous Based Cu Nanoparticle Ink For Printing Well-Defined Highly Conductive Features On A Plastic Substrate. Langmuir 27, 3144-3149.

Jiang, L., Fan, Z. (2014). Designed of advanced porous materials: from graphene nanomesh to 3D architectures. Nanoscale 6, 1922-1945.

Johnson, D.W., Dobson, B.P., Coleman, K.S. (2015). A manufacturing perspective on graphene dispersions. Current Opinion in Colloid & Interface Science 20, 367-382.

Johra, F.T., Lee, J.W., Jung, W.G. (2014). Facile and safe graphene dispersion on solution based platform. Journal of Industrial and Engineering Chemistry 20, 2883-2887.

Jun, Y.S., Um, J.G., Jiang, G., Lui, G., Yu, A. (2018). Ultra-large sized graphene nano-platelets (GnPs) incorporated polypropylene(PP)/GnPs composites engineered by melt compounding and its thermal, mechanical, and electrical properties. Compos. Part B 133, 218-225.

Kamyshny, A., Ben-Moshe, M., Aviezer, S., Magdassi, S. (2005). Ink-jet printing of metallic nanoparticles and microemulsions. Macromol. Rapid Commun. 26, 281-288.

Kamyshny, A., Magdassi, S. (2014). Conductive Nanomaterials For Printed Electronics. Small 10, 3515-3535.

Kang, J.S., Kim, H.S., Ryu, J., Hahn, H.T., Jang, S., Joung, J.W. (2010). Inkjet printed electronics using copper nanoparticle ink, J. Mater. Sci.: Mater. Electron. 21, 1213-1220.

Karim, N., Afroj, S., Malandraki, A., Butterworth, S., Beach, C., Rigout, M., Novoselov, K.S., Casson, A.J., Yeates, S.G. (2017). All inkjet-printed graphene-based conductive patterns for wearable e-textile applications. J. Mater. Chem. C 5, 11640-11648.

Kastner, J., Faury, T., Außerhuber, H.M., Obermüller, T., Leichtfried, H., Haslinger, M.J., Liftinger, E., Innerlohinger, J., Gnatiuk, I., Holzinger, D., Lederer, T. (2017). Silver-based reactive ink for inkjet-printing of conductive lines on textiles. Microelectron Eng. 176, 84-88.

Kernan, D.M., Blau, W.J. (2008). Exploring the mechanisms of carbon-nanotube dispersion aggregation in a highly polar solvent. Europhys. Lett. 83, 66009.

Khan, S., Lorenzelli, L., Dahiya, R.S. (2015). Technologies for Printing Sensors and Electronics Over Large Flexible Substrates: A Review. IEEE Sens. J. 15, 3164-3185.

Khan, U., O'Neill, A., Lotya, M., De, S., Coleman, J.N. (2010). High-concentration solvent exfoliation of graphene. Small 6(7), 864-871.

Khondoker, M.A.H., Mun, S.C., Kim, J. (2013). Synthesis and characterization of conductive silver ink for electrode printing on cellulose film. Applied Physics A, 112(2), 411-418.

Kim, D.S., Kim, J.S., Lee, M.C. (2014). Thin film forming technique based on hybrid spray coating using electrostatic force and air pressure. Japanese Journal of Applied Physics 53, 1-8.

Kim, I., Lee, T.M., Kim, J. (2014). A study on the electrical and mechanical properties of printed Ag thin films for flexible device application. J. Alloy Compd. 596, 158-163.

Kim, Y.H., Sachse, C., Machala, M.L., May, C., Müller-Meskamp, L., Leo, K. (2011). Highly Conductive PEDOT:PSS Electrode with Optimized Solvent and Thermal Post-Treatment for ITO-Free Organic Solar Cells. Adv. Funct. Mater. 21, 1076-1081.

Konkena, B., Vasudevan, S. (2012). Understanding aqueous dispersibility of graphene oxide and reduced graphene oxide through pka measurements. J. Phys. Chem. Lett. 3, 867-872.

Kordás, K., Mustonen, T., Tóth, G., Jantunen, H., Lajunen, M., Soldano, C., Talapatra, S., Kar, S., Vajtai, R., Ajayan, P.M. (2016). Inkjet printing of electrically conductive patterns of carbon nanotubes. Small 2, 1021-1025.

Kulkarni, M.V., Apte, S.K., Naik, S.D., Ambekar, J.D., Kale, B.B. (2013). Ink-jet printed conducting polyaniline based flexible humidity sensor. Sens Actuators B-Chem. 178, 140-143.

Laflamme, S., Kollosche, M., Connor, J.J., Kofod, G. (2012). Robust flexible capacitive surface sensor for structural health monitoring applications. Journal of Engineering Mechanics 139(7), 879-885.

Lau, G.K., Shrestha, M. (2017). Ink-Jet Printing of Micro-Electro-Mechanical Systems (MEMS). Micromachines 8, 194.

Le, H.P. (1998). Progress and trends in ink-jet printing technologies. J. Imaging Sci. Technol. 42, 49-62.

Lee, Y., Choi, J.R., Lee, K.J., Stott, N.E., Kim, D. (2008). Large-scale synthesis of copper nanoparticles by chemically controlled reduction for applications of inkjet-printed electronics. Nanotechnology 19, 415604.

Lewis, G.N. (1923). Valence and the structure of atoms and molecules, Chemical Catalog Co., New York.

Li, D., Huang, J., Kaner, R.B. (2009). Polyaniline nanofibers: a unique polymer nanostructure for versatile applications. Acc. Chem. Res. 42, 135-145.

Li, J., Ye, F., Vaziri, S., Muhammed, M., Lemme, M.C., Östling, M. (2013). Efficient inkjet printing of graphene. Advanced Materials 25, 3985-92.

Li, L., Gao, M., Guo, Y., Sun, J., Li, Y., Li, F., Song, Y., Li, Y. (2017). Transparent Ag@Au–graphene patterns with conductive stability via inkjet printing. J. Mater. Chem. C 5, 2800-2806.

Li, P., Tao, C.A., Wang, B., Huang, J., Li, T., Wang, J. (2018). Preparation of Graphene Oxide-Based Ink for Inkjet Printing. J. Nanosci. Nanotechnol. 18, 713-718.

Li, Y., Lu, D., Wong, C.P. (2010). Electrical Conductive Adhesives with Nanotechnologies. Springer US.

Li, Y., Yang, Q., Li, M., Song, Y. (2016). Rate-dependent interface capture beyond the coffee-ring effect. Scientific Reports 6, 24628.

Lin, Y., Liu, S., Chen, S., Wei, Y., Dong, X., Liu., L. (2016). A highly stretchable and sensitive strain sensor based on graphene-elastomer composites with a novel double-interconnected network. J. Mater. Chem. C 4, 6345-6352.

Lipomi, D.J., Vosgueritchian, M., Tee, B.C.K., Hellstrom, S.L., Lee, J.A., Fox, C.H., Bao, Z. (2011). Skin-like pressure and strain sensors based on transparent elastic films of carbon nanotubes. Nature Nanotechnology 6, 788-792.

Liu, C.X., Choi, J.W. (2014). Analyzing resistance response of embedded PDMS and carbon nanotubes composites under tensile strain. Microelectronics Engineering 117, 1-7.

Liu, H., Gao, J., Huang, W., Dai, K., Zheng, G., Liu, C. (2016). Electrically conductive strain sensing polyurethane nanocomposites with synergistic carbon nanotubes and graphene bifillers. Nanoscale 8, 12977-12989.

Liu, J., Takeshi, D., Sasaki, K., Lyth, S.M. (2014). Defective graphene foam: A platinum catalyst support for PEMFCs. Journal of the Electrochemical Society 161, 838-844.

Liu, L., Wan, X., Sun, L., Yang, S., Dai, Z., Tian, Q., Lei, M., Xiao, X., Jiang, C., Wu, W. (2015). Anion-mediated synthesis of monodisperse silver nanoparticles useful for screen printing of high-conductivity patterns on flexible substrates for printed electronics. RSC Adv. 5, 9783-9791.

Liu, W.W., Wang, J.N., Wang, X.X. (2012). Charging of unfunctionalized graphene in organic solvents. Nanoscale 4, 425-428.

Lotya, M., Hernandez, Y., King, P.J., Smith, R.J., Nicolosi, V., Karlsson, L.S., *et al*., (2009). Liquid phase production of graphene by exfoliation of graphite in surfactant/water solutions. J. Am. Chem. Soc. 131(10), 3611-3620.

Lotya, M., King, P.J., Khan, U., De, S., Coleman, J.N. (2010). High-concentration, surfactant-stabilized graphene dispersions. ACS Nano. 4(6), 3155-3162.

Low, C.T.J., Walsh, F.C., Chakrabarti, M.H., Hashim, M.A., Hussain, M.A. (2013). Electrochemical Approaches to the Production of Graphene Flakes and their Potential Applications. Carbon 54, 1-21.

Lyklema, J. (1999). The surface tension of pure liquids- thermodynamic components and corresponding states. Colloids Surf. A 156, 413-421.

Ma, J., Wang, J., He, Y.S., Lioa, X.Z., Chen, J., Wang, J.Z., Yuan, T., Ma, Z.F. (2014). A solvothermal strategy: one-step in situ synthesis of self-assembled 3D graphene-based composites with enhanced lithium storage capacity. Journal of Materials Chemistry A 2, 9200-9207.

Ma, J., Zhou, X., Ding, S., Liu, Z. (2017). Solvent evaporation induced self-assembly of graphene foam for thermally conductive polymers. RSC Adv. 7, 15469-15474.

Ma, M., Zhu, Z., Wu, B., Chen, S., Shi, Y., Wang, X. (2017). Preparation of highly conductive composites with segregated structure based on polyamide-6 and reduced graphene oxide. Mater. Lett. 190(1), 71-74.

Majee, S., Liu, C., Wu, B., Zhang, S.L., Zhang, Z.B. (2017). Ink-jet printed highly conductive pristine graphene patterns achieved with water-based ink and aqueous doping processing. Carbon 114, 77-83.

Majee, S., Song, M., Zhang, S.L., Zhang, Z.B. (2016). Scalable inkjet printing of shear-exfoliated graphene transparent conductive films. Carbon 102, 51-57.

Manoratne, C.H., Rosa, S.R.D., Kottegoda, I.R.M., XRD-HTA, UV Visible, FTIR and SEM interpretation of reduced graphene oxide synthesized from high purity vein graphite. Mat. Sci. Res. India 14(1), 19-30.

Mariani, P., Vesce, L., Di Carlo A. (2015). The role of printing techniques for large-area dye sensitized solar cells. Semicond. Sci. Technol. 30, 104003.

Meng, Q., Liu, Z., Han, S., Xu, L., Araby, S., Cai, R., Zhao, Y. (2019). A facile approach to fabricate highly sensitive, flexible strain sensor based on elastomeric/graphene platelet composite film. Journal of Materials Science https://doi.org/10.1007/s10853-019-03650-1.

Mengistie, D.A., Ibrahem, M.A., Wang, P.C., Chu, C.W. (2014). Highly conductive PEDOT:PSS treated with formic acid for ITO-free polymer solar cells. ACS Appl. Mater. Interfaces 6, 2292-2299.

Miao, F., Majee, S., Songa, M., Zhao, J., Zhang, S.L., Zhang, Z.B. (2016). Inkjet printing of electrochemically-exfoliated graphene nanoplatelets. Synth. Met. 220, 318-322.

Michel, M., Desai, J.A., Biswas, C., Kaul, A.B. (2016). Engineering chemically exfoliated dispersions of two-dimensional graphite and molybdenum disulphide for inkjet printing. Nanotechnology 27, 485602.

Müller, R.H., Schwarz, C., zur Mühlen, A., Mehnert, W. (1994). Incorporation of lipophilic drugs and drug release profiles of carsolid lipid nanoparticles (SLN). Int. Symp. Control Bioact. Mater. 21, 146-147.

Nanda, K.K., Maisels, A., Kruis, F.E., Fissan, H., Stappert, S. (2003). Higher surface energy of free nanoparticles. Physical review letters 91(10), 106102.

Nethravathi, C., Rajamathi, M. (2008). Chemically modified graphene sheets produced by the solvothermal reduction of colloidal dispersions of graphite oxide. Carbon 46, 1994-1998.

Nicolosi, V., Chhowalla, M., Kanatzidis, M.G., Strano, M.S., Coleman, J.N. (2013). Liquid exfoliation of layered materials. Science 340, 1226419.

Nie, X., Wang, H., Zou, J. (2012). Inkjet printing of silver citrate conductive ink on PET substrate, Appl Surf Sci. 261, 554-560.

Novoselov, K.S., Geim, A.K., Morozov, S.V., Jiang, D., Zhang, Y., Dubonos, S.V., Grigorieva, I.V., Firsov, A.A. (2004). Electric field effect in atomically thin carbon films. Science 306, 666-669.

Novoselov, K.S., Fal'ko, V.I., Colombo, L., Gellert, P.R., Schwab, M.G., Kim, K. (2012). A roadmap for graphene. Nature 490, 192-200.

O'Mahony, C., Haq, E.U., Silien, C., Tofail, S.A.M. (2019). Rheological issues in carbon-based inks for additive manufacturing. Micromachines (Basel) 10(2), 99.

Öhlund, T., Örtegren, J., Forsberg, S., Nilsson, H.E. (2012). Paper surfaces for metal nanoparticle inkjet printing. Appl. Surf. Sci. 259, 731-739.

Ownby, P.D., Yang, X., Liu, J. (1992). Calculated X-ray diffraction data for diamond polytypes. J. Am. Ceram. Soc. 75, 1876-83.

Pan, L., Chortos, A., Yu, G., Wang, Y., Isaacson, S., Allen, R., Bao, Z. (2014). An ultra-sensitive resistive pressure sensor based on hollow-sphere microstructure

induced elasticity in conducting polymer film. Nature Communications 5, 3002.

Park, H.Y., Kang, B.J., Lee, D., Oh, J.H. (2013). Control of surface wettability for inkjet printing by combining hydrophobic coating and plasma treatment. Thin Solid Films 546, 162-166.

Park, Y.T., Qian, Y., Chan, C., Suh, T., Nejhad, M.G., Macosko, C.W., Stein, A. (2015). Epoxy toughening with low graphene loading. Adv. Func. Mater. 25, 575-585.

Parvez, K., Yang, S., Feng, X., Müllen, K. (2015). Exfoliation of graphene via wet chemical routes. Synthetic Metals 210, 123-132.

Pei, S., Cheng, H.M. (2012). The reduction of graphene oxide. Carbon 50, 3210-3228.

Peng, S., Fan, X., Li, S., Zhang, J. (2013). Green synthesis and characterization of graphite oxide by orthogonal experiment. J. Chil. Chem. Soc. 58.

Penn State (2013). Flexible electronics could transform the way we make and use electronic devices. Retrieved from: https://news.psu.edu/story/272086/2013/04/08/research/flexible-electronics-could-transform-way-we-make-and-use-electronic [Accessed May 2019].

Perinka, N., Kim, C.H., Kaplanova, M., Bonnassieux, Y. (2013). Preparation and Characterization of Thin Conductive Polymer Films on the base of PEDOT:PSS by Ink-Jet Printing. Physics Procedia 44, 120-129.

Pietrikova, A., Lukacs, P., Jakubeczyova, D., Ballokova, B., Potencki, J., Tomaszewski, G., Pekarek, J., Prikrylova, K., Fides, M. (2016). Surface

analysis of polymeric substrates used for inkjet printing technology. Circuit World 42, 9-16.

Popli, S.A., Patel, U.D. (2015). Electrochemical decolourization of Reactive Black 5 in an undivided cell using Ti and graphite anodes: Effect of polypyrrole coating on anodes. J. Electrochem. Sci. Eng. 5, 145-156.

Rajan, K., Roppolo, I., Chiappone, A., Bocchini, S., Perrone, D., Chiolerio, A. (2016). Silver nanoparticle ink technology: State of the art. Nanotechnol. Sci. Appl. 9, 1-13.

Sabba, Y., Thomas, E.L. (2004). High-Concentration Dispersion of Single-Wall Carbon Nanotubes. Macromolecules 37, 4815-4820.

Saghaei, J., Fallahzadeh, A., Yousefi, M.H. (2015). Improvement of electrical conductivity of PEDOT:PSS films by 2-methylimidazole post treatment. Organic Electronics 19, 70-75.

Sahoo, S.K., Mallik, A. (2015). Synthesis and characterization of conductive few layered graphene nanosheets using an anionic electrochemical intercalation and exfoliation technique. J. Mater. Chem. C 3, 10870-10878.

Saion, E., Gharibshahi, E., Naghavi, K. (2013). Size-controlled and optical properties of monodispersed silver nanoparticles synthesized by the radiolytic reduction method. Int. J. Mol. Sci. 14, 7880-7896.

Salunkhe, R.R., Tang, J., Kobayashi, N., Kim, J., Ide, Y., Tominaka, S., Kim, J.H., Yamauchi, Y. (2016). Ultrahigh performance supercapacitors utilizing core-shell nanoarchitectures from a metal-organic framework-derived nanoporous carbon and a conducting polymer. Chem. Sci. 7, 5704-5713.

Schlenoff, J.B., Xu, H. (1992). Evolution of Physical and Electrochemical Properties of Polypyrrole during Extended Oxidation. J. Electrochem Soc. 139, 2397-2401.

Schramm, L. (2005), Emulsions, foams, and suspensions: fundamentals and applications. Hoboken: Wiley.

Secor, E.B., Prabhumirashi, P.L., Puntambekar, K., Geier, M.L., Hersam, M.C. (2013). Inkjet Printing of High Conductivity, Flexible Graphene Patterns. J. Phys. Chem. Lett. 4, 1347-51.

Secor, E.B., Ahn, B.Y., Gao, T.Z., Lewis, J.A., Hersam, M.C. (2015). Rapid and Versatile Photonic Annealing of Graphene Inks for Flexible Printed Electronics. Adv. Mater. 27, 6683-8.

Secor, E.B., Gao, T.Z., Islam, A.E., Rao, R., Wallace, S.G., Zhu, J., Putz, K.W., Maruyama, B., Hersam, M.C. (2017). Enhanced Conductivity, Adhesion, and Environmental Stability of Printed Graphene Inks with Nitrocellulose. Chem. Mater. 29, 2332-2340.

Sharbati, M.T. (2016). Graphene Quantum Dot-Based Organic Loght Emitting Diodes Master's Thesis, University of Pittsburgh.

Shaw, D.J. (1996). Introduction to Colloid and Surface Chemistry, 4th Edition Butterworth-Heinemann, Oxford.

Shen, H., Zhang, L., Liu, M., Zhang, Z. (2012). Biomedical applications of graphene. Theranostics. 2, 283-94.

Shengbo, S., Lihua, L., Aoqun, J., Qianqian, D., Jianlong, J., Qiang, Z., Wendong, Z. (2018). Highly sensitive wearable strain sensor based on silver nanowires and nanoparticles. Nanotechnology 29(25), 255202.

Singh, M., Haverinen, H.M., Dhagat, P., Jabbour, G.E. (2010). Inkjet printing-process and its applications. Adv. Mater. 22, 673-85.

Song, E., Tortorich, R.P., da Costa, T.H., Choi, J.W. (2015). Inkjet printing of conductive polymer nanowire network on flexible substrates and its application in chemical sensing. Microelectron. Eng. 145, 143-148.

Speyer, L., Fontana, S., Cahen, S., Ghanbaja, J., Medjahdi, G., Hérold, C. (2015). Multi-scale Characterization of Graphenic Materials Synthesized by a Solvothermal Based Process: Influence of the Thermal Treatment. Solid State Sci. 50, 42-51.

Speyer, L., Fontana, S., Cahen, S., Hérold, C. (2018). Simple production of high-quality graphene foams by pyrolysis of sodium ethoxide. Mater. Chem. Phys. 219, 57-66.

Stempien, Z., Rybicki, T., Rybicki, E., Kozanecki, M., Szynkowska, M.I. (2015). *In-situ* deposition of polyaniline and polypyrrole electroconductive layers on textile surfaces by the reactive ink-jet printing technique. Synth. Met. 202, 49-62.

Stoppa, M., Chiolerio, A. (2014). Wearable electronics and smart textiles: a critical review. Sensors (Basel) 14, 11957-11992.

Suganuma, K. (2014). Introduction to Printed Electronics: SpringerBriefs in Electrical and Computer Engineering. Springer-Verlag New York.

Tang, J., Yamauchi, Y. (2016). Carbon materials: MOF morphologies in control. Nat. Chem. 8, 638-639.

Tang, Z., Zhang, L., Zeng, C., Lin, T., Guo, B. (2012). General route to graphene with liquid-like behavior by non-covalent modification. Soft Matter. 8, 9214-9220.

Tian, H., Shu, Y., Cui, Y.L., Mi, W.T., Yang, Y., Xie, D., Ren, T.L. (2014). Scalable fabrication of high-performance and flexible graphene strain sensors. Nanoscale 6, 699-705.

Torrisi, F., Carey, T. (2018). Graphene, related two-dimensional crystals and hybrid systems for printed and wearable electronics. Nanotoday 23, 73-96.

Tran, T.S., Dutta, N.K., Choudhury, N.R. (2018). Graphene inks for printed flexible electronics: Graphene dispersions, ink formulations, printing techniques and applications. Adv. Colloid Interface Sci. 261, 41-61.

Tsai, C.Y., Chang, W.C., Chen, G.L., Chung, C.H., Liang, J.X., Ma, W.Y., Yang, T.N. (2015). A Study of the Preparation and Properties of Antioxidative Copper Inks with High Electrical Conductivity. Nanoscale Res. Lett. 10, 357.

Turkdogan, E.T., Vinters, J.V. (1969). Kinetics of oxidation of graphite and charcoal in carbon dioxide. Carbon 7(1), 101-117.

Vallés, C., Young, R.J., Lomax, D.J., Kinloch, I.A. (2014). The rheological behavior of concentrated dispersions of graphene oxide. Journal of Materials Science 49(18), 6311-6320.

Varrla, E., Balasubramaniam, K., Sundara, R. (2011). Functionalized graphene reinforced thermoplastic nanocomposites as strain sensors in structural health monitoring. Journal of Materials Chemistry 21(34), 12626-12628.

Vaseem, M., Lee, K.M., Hong, A.R., Hahn, Y.B. (2012). Inkjet printed fractal-connected electrodes with silver nanoparticle ink. ACS Appl. Mater. Interfaces 4, 3300-3307.

Viswanath, D.S., Ghosh, T., Prasad, D.H.L., Dutt, N.V.K., Rani, K.Y. (2007). Visocsity Of Liquids, Netherlands, Springer.

Wallace, D., Hayes, D., Chen, T., Shah, V., Radulescu, D., Cooley, P., Wachtler, K., Nallani, A. (2007). Ink-Jet as a MEMS Manufacturing Tool. Proceedings of the First International Conference on Integration and Commercialization of Micro and Nanosystems, China, 1161-1168.

Wallace, P.R. (1947). The Band Theory of Graphite. Phys. Rev. 71, 622.

Wan, Y., Luo, J., Xu, J., Zhang, X., Yu, H. (2013). Experimental study of surface roughness effects on wettability. Proceedings of the International Conference on Manipulation, Manufacturing and Measurement on the Nanoscale, IEEE 97-100.

Wang, B., Lee, B.K., Kwak, M.J., Lee, D.W. (2013). Graphene/polydimethylsiloxane nanocomposite strain sensor. Rev. Sci. Instrum. 84(10), 105005.

Wang, C., Chiu, Y.C., Huang, C.L. (2015). Electrical percolation and cyrstallization kinetics of semi-crystalline polystyrene composites filled with graphene nanosheets. Mater. Chem. Phys. 164, 206-213.

Wang, P., Chong, H., Zhang, J., Yang, Y., Lu, H. (2018). Ultralow electrical percolation in melt-compounded polymer composites based on chemically expanded graphite. Compos. Sci. Technol. 158, 147-155.

Wang, Y., Wang, L., Yang, T., Li, X., Zang, X., Zhu, M., *et al*. (2014). Wearable and highly sensitive graphene strain sensors for human motion monitoring. Adv. Func. Mater. 24, 4666-4670.

Woo, K., Jang, D., Kim, Y., Moon, J. (2013). Relationship between printability and rheological behavior of ink-jet conductive inks. Ceram. Int. 39, 7015-7021.

Wu, J.T., Hsu, S.L.C., Tsai, M.H., Hwang, W.S. (2009). Conductive silver patterns via ethylene glycol vapor reduction of ink-jet printed silver nitrate tracks on a polyimide substrate. Thin Solid Films 517, 5913-5917.

Xu, Y., Hennig, I., Freyberg, D., Strudwick, A.J., Schwab, M.G., Weitz, T., Cha, K.C.P. (2014). Inkjet-printed energy storage device using graphene/polyaniline inks, J. Power Sources 248, 483-488.

Yang, D., Velamakanni, A., Bozoklu, G.L., Park, S., Stroller, M., Piner, R.D., Stankovich, S., Jung, I., Field, D.A., Ventrice Jr., C.A., Ruoff, R.S. (2009). Chemical analysis of graphene oxide films after heat and chemical treatments by X-ray photoelectron and Micro-Raman spectroscopy. Carbon 47, 145-152.

Yu, F., Chen, Y., Liang, X., Xu, J., Lee, C., Liang, Q., Tao, P., Deng, T. (2017). Dispersion stability of thermal nanofluids. Pro. Nat. Sci.-Mater. 27, 531-542.

Zabihi, F., Xie, Y., Gao, S., Eslamian, M. (2015). Morphology, conductivity, and wetting characteristics of PEDOT:PSS thin films deposited by spin and spray coating. Applied Surface Science 338, 163-177.

Zervos, H. (2016). Printed Electronics Market Update - Opportunities for the Printing Industry. Retrieved from: http://www.inprintshow.com/usa/conference/pdf/Harry-Zervos.pdf [accessed September 2018]

Zhang, W., Bi, E., Li, M., Gao, L. (2016). Synthesis of Ag/RGO composite as effective conductive ink filler for flexible inkjet printing electronics. Colloids and Surfaces A: Physicochem. Eng. Aspects 490, 232-240.

Zhang, W., Yin, B., Wang, J., Mohamed, A., Jia, H. (2019). Ultrasensitive and wearable strain sensors based on natural rubber/graphene foam. Journal of Alloys and Compounds 785, 1001-1008.

Zhang, Z., Zhu, W. (2015). Controllable synthesis and sintering of silver nanoparticles for inkjet-printed flexible electronics. J Alloy Compd. 649, 687-693.

Zhou, D., Cheng, Q.Y., Han, B.H. (2011). Solvothermal synthesis of homogeneous graphene dispersion with high concentration. Carbon 49, 3920-3927.

Zhou, L., Jung, S., Brandon, E., Jackson, T.N. (2006). Flexible substrate microcrystalline silicon and gated amorphous silicon strain sensors. IEEE Transactions on Electron Devices 53(2), 380-385.

Zhou, Y., Bao, Q.L., Tang, L.A.L., Zhong, Y., Loh, K.P. (2009). Hydrothermal dehydration for the “green” reduction of exfoliated graphene oxide to graphene and demonstration of tunable optical limiting properties. Chem. Mater. 21(13), 2950-2956.

LIST OF PUBLICATIONS

Saidina, D.S., Zubir, S.A., Mariatti, M., Fontana, S., Hérold. C (2019). Morphology and Thermal Stability of Various Types of Carbon Nanoparticles for Conductive Ink Applications. AIP Conference Proceedings 2068, 020089.

Saidina, D.S., Eawwiboonthanakit, N., Mariatti, M., Fontana, S., Hérold, C. (2019). Recent development of graphene-based ink and other conductive material-based inks for flexible electronics. Journal of Electronic Materials 48(6), 3428-3450.

Saidina, D.S., Zubir, S.A., Fontana, S., Hérold, C., Mariatti, M. (2019). Synthesis and characterization of graphene-based inks for spray coating applications. Journal of Electronic Materials 48(9), 5757-5770.

Saidina, D.S., Mariatti, M., Zubir, S.A., Fontana, S., Hérold, C., (2019). Performance of graphene hybrid-based ink for flexible electronics, Journal of Materials Science: Materials in Electronics (accepted with minor revisions).

1. Introduction

Le graphène présente des propriétés électriques, physico-chimiques et mécaniques intéressantes qui le rendent largement utilisé dans diverses applications électroniques, y compris comme encre conductrice pour l'électronique flexible imprimable (Arapov et al., 2014, Ghany et al., 2017). L'encre conductrice devient un élément important dans l'industrie de l'impression par jet d'encre, par sérigraphie, par vernissage, par pulvérisation, par l'héliogravure, etc. La plupart des encres à base de graphène rapportées dans la littérature ont été préparées en utilisant de l'oxyde de graphène (GO) comme charge.

Le GO est connu pour sa bonne solubilité dans divers types de solvants courants en raison de sa nature hydrophile (Le et al., 2011, Geng et al., 2009). Huang et ses collaborateurs (2011) ont préparé du GO monocouche soluble dans l'eau et du GO monocouche à faible épaisseur (FGO) pour l'impression jet d'encre. Ils ont signalé que la conductivité électrique du GO est inférieure à celle du FGO après 25 couches imprimées avec des valeurs de $5{,}0 \times 10^2$ $S.m^{-1}$ et $9{,}0 \times 10^2$ $S.m^{-1}$, respectivement, en raison du nombre élevé de groupes contenant de l'oxygène dans l'échantillon GO. Par conséquent, le procédé de réduction est important pour éliminer les groupes fonctionnels, mais ce procédé implique des matériaux hautement toxiques, comme l'hydrazine qui n'est pas écologique et introduit des défauts qui compromettent la conductivité (Tran et al., 2018 ; Pei et Cheng, 2012). Pour cette raison, il est préférable d'utiliser un matériau alternatif de type graphène, ayant une bonne conductivité électrique et exempt de défauts, pour la préparation d'encre conductrice. D'après les études bibliographiques, les nanoplaquettes de graphite (GNPs) produites par exfoliation en phase liquide sont très connues pour leur excellente conductivité électrique, leur faible coût (Tran et al., 2018). La mousse de graphène (GF) synthétisée par dépôt chimique en phase vapeur et par réaction solvothermale a une structure poreuse et une grande surface spécifique (Ning et al., 2013 ; Speyer et al., 2015). Selon Tang et al. (2016), Salunkhe et al. (2016) et Ma et al. (2017), la structure unique de GF, qui est constituée d'un réseau interconnecté en trois dimensions (3D) pour éviter l'agrégation tout en maintenant la conductivité électrique, peut être considérée comme explorée pour la fabrication d'encre au graphène.

Coleman (2013) et Nicolosi et al. (2013) ont rapporté que la plupart des encres à base de graphène étaient produites en utilisant des solvants efficaces tels que la N-méthyl-2-pyrrolidone (NMP), le diméthyl sulfoxyde (DMSO) et le N,N-Diméthylformamide (DMF) en raison de la tension superficielle qui est autour de 40 $mJ.m^{-2}$. Cependant, ces solvants présentent une toxicité qui peut affecter la respiration humaine, la reproduction, l'irritation de la peau et des yeux, etc. De plus, ces solvants ont des points d'ébullition élevés (>150 °C) qui ne sont pas appropriés pour être utilisés avec des substrats plastiques, qui nécessitent une température de traitement basse. Un solvant alternatif à bas point d'ébullition, moins toxique et à tension superficielle élevée est préférable pour la préparation d'une encre conductrice à bonne dispersion. L'acétone, le 2-propanol (IPA) et l'éthanol font partie des solvants alternatifs courants dont le point d'ébullition est faible, mais ces solvants présentent une faible tension superficielle d'environ 23 $mJ.m^{-2}$, ce qui entraîne une mauvaise dispersion de l'encre (Tran et al., 2018). D'après l'analyse documentaire, les rapports sur la préparation d'encre à base de graphène en utilisant de l'éthylène glycol (EG) et du propylène glycol (PG) sont limités. Ces solvants ont une tension superficielle proche de 40 $mJ.m^{-2}$ et moins toxique, mais ces solvants ont des points d'ébullition élevés. On s'attend à ce qu'en mélangeant ces solvants avec d'autres solvants moins toxiques et à bas point d'ébullition, on obtienne une encre à base de graphène ayant une bonne stabilité de dispersion.

L'objectif principal de ce travail de recherche est de produire des encres à base de graphène en utilisant des solvants alternatifs moins toxiques pour l'électronique imprimée. Pour y parvenir, les étapes suivantes sont nécessaires :

i. Comparer les caractéristiques de la mousse de graphène synthétisée avec celles des nanoplaquettes de graphite commerciales et du graphite synthétique.
ii. Étudier les propriétés de l'encre des matériaux à base de graphène mélangés à un liant de vernis polyester et déterminer la conductivité électrique des motifs pulvérisés.
iii. Déterminer la stabilité des nanoplaquettes de graphite et de la mousse de graphène dispersées dans des solvants mixtes moins toxiques.
iv. Identifier la stabilité et les propriétés électriques des encres à base de graphène et des encres hybrides à base de graphène.

2. Matériels et méthodes

2.1 Matériaux

Plusieurs types de matériaux à base de graphène ont été utilisés comme charge dans la préparation des encres conductrices. Il s'agit notamment de la mousse de graphène (GF), des nanoplaquettes de graphite (GNPs) et du graphite synthétique (SG). GF avec une densité de 1,06 gcm^{-3} a été préparé en utilisant une méthode de réaction solvothermale basée sur des travaux antérieurs (Speyer et al., 2015). Les GNPs et les SG d'une densité de 2,2 gcm^{-3} et 3,0 gcm^{-3} ont été fournis par Timcal Group, Suisse. Les nanoparticules d'argent (AgNPs) et le polymère conducteur de poly(styrène-sulfonate de poly(3,4-éthylènedioxythiophène) (PEDOT:PSS) ont été fournis par Sigma Aldrich et utilisés comme charge hybride dans la production d'encre à base de graphène.

Tous les solvants utilisés pour disperser les matériaux à base de graphène et les produits chimiques impliqués dans cette recherche ont été achetés auprès de fournisseurs locaux et étrangers. Un vernis polyester (PV) d'une densité de 0,92 gcm^{-3} a été utilisé comme liant dans la préparation d'encres à base de graphène pour revêtement par pulvérisation et fourni par AEV Ltd, Royaume-Uni. Le diluant de xylène a été utilisé comme solvant pour le PV et également fourni par AEV Ltd, Royaume-Uni. Des solvants comprenant de l'éthylène glycol (EG) et du 2-propanol (IPA) d'une densité de 1,11 et 0,786, respectivement, ont été utilisés pour disperser des matériaux à base de graphène dans la préparation d'encre conductrice pour impression à jet d'encre. Les solvants EG et IPA ont été fournis par Merck.

2.2 Méthodes

2.2.1 Synthèse de la mousse de graphène

La mousse de graphène (GF) a été préparée par réaction solvothermale selon la méthode décrite par Speyer et al. (2015). Dans cette méthode, 15 mL d'éthanol et 6 g de sodium ont été mélangés (mélange stoechiométrique 1:1) sous atmosphère inerte dans un autoclave Parr. De l'azote gazeux à une pression de 100 bar a ensuite été injecté dans le réacteur. Ensuite, l'autoclave a été chauffé à 220 °C jusqu'à ce que la pression interne atteigne 200 bar pendant 72 h et finalement refroidi à température ambiante. Le produit solvothermale, del'éthoxyde de sodium a ensuite été recueilli sous atmosphère d'argon.

Environ 5 g d'éthoxyde de sodium ont été pesés et placés dans un four tubulaire vertical. Le four a été chauffé à 850 °C à une vitesse de chauffage de 20 $Cmin^{-1}$ pendant 4 h, puis refroidi à la température ambiante. Les produits de pyrolyse contenaient du carbone, du carbonate de sodium, de l'hydroxyde de sodium et des hydrocarbures gazeux. Les produits de pyrolyse ont été soniqués et lavés avec de l'éthanol, de l'acide chlorhydrique et de l'eau distillée pour éliminer le carbonate de sodium et l'hydroxyde de sodium, et finalement filtrés par filtration sous vide. L'échantillon lavé a ensuite été séché à 100 °C pendant 24 h.

2.2.2 Production d'encre à base de graphène pour revêtement par pulvérisation

La charge des matériaux à base de graphène dans le liant PV variait de 2 % en volume à 20 % en volume. Les formulations ont été soniquées à température ambiante pendant 15 minutes avec une densité de puissance de 175 W afin d'obtenir une dispersion uniforme et homogène de la charge dans le liant PV. Un revêtement par pulvérisation d'air commandé par moteur a été fabriqué sur mesure pour déposer le mélange d'encre conductrice et de PV sur un substrat flexible. Le substrat flexible utilisé dans cette étude était un film transparent organique. Le substrat flexible a été placé sur le substrat métallique préchauffé. La température du substrat métallique, la longueur de pulvérisation et la pression d'air ont été fixées à 100 °C, 0,16 m et 4 psi, respectivement. Le motif d'encre conductrice produit par revêtement par pulvérisation a été durci à 130 °C pendant 4 h. Le schéma du travail d'écoulement pour le processus de fabrication du motif d'encre conductrice est illustré à la Figure 1.

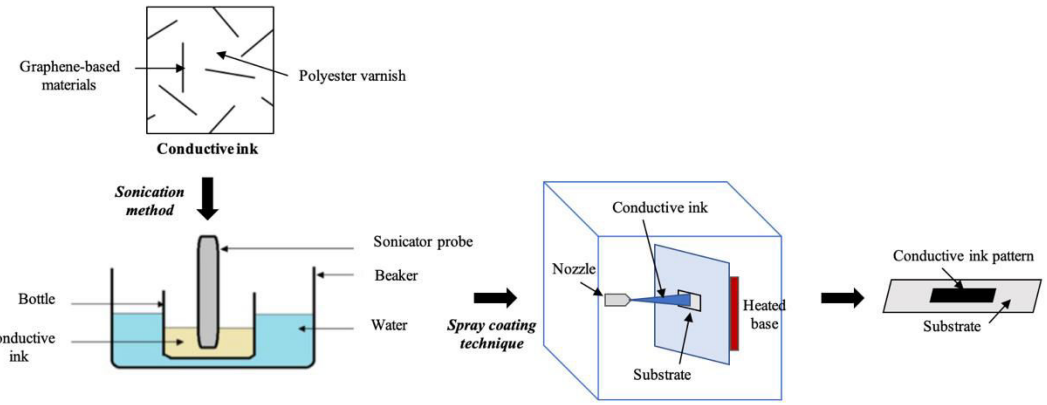

Figure 1 Schéma du procédé de fabrication d'un motif d'encre conductrice en utilisant la technique de revêtement par pulvérisation

2.2.3 Production d'encre à base de graphène pour l'impression par jet d'encre

2.2.3(a) Solvants mixtes moins toxiques

Concentration d'environ 0,05 mgmL^{-1} de GNPs dispersés dans le mélange de solvants IPA et EG. Le rapport des solvants mixtes de l'IPA:EG variait de 1:4, 2:3, 1:1, 3:2 et 4:1, respectivement. Les formulations ont été soniquées à température ambiante pendant une heure avec une amplitude de 50 % et un cycle de sonication de 0,5 cycle. Une fois la sonication terminée, le surnageant de l'encre GNPs a été recueilli. Les mêmes procédures que celles décrites dans la présente section pour produire les encres GNPs ont été utilisées pour préparer des encres à base de GF à des fins de comparaison.

2.2.3(b) Fabrication d'un motif d'encre conductrice

La concentration de l'encre GF, de l'encre hybride GF/AgNPs et de l'encre hybride GF/PEDOT:PSS dispersées dans les solvants IPA:EG à raison de 1:1 ont été fixées à 4 mg.mL^{-1}. La même procédure a été utilisée pour la préparation de l'encre GF, comme indiqué à la section 2.2.3(a). Dans cette étude, les couches d'impression ont varié de 10 à 50 couches. Le processus d'impression a été effectué à l'aide d'une imprimante Squink Multilayer PCB Printer (BotFactory Inc., États-Unis) avec une taille de buse d'environ 6 µm et une température du substrat métallique de 80°C. Le substrat flexible utilisé était le polyéthylène téréphtalate (PET), fabriqué par DuPont Mylar A (GTS Flexible Materials Ltd., Royaume-Uni). Le schéma du travail d'écoulement pour le processus de fabrication du motif d'encre conductrice est illustré à la Figure 2.

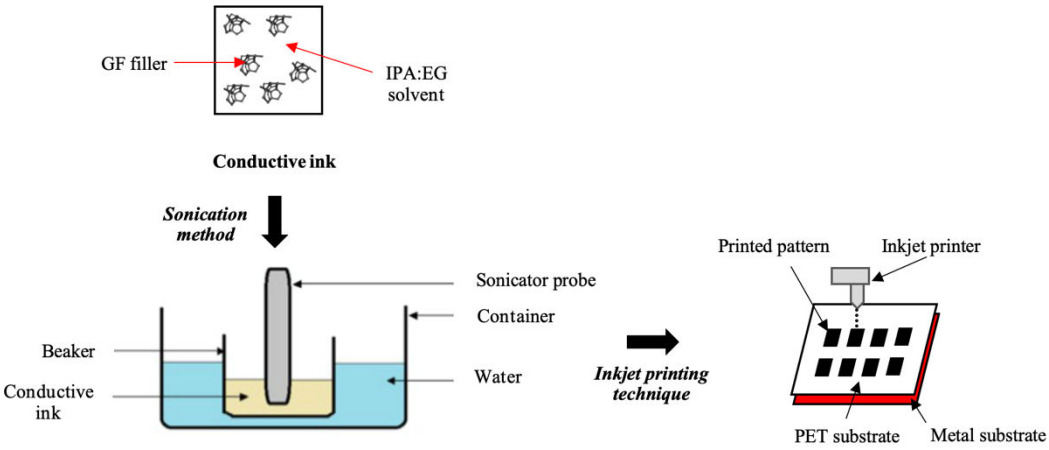

Figure 2 Schéma du procédé de fabrication d'un motif d'encre conductrice par la technique d'impression à jet d'encre

3. Résultats et discussion

3.1 Propriétés de la mousse de graphène et des matériaux commerciaux à base de graphène

Le premier objectif de la présente recherche est de comparer les caractéristiques du GF synthétisé par réaction solvothermale avec les GNPs et SG commerciaux. Dans ce travail, la morphologie, la formation des phases, les fonctionnalités, les caractéristiques structurelles et les propriétés électriques des matériaux à base de graphène ont été étudiées.

La Figure 3 montre les images au microscope électronique à balayage (MEB) des matériaux à base de graphène ; (a) GF, (b) GNPs et (c) SG. D'après les micrographies, on a observé que la structure du GF est un réseau poreux en 3D. Le GF poreux a été formé en raison de la réaction entre l'éthanol et le sodium pendant le processus solvothermale. L'éthanol est encapsulé dans le sodium dans une structure de type clathrate. Pendant ce temps, le réseau 2D des GNPs et des SG représente la morphologie typique d'une feuille. Les couches de graphène sont empilées les unes sur les autres par de faibles forces de van der Waals.

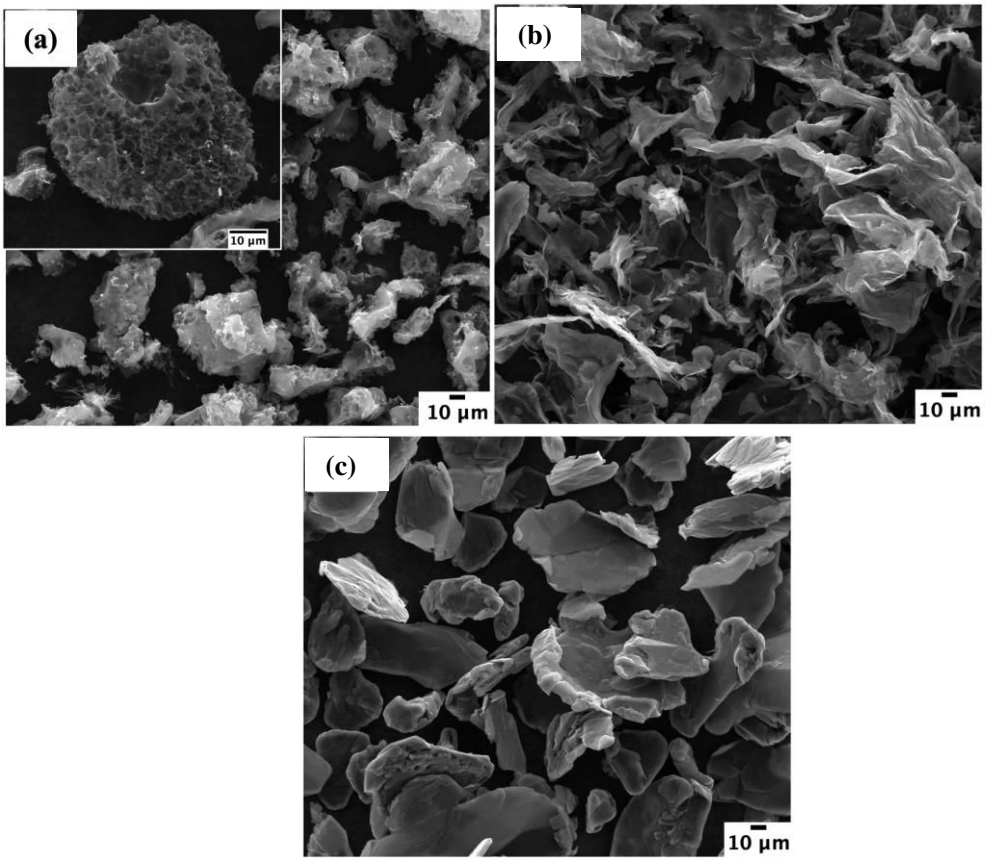

Figure 3 Micrographies MEB de (a) GF, (c) GNPs et (e) particules de SG [1000X mag.], l'encart est une image de GF poreux à 2000X mag.

La Figure 4 illustre les images en microscopie électronique à transmission à haute résolution (METHR) de (a, b) GF, (c, d) GNPs et (e, f) particules SG. D'après la figure 4 (a), on observe que le GF se compose de structures graphéniques repliées sur elles-même ; des régions de carbone amorphe peuvent être observées. La présence d'une région de carbone amorphe est due à la cristallisation du GF qui est considérée par Speyer et al. (2015) comme incomplète. Onze lignes parallèles ont pu être observées à partir de l'image capturée par METHR, une indication qu'il s'agissait d'un graphène multicouche. Les échantillons de PNB et de SG indiquaient des structures transparentes en forme de feuille et suggéraient que les particules de carbone présentaient une meilleure cristallinité avec des régions planes ordonnées. Le nombre de couches de graphène pour le GNPs et le SG est respectivement de 10 et 46 couches. En outre, le GNPs et le SG présentaient également des bords froissés et moins pliés que le GF. Les bords pliés apparaissaient plus dans les structures GF que dans les structures GNPs et SG. Ceci est dû à la tendance des particules de GF à se chevaucher, en raison de la grande surface

des couches minces étendues. La distance entre les couches pour GF, GNPs et SG était de 0,33 nm, 0,34 nm et 0,33 nm, respectivement.

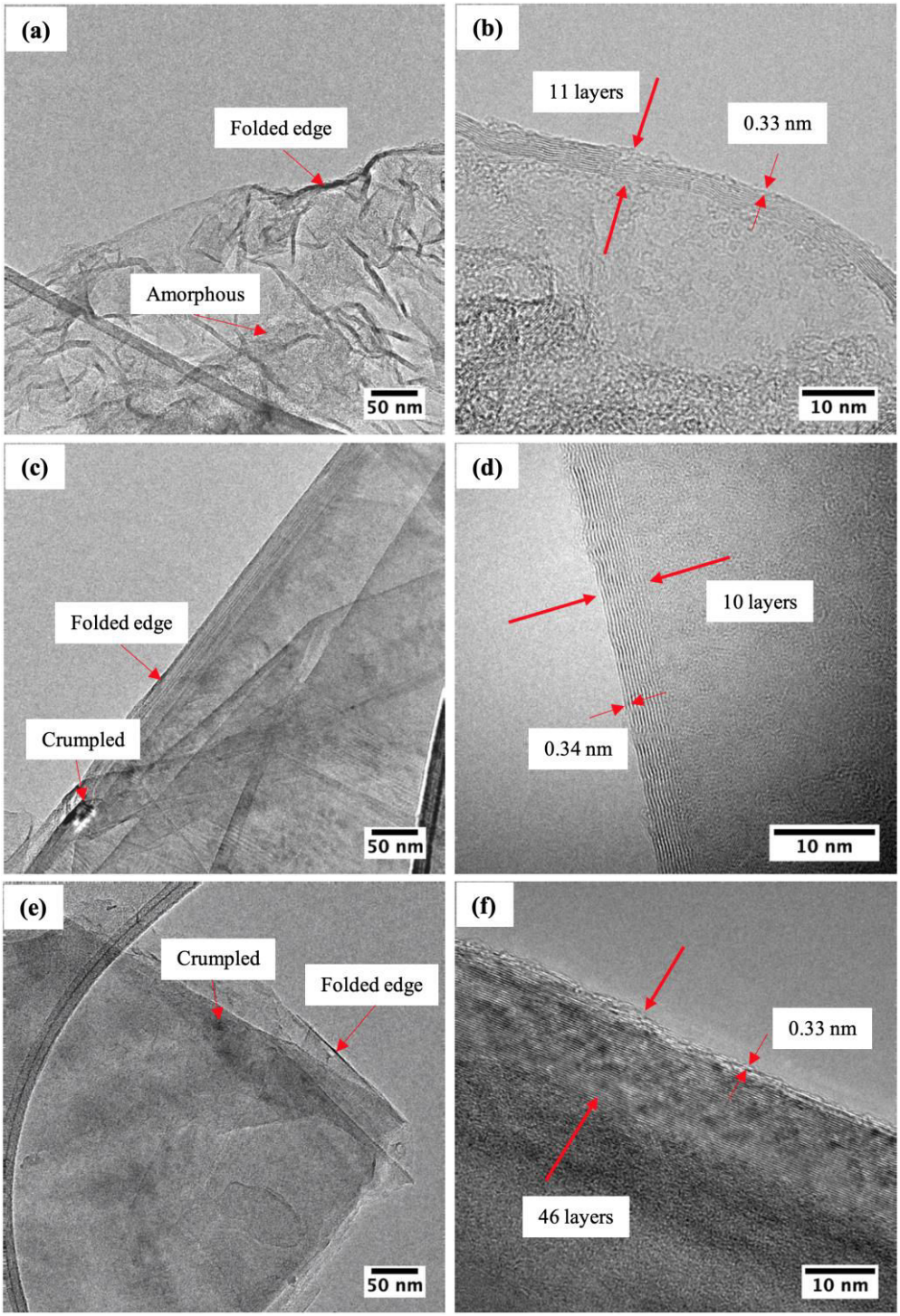

Figure 4 Micrographies METHR de (a, b) GF, (c, d) GNPs et (e, f) particules de SG à des grossissements de (a, c, e) 97kX et (b, d, f) 690 kX

Les propriétés générales des matériaux à base de graphène caractérisés à l'aide du MEB, de la physisoprtion de diazote à 77K, de la spectroscopie Raman et de la spectroscopie de photo-émission (XPS) sont présentées au Tableau 1. Le GF présentait la superficie et le volume de pores les plus élevés. Comme le rapportent Chen et al. (2011), la structure du GF a une surface spécifique élevée en raison de sa porosité très importante.

Le défaut des particules peut être déterminé en mesurant le rapport d'intensité des pics D et G (I_D/I_G) (Tang et al., 2012) en spectroscopie Raman. D'après le Tableau 1, les rapports d'intensité de la bande D par rapport à la bande G (I_D/I_G) du GF, du GNPs et de la SG ont été calculés à 1,07, 0,34 et 0,56, respectivement. Une valeur plus élevée d'I_D/I_G peut être liée à une concentration plus élevée de défauts. D'après les résultats obtenus, l'échantillon de GF présentait la valeur I_D/I_G la plus élevée par rapport à ceux des GNPs et des échantillons de SG, ce qui signifie qu'une grande surface de mousse de graphène a une faible qualité structurelle. En outre, pour le graphène empilé, le nombre de couches pourrait être dérivé du rapport des intensités de pics pour 2D et G (I_{2D}/I_G). Les rapports I_{2D}/I_G pour GF, GNPs et SG étaient respectivement de 0,42, 0,70 et 0,74, ce qui indique que les matériaux à base de graphène sont constitués de graphène multicouches.

Le rapport O/C a été obtenu par la mesure de l'analyse élémentaire par analyse XPS. Les matériaux à base de graphène présentaient un rapport pondéral carbone /oxygène d'environ 0,050, 0,008 et 0,017 correspondant respectivement aux particules GF, GNPs et SG. Une teneur plus élevée en oxygène dans les particules GF est attribuée au carbonate de sodium formé pendant la réaction de pyrolyse et toujours présent même après lavage.

Tableau 1 Propriétés générales des matériaux à base de graphène

Échantillon	**GF**	**GNPs**	**SG**
Taille latérale moyenne (μm)	32	38	44
Surface BET (m^2g^{-1})	2136	25	3
Volume des pores (cm^3g^{-1})	0.138	0.003	0.001
I_D/I_G	1.07	0.34	0.56
I_{2D}/I_G	0.42	0.70	0.74
O/C	0.050	0.008	0.017

3.2 Propriétés des matériaux à base de graphène mélangés à un liant de vernis polyester

Le deuxième objectif de la présente recherche est d'étudier les propriétés de l'encre des matériaux à base de graphène mélangés à un liant de vernis polyester (PV) et de déterminer la conductivité électrique des motifs pulvérisés. Les propriétés des encres conductrices fabriquées à partir de divers matériaux de type graphène, notamment la viscosité, l'angle de contact et l'énergie de surface, ont été étudiées.

La Figure 5 (a) illustre les courbes de viscosité, η des encres à base de graphène à 5 % en volume en fonction du taux de cisaillement. On a observé que la valeur de η pour toutes les encres diminuait avec l'augmentation du taux de cisaillement dans une plage de 1,5 à 500 s^{-1}, ce qui indique des comportements d'écoulement par cisaillement. Le η est considéré comme stable à des taux de cisaillement élevés. L'attraction entre les matériaux à base de graphène induit une floculation dans les encres qui provoque une immobilité du solvant en suspension dans les particules et augmente donc le η à faible vitesse de cisaillement (Woo et al., 2013). En comparaison, à un taux de cisaillement plus élevé, la floculation se décompose et favorise la mobilité du solvant piégé entre les particules, ce qui entraîne une diminution du η.

La Figure 5 (b) montre la variation de η en fonction des charges de remplissage. Il est clairement indiqué que l'ajout de matériaux à base de graphène à 5 % en volume, à un taux de cisaillement de 500 s^{-1}, a montré une augmentation de 114 % (encre GNPs), 55 % (encre SG) et 16 % (encre GF) par rapport au liant PV non chargé (η = 0,18 Pas). Les valeurs η des encres étaient différentes même avec la même charge de remplissage en raison de la taille et de la forme différentes des encres. Même si GF présentait la surface BET la plus élevée par rapport aux GNPs et SG qui étaient censés augmenter la valeur de l'encre sur η, une tendance différente a été observée. La faible augmentation de la valeur η de l'encre GF est attribuée à l'agrégation entre les particules GF, comme le confirme l'analyse METHR à la section 3.1. Vallés et ses collaborateurs (2014) ont observé une observation similaire, car la viscosité de la suspension de GO a légèrement augmenté en raison de l'agrégation entre les flocons de GO.

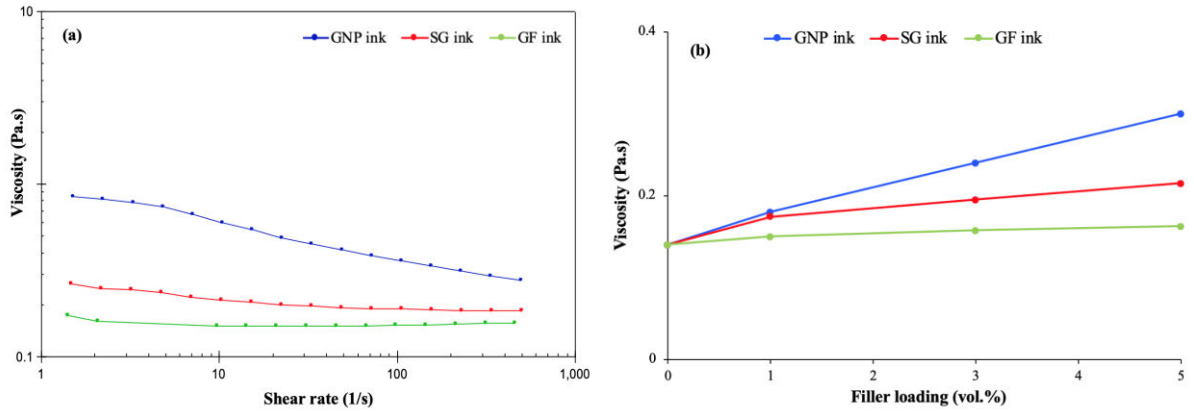

Figure 5 (a) Courbes de viscosité des encres conductrices à 5 % en volume en fonction du taux de cisaillement et (b) variation de viscosité en fonction des charges de remplissage à 500 s^{-1} de cisaillement

La Figure 6 (a) indique que le θ_c pour toutes les encres conductrices augmente avec l'augmentation des charges de charge dans le liant PV. L'augmentation du nombre de matériaux à base de graphène dans les liants PV affecte également la gouttelette θc sur le substrat en raison de la modification de η mais les encres conductrices présentant encore des caractéristiques hydrophiles, $\theta_c <$ 90° qui permettent une meilleure combinaison encre-substrat. En outre, l'énergie de surface, γ_{SL}, calculée à partir du θc mesuré pour toutes les encres conductrices, a été calculée et présentée à la figure 6 (b). Le γ_{SL} a légèrement diminué avec une augmentation des charges de matériaux à base de graphène. Ceci est attribué aux grandes quantités de matériaux à base de graphène présentées à la surface des gouttelettes lors de fortes charges de remplissage et, par conséquent, a réduit le γ_{SL} des encres conductrices. Cependant, la légère diminution de γ_{SL} n'a pas eu d'influence sur la qualité du motif pulvérisé entre l'encre conductrice et le substrat, où le θ_c est toujours <90°.

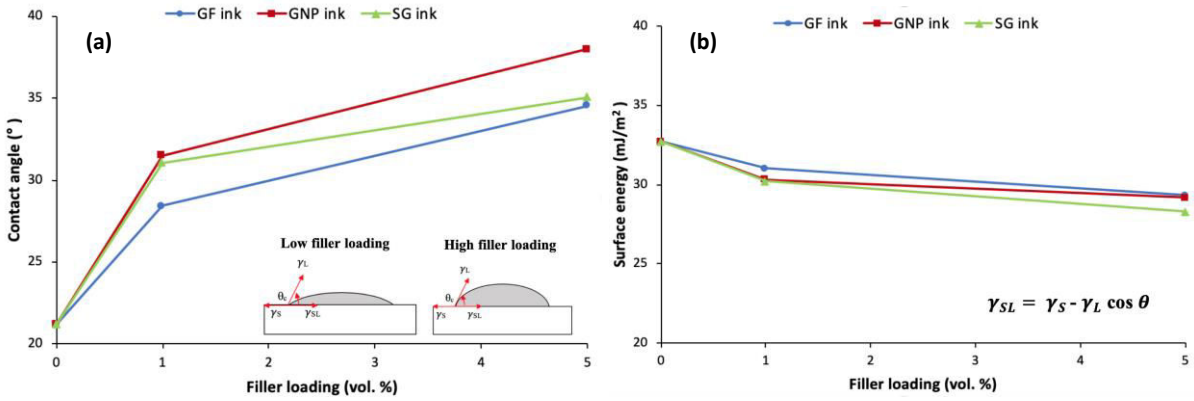

Figure 6 (a) variation de l'angle de contact en fonction des charges de remplissage, encadré montrant (i) un petit angle de contact et (ii) un angle de contact élevé et (b) l'énergie de surface en fonction des charges de remplissage, y compris l'équation de Young

Pour déterminer le seuil de percolation, on a fabriqué des motifs d'encre conducteurs à partir de divers matériaux à base de graphène sous différentes charges dans un liant PV. La Figure 7 présente la conductivité électrique de différentes encres conductrices en fonction des charges de remplissage. Des charges de remplissage différentes évidentes ont été utilisées dans la formulation d'encres conductrices grâce. D'après les formulations, une plus grande quantité de charge GF a été utilisée pour mélanger avec du vernis polyester que pour les GNPs et les SG avec la même charge de charge en raison de la faible densité du GF. Cependant, les encres conductrices deviennent très difficiles à distribuer avec une charge de remplissage plus élevée en raison du taux élevé de η.

On peut observer que la conductivité électrique de tous les échantillons augmente manifestement avec l'augmentation du taux de charges (Figure 7). Les encres conductrices composées de GNPs présentent la conductivité électrique la plus élevée, suivies par les encres SG et GF pour toutes les charges de remplissage. Même si GF présentait la surface spécifique BET la plus élevée par rapport aux GNPs et aux SG qui étaient supposés augmenter la conductivité électrique du motif d'encre conductrice, une tendance différente a été observée. Ceci est dû à d'autres facteurs qui ont influencé la conductivité électrique de l'encre GF, notamment la taille latérale, la cristallinité, la teneur en oxygène et la qualité des particules GF, comme discuté dans les analyses BET, MEB, XPS et Raman. Dans le même temps, la conductivité électrique plus élevée de toutes les charges d'encre GNPs et d'encre SG a été attribuée à la grande taille latérale, à la structure cristalline élevée et à la haute qualité des flocons GNPs et SG.

Pour l'encre GNPs, le seuil de percolation est obtenu entre 4 % en volume et 4,5 % en volume GNPs. En cas d'augmentation supplémentaire de la charge du GNPs, la conductivité électrique est augmentée avec des valeurs de 1,26 Scm^{-1} à 5 % en volume à 1,86 Scm^{-1} à 10 % en volume. Dans le cas des encres SG et GF, le seuil de percolation a pu être observé lorsque le taux de charge SG se situe entre 8 % et 9 % en volume et lorsque celui des charge GF se situe entre 9 % et 10 % en volume.

Un circuit électronique simple était composé d'une pile de 9,0 V, d'un motif conducteur pulvérisé, d'un condensateur et de la LED pour démontrer le comportement des motifs d'encre conducteurs vis-à-vis de la luminosité de la LED. Les encres GNPs présentaient une amélioration remarquable de la conductivité électrique, suivies par les encres SG et GF à 10 % en volume par rapport aux liants de vernis polyester non chargés, de 186 %, 40 % et 10 %, respectivement.

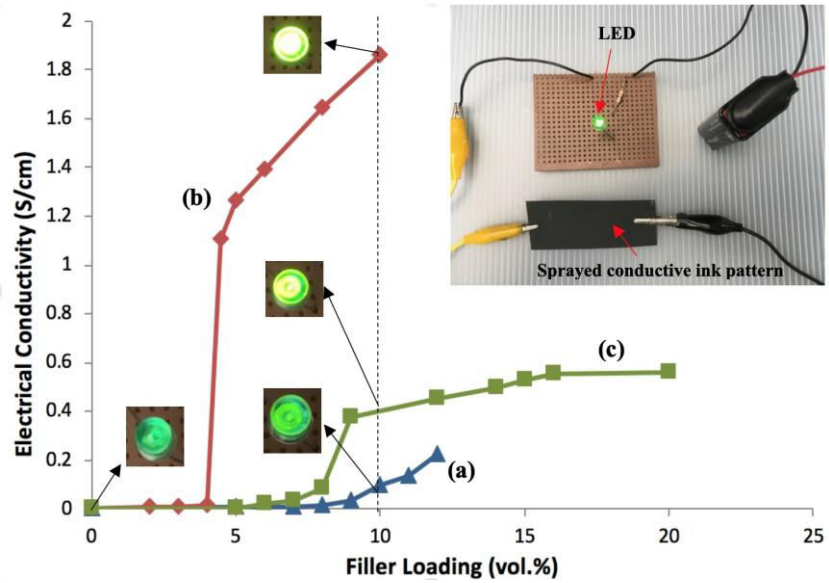

Figure 7 Conductivité électrique de (a) l'encre GF, (b) l'encre GNPs et (c) l'encre SG en fonction de la charge de remplissage, encadré montrant les images numériques d'un circuit électronique configuré et la luminosité des LED pour différents types de motifs d'encre conducteurs à 10 % en volume

La conductivité électrique des motifs d'encres conductrices dépend fortement de leur morphologie qui a été étudiée par analyse MEB. La Figure 8 (a-e) montre la morphologie des motifs d'encre conductrice de la section transversale par rapport aux charges de charge, ce qui donne un aperçu du processus de formation du réseau conducteur. Les traces d'encre conductrice aux faibles charges de remplissage (illustrées à la Figure 8 (a) et (c)) indiquent que certains chemins conducteurs n'étaient pas

connectés, ce qui indique que les faibles taux de charge de remplissage n'étaient pas suffisants pour supporter un réseau complet et qu'on pouvait voir plus de vides. Cependant, lorsque la quantité de matériaux à base de graphène a augmenté, comme le montre la Figure 8 (b), (d) et (e), le réseau est devenu visiblement plus dense et les chemins conducteurs étaient bien établis, comme le montre la flèche rouge.

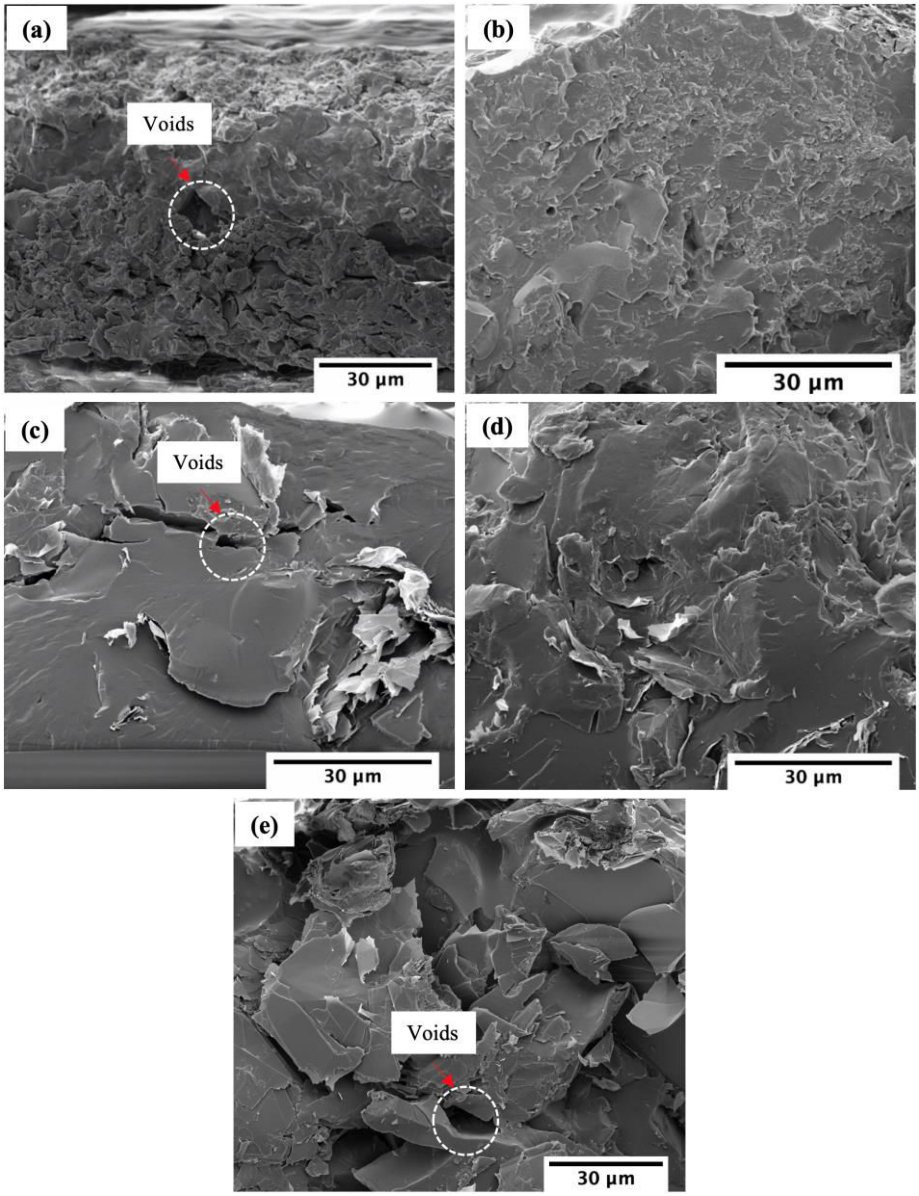

Figure 8 Micrographies MEB de modèles d'encres conductrices en coupe transversale constituées de (a) 7 % en volume de GF (b) 12 % en volume de GF, (c) 2 % en volume de GNPs (d) 4,5 % en volume de GNPs (e) 9 % en volume de SG[2,500-3,500X mag]

3.3 Propriétés des encres à base de graphène

D'après les propriétés physiques et électriques indiquées à la section 3.2, des nanoplaquettes de graphite (GNPs) et de la mousse de graphène (GF) ont été choisies pour des études plus poussées. Le troisième objectif est de déterminer la stabilité des GNPs et des GF dispersés dans des solvants mixtes moins toxiques. La stabilité de dispersion des encres à base de graphène a été étudiée par observation visuelle, zétasizer, spectroscopie UV-Vis, rhéomètre et ganiomètre.

Les GNPs et les GF dispersés dans divers rapports IPA:EG ont été observés visuellement dans le temps, entre le jour 1 (après la sonication) et le jour 7, comme le montre la Figure 9. Comme on peut l'observer, les encres GF présentaient une meilleure stabilité de dispersion car la dispersion restait d'une couleur foncée uniforme par rapport aux encres GNPs. Une teneur plus élevée en oxygène dans le GF d'environ 4,64 % en poids (comme le confirme l'analyse XPS du Tableau 1) a montré que le GF est plus hydrophile que les GNPs de 0,83 % en poids et qu'il est donc plus facile à disperser dans le solvant. La Figure 9 (d-f) montre qu'une sédimentation minimale a pu être observée dans les encres GF ayant un aspect foncé après le 7e jour de stockage. Le GF dispersé dans un solvant IPA:EG à un rapport de 1:1 montre la meilleure stabilité de dispersion par rapport aux encres GF à des rapports de mélange de 1:4 et 4:1, respectivement. En ce qui concerne les encres à base de GNPs, on observe que les GNPs s'agglomèrent et sédimentent au fonde la bouteille après 7 jours. Nethravathi et Rajamathi (2008) et Zhou et al. (2011) ont rapporté que l'agglomération est due à l'augmentation de l'hydrophobicité et à l'interaction d'empilement entre les feuilles de GNPs, comme le confirme la Figure 1 (a, b).

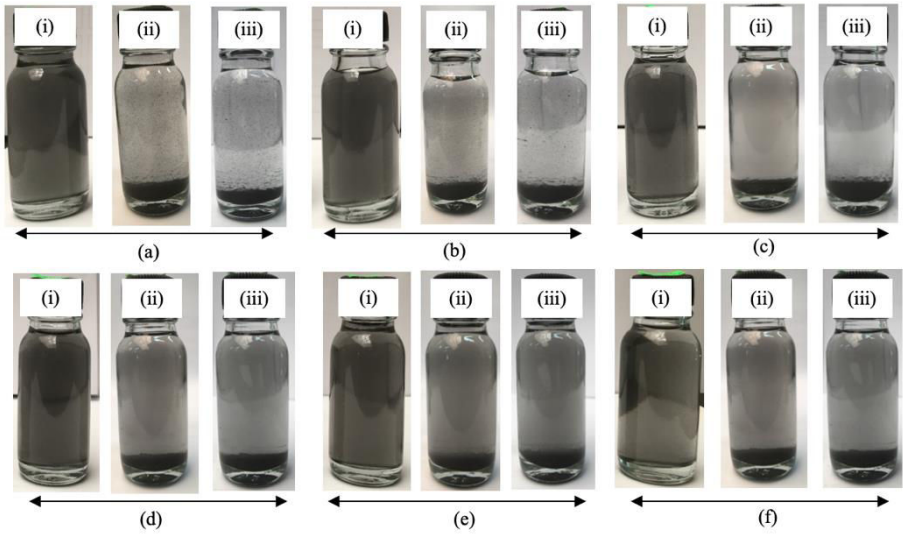

Figure 9 Photographies des GNPs (a-c) et des FG (d-f) dans différents rapports IPA:EG solvants mixtes. Figure (a, d) IPA:4EG, (b, e) IPA:EG et (c, f) 4IPA:EG font référence à l'image après sonication (jour 1), jour 3 et jour 7, respectivement

La Figure 10 montre le potentiel ζ des GNPs et des GF dispersés dans différents rapports IPA:EG de solvants mixtes. Le pH mesuré des GNPs et des encres GF après sonication était de 5, les GNP et les surfaces GF étant chargés négativement dans toutes les dispersions principalement attribuées au transfert de charge de Lewis des molécules de solvant interfacial et aux GNPs et particules GF (Johnson et al., 2015). Les valeurs du potentiel ζ indiquent que toutes les teneurs en GF dans les solvants mélangés sont stables, alors que pour les dispersions du GNPs, elles ne sont stables qu'à des rapports de 3:2 et 4:1, respectivement. Selon Rajan et al. (2016), les potentiels de ζ avec des valeurs absolues supérieures à $\pm$30 mV indiquent une dispersion stable en raison de la répulsion électrostatique des particules entre elles. Il est évident que les encres GF sont plus stables que les encres GNPs à tous les rapports mixtes.

La stabilité des GNPs et des GF dispersés dans le solvant IPA:EG à une certaine période de temps a été étudiée par spectroscopie UV-Vis. La figure 11 montre les spectres d'absorption UV-Vis de l'encre GNPs et de l'encre GF dans le solvant IPA:EG à différentes périodes de temps, entre le jour 1 (voir D1), le jour 3 (voir D3) et le jour 5 (voir D5). On a constaté que les encres GNP et GF présentaient toutes deux, le pic d'absorption le plus élevé à 265 nm, ce qui est attribué aux liaisons sp^2 C=C. L'intensité d'absorption de l'encre GF a légèrement diminué au fil du temps par rapport à celle de l'encre

GNPs, comme le montre la Figure 11, ce qui confirme que l'encre GF a une meilleure stabilité de dispersion. L'intensité de toutes les encres a progressivement diminué avec le temps, probablement en raison de la ré-agglomération des particules.

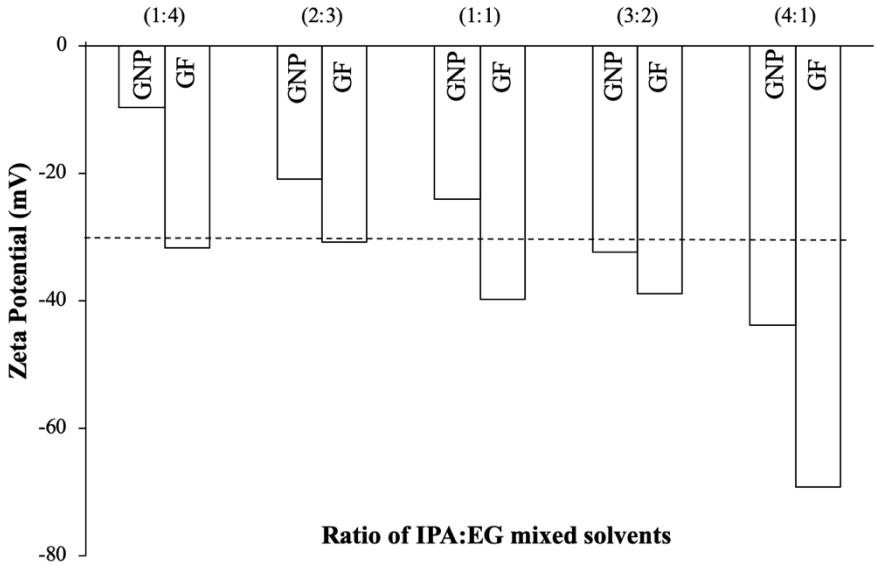

Figure 10 Potentiels zêta des GNPs et des GF dispersés dans différents rapports IPA:EG solvants mixtes

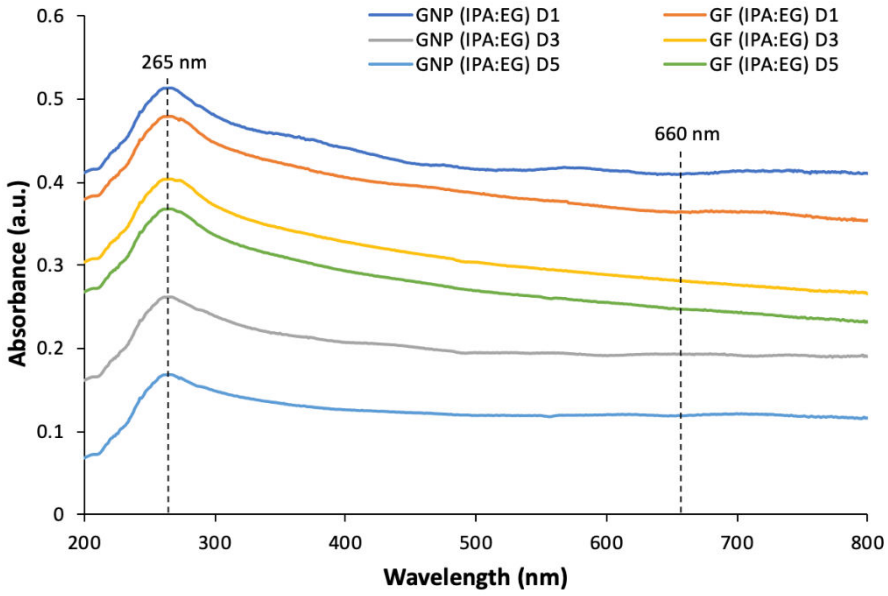

Figure 11 Spectre d'absorption UV-Vis des encres GNPs et des encres GF dans le solvant IPA:EG à différentes périodes de temps

En outre, la stabilité de la dispersion des GNPs et des GF dans les solvants mixtes a été évaluée en étudiant leurs concentrations sur certaines périodes de temps, comme le montre la figure 12. D'après les concentrations calculées à la Figure 12, les GNPs dispersés dans l'IPA:EG à des ratios mixtes de 1:4 et 4:1 montrent une diminution significative après un mois (>90%) par rapport aux GNPs dispersés dans l'IPA:EG à des ratios de 1:1 (>80%). Dans le cas des dispersions de GF, une légère diminution

après un mois a été observée dans le GF dispersé dans des solvants mélangés à un rapport de 1:1 (~50%) par rapport à ceux des rapports 1:4 et 4:1 mélangés, la diminution en pourcentage étant de 60% environ. Ces observations suggèrent fortement que le GF dispersé dans les solvants mixtes IPA:EG, tous rapports confondus, était stable par rapport aux dispersions du GNPs. Ceci est conforme à l'observation visuelle et à l'analyse du potentiel de ζ qui ont été discutées dans les Figures 9 et 10.

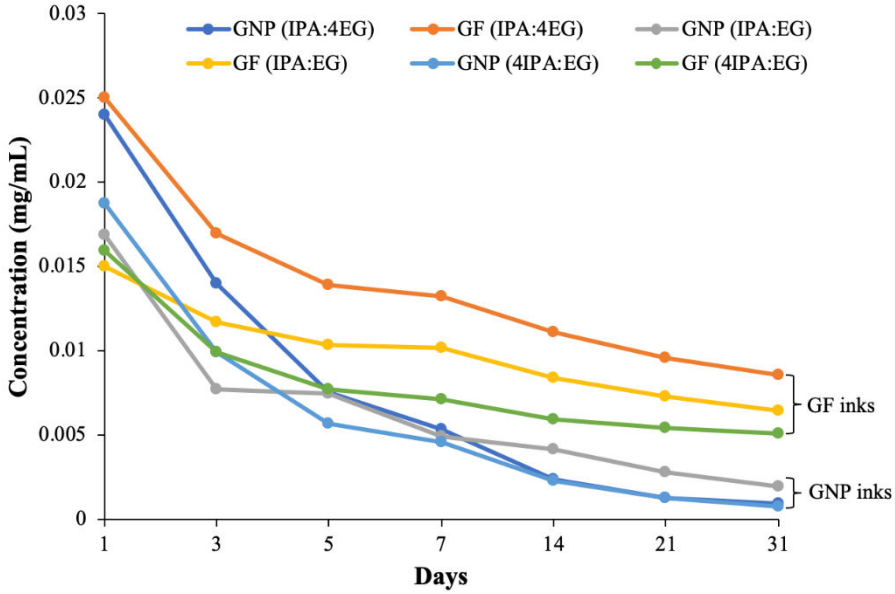

Figure 12 Concentration des encres GNPs et des encres GF dans différents rapports IPA:EG solvants mixtes en fonction du temps

Le Tableau 2 présente la viscosité, les valeurs η des solvants mélangés et les valeurs η des GNPs et des GF dispersés dans divers rapports IPA:EG des solvants mélangés. On observe que les valeurs η de toutes les encres ont augmenté avec l'addition des GNPs et des GF dans les solvants mixtes à tous les rapports. De plus, les valeurs η des encres GNPs et GF ont diminué avec l'augmentation de la teneur en IPA dans les solvants mixtes IPA:EG. Ceci est en accord avec le faible η de l'IPA (1,3 mPas) que de l'EG (14,5 mPas). On observe que les valeurs η des encres GNPs et des encres GF se situaient respectivement entre 3,5 et 14 et entre 5 et 14,3 mPas. Ces résultats suggèrent que les encres GNPs et GF peuvent être considérées comme acceptables pour l'impression jet d'encre. En outre, il a été constaté que le η de l'encre GF était légèrement supérieur à celui de l'encre GNPs, même avec le même rapport de mélange. D'après les formulations, une plus grande quantité de charge GF au même pourcentage en volume est due à la faible densité de GF avec une valeur de 1,06 gcm^{-3} par rapport à un GNPs de 2,2 gcm^{-3}.

Tableau 2 Viscosité du solvant mélangé et viscosité des GNPs et des GF dans différents rapports IPA:EG solvants mélangés

Échantillon	Ratio mixte IPA:EG	Viscosité du solvant mélangé (mPas)	Viscosité de l'encre GNPs (GF) (mPas)
GNPs (GF)	1:4	11.3	14 (14.3)
	2:3	8.2	9.5 (11)
	1:1	6.9	8 (10)
	3:2	5.2	6 (8)
	4:1	2.5	3.5 (5)

* les valeurs entre parenthèses se réfèrent aux dispersions GF

La Figure 13 montre l'angle de contact et l'énergie de surface des GNPs et des GF dans différents rapports IPA:EG solvants mixtes. D'après les valeurs de θ_c, on constate que le θ_c des GNPs et des dispersions de GF tend à diminuer avec une augmentation de la teneur en IPA dans les solvants mélangés. Comme prévu, une meilleure mouillabilité a pu être observée pour les encres GF par rapport aux encres GNPs en raison d'une amélioration de la stabilité à la dispersion des encres GF, ce qui a conduit à des valeurs plus faibles pour les encres GF. Selon Park et al. (2013) et Wan et al. (2013), un petit θ_c provoque une évaporation rapide de l'encre et une absorption excessive. La γ_{SL} de la θ_c mesurée des GNPs et des GF dans différents rapports IPA:EG de solvants mélangés a augmenté avec une augmentation de la teneur en IPA dans les solvants mélangés. Comme on peut le constater, la différence en γ_{SL}des encres GF à tous les rapports mixtes était très faible, de 6 % par rapport à celles des encres GNPs de 17 %. Les particules doivent interagir correctement avec le solvant afin de réduire le γ_{SL}du système.

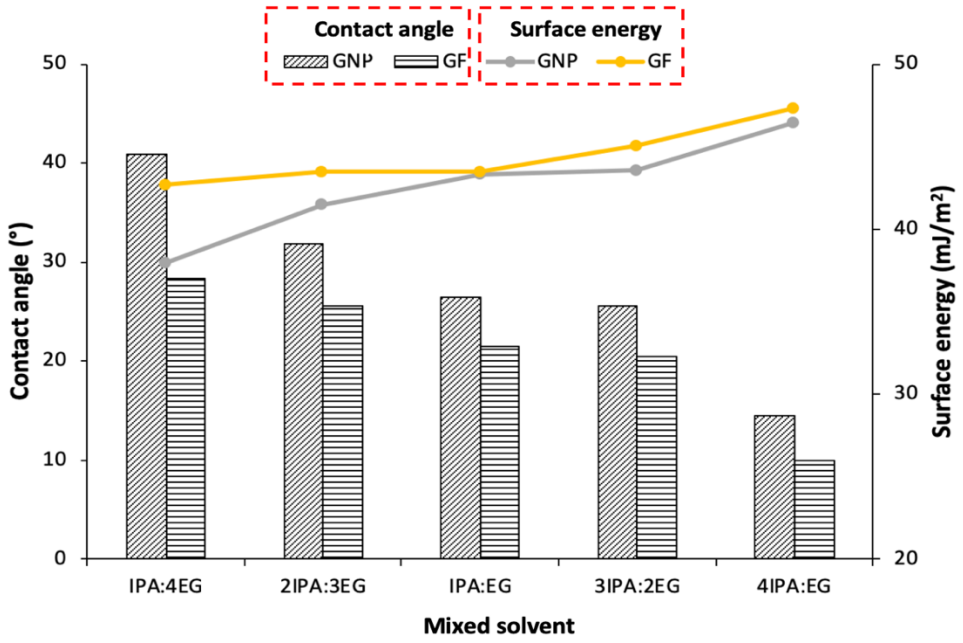

Figure 13 Angle de contact et énergie de surface des GNPs et des GF dans différents rapports IPA:EG solvants mixtes

La morphologie du GF dispersé dans le rapport IPA:EG à 1:1 a été observée pour identifier l'effet de stabilité au jour 1 et au jour 5. Les images METHR du GF dans le rapport IPA:EG à 1:1 sont illustrées à la Figure 14. Notons que les agglomérats apparaissent comme des régions sombres sur les images METHR. D'après la Figure 14, on a pu observer une région plus foncée pour la dispersion du GF après le jour 5 (Figure 14 (iii)), ce qui indique que les particules étaient agglomérées comparativement aux particules du GF au jour 1 (Figure 14 (i)). Ces résultats concordent avec l'observation visuelle et l'analyse des UV-Vis, tel qu'indiqué aux Figures 9 et 11, respectivement.

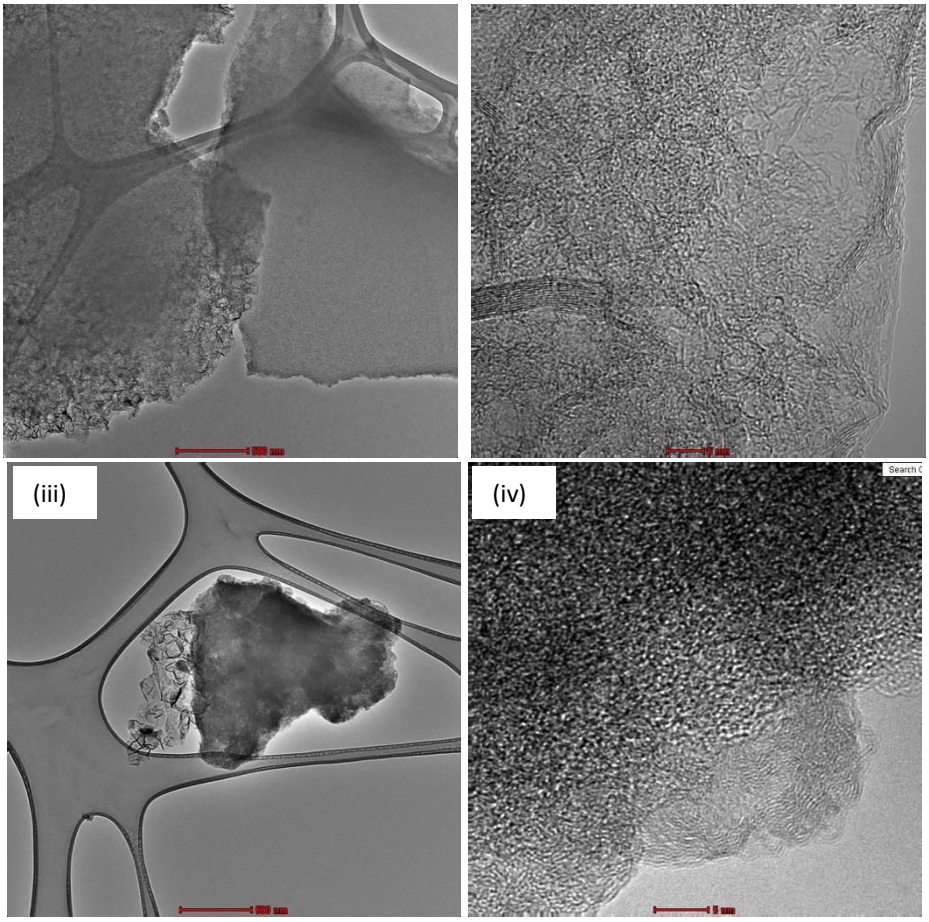

Figure 14 Micrographies METHR de particules de GF dans des solvants mixtes IPA:EG au rapport 1:1 à des grossissements de (i, iii) 15kX et (ii, iv) 690kX. Les figures (i-ii) et (iii-iv) se rapportent à l'image après la sonication (jour 1) et jour 5, respectivement

3.4 Propriétés des encres à base de graphène et des encres hybrides au graphène

Dans ce travail, des encres à base de graphène et des encres hybrides à base de graphène à des concentrations fixes de 4 mgmL^{-1} ont été préparées en utilisant des solvants mixtes IPA:EG au rapport 1:1. Deux matériaux ont été utilisés pour les encres hybrides à base de graphène, notamment les AgNPs et PEDOT:PSS. L'effet du graphène sur la stabilité, la viscosité, la mouillabilité de surface, la conductivité électrique et la morphologie du graphène et du graphène hybride comme encres conductrices a été étudié.

L'observation visuelle des encres hybrides GF, GF/AgNPs et GF/PEDOT:PSS à une concentration de 4 mgmL^{-1} observée du jour 1 (après la sonication) au jour 7 est illustrée à la Figure 15. Pour l'encre GF (Figure 15 (a)), une sédimentation a été observée au jour 7, indiquant que le GF est partiellement stable jusqu'à une semaine. En revanche, l'encre hybride GF/AgNPs n'est restée stable qu'une seule journée, l'encre hybride semblant plus claire au septième jour. La sédimentation de grandes quantités de GF et d'AgNPs a été observée au fond de la bouteille au jour 7, ce qui indique que la dispersion du GF et des AgNPs dans les solvants IPA:EG n'était pas stable. Ceci est attribué à la forte tension interfaciale entre GF (~40 mJm^{-2}) et AgNPs (~7,2 Jm^{-2}) ainsi qu'à la densité élevée des AgNPs (10,49 gcm^{-3}) qui conduit à une faible stabilité de la dispersion (Nanda et al., 2003). Cependant, pour l'encre hybride GF/PEDOT:PSS, on peut voir que l'encre hybride était visuellement homogène avec un aspect sombre jusqu'au jour 7, ce qui indique que la dispersion de l'hybride GF avec PEDOT:PSS dans les solvants mixtes IPA:EG était stable pendant une longue période. Une faible tension interfaciale entre

GF (~40 mJm^{-2}) et PEDOT:PSS (~42,5 mJm^{-2}) conduit à une bonne stabilité de la dispersion de l'encre hybride (Dabczyński et al., 2018).

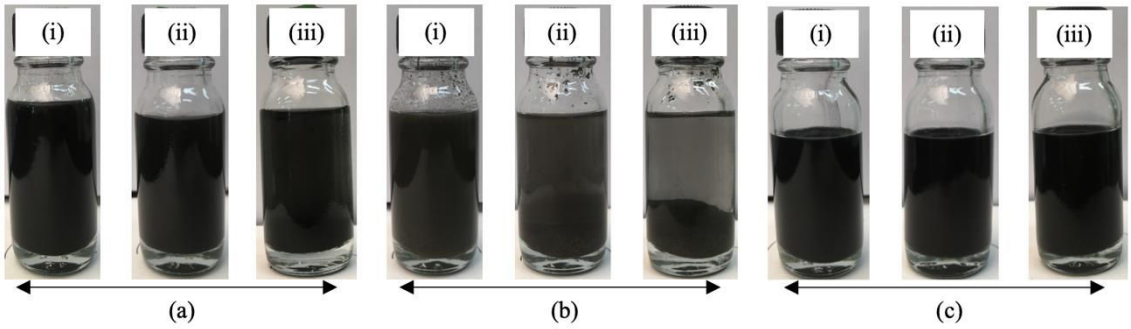

Figure 15 Photographies de (a) l'encre GF, (b) l'encre hybride GF/AgNPs et (c) l'encre hybride GF/PEDOT:PSS. Les figures (i), (ii) et (iii) se réfèrent à l'image après sonication (jour 1), jour 3 et jour 7, respectivement

La spectroscopie UV-Vis a été utilisée pour analyser la qualité, la nature et la stabilité des encres GF et GF hybrides. Les spectres d'absorption UV-Vis des encres GF et des encres hybrides GF sont représentés à la Figure 16. Comme le montre la Figure 16 (a), le pic d'absorption le plus élevé pour l'encre GF a été observé à 265 nm et attribué à la transition π- π^* du cycle aromatique C-C dans l'encre GF (Johra et al., 2014). La formation d'AgNPs et de PEDOT:PSS dans les encres hybrides GF a été confirmée par les pics d'absorption dans les spectres UV-Vis, comme le montre la Figure 16 (b-c), respectivement. Comme on peut le constater, l'encre hybride GF/AgNPs avait un pic d'absorbance à 418 nm, montrant un pic associé à la résonance plasmonique de surface des AgNPs. Saion et al. (2013) et Campillo et al. (2017) ont signalé un pic maximal de AgNPs entre 404 et 418 nm. Dans le cas de l'encre GF/PEDOT:PSS, l'absorption maximale a été observée à 227 nm, ce qui fait référence aux cycles aromatiques du PSS (Mengistie et al., 2014 ; Saghaei et al., 2015).

La stabilité de dispersion des encres GF et GF hybrides dans les solvants mixtes IPA:EG a été étudiée en mesurant leurs concentrations pendant un mois, comme le montre la Figure 17. D'après les concentrations calculées à l'aide de l'équation de Lambert-Beer, l'encre hybride GF/PEDOT:PSS présente une légère diminution après un mois (30 %) par rapport à celles de l'encre GF et de l'encre hybride GF/AgNPs, la diminution en pourcentage étant respectivement de 50 et 70 % environ. D'après cette observation, l'encre hybride GF/PEDOT:PSS était stable par rapport à ces encres conductrices. Ce résultat est parallèle à l'observation visuelle dont il a été question à la Figure 15.

Le Tableau 3 présente la diminution de la concentration et la zêta, ζ valeurs potentielles des encres hybrides GF et GF. Les valeurs des potentiels ζ indiquent que toutes les encres sont dans une bonne stabilité car les encres conductrices ont des valeurs de potentiel ζ inférieures à -30 mV (Rajan et al., 2016). L'encre hybride GF/PEDOT:PSS présentait le potentiel ζ le plus faible avec une valeur de -80,4 mV par rapport aux autres encres conductrices, ce qui indique que cette encre hybride a la meilleure stabilité que l'encre GF et l'encre hybride GF/AgNPs, respectivement. Les résultats du potentiel zêta présentés au Tableau 3 corroborent généralement les résultats de l'observation visuelle et de l'analyse UV-Vis.

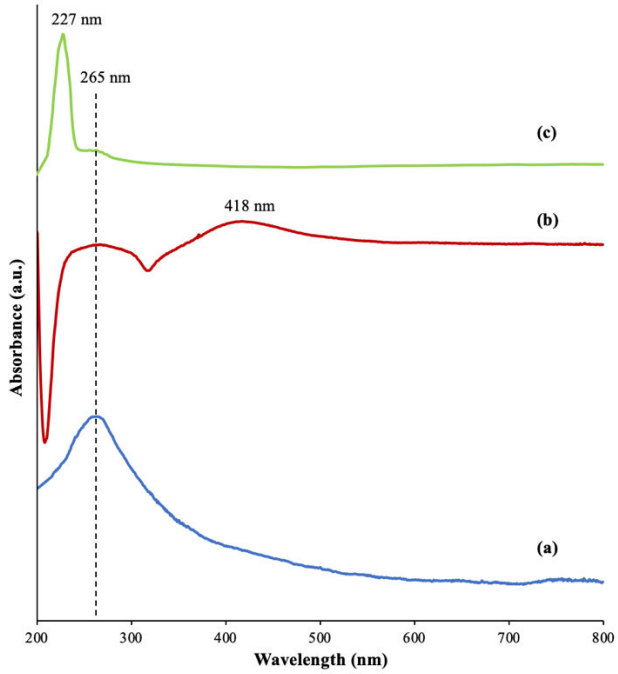

Figure 16 Spectre d'absorption UV-Vis de (a) GF, (b) Encre hybride GF/AgNPs, et (c) Encre hybride GF/PEDOT:PSS

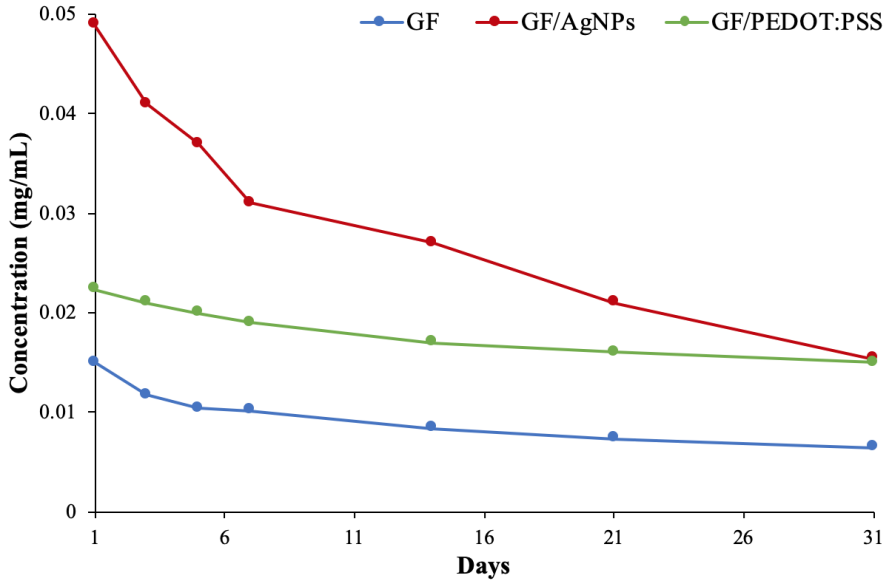

Figure 17 Concentration de l'encre GF, de l'encre hybride GF/AgNPs et de l'encre hybride GF/PEDOT:PSS en fonction du temps

Tableau 3 Diminution de la concentration et potentiel zêta des encres hybrides GF et GF

Encre	Diminution de la concentration (%)	Potentiel zêta (mV)
GF	50	-38.9
GF/AgNPs	70	-50
GF/PEDOT:PSS	30	-80.4

Le Tableau 4 présente la viscosité, l'angle de contact η, θ_c et l'énergie de surface, γ_{SL} valeurs des encres hybrides GF et GF. Le η pour toutes les encres varie entre 7,5 et 11,9 mPas, ce qui indique que toutes les encres sont acceptables pour l'impression jet d'encre. La Figure 18 illustre les courbes η des encres GF et des encres hybrides GF. Le η pour l'encre GF et les encres hybrides GF a diminué avec l'augmentation du taux de cisaillement, ce qui indique un comportement pseudoplastique (écoulement d'amincissement par cisaillement). L'amincissement par cisaillement est un phénomène dans lequel la viscosité de l'encre conductrice diminue avec l'augmentation de la contrainte de cisaillement. Ce phénomène est bon en impression jet d'encre où l'encre conductrice a une viscosité élevée dans des conditions normales mais une faible viscosité lors du passage à travers la tête d'impression afin d'éviter le colmatage des buses (O'Mahony et al., 2019).

Selon Khondoker et al. (2013), la mouillabilité de la surface de l'encre conductrice avec le support joue un rôle important qui influence considérablement la qualité d'impression. Les valeurs mesurées des encres GF et des encres hybrides GF sur le substrat PET sont indiquées dans le Tableau 4. Sur la base du Tableau 4, il a été constaté que le θ_c pour les encres hybrides augmentait légèrement avec l'ajout d'un matériau hybride; AgNPs et PEDOT:PSS. Cependant, le θ_c est toujours en dessous de 90°, ce qui est considéré comme une bonne adhérence entre l'encre conductrice et le substrat PET. Le γ_{SL} de l'encre GF et des encres hybrides GF mesuré sur le site θ_c se situe entre 39,4 et 41,1 mJm^{-2}, ce qui fait que les encres GF et hybrides GF ont tendance à devenir moins réactives avec l'environnement.

Tableau 4 Comparaison des propriétés physiques des encres hybrides GF et GF

Encre	Viscosité (mPas)	Angle de contact (°)	Énergie de surface (mJm^{-2})
GF	7.5	32.9	41.1
GF/AgNPs	9.8	33	41.1
GF/PEDOT:PSS	11.8	37.3	39.4

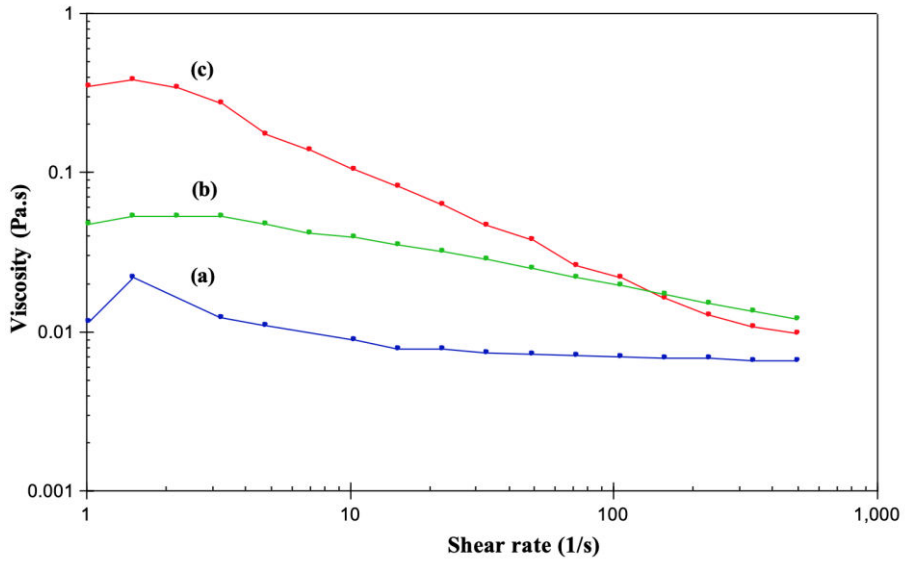

Figure 18 Courbes de viscosité de (a) l'encre GF, (b) l'encre hybride GF/PEDOT:PSS et (c) l'encre hybride GF/AgNPs en fonction du taux de cisaillement

La Figure 19 montre les encres hybrides GF et GF imprimées sur substrat PET à différents nombres de couches d'impression. D'après la Figure 19, comme prévu, la couleur imprimée au jet d'encre est devenue plus foncée avec l'augmentation du nombre de couches d'impression, en particulier

pour l'encre hybride GF/PEDOT:PSS. Cependant, pour l'encre GF et l'encre hybride GF/AgNPs, la couleur imprimée était moins foncée que l'encre hybride GF/PEDOT:PSS. On croit que l'échantillon imprimé avec une couleur plus foncée a une meilleure connexion et pourrait influencer les propriétés électriques. Denneulin et ses collaborateurs (2009) ont signalé qu'à mesure que le nombre de couches d'impression augmentait, le film conducteur se connectait les uns aux autres et réduisait donc la résistance de la feuille.

Les motifs d'encres conductrices composés d'encres GF et d'encres hybrides GF sur différentes couches d'impression ont été fabriqués par impression jet d'encre afin de déterminer le comportement de la conductivité. La Figure 20 (a, b) présente la conductivité de surface de l'encre GF et des encres hybrides GF en fonction de la couche d'impression. Comme on peut le constater, la conductivité de surface de tous les échantillons imprimés au jet d'encre augmente avec l'augmentation de l'épaisseur de la couche d'impression. L'encre conductrice en GF/PEDOT:PSS hybride présente la conductivité de surface la plus élevée par rapport à celle de l'encre GF et de l'encre hybride GF/AgNPs sur toutes les couches d'impression. L'encre hybride GF/PEDOT:PSS a montré une amélioration remarquable de la conductivité de surface de 10 à 50 couches d'impression, suivie par l'encre hybride GF/AgNPs et l'encre GF de 100%, 55% et 54%, respectivement.

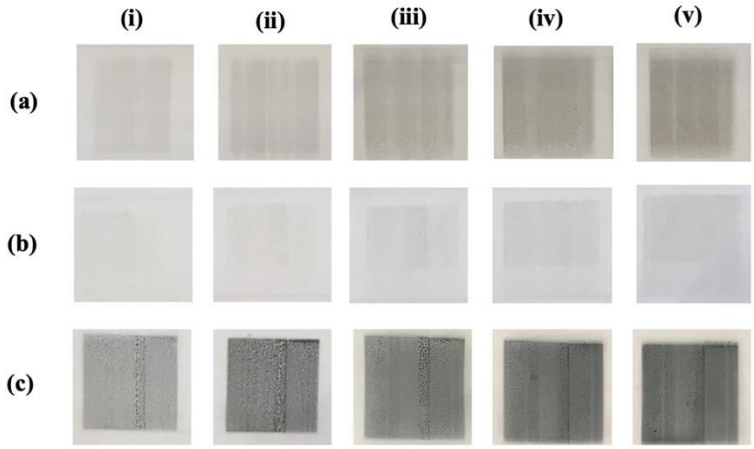

Figure 19 Photographies de l'encre imprimée (a) GF, (b) de l'encre hybride GF/AgNPs et (c) de l'encre hybride GF/PEDOT:PSS sur substrat PET avec différentes couches d'impression (i) 10 couches, (ii) 20 couches, (iii) 30 couches, (iv) 40 couches et (v) 50 couches

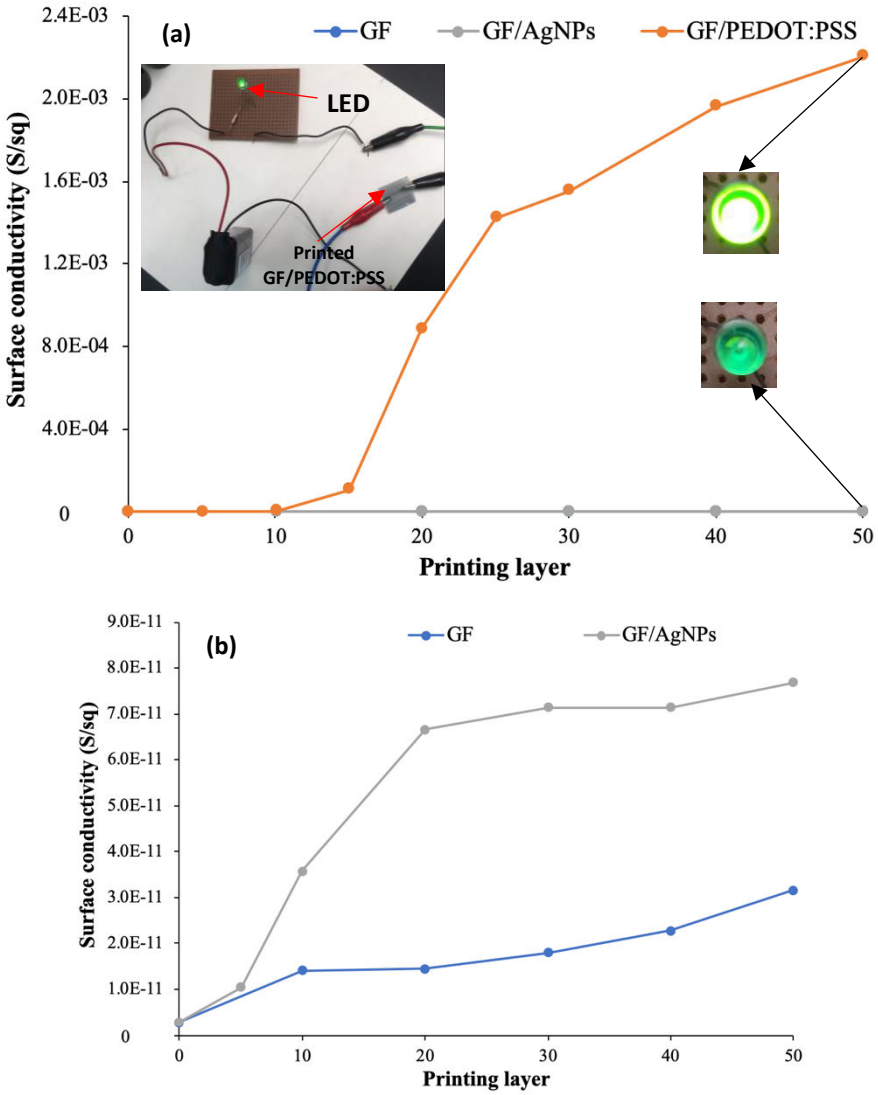

Figure 20 (a) Conductivité superficielle de l'encre GF et des encres hybrides GF en fonction de la couche d'impression et (b) agrandissement de la conductivité superficielle de l'encre GF et de l'encre hybride GF/AgNPs, encadré montrant des images numériques d'un circuit électronique configuré et la luminosité des LED pour les encres GF et GF hybrides imprimées

Même si la conductivité électrique du GF pur et des AgNPs était supérieure à celle du PEDOT:PSS pur, il y a aussi d'autres facteurs qui ont influencé la conductivité de surface des motifs imprimés, notamment la stabilité de l'encre. Dang et ses collaborateurs (2013) ont indiqué que l'encre conductrice devrait être stable au moins pendant le processus d'impression. Comme indiqué à la section 3.4, le GF/PEDOT:PSS présente la meilleure stabilité parmi toutes les encres conductrices. Une mauvaise stabilité de l'encre peut entraîner plusieurs problèmes au cours du processus d'impression, notamment l'obstruction de la buse et la présence d'un matériau conducteur sur le filtre de la cartouche d'encre, comme le montre la Figure 21. La Figure 21 (a, b) montre une buse bouchée et un matériau conducteur piégé sur le filtre de la cartouche d'encre en raison d'une mauvaise stabilité de l'encre. Il en résulte une qualité d'impression médiocre, ce qui affecte la conductivité superficielle des motifs imprimés, comme le montre la Figure 20.

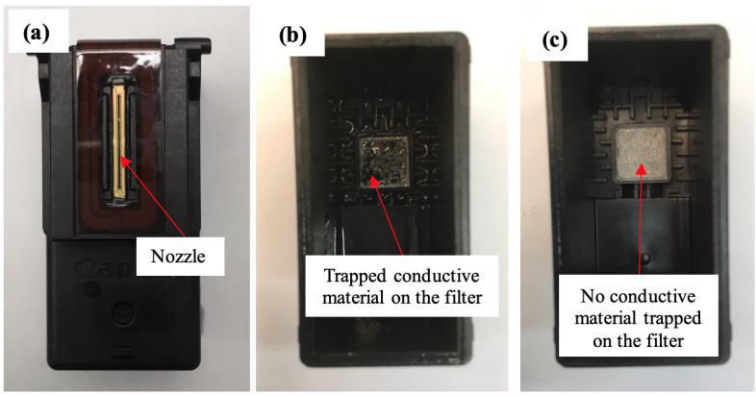

Figure 21 Photographies des problèmes de stabilité des cartouches d'encre dus à une mauvaise stabilité, y compris (a) la buse obstruée et (b) l'encre conductrice piégée sur le filtre à cartouche d'encre; en comparaison avec (c) aucun matériau conducteur piégé sur le filtre à cartouche

De plus, la conductivité superficielle des motifs imprimés est complètement influencée par leur morphologie. La Figure 22 montre la morphologie de la surface supérieure imprimée de l'encre GF et des encres hybrides GF par rapport à la couche d'impression qui fournit des informations sur la formation du réseau conducteur. La Figure 22 (a-d) montre que les chemins conducteurs n'étaient pas connectés et répartis de façon aléatoire sur le substrat, ce qui montre que la quantité de GF et d'hybrides GF/AgNPs n'étaient pas suffisants pour supporter un réseau complet. Dans le cas de l'hybride GF/PEDOT:PSS (Figure 22 (e-f)), le réseau devient plus dense et le réseau conducteur est entièrement formé. La continuité des motifs imprimés s'est améliorée avec l'augmentation de la couche d'impression de 10 à 50 couches. La qualité d'impression des encres conductrices s'est améliorée à mesure que le nombre de couches d'impression augmentait. Cette observation est conforme au précédent rapport de Gao et al. (2014) sur la fabrication de motifs en graphène sur le substrat en verre par impression à jet d'encre.

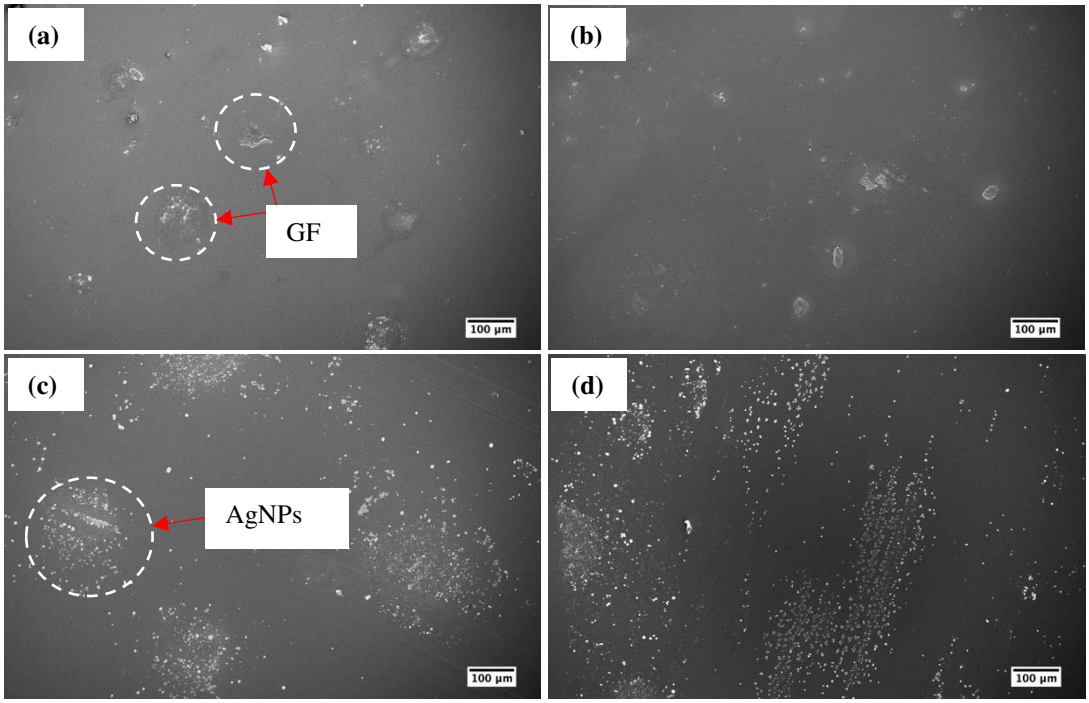

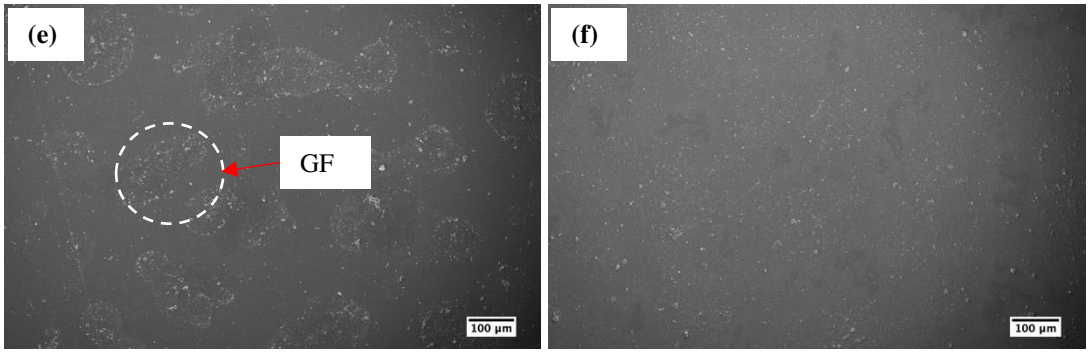

Figure 22 Micrographies MEB de la surface supérieure imprimée en (a, b) encre GF, (c, d) encre hybride GF/AgNPs et (e, f) encre hybride GF/PEDOT:PSS à (a), (c), (e) 10 couches d'impression et (b), (d), (f) 50 couches d'impression [mag. 100X]

4. Conclusions

D'après les résultats de l'enquête menée dans le cadre de la présente recherche, les conclusions suivantes sont résumées d'après les objectifs généraux:

1. Trois différents types de matériaux semblables au graphène; GF, GNPs et SG ont été utilisés pour fabriquer des encres conductrices. Le GF a été synthétisé par réaction solvothermique et les propriétés ont été comparées avec les GNPs et les SG commercialisés. Les résultats ont montré que le GF présentait la surface spécifique et le volume de pores BET les plus élevés, tandis que les GNPs et les SG présentaient une grande taille latérale, une structure cristalline élevée et une haute qualité des particules. Cependant, la petite taille latérale, la faible structure cristalline et la forte teneur en oxygène des particules GF ont réduit ses propriétés électriques.
2. Des matériaux de type graphène ont été mélangés à un liant PV pour produire des encres à base de graphène et les propriétés ont été étudiées. D'après les résultats, l'ajout de charges de remplissage a augmenté la viscosité et l'angle de contact des encres conductrices. Les encres conductrices fabriquées à partir de GNPs présentent une amélioration de 186 % de la conductivité électrique à 10 % en volume de la charge de remplissage, contre 40 % et 10 % pour SG et GF, respectivement. Les micrographies de matériaux de type graphène dans un liant PV ont montré que les encres conductrices étaient pulvérisées de façon uniforme sur le substrat. Les résultats indiquent que les propriétés de l'encre utilisée dans le revêtement par pulvérisation affectent la qualité d'un motif produit.
3. Les encres conductrices GNPs ont été produites avec succès en utilisant des solvants moins toxiques tels que EG, PG et IPA. On observe que le GNPs dispersé dans l'EG présentait une meilleure stabilité de dispersion, viscosité et mouillabilité que celui du GNPs dispersé dans le PG et l'IPA. En revanche, les GNPs dispersés dans les solvants NMP et DMF présentaient également une bonne stabilité de dispersion et une bonne mouillabilité, mais il n'était pas recommandé d'utiliser ces solvants dans l'industrie de l'imprimerie en raison de leur toxicité et des points d'ébullition élevés.
4. Les dispersions de GNPs à différents rapports IPA:EG de solvants mixtes ont été comparées aux dispersions de GF. Il a été constaté que la dispersion des encres GF présentait une meilleure stabilité, viscosité et mouillabilité que celles des encres GNPs à tous les rapports mixtes, ce qui a été confirmé par le potentiel zêta, la spectroscopie UV-Vis, le test d'observation, le rhéomètre, l'angle de contact et les mesures de l'énergie de surface. Seulement 50 % de moins que sa concentration initiale de GF dispersée dans l'IPA:EG à un rapport mixte de 1:1. Cela montre que cette dispersion a la meilleure stabilité de dispersion parmi toutes les encres préparées et qu'elle peut être utilisée comme encre conductrice pour l'électronique d'impression.
5. L'encre hybride GF/PEDOT:PSS a une meilleure stabilité que l'encre GF et l'encre hybride GF/AgNPs avec une légère diminution de sa concentration après un mois avec des valeurs de 30%, 50% et 69%, respectivement. De plus, l'encre conductrice en GF/PEDOT:PSS hybride présente une

amélioration de 100 % de la conductivité de surface de 10 à 50 couches d'impression, contre 55 % et 54 % pour l'hybride GF/AgNPs et GF, respectivement.

References

Arapov, K., Abbel, R., de With, G., Friedrich, H. (2014). Inkjet printing of graphene. Faraday Discuss. 173, 323-336.

Campillo, G.E., Vélez, E., Morales, G., Hincapié, C., Osorio, J., Arnache, O., Uribe, J.I., Jaramillo, F. (2017). Synthesis of silver nanoparticles (AgNPs) with antibacterial activity. IOP Conf. Series: Journal of Physics: Conf. Series 850, 012023.

Chen, Z., Ren, W., Gao, L., Liu, B., Pei, S., Cheng, H.M. (2011). Three-dimensional flexible and conductive interconnected graphene networks grown by chemical vapour deposition. Nature Materials 10, 424-428.

Coleman, J.N. (2013). Liquid exfoliation of defect-free graphene. Acc. Chem. Res. 46(1), 14-22.

Dabczyński, P., Marzec, M.M., Pięta, Ł., Fijałkowski, K., Raczkowska, J., Bernasik, A., Budkowski, A., Rysz, J. (2018). Engineering a poly(3,4-ethylenedioxythiophene):(polystyrene sulfonate) surface using self-assembling molecules- a chemical library approach. ACS Omega 3, 3631-3639.

Dang, M.C., Dang, T.M.D., Fribourg-Blanc, E. (2013). Inkjet printing technology and conductive inks synthesis for microfabrication techniques. Adv. Nat. Sci: Nanosci. Nanotechnol. 4, 015009.

Denneulin, A., Bras, J., Blayo, A., Khelifi, B., Roussel-Dherbey, F., Neuman, C. (2009). The influence of carbon nanotubes in inkjet printing of conductive polymer suspensions. Nanotechnology, 20(38), 385701.

Gao, Y., Shi, W., Wang, W., Leng, Y., Zhao, Y. (2014). Inkjet printing patterns of highly conductive pristine graphene on flexible substrates. Ind. Eng. Chem. Res. 53, 16777-16784.

Geng, Y., Wang, S.J., Kim, J.K. (2009). Preparation of graphite nanoplatelets and graphene sheets. J Colloid Interface Sci 336(2), 592-598.

Ghany, N.A.A., Elsherif, S.A., Handal, H.T. (2017). Revolution of graphene for different applications: state-of-the-art. Surfaces and Interfaces 9, 93-106.

Huang, L., Huang, Y., Liang, J., Wan, X., Chen, Y. (2011). Graphene-based conducting inks for direct printing of flexible conductive patterns and their applications in electric circuits and chemical sensors. Nano Res. 4, 675-684.

Johnson, D.W., Dobson, B.P., Coleman, K.S. (2015). A manufacturing perspective on graphene dispersions. Current Opinion in Colloid & Interface Science 20, 367-382.

Johra, F.T., Lee, J.W., Jung, W.G. (2014). Facile and safe graphene dispersion on solution based platform. Journal of Industrial and Engineering Chemistry 20, 2883-2887.

Khondoker, M.A.H., Mun, S.C., Kim, J. (2013). Synthesis and characterization of conductive silver ink for electrode printing on cellulose film. Applied Physics A, 112(2), 411-418.

Le, L.T., Ervin, M.H., Qiu, H., Fuchs, B.E., Lee, W.Y. (2011). Graphene supercapacitor electrodes fabricated by inkjet printing and thermal reduction of graphene oxide. Electrochem Commun 13(4), 355-358.

Ma, M., Zhu, Z., Wu, B., Chen, S., Shi, Y., Wang, X. (2017). Preparation of highly conductive composites with segregated structure based on polyamide-6 and reduced graphene oxide. Mater. Lett. 190(1), 71-74.

Mengistie, D.A., Ibrahem, M.A., Wang, P.C., Chu, C.W. (2014). Highly conductive PEDOT:PSS treated with formic acid for ITO-free polymer solar cells. ACS Appl. Mater. Interfaces 6, 2292-2299.

Nanda, K.K., Maisels, A., Kruis, F.E., Fissan, H., Stappert, S. (2003). Higher surface energy of free nanoparticles. Physical review letters 91(10), 106102.

Nethravathi, C., Rajamathi, M. (2008). Chemically modified graphene sheets produced by the solvothermal reduction of colloidal dispersions of graphite oxide. Carbon 46, 1994-1998.

Nicolosi, V., Chhowalla, M., Kanatzidis, M.G., Strano, M.S., Coleman, J.N. (2013). Liquid exfoliation of layered materials. Science 340, 1226419.

Ning, G., Xu, C., Cao, Y., Zhu, X., Jiang, Z., Fan, Z., Qian, W., Wei, F., Gao, J. (2013). Chemical vapor deposition derived flexible graphene paper and its application as high performance anodes for lithium rechargeable batteries. J Mater Chem A 1, 408-414.

O'Mahony, C., Haq, E.U., Silien, C., Tofail, S.A.M. (2019). Rheological issues in carbon-based inks for additive manufacturing. Micromachines (Basel) 10(2), 99.

Park, H.Y., Kang, B.J., Lee, D., Oh, J.H. (2013). Control of surface wettability for inkjet printing by combining hydrophobic coating and plasma treatment. Thin Solid Films 546, 162-166.

Pei, S., Cheng, H.M. (2012). The reduction of graphene oxide. Carbon 50, 3210-3228.

Rajan, K., Roppolo, I., Chiappone, A., Bocchini, S., Perrone, D., Chiolerio, A. (2016). Silver nanoparticle ink technology: State of the art. Nanotechnol. Sci. Appl. 9, 1-13.

Saghaei, J., Fallahzadeh, A., Yousefi, M.H. (2015). Improvement of electrical conductivity of PEDOT:PSS films by 2-methylimidazole post treatment. Organic Electronics 19, 70-75.

Saion, E., Gharibshahi, E., Naghavi, K. (2013). Size-controlled and optical properties of monodispersed silver nanoparticles synthesized by the radiolytic reduction method. Int. J. Mol. Sci. 14, 7880-7896.

Salunkhe, R.R., Tang, J., Kobayashi, N., Kim, J., Ide, Y., Tominaka, S., Kim, J.H., Yamauchi, Y. (2016). Ultrahigh performance supercapacitors utilizing core-shell nanoarchitectures from a metal-organic framework-derived nanoporous carbon and a conducting polymer. Chem. Sci. 7, 5704-5713.

Speyer, L., Fontana, S., Cahen, S., Ghanbaja, J., Medjahdi, G., Hérold, C. (2015). Multi-scale Characterization of Graphenic Materials Synthesized by a Solvothermal Based Process: Influence of the Thermal Treatment. Solid State Sci. 50, 42-51.

Tang, J., Yamauchi, Y. (2016). Carbon materials: MOF morphologies in control. Nat. Chem. 8, 638-639.

Tang, Z., Zhang, L., Zeng, C., Lin, T., Guo, B. (2012). General route to graphene with liquid-like behavior by non-covalent modification. Soft Matter. 8, 9214-9220.

Tran, T.S., Dutta, N.K., Choudhury, N.R. (2018). Graphene inks for printed flexible electronics: Graphene dispersions, ink formulations, printing techniques and applications. Adv. Colloid Interface Sci. 261, 41-61.

Vallés, C., Young, R.J., Lomax, D.J., Kinloch, I.A. (2014). The rheological behavior of concentrated dispersions of graphene oxide. Journal of Materials Science 49(18), 6311-6320.

Wan, Y., Luo, J., Xu, J., Zhang, X., Yu, H. (2013). Experimental study of surface roughness effects on wettability. Proceedings of the International Conference on Manipulation, Manufacturing and Measurement on the Nanoscale, IEEE 97-100.

Woo, K., Jang, D., Kim, Y., Moon, J. (2013). Relationship between printability and rheological behavior of ink-jet conductive inks. Ceram. Int. 39, 7015-7021.

Zhou, D., Cheng, Q.Y., Han, B.H. (2011). Solvothermal synthesis of homogeneous graphene dispersion with high concentration. Carbon 49, 3920-3927.

Résumé

Les propriétés prometteuses et exceptionnelles du graphène ont suscité beaucoup d'intérêt de la part de nombreux chercheurs, surtout pour son application dans le domaine de l'électronique. L'objectif principal de cette étude est de fabriquer une encre à base de graphène ayant une très bonne stabilité ainsi que d'excellentes propriétés physico-chimiques pour le développement de dispositifs électroniques flexibles. Des techniques de revêtement par pulvérisation ou par impression à jet d'encre ont été employées pour la fabrication des motifs imprimés. Dans un premier temps, la comparaison des différents matériaux carbonés, i.e. mousse graphénique (GF), nanoplaquettes de graphite (GNPs) et graphite synthétique (SG), a montré que GF avait le plus important volume poreuxet la surface spécifique la plus élevée, avec des valeurs de 0,138 $cm^3.g^{-1}$ et 2136 $m^2.g^{-1}$respectivement. En revanche, GNPs et SG présentent des structures bien cristallisées avec de grandes tailles latérales comprises entre 38 et 44 µm ainsi que des particules de haute qualité ayant un rapport ID / IG compris entre 0,34 et 0,56. Dans un second temps, l'ajout de GF, de GNPs et de SG dans un liant à base de vernis polyester (PV) a été étudié. Les résultats ont montré que la viscosité et l'angle de contact des encres conductrices augmentaient de manière significative lorsque la teneur en charges carbonées dans le liant PV augmentait. L'intégration de 10% en volume de GNPs a amélioré la conductivité électrique du PV de 186% mais seulement de 40% et de 10% pour SG et GF respectivement. Ensuite, la stabilité des encres à base de matériaux graphéniques utilisant des solvants moins toxiques pour l'impression à jet d'encre a été étudiée. Il a été constaté que les GNPs dispersés dans de l'éthylène glycol (EG) montraient de meilleures propriétés en matière de viscosité, de mouillabilité et de stabilité, avec une diminution de 85% de leur concentration initiale au bout d'un mois, comparées à celles du propylène glycol (PG) et du 2-propanol (IPA). Cependant, dans le cas des particules de GF dispersées dans le mélange équimolaire IPA-EG, leur concentration n'a diminué que de 50% après un mois.. Dans la dernière partie, l'encre GF, l'encre hybride GF/poly (3,4-éthylènedioxythiophène) poly (styrène sulfonate) (PEDOT:PSS) et l'encre hybride GF/nanoparticules d'argent (AgNPs) ont été préparées en utilisant des solvants équimolaires de IPA-EG. L'encre hybride GF/PEDOT:PSS a montré une meilleure stabilité que l'encre GF et l'encre hybride GF/AgNPs car elle présentait une diminution de 30% en concentration après un mois d'observation. L'encre conductrice fabriquée à partir de l'encre hybride GF/PEDOT:PSS a montré une amélioration de 100% de la conductivité de surface à 50 couches imprimées et de 55% et de 54% dans le cas de l'encre hybride GF/AgNPs et de l'encre GF respectivement. Le capteur de contrainte imprimé avec de l'encre hybride GF/PEDOT:PSS présente un facteur de jauge de 4,3. En conclusion, l'encre hybride GF/PEDOT:PSS a un fort potentiel pour être utilisée dans les capteurs de contrainte.

Mots clés : polymères, encres, graphène, graphite, électronique souple

Abstract

Les propriétés prometteuses et exceptionnelles du graphène ont suscité beaucoup d'intérêt de la part de nombreux chercheurs, surtout pour son application dans le domaine de l'électronique. L'objectif principal de cette étude est de fabriquer une encre à base de graphène ayant une très bonne stabilité ainsi que d'excellentes propriétés physico-chimiques pour le développement de dispositifs électroniques flexibles. Des techniques de revêtement par pulvérisation ou par impression à jet d'encre ont été employées pour la fabrication des motifs imprimés. Dans un premier temps, la comparaison des différents matériaux carbonés, i.e. mousse graphénique (GF), nanoplaquettes de graphite (GNPs) et graphite synthétique (SG), a montré que GF avait le plus important volume poreuxet la surface spécifique la plus élevée, avec des valeurs de 0,138 cm3.g-1 et 2136 m2.g-1respectivement. En revanche, GNPs et SG présentent des structures bien cristallisées avec de grandes tailles latérales comprises entre 38 et 44 µm ainsi que des particules de haute qualité ayant un rapport ID / IG compris entre 0,34 et 0,56. Dans un second temps, l'ajout de GF, de GNPs et de SG dans un liant à base de vernis polyester (PV) a été étudié. Les résultats ont montré que la viscosité et l'angle de contact des encres conductrices augmentaient de manière significative lorsque la teneur en charges carbonées dans le liant PV augmentait. L'intégration de 10% en volume de GNPs a amélioré la conductivité électrique du PV de 186% mais seulement de 40% et de 10% pour SG et GF respectivement. Ensuite, la stabilité des encres à base de matériaux graphéniques utilisant des solvants moins toxiques pour l'impression à jet d'encre a été étudiée. Il a été constaté que les GNPs dispersés dans de l'éthylène glycol (EG) montraient de meilleures propriétés en matière de viscosité, de mouillabilité et de stabilité, avec une diminution de 85% de leur concentration initiale au bout d'un mois, comparées à celles du propylène glycol (PG) et du 2-propanol (IPA). Cependant, dans le cas des particules de GF dispersées dans le mélange équimolaire IPA-EG, leur concentration n'a diminué que de 50% après un mois.. Dans la dernière partie, l'encre GF, l'encre hybride GF/poly (3,4-éthylènedioxythiophène) poly (styrène sulfonate) (PEDOT:PSS) et l'encre hybride GF/nanoparticules d'argent (AgNPs) ont été préparées en utilisant des solvants équimolaires de IPA-EG. L'encre hybride GF/PEDOT:PSS a montré une meilleure stabilité que l'encre GF et l'encre hybride GF/AgNPs car elle présentait une diminution de 30% en concentration après un mois d'observation. L'encre conductrice fabriquée à partir de l'encre hybride GF/PEDOT:PSS a montré une amélioration de 100% de la conductivité de surface à 50 couches imprimées et de 55% et de 54% dans le cas de l'encre hybride GF/AgNPs et de l'encre GF respectivement. Le capteur de contrainte imprimé avec de l'encre hybride GF/PEDOT:PSS présente un facteur de jauge de 4,3. En conclusion, l'encre hybride GF/PEDOT:PSS a un fort potentiel pour être utilisée dans les capteurs de contrainte.

Keywords: polymer, ink, graphène, graphite, flexible elctronics